Atmospheric Cerenkov astronomy of cataclysmic variables & other potential gamma ray sources

Bradbury, Stella Marie

Atmospheric Cerenkov Astronomy of Cataclysmic Variables & Other Potential Gamma Ray Sources

by

Stella Marie Bradbury, B.Sc.

A thesis submitted to the University of Durham in accordance with the regulations for admittance to the degree of Doctor of Philosophy

Department of Physics
University of Durham

November 1993

ABSTRACT

Recent developments in the application of the atmospheric Cerenkov technique to γ-ray astronomy are reviewed here. These include new methods of signal to noise enhancement and the increasing diversity of stellar systems positively identified as Very High Energy γ-ray sources.

Four Cataclysmic Variable systems were observed using the University of Durham Atmospheric Cerenkov telescopes during the course of 1990 and 1991. The statistical analysis performed in the search for a γ-ray signal, above a threshold energy of approximately 0·4 TeV, from three of these objects, HO253+193, EF Eridani and VW Hydri, is described here. The results of this brief survey are discussed in the context of current ideas as to the mechanisms by which Very High Energy γ-rays may be emitted from accreting binary star systems of this type.

The analysis techniques applied to Cataclysmic Variable data were extended to an x-ray binary system, Sgr X-7. For comparison, the analysis of data recorded on two radio pulsars, PSR 1855+09 and PSR 1509-58, having more accurately known pulse signatures than the accreting systems is also described here, together with that of the globular cluster 47 Tucanae, which may emit a steady γ-ray flux; an upper limit is placed upon the level of Very High Energy γ-ray emission from this object.

Extension of the Very High Energy γ-ray source catalogue will require a further improvement beyond the current signal to noise ratios of atmospheric Cerenkov telescopes. Some features characteristic of the atmospheric Cerenkov emission triggered by Very High Energy γ-rays as opposed to other cosmic ray particles, which could be exploited in an attempt to reduce interference from the latter, are reviewed. The first attempt to obtain directional information from the relative time of arrival of a Cerenkov flash at the telescopes at the University of Durham Southern Hemisphere site, and thus isolate an anisotropic γ-ray flux is reported here.

CONTENTS

PREFACE

The analysis of data obtained using the University of Durham Atmospheric Cerenkov telescopes is presented here. The author made a special study of the feasibility of obtaining information as to the direction of origin of a flash of Cerenkov light from the difference in its arrival time at separate telescopes, with a view to improving the signal to noise ratio of the atmospheric Cerenkov technique.

The author assessed the theoretical basis for according Cataclysmic Variables the status of Very High Energy γ-ray source candidates, and compared the results of her analysis of observational data on three such systems with their expected behaviour. She also undertook the analysis of four datasets, to which her own observations had contributed; those pertaining to the x-ray binary Sgr X-7, the globular cluster 47 Tucanae and the pulsars PSR 1855+09 and PSR 1509-58.

In addition, the author contributed to the routine operation and maintenance of the Mark III and Mark IV telescopes during a total of seven dark Moon periods from 1990 to 1993, and assisted in the commissioning of the Mark V telescope at Bohena Settlement, New South Wales. The author was, in part, responsible for the design and testing of a photomultiplier based detector package for use in the Mark V telescope. She also shared in routine data processing tasks and the modification of various analysis programs.

None of the work presented in this thesis has been submitted previously for admittance to a degree in this or in any other university.

ACKNOWLEDGEMENTS

I thank Professor A.D. Martin for the provision of the facilities of the Department of Physics throughout my studies, and my supervisor Dr K.J. Orford for his sense of humour. I also acknowledge the financial support of the Science and Engineering Research Council.

My gratitude and sympathy goes to Pete Edwards and David Buck for their attempts to curb my wilder flights of fancy.

I should like to thank the past and present inmates of The Observatory and of Shincliffe Hall for their moral support; they know who they are, and also Kerri, Chris, Trish and Ross for being, well, Australian.....

CHAPTER ONE

An Introduction to Gamma Ray Astronomy

1.1 preamble

Ninety years have passed since Rutherford and Cooke (1903) first discovered that the discharge time of a gold leaf electroscope could be prolonged by encasing it in metal. The rapid rate of discharge in open surroundings was attributed to the agency of some form of penetrating radiation. Within a decade of this finding, Goekel (1910) and Hess (1911) had observed the same phenomenon during balloon borne experiments. It was noted that the discharge time of an electroscope reached a maximum at approximately 1 km above sea level, then fell steadily as the balloon continued to rise. The "recovery" at high altitudes was attributed to penetrating radiation of an extraterrestrial origin. It is now known that the "cosmic rays" studied by Goekel and Hess were highly energetic, charged particles. The mean energy of cosmic rays accelerated within the galaxy is $\sim 10^9$ eV and their energy density at Earth is ~ 1 eV cm^{-3} (Silberberg, Tsao & Letaw, 1993). In fact, their energy density is approximately equivalent to the galactic energy density of starlight, of the thermal gas in the inter-stellar medium (ISM) and of galactic magnetic fields, yet the precise origin of cosmic rays still remains a mystery.

The cosmic ray flux in the vicinity of Earth consists principally of charged particles, of which the majority are protons, electrons and light nuclear fragments, which are susceptible to acceleration by electro-magnetic fields. These particles are deflected during their passage through the background magnetic field of the galaxy (of strength $\sim 3\mu G$). The directions from which all but the most energetic particles are seen to have come therefore bear no relation to their place of origin, and the overall

flux appears isotropic. Only γ-rays (photons of energy greater than 0·511 MeV, the rest mass energy of the electron), which make up approximately one ten thousandth of the cosmic ray number density, and a very few long-lived neutral particles can be traced to their origin at a discrete "point source".

The measured nuclear composition and energy spectrum of cosmic rays can be used to constrain models of stellar evolution and nucleosynthesis and of shock wave propagation in the ISM. Conversely, Gamma Ray Astronomers seek to study only the small photonic component of the cosmic ray flux. Photons retain not only directional information, leading to the identification of a source of γ-rays with an object observed at other wavelengths, but also the temporal characteristics associated with a specific acceleration mechanism and source geometry.

Most of the processes of γ-ray production described in the following pages are inextricably linked to the presence of energetic, charged particles. Any celestial body which exhibits continuum emission at γ-ray wavelengths is almost certainly contributing to the universal flux of charged cosmic ray particles. Gamma Ray Astronomy therefore has a vital role to play in establishing the fundamental origin of cosmic rays.

1.2 γ-ray production mechanisms

A number of production mechanisms must be invoked in order to account for the strong flux of cosmic γ-rays arriving at Earth. Radioactive decay may contribute γ-rays carrying a specific energy in the range 1 MeV to 100 MeV. However, the radioactive nuclei which give rise to this discrete γ-ray line emission are confined to regions where nuclear reprocessing has recently occurred. For example, Kurfess et al. (1992) have observed γ-ray line emission from the remnant of the supernova SN1987A which is characteristic of the decay of ^{57}Co.

The spectrum of black body radiation cannot extend beyond the low

energy γ-rays produced in the aftermath of a supernova event, where shock heating may raise the local temperature to $\sim 10^{10}$ K. Some more prevalent γ-ray continuum emission mechanisms are presented below.

1.2.1 particle - electro-magnetic field interactions

A particle of charge q which enters an electro-magnetic field at an oblique angle experiences an acceleration, **a**, and radiates energy in the form of electo-magnetic waves at a rate given by:

$$-\frac{dE}{dt} = \frac{q^2 |\mathbf{a}|^2}{6\pi\varepsilon_o c^3} \qquad \text{eqn. 1.2a}$$

(Longair, 1981). Since the accelerating force is a function of charge but not of mass, of two particles both carrying charge q, the less massive will experience the greater acceleration. For this reason, models of γ-ray emission are often simplified by the omission of all potentially radiating particles other than electrons and positrons. A survey of some of the most common astrophysical particle - electro-magnetic field encounters follows.

(i) bremsstrahlung radiation

When one charged particle enters the Coulomb field of another at a relative velocity **v**, it experiences an electro-static attraction or repulsion which causes it to change direction. As it is accelerated it radiates according to equation 1.2a (a detailed treatment has been presented by Longair, 1981). The spectrum of emitted radiation is level until a frequency of $\nu = \gamma v/b$ is reached (where b is the perpendicular distance from the original path of the first particle to the second and $\gamma = (1 - (v/c)^2)^{-1/2}$) above which it rapidly declines.

(ii) magneto-bremsstrahlung radiation

If a particle of charge q, mass m and velocity v enters a uniform magnetic field B (G), it experiences a Lorentz force in the direction of v x B, giving an acceleration of:

$$\mathbf{a} = \frac{q}{\gamma m} \mathbf{v} \times \mathbf{B}$$

where γ is the Lorentz factor of the incident particle. The particle is therefore constrained to follow a helical path about B.

If $\gamma \approx 1$, then the photons emitted are much less energetic than the radiating particle. According to Longair (1981), the frequency of the "cyclotron radiation" obtained approximates to $\nu = 2{\cdot}8$ MHz G^{-1} and it does not extend to the γ-ray region.

If the incoming particle is travelling at a relativistic speed such that γ can no longer be approximated to 1, then γ-rays may be obtained. This is "synchrotron radiation".

(iii) curvature radiation

As a charged particle loses energy via magneto-bremsstrahlung radiation, the gyro-radius of its motion about a magnetic field line dwindles until v is aligned with B. If the field line is curved, then the direction of motion of a particle which follows it will vary accordingly. Particles accelerated in this fashion emit photons of "curvature radiation" of energy E_{curv} given by:

$$E_{curv} \approx 3hc\gamma^3/4\pi r_c \qquad \text{eqn. 1.2b}$$

where r_c is the radius of curvature of the field line and γ is the Lorentz factor of the charged particle (Ramana Murthy & Wolfendale, 1986).

(iv) inverse Compton scattering

None of the above mechanisms is sufficient, in itself, to supply the flux of γ-rays observed at Earth which have energies of 10^{12} eV and above. The low energy γ-ray photons which *are* obtained can however be boosted to this energy range through electro-magnetic coupling to relativistic particles.

A photon of energy E_{ph} which encounters a relativistic electron of energy $E_e = \gamma\, m_o\, c^2$, will, on average, leave the collision site with an energy of $^4/_3\, \gamma^2\, E_{ph}$ (Lang, 1986). The number of photons scattered per unit time is proportional to the energy density of the incident photon flux.

1.2.2 meson decay

Unstable secondary mesons can be produced as a result of collisions between highly energetic cosmic ray nucleons, the most common interaction is:

$$p^+ + p^+ \rightarrow p^+ + p^+ + \pi^o$$

Neutral pions of Lorentz factor γ in an observer's rest frame appear to decay after $\gamma(10^{-16})$ s, the principal decay mode being: $\pi^o \rightarrow \gamma + \gamma$ (branching ratio ~99% (Griffiths, 1987)). The threshold energy for the above reaction is 1·2 GeV and there the pion will decay to two photons each of 75 MeV energy.

Collisions between protons of energy $\geq 10^{20}$ eV and photons of the 2.7 K cosmic microwave background (MWB) may also contribute to the production of π^o decay γ-rays. The following photo-pion production mechanisms are supportable:

$$p^+ + \text{MWB} \rightarrow n + \pi^+$$

$$p^+ + \text{MWB} \rightarrow p^+ + \pi^o$$

$$p^+ + \text{MWB} \rightarrow p^+ + n\pi$$

The neutral pions produced in the second reaction above can decay to give γ-rays of energy $\geq 10^{19}$ eV.

1.3 celestial origins

The production of an intense γ-ray flux through meson decay or as Bremsstrahlung radiation can occur only in regions having a high density of matter. The magneto-bremsstrahlung radiation mechanism by definition requires a strong magnetic field. These conditions may be met near the surface of a degenerate star or in the vicinity of an active galactic nucleus (AGN).

The electro-motive force experienced by charged particles at the surface of a rotating degenerate star can cause them to flow outwards along the direction of its dipole field. According to equation 1.2b, an electron following a magnetic field line having a radius of curvature comparable to ten times the radius of (i) a neutron star or (ii) a white dwarf, would have to carry an energy of (i) 35 TeV or (ii) 300 TeV in order to emit a photon of curvature radiation of energy $E_{curv} = 10^{12}$ eV. The relativistic particle flux which is continually replenished from the stellar surface can sustain the inverse Compton scattering of these photons and of any local synchrotron radiation.

In the ISM, inverse Compton scattering off relativistic cosmic ray particles may convert a photon of the 2·7 K microwave background to a 10 MeV γ-ray or an optical photon to a 100 MeV γ-ray.

1.3.1 γ-ray absorption

Two photons of energy E_1 and E_2 respectively can combine to form a pair of leptons if they satisfy the condition:

$$E_1 > \frac{2\ m^2c^4}{E_2(1-\cos(\theta))}$$

where m is the mass of each daughter particle (generally an electron and a positron are considered) and θ is the angle between the photons' pre-

collision trajectories (Ramana Murthy & Wolfendale, 1986). According to this relationship, a γ-ray having an energy of 1 TeV or above can be lost through the interaction:

$$\gamma + \text{MWB} \rightarrow e^+ + e^-$$

as it passes through the 2·7 K microwave background. The photon number density of the microwave background is sufficiently low (~400 photons cm^{-3} (Protheroe & Stanev, 1992)) that little attenuation of any γ-ray flux occurs over interstellar distances. However, the substantial flux of visible light produced within a binary star system where mass transfer is taking place, may hinder the escape of γ-rays by promoting pair production. The γ-ray flux from AGN which lie many megaparsecs from Earth *is* significantly attenuated by this mechanism. Protheroe & Stanev (1992) considered a scenario in which the electron - positron pairs produced in the ISM inverse Compton scatter infra-red background photons (from nearby galaxies or red-shifted optical emission from distant sources). They concluded that the γ-ray spectra of AGN would thus be enhanced in the 1 GeV region.

A γ-ray photon of energy E_1 (eV) can pair produce in conjunction with a virtual photon of a magnetic field of strength B (G), provided that $E_1 \approx 4 \times 10^{18} B^{-1}$ (Manchester & Taylor, 1977). At a distance r from a compact star of radius r_s and magnetic dipole field strength B_s, $B = B_s(r_s/r)^3$. Therefore, γ-rays produced within ~3 r_s of a white dwarf ($B_s \approx 10^8$ G) or 60 r_s of a neutron star ($B_s \approx 10^{12}$ G) may be re-absorbed via this mechanism.

Photons of energies >> 1 MeV interact with matter principally through pair production with virtual photons in the Coulomb fields of nuclei. A γ-ray flux will be attenuated by a factor of two by this process after its passage through a column depth of baryonic material of ~40 g cm^{-2}. This thickness is often exceeded in the environs of accreting stellar binaries, so that the duty cycle of their γ-ray emission can reveal the location of matter within such a system.

1.3.2 favoured sources

In general terms, all astronomical objects which radiate at longer wavelengths, particularly in the X-ray region, in a manner which is indicative of a violent redistribution of matter and/or energy, are potential targets for Gamma Ray Astronomers. These objects range from nearby AGN, through binary systems in which a degenerate star is accreting matter from its companion, to supernova remnants and single, rapidly rotating, magnetised, degenerate stars. For example, many X-ray binaries emit polarised light which is attributed to synchrotron radiation by relativistic particles which may, in due course, take part in inverse Compton scattering and produce γ-rays. The X-ray binaries Cyg X-3, Her X-1, Vela X-1, 4U0115+63 and Cen X-3 have been seen to emit γ-rays of energy $\sim$1 TeV. Other confirmed sources include the Cataclysmic Variable AE Aquarii, the Crab Pulsar and the Crab Nebula (see Chadwick, McComb & Turver (1992) and references therein).

If the low energy photon emission from an object exhibits a well-documented time-variability, then a similar periodicity may be searched for in γ-ray data, as an aid to the identification of a weak source. If no such trial period is available, then a longer exposure will be required before a γ-ray signal is distinguishable from the cosmic ray background flux. For this reason, systems which support beamed emission from a rapidly spinning, degenerate star dominate the list of cosmic γ-ray sources which have been detected by independent observers.

1.4 observational methods

A variety of photon - matter interactions are exploited, each entailing a different detector configuration, in order to scan the γ-ray spectrum from 10^6 eV to 10^{18} eV and above. The number density of cosmic γ-rays falls off as the energy per photon rises. The most penetrating photons are therefore

studied from the ground, rather than via satellite or balloon borne instruments of restricted sensitive area. The latter are used to detect those low energy γ-rays which would be rapidly absorbed by Earth's atmosphere. The γ-ray region is subdivided into energy bands which reflect the coverage which may be obtained by each observational technique (see figure 1.4).

1.4.1 satellite and balloon borne instruments

The first well-substantiated detection of cosmic γ-rays (at an energy $\geq$ 100 MeV) was obtained using the OSO-III satellite, which recorded an enhanced flux density in the direction of the galactic centre (Kraushaar et al., 1967). Satellite and balloon experiments designed to detect γ-rays of energy 1 MeV to 30 GeV generally carry some combination of the scintillation detectors and spark chambers described below.

(i) Low Energy γ-ray detectors

Those γ-ray photons of energy less than 10 MeV interact with matter primarily through Compton scattering, for example by giving up energy to an electron according to:

$$\gamma + e^- \rightarrow \gamma + e^-$$

An incoming γ-ray can thus liberate an electron from its lattice position, to create an electron - hole pair in a semiconductor. This mechanism forms the basis for solid state γ-ray detectors of small sensitive area but high spectral resolution, in which the charge delivered is trapped in artificially maintained potential wells, then read out using charge coupling techniques.

If high spectral resolution is not a prime consideration then scintillation detectors can be employed. When a γ-ray ejects an electron

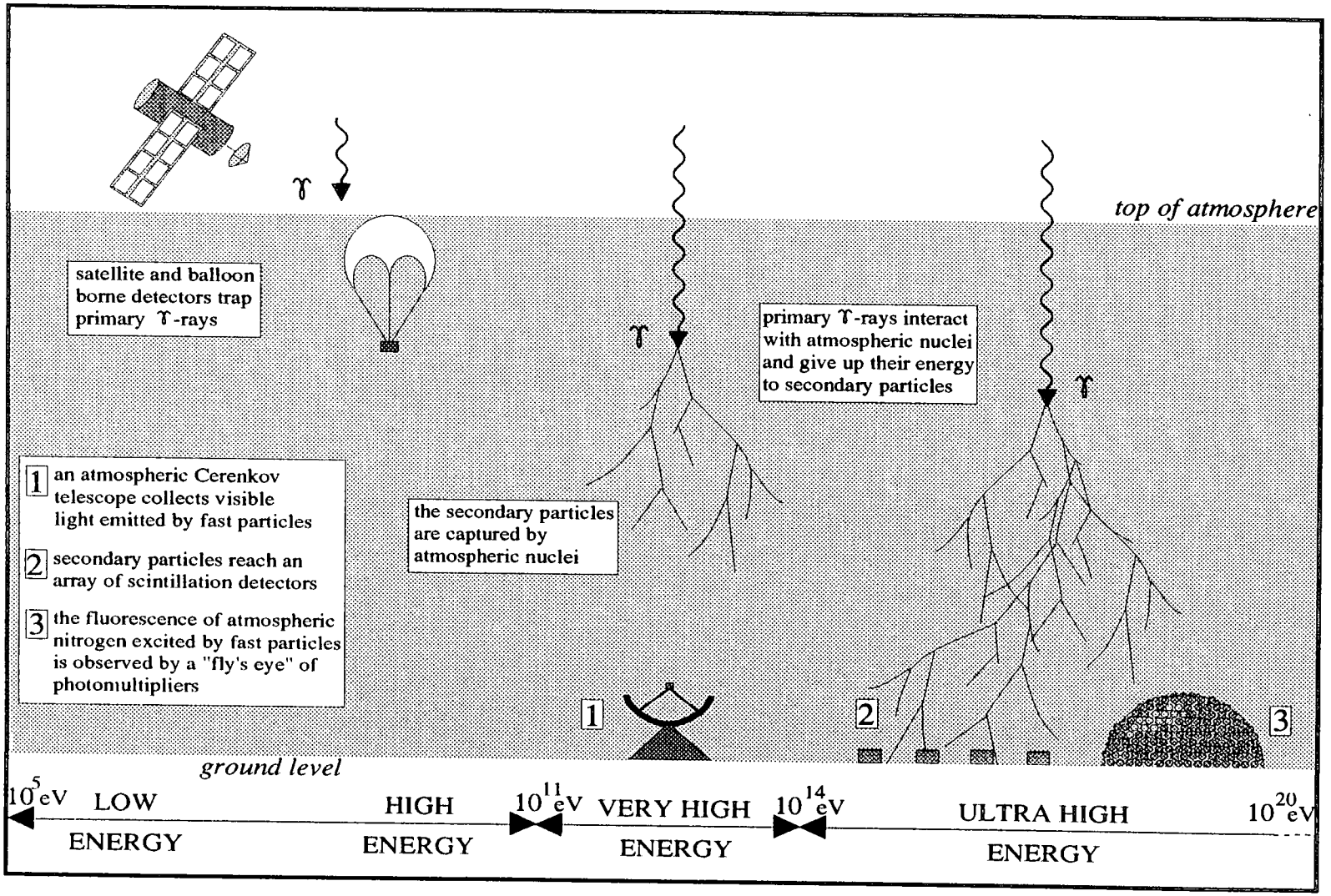

Figure 1.4 : schematic view of some techniques employed in the study of gamma rays of Low/ High Energy, Very High Energy (VHE) and Ultra High Energy (UHE). The photon energies (in eV) to which these sub-divisions of the spectrum correspond are given beneath their associated detectors.

from an atom of scintillating material, the fluorescent light, which is a by-product of this ionisation, is sampled by a photo-sensitive transducer. Crystals of NaI or CsI, or organic scintillators in liquid or plastic form are most frequently used. Scintillators can be produced with a larger surface area and are generally more robust than solid state devices. See Hillier (1984, 55) for an in-depth comparison of the two techniques.

The multiple Compton scattering of low energy γ-rays precludes any attempt to identify their direction of incidence at a detector from the path which they, and the electrons which they liberate, follow within it. Their approximate point of origin on the sky is inferred from the instrument's aperture, which may be subdivided by a matrix of collimators.

Electrons scattered by a photon of energy > 3 MeV do retain the approximate direction of motion of the incoming γ-ray. In Compton telescopes, the locations of the interactions of such a photon during its passage through several separate layers of scintillating material are measured, together with the energy deposited in each tier, so that its direction of incidence can be reconstructed.

(ii) High Energy γ-ray detectors

For photons having an energy in the range 10 MeV to 1 GeV, pair production supplants Compton scattering as the principal absorption process. Spark chambers are used to detect γ-rays via the charged daughter particles which they produce within a slab of dense target material (e.g. crystalline NaI or CsI). Each chamber is filled with an inert gas (e.g. Neon or Argon) and contains a series of parallel metal plates connected to a high voltage supply, interleaved with similar plates maintained at earth potential. The charged particles ionise the gas through which they pass. Breakdown between adjacent plates occurs along the trail of residual ions, so that the particles' paths can be traced through the electrode stack as the electrical discharge gives rise to a succession of visible sparks. The sparks are

registered by fast photomultipliers. Spark chambers can be made sufficiently small to be deployed in a three dimensional array, behind the target slab forming the window of a telescope, thus allowing the direction of incidence of the γ-ray to be determined.

(iii) the Compton Gamma Ray Observatory

The Compton Gamma Ray Observatory (CGRO), which was launched in April 1991, comprises the most comprehensive suite of satellite borne γ-ray detectors currently in operation. Targeting by CGRO has provided the impetus for contemporaneous ground-based γ-ray observations of various objects, such as PSR 1509-58 and the globular cluster 47 Tucane (see chapter seven). The four instruments carried on-board the satellite are listed below (information taken from Schönfelder, 1989).

Name	Detector type	Energy range	Dedicated to:
BATSE	8 un-collimated NaI (Tl) scintillation detectors	20 keV to 100 MeV	all sky monitoring of bursts and transient sources
OSSE	scintillation spectrometer - four NaI/CsI detectors plus tungsten collimators	100 keV to 10 MeV	studying spectra & time-variability of discrete sources
COMPTEL	imaging Compton telescope - a liquid scintillator above NaI blocks	1 MeV to 30 MeV	detection of point sources to high spectral resolution
EGRET	spark chamber above a NaI absorber (to give energy resolution)	20 MeV to 30 GeV	location of point sources to high angular resolution

1.4.2 atmospheric particle cascades

A cosmic γ-ray, of energy ~1 TeV or above, which enters Earth's atmosphere, will encounter atmospheric nuclei and undergo pair production as per section 1.3.1. The charged daughter particles (which retain most of

their parent's momentum) may then go on to emit secondary γ-rays as bremsstrahlung radiation lower in the atmosphere. A cascade of charged particles and high energy photons is formed, which continues to branch out until the the energy per particle is low enough for ionisation to supplant bremsstrahlung radiation as the dominant energy loss mechanism. The Extensive Air Shower (EAS) particles produced by a primary γ-ray of energy $> 10^{14}$ eV may survive to ground level. Less energetic showers which dissipate in the middle atmosphere are studied via the photons of visible light, emitted by the charged particle component, which do reach ground-based detectors. Air shower propagation is reviewed further in section 5.1.

(i) Very High Energy γ-ray detectors

During their passage through the atmosphere, charged particles moving at relativistic speeds trigger a flash of blue Cerenkov light, which is highly collimated along their direction of motion. Atmospheric Cerenkov Telescopes consist of mirrored dishes which collect this light at ground level and focus it onto an array of photomultiplier tubes. The arrival direction at Earth of cosmic γ-rays of energy $\sim 10^{11}$ eV to 10^{14} eV can be specified to within 1°. This technique is described in detail in chapter two.

(ii) Ultra High Energy γ-ray detectors

Air shower particles which reach the ground are recorded using extensive arrays of scintillation detectors. At a mountain altitude of ~2 km, an air shower generated by a single cosmic γ-ray of energy 100 TeV may contain $\sim 10^6$ electrons and positrons, spread over an area of 10^5 m^2 (Carraminana, 1991). The combination of air shower particle arrival times, recorded by different detector modules, is used to determine the point on the sky from which the primary particle came (see for example Edwards, 1990).

A cosmic γ-ray having an energy in excess of 10^{17} eV can be detected via the fluorescent light emitted by atmospheric nitrogen, when it is ionised by secondary particles of ultra high energy. An array of photomultiplier tubes directed towards the sky is used to record the particle tracks. A detection, by this method, of γ-rays of energy 5×10^{17} eV from the x-ray binary Cygnus X-3 was reported by Cassiday et al. (1989). In common with Atmospheric Cerenkov Telescopes, the Nitrogen Fluorescence Technique is only operable on clear, moonless nights, whereas EAS particle detector arrays potentially have a 100% duty cycle.

CHAPTER TWO

The Atmospheric Cerenkov Technique

This chapter contains a summary of the Cerenkov radiation mechanism, notes on the emission of Cerenkov light in Earth's atmosphere and a brief description of the atmospheric Cerenkov technique employed in the study of cosmic γ-rays.

2.1 Cerenkov radiation mechanism

Swamped by the more conspicuous effects of fluorescence and phosphorescence, the production of a pale blue light in transparent media in the vicinity of radioactive substances was not studied in earnest until sixteen years after its appearance in 1910 in the radium filled glass phials of Marie Curie (described in E. Curie, 1938, 173). Mallet (1926) established that this emission was consistently of a blue-white hue in a variety of clear liquids and was continuous i.e. it contained no spectral lines characteristic of atomic excitation. Cerenkov (1934, 1937) following an entirely independent investigation, determined that unlike fluorescence this effect could not be suppressed by the introduction of chemical impurities into the transmitting liquid. He also discovered that a magnetic field could influence the site of the luminosity. Thus if a γ-ray source was in use, the light emission must be due to the presence of charged secondary particles. Cerenkov's results, although limited by the sensitivity of his light detectors, confirmed the theoretical explanation of the phenomenon put forward by Frank and Tamm (1937). This classical electrodynamical treatment has only recently been found to have been presaged by the work of Heaviside (1892). The term "Cerenkov radiation" was coined when Ginsburg (1940) published a quantum mechanical treatment of the radiation process.

A summary of the classical mechanism for Cerenkov radiation follows. The quantum mechanical interpretation differs from the classical, in that it includes the effect upon the motion of the parent particle of momentum conservation during the emission of a photon, a negligible consideration for the purposes of this study. A detailed description may be found in the review by J.V. Jelley (1958) or in Wilson & Wouthuysen (1967).

The passage of a charged particle through a dielectric medium results in the temporary polarisation of its constituent atoms or molecules. This polarisation will be symmetric about the position of the particle if its motion is sufficiently slow, and therefore at a large distance there will be no net field.

If the velocity of the particle is comparable to the phase velocity of light in the medium, then the influence of the particle will be apparent after it has moved on, as illustrated for an electron in figure 2.1a. A pattern of polarisation is set up which is symmetric about the line of passage AB, but which is asymmetric along its length. Thus at point C, some distance away, an instantaneous dipole field exists which induces a retarded electric potential $V(r,\theta,\varphi,t)$ which will propagate outwards like a shock wave. Generally, destructive interference occurs between waves centred on different points along the particle track. However, some constructive interference is possible, as illustrated in figure 2.1b. It is assumed that any deceleration which the charged particle may experience, through ionisation or Bremsstrahlung radiation, is negligible compared with the phase velocity of the electromagnetic shock wave. If the wave traverses the distance PX in the time Δt in which the particle moves from P to P', then a plane wavefront is preserved along the line P'X. Since this pattern is axially symmetric a hollow cone of light is produced. The semi-apex of this cone is defined as follows. From figure 2.1b:

$$\cos\theta = \frac{c/n \times \Delta t}{\beta \times c \times \Delta t}$$

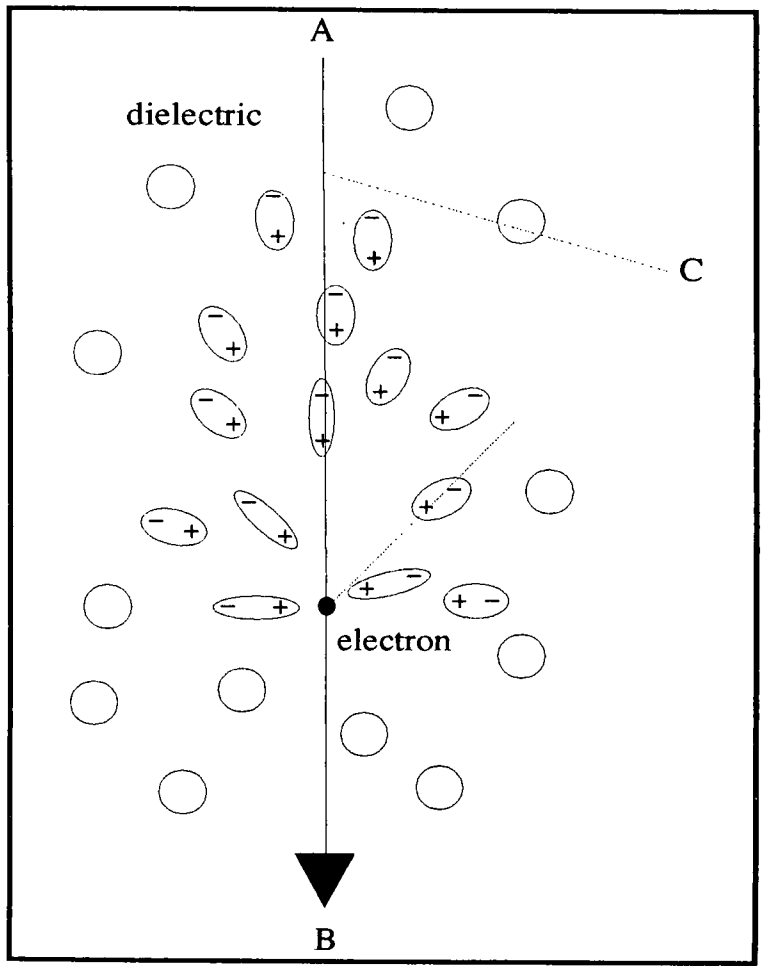

Figure 2.1a : the polarisation of a dielectric medium on the passage of an electron.

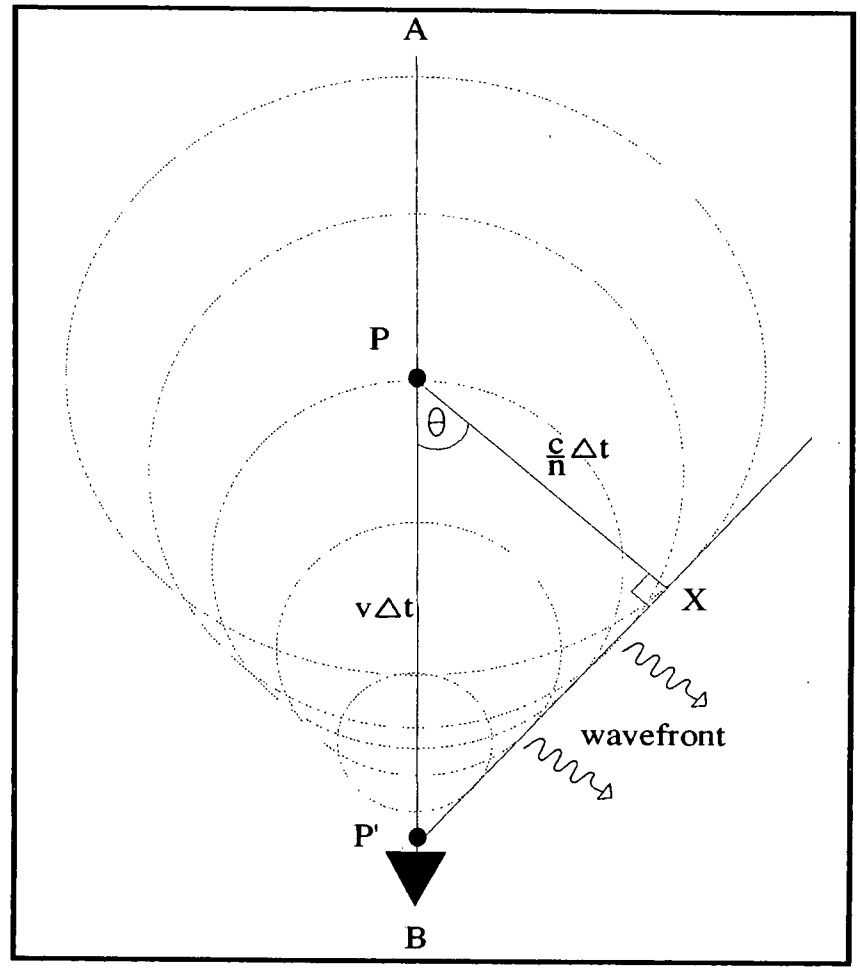

Figure 2.1b : the formation of a Cerenkov cone through constructive interference.

$$\cos\theta = (\beta n)^{-1} \qquad \text{eqn. 2.1a}$$

where n is the refractive index of the dielectric and β is the fraction of the speed of light at which the particle is travelling. This equation 2.1a is the Cerenkov relation and θ is commonly known as the Cerenkov angle.

Clearly, if $\beta < {}^{1}/_{n}$ Cerenkov radiation is not observed. This is always the case for X-ray wavelengths and above, at which the refractive index is less than unity. Cerenkov radiation is usually manifest in the visible and ultra-violet wavebands. The maximum possible Cerenkov angle, for an ultra-relativistic particle (i.e. $\beta \approx 1$), is a mere $1{\cdot}4^{\circ}$ in air at S.T.P. as opposed to $41{\cdot}5^{\circ}$ in water.

As indicated above, for substantial coherent radiation, the kinetic energy loss of the particle must be slight. Frank & Tamm (1937) derived an expression for the energy loss by Cerenkov radiation of a particle of charge ze, which may be reduced to:

$$dE = \frac{z^2 e^2}{c^2} \sin^2(\theta)\ \omega\ d\omega\ dl \qquad \text{eqn. 2.1b}$$

where dE (J) is the amount of energy radiated from an element of the particle track of length dl (m) in an angular frequency bandwidth $d\omega$ (rad s^{-1}) centred upon ω (Protheroe, 1977). Thus taking the above value of θ_{air}, for wavelengths in the visible range from 350 nm to 550 nm, a rate of emission of $5\text{x}10^{-17}$ Jm^{-1} is obtained. This is roughly equivalent to the emission of 20 optical photons per metre of track, which is a poor yield when compared with the 15,000 photons per metre predicted, by the same method, for Cerenkov radiation in water. This being the case, it is hardly surprising that the first positive detection of Cerenkov radiation in air did not occur until 1954 (Ascoli Balzanelli & Ascoli, 1954).

2.2 Cerenkov radiation as a trace of cosmic rays

The detection of Cerenkov light in gases was made possible by the development of the photomultiplier. Photographic methods requiring long exposures to a high light intensity quickly became obsolete, together with photosensitive Geiger counters which suffered from a low energy efficiency and the tendency to respond to randomly incident particles as well as to a Cerenkov beam. The high gain, wide effective bandwidth in the visible region, directional response and straightforward electronics of the photomultiplier made the observation of Cerenkov light a practicable tool in the field of high energy physics.

2.2.1 integral Cerenkov detectors

The Cerenkov relation is the key to a simple test of the velocity of a charged particle, as Cerenkov light is observed only at particle speeds greater than an easily quantifiable threshold value. Since the threshold velocity is dependent upon the refractive index of the transmitting medium, a block of dielectric material viewed by a photomultiplier can be used to discriminate between slow moving particles and faster ones for which condition 2.1a is fulfilled. A layered target of varied composition is used to place bounds upon the velocity of a transient particle. It may consist of a gas at a range of pressures or of sheets of clear plastic, for threshold velocities approximating to the speed of light or to two thirds of this value respectively. Gas-filled Cerenkov threshold detectors have proved their worth in satellite experiments, being well adapted to discriminate between cosmic ray electrons and the similarly energetic yet slower moving background nucleons.

A suitably shielded dielectric and photomultiplier assembly can be used to measure the amount of light emitted in a Cerenkov event. The sum of the energy thus deposited, combined with a velocity estimate, can be used

to determine the charge upon the incident particle according to equation 2.1b. In satellite and balloon borne cosmic ray experiments, a Cerenkov counter is often run in conjunction with a spark chamber array, from which the direction of incidence of a particle and hence its exact path length through the dielectric can be determined.

The use of Cerenkov detectors is not limited to the study of charged primary particles. The energy of an uncharged particle may be inferred from the Cerenkov radiation of the charged daughter particles which it produces on collision with a suitable target material. For example, in the γ-ray telescope flown on board the OSO-III satellite, an incoming gamma ray was immediately converted to an electron-positron pair within a CsI target crystal. These charged fragments then encountered the clear plastic dielectric of a Cerenkov counter (Longair, 1981).

The ability to determine velocity independently of momentum is unique to Cerenkov counters. For most other applications, the scintillation counter is a viable alternative. Both techniques have the capacity for spectrometry by absorption, and measurement of particle flux irrespective of energy. Their uniform response over areas in excess of 1 m^2 makes them suitable for use in ground-based ultra high energy cosmic ray detectors, since an experiment seeking to determine the total energy of a particle requires the volume of the detector to be such that the particle effectively comes to rest within it.

Cerenkov emission is weaker than the light emitted in a scintillator, although it is not re-absorbed in the target medium and photomultipliers may be placed so as to take full advantage of its directionality. Cerenkov detectors are often preferred for financial reasons, as scintillation generally requires a refined medium, whereas Cerenkov emission can be observed in readily available materials and is not affected by small impurities. A case in point is the Deep Underwater Muon And Neutrino Detector (DUMAND) project, the aim of which is to detect cosmic neutrinos

of TeV energies via the charged muons produced in their interactions in sea water. These muons cause Cerenkov emission themselves and may also initiate a shower of electrons. The prototype detector consisted of a 250 m x 250 m x 500 m array of 756 photomultiplier packages, suspended in the ocean off Hawaii at a depth of 4·5 km (Stenger, 1983).

2.2.2 Cerenkov light from extensive air showers

So far, this discussion has concentrated upon Cerenkov detectors in which the dielectric medium is an integral part of the detection device. For cosmic rays of energies in the TeV region, which are too rare to be studied by small aperture satellites and not sufficiently energetic to reach ground based detectors, it is the Earth's atmosphere which acts as a medium for Cerenkov emission.

The threshold energy for the Cerenkov effect in air may be calculated for a particle of known mass using the Cerenkov relation. From a comparison of the threshold energies of the most abundant extensive air shower (EAS) particles, electrons (21 MeV), muons (4·4 GeV) and protons (39 GeV), it is clear that electrons will contribute the most Cerenkov light. Boley (1964) states that 85% of sea level EAS electrons lie above the 21 MeV threshold.

It was Blackett (1948) who first predicted the existence of Cerenkov radiation produced by the passage of cosmic rays through the atmosphere. He estimated that this phenomenon must contribute one ten thousandth of the total night sky brightness. It was a fortuitous encounter in 1958 between Blackett and the cosmic ray physicists Galbraith and Jelley which prompted the latter to make the first observations of atmospheric Cerenkov light (Jelley, 1987). They constructed a detector like that outlined in figure 2.2 (after Jelley, 1958, 213) having a field of view of 0·13 steradians. After simultaneous observation with this "light bucket" and an array of geiger counters, they reported that 44% of the recorded light flashes were

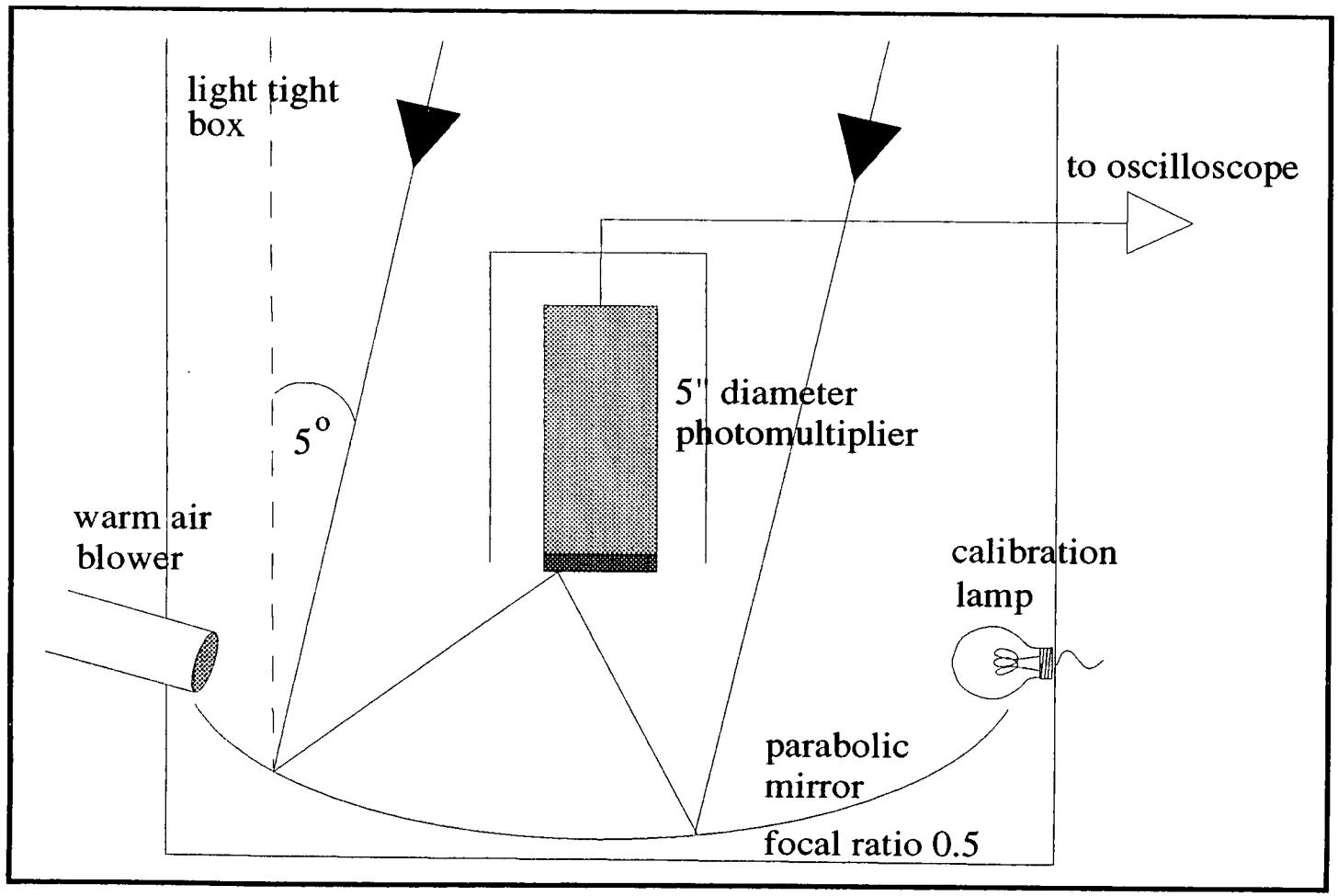

Figure 2.2 : the Galbraith and Jelley "light bucket".

coincident with a geiger counter particle response.

Returning to the concept of the Cerenkov cone, the radius of the light ring on the ground may be estimated using equation 2.1 and a value of refractive index appropriate to the assumed altitude of maximum emission. The variation in refractive index with height (h) is described by:

$$n(h) = 1 + (n_o - 1)\exp(-h/h_o)$$

where n_o is the refractive index of air at S.T.P. and h_o is the scale height of the atmosphere. Simulations suggest that the number of electrons in a shower reaches a maximum at a height (h) of approximately 8 km. The corresponding Cerenkov angle is $0{\cdot}9^\circ$. Thus the emission from a length Δh of the air shower axis will illuminate a ring of radius $\theta h \approx 125$ m and width $\theta\Delta h$.

Galbraith and Jelley measured the coincidence rate between two light bucket detectors as a function of the angle between their optic axes. They found an angular dependence, which was consistent with Cerenkov emission if the effective angle θ was allowed to have diverged, by up to a factor of ten, due to the perturbing effect of coulomb scattering between the shower electrons and atmospheric nuclei. One contemporary experiment, in which coincident events between an EAS array and a zenith pointing photomultiplier were recorded, showed that flashes could be observed as far as 30° away from the shower axis. In another, Cerenkov light was focused onto an image intensifier and photographed. The resultant images were bright circular and elliptical spots of 2° to 5° in diameter. These results demonstrate that although Coulomb scattering can produce large angle dispersion, the light intensity is considerably greater towards the shower axis and may thus be brought to a tightly focused image.

During their experiments, Galbraith and Jelley observed that the light flash count rate fell in the presence of high cloud. This was a sign that under clear skies a significant amount of the observed Cerenkov light had

its origin in the higher regions of the shower. Thus, Cerenkov radiation could provide new information on the history of an extensive air shower, which could not be deduced from particles detected at ground level, most of which come into existence only in the final stages of shower development.

An atmospheric Cerenkov instrument is often used as a supplement to an array of particle detectors. The amount of Cerenkov light is a reliable indication of the energy of a cosmic ray particle, whereas the number and energy of EAS particles at ground level is highly dependent upon the depth of the shower maximum in the atmosphere. The ratio of Cerenkov radiation to secondary particles can be used to estimate the mass of a primary particle, and so to distinguish between nucleon and photon initiated cascades. The directional information obtained from a Cerenkov flash can be used to calibrate the response of a particle array, thus allowing it to function as a point source detector.

2.3 astronomy by the atmospheric Cerenkov technique

The development of atmospheric Cerenkov detectors coincided with the discovery of radio pulsars. Knowing that radio emission was associated with charged particle acceleration, physicists set out to detect these potential point sources of cosmic rays.

In order to retain directional information, a charged cosmic ray particle must travel at a speed sufficient for it to pass through galactic and local magnetic fields without significant deviation. This is remotely possible at ultra high energies, but particles of TeV energies and below appear isotropically distributed. A VHE astronomy of discrete sources must therefore rely upon the detection of neutral particles and γ-rays.

Studies of the fractional electron composition of extensive air showers suggested that one in three hundred was initiated by a high energy photon. It was thought that if these γ-ray induced showers could be preferentially selected, then the directional capability of a Cerenkov

detector would allow observers to pin-point the astronomical source. So, the first atmospheric Cerenkov telescopes were commissioned, and the struggle towards an efficient method of background rejection began.

2.3.1 telescope design

Atmospheric Cerenkov telescopes, although sporting many and varied refinements, are based upon the simple Galbraith and Jelley light bucket, mounted in much the same fashion as the dishes of a radio telescope. Light is reflected from a mirrored surface on to a detector package of one or more photomultiplier tubes. The photomultiplier response is digitised and recorded for analysis at a later date.

The duration of an atmospheric Cerenkov pulse is equivalent to the difference in ground arrival times between light emitted at the top of a shower, and any particles remaining above the Cerenkov threshold. This delay (Δt) is given by:

$$\Delta t = \frac{h}{c/n} - \frac{h}{\beta \times c}$$

for Cerenkov radiation initiated at a height h by a particle travelling at a fraction β of the speed of light. For ultra-relativistic particles, the pulse duration is of the order of a few nanoseconds. Thus, the choice of photomultiplier is restricted to those having a short rise time and rapid recovery. If the response of the photocathode is gradual, the resultant voltage may never reach an instantaneous value sufficient to fire the pulse discriminating system. The system dead time, that is the time taken for the photomultiplier and recording electronics to return to their receptive state, must be minimised to achieve a high pulse count rate.

The brightness of the night sky is sufficient to swamp the response of a photomultiplier to Cerenkov flashes, unless it is run at a very low gain. To achieve a greater sensitivity, several photomultipliers may be run in unison, such that only light pulses which fire more than one tube are

recorded and the multiple triggers must occur within a predetermined gate time e.g. 10 ns. Such a system may be run at a higher gain as statistical fluctuations from individual tubes are ignored.

The duty cycle of an atmospheric Cerenkov telescope is limited by the need for a moonless sky. Operation is difficult at low zenith angles, as the greater atmospheric path length causes showers to maximise further from the detector. Less light is received than would be received from a similar vertical shower, so the energy threshold for event recognition is greater towards the horizon. Cloud also reduces the event count rate and poses problems of data analysis which are discussed in chapter four.

(i) the Dugway experiment

The number of atmospheric Cerenkov observatories has gradually increased, from the three pioneering experiments of the mid nineteen sixties to the thirteen currently in operation (Brazier, 1991). There follows a brief history of the first University of Durham telescopes, which are described in greater detail by Chadwick (1987).

In 1981, the University of Durham constructed an array of four atmospheric Cerenkov telescopes at a site in Dugway, Utah. Each "Mark I" telescope consisted of three paraxially mounted 1·5 m diameter searchlight mirrors, which could be positioned in altitude and azimuth to an accuracy of 0·1° by computer control. Every mirror had a 5 cm wide circular aperture at its cassegrain focus, restricting the field of view of the single 12·5 cm photomultiplier tube behind it to 1·75°. The photomultiplier was offset slightly from the focus in order to obtain a uniform response across such a large photocathode. Only flashes registered by all three photomultipliers were recorded.

The telescopes were positioned at the apices and centre of an equilateral triangle. Although they were otherwise self-contained instruments, a common time base allowed selection, during analysis, of

flashes which were seen simultaneously by some combination of the four. Such a subset should contain a higher proportion of events occuring in the mutual target direction, and therefore display an improved signal to noise ratio.

In 1983, one of the detectors was re-engineered in an attempt to improve its optical characteristics. This then became the "Mark II" telescope. The inferior search light mirrors were replaced by sets of seven 60 cm diameter, solid aluminium reflectors, in a hexagonal formation. A secondary mirror was no longer needed to ensure fair optical quality, so the 2" photomultiplier, which replaced the 12·5 cm model, was located at the prime focus. The field of view was narrowed to 1·25°. It was clear, from simultaneous Mark I and Mark II observations, that the aperture reduction increased the ratio of γ-ray to cosmic ray background detections.

The Dugway telescopes were operated until September 1984. The technique of background rejection by careful aperture design was then taken a stage further, in the planning of the University of Durham Mark III telescope.

(ii) aperture rejection

Cosmic ray nucleons create wider air showers than γ-ray primaries, due to the large emission angles of pions in nuclear collisions. This is manifest in the breadth and irregularity of the received Cerenkov image. With the aid of computer simulations, it is possible to tailor the size of a telescope aperture, to obtain the optimum ratio of γ-ray induced photons to those associated with nucleons and the general sky background.

The pre-analysis selection of events, by the choice of appropriate hardware, does not require a detailed record of the characteristics of each Cerenkov pulse. It is therefore possible to work on very low energy showers which trigger a minimal photomultiplier response. A

low energy threshold is desirable as the fraction of atmospheric Cerenkov light due to γ-rays is greater at low energies. This is because increasingly energetic cosmic ray protons give rise to proportionally more secondary pions and hence to a greater relative Cerenkov yield.

The successful detection of 100 MeV γ-rays, by the SAS 2 and COS B satellites, was an incentive to atmospheric Cerenkov astronomers to work towards lower energy thresholds.

The energy thresholds of the Durham Mk I and Mk II telescopes were estimated by comparison of the actual count rate with simulations. They were found to be 1 TeV and 800 GeV respectively when pointing to the zenith at the 1450 m altitude of the Dugway site. Experience led the University of Durham group to choose a smaller, 1° aperture for their next detector, together with a large mirror area giving sensitivity to low energy flashes whilst diluting the effect of fluctuations in night sky background illumination on tube performance. This "Mk III" telescope had a threshold energy of 250 GeV (Brazier et al., 1989), but has since been subject to various modifications. It is described in greater detail in the following chapter.

(iii) the imaging technique

The University of Durham group is working towards a new generation of hybrid telescopes, combining the technique of aperture rejection with the imaging method of event selection.

Weekes and Turver (1977) first suggested that the shape and orientation of the image of a Cerenkov flash could be used to discriminate between γ-ray and nucleon initiated showers. A Cerenkov telescope could be modified to focus light onto a close packed cluster of photomultiplier "pixels". This would entail not only increasingly complex electronics, but also the sacrifice of low threshold energies in favour of obtaining more information from a substantial pulse.

A Crimean group started to build such a detector, with 37 photomultiplier tubes at its focus, in 1983. A similar device was constructed at the Fred Whipple observatory in Arizona, the successful operation of which encouraged the Whipple group to devise a larger "high resolution camera" (HRC), which came into operation in 1988. The camera consists of 91 photomultiplier tubes having an angular diameter on the sky of 0.25°, surrounded by a ring of 18 tubes each subtending an angle of 0.5°, and is located at the focus of a mirror of 10 m in diameter. The instrument has a 3.5° field of view and 0.12° resolution (Cawley et al., 1990). A Cerenkov event is registered when a response is obtained from two or more of the inner 91 photomultipliers.

The ellipticity of a two dimensional Cerenkov image is dependent upon the air shower impact parameter (the perpendicular distance between the telescope axis and the shower axis). Those whose major axes point towards the centre of the field of view are accepted as being due to showers from the source direction, whilst others of random orientation are rejected. Wide, irregular images are assumed to be a result of core multiplicity in nucleon induced showers. An extended footprint is a sign that the light contribution spanned a lengthy nucleon track, rather than a short electron-photon cascade. The Whipple group select Cerenkov events on the basis of the geometrical parameters shown in figure 2.3, the total light received and the ratio of the two strongest tube responses to the sum of all (Fegan, 1992). Hillas and co-workers (Hillas and Patterson,1987) report that the greatest single distinction, between tight γ-ray related profiles and the diffuse images attributed to nucleons, lies in the azwidth parameter. It is worth noting that this information was obtained solely through the use of numerical simulations, since detailed measurements of air shower development were simply not feasible.

Aside from placing reliance upon theoretical models, the experimentalist must achieve a high degree of accuracy in the calibration

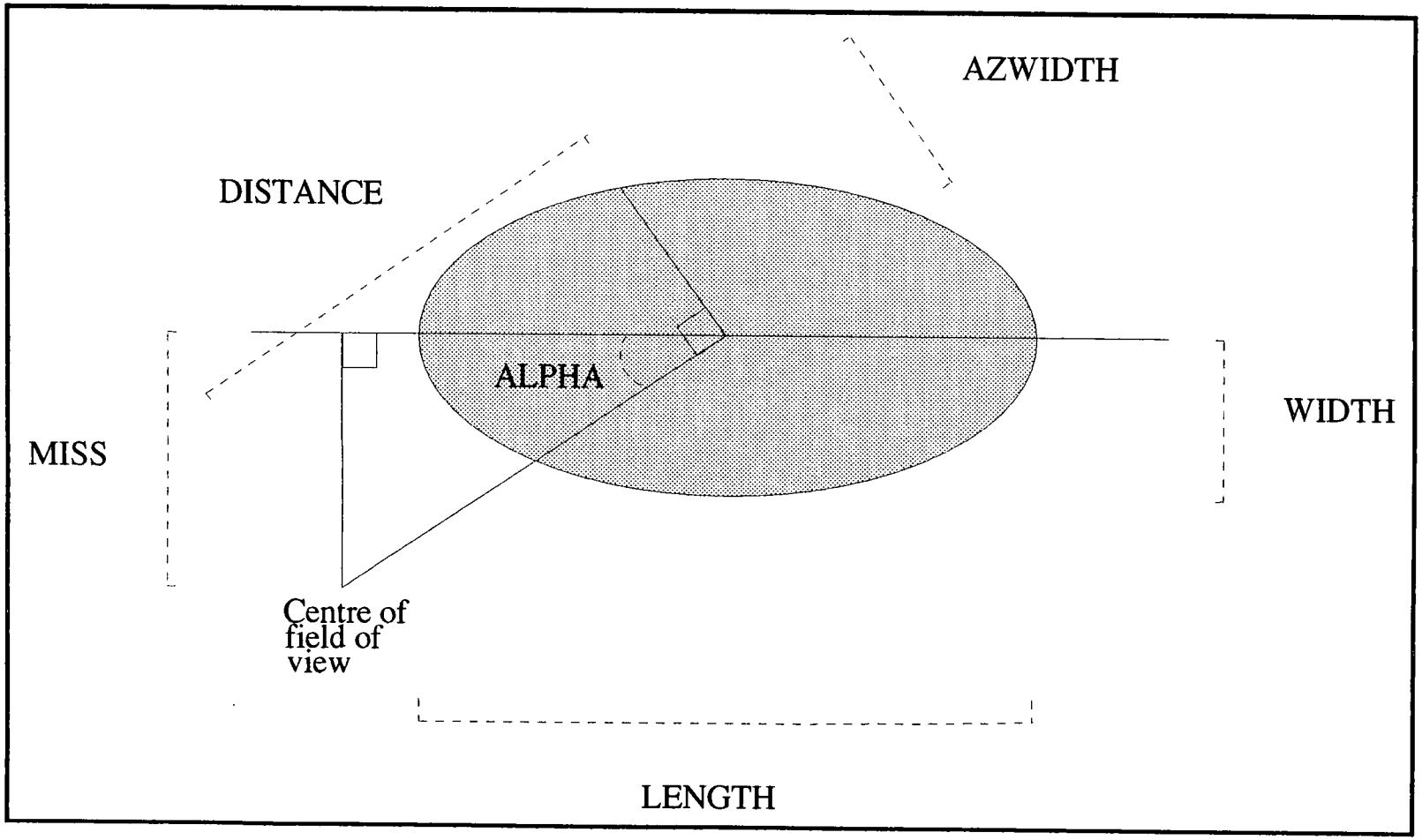

Figure 2.3 : parameters used to describe the elliptical image of a Cerenkov flash in the focal plane of an atmospheric Cerenkov telescope.

of the photomultiplier package, in order to benefit from the imaging technique. The subtraction of pedestal values and gain normalisation between photomultipliers, to achieve a uniform cross-camera response, is referred to as flat-fielding. This process, which is far from simple as characteristics vary from tube to tube according to temperature and sky brightness, is further complicated by the passage of stars through the field of view. However, it is possible to rotate a camera during an observation, such that a background star remains in the sight of a given photomultiplier, which may then be ignored throughout.

2.3.2 contemporary atmospheric Cerenkov observations

The distribution of atmospheric Cerenkov observatories has changed little since a comprehensive listing was given by Mannings (1990). Of the experiments operational at that time, only the Whipple collaboration had made the move from aperture rejection to become reliant upon the imaging technique, although it was the stated intention of the University of Adelaide group to develop a similar camera. As a consequence, the Whipple results were regarded with a great deal of speculative interest, particularly since they seemed to refute some of Cerenkov astronomy's most convincing source detections.

Atmospheric Cerenkov observations have frequently given rise to reports of VHE γ-ray emission based upon a periodicity in the event count rate of low, and in some cases somewhat dubious, statistical significance. A limited number of objects have been confirmed as VHE γ-ray sources by more than one independent group. These are the Crab, Cygnus X-3 and Geminga pulsars, the X-ray binaries 4U0115+63, Hercules X-1, Vela X-1 and Centaurus X-3 and the cataclysmic variable AE Aquarii. However, detections are rare and have not been reproduced on a regular basis. The standard candle of VHE γ-ray astronomy still eludes observers, unless it be the Crab nebula and its pulsar dynamo, from which the Whipple group report a

persistent unpulsed (or "DC") flux.

The Whipple HRC measured a small count rate excess from the direction of the Crab nebula, which became a nine standard deviation effect after application of the azwidth "cut". This detection, although of far greater statistical significance than previous results, was perplexing, since other groups had found evidence for pulsed emission but none for the existence of a DC component. Indeed, satellite observations had shown that above 0.4 GeV, the unpulsed nebula emission fell and the pulsed fraction became dominant. Perhaps the imaging technique introduced a bias against the most energetic Cerenkov events. When the same cut was applied to raw data on other objects, the periodicity which had been apparent did not appear in the reduced data set. Claimed detections of Hercules X-1 and 4U0115+63 were withdrawn as a result. Three years passed between the Crab result and the HRC detection of a second non-pulsating source; the active galaxy Markarian 421 (Punch et al., 1992).

Is the apparent failure of the HRC to detect pulsed emission due to a flaw in the imaging technique? It is possible that not enough care has been taken to assess the number of degrees of freedom involved in periodicity tests, resulting in the presentation of statistical fluctuations as bona fide pulsed emission. However, it would be pessimistic to assume that so many researchers could make the same errors. It is unlikely that models of cascade development are wildly at fault, since many of the interactions on which they are based have been reproduced in particle accelerators. Macrae (1985) did express some doubt, as to whether predicted variations in the generic images of nucleon associated and γ-ray initiated showers were in fact greater than those obtained from random fluctuations between showers of a similar composition. The Whipple results do seem to confirm the superiority of the azwidth cut predicted by Hillas, although a multi-parameter "wedge" cut achieves the most significant effect (Fegan, 1992).

Ideally, the Whipple results should be corroborated by observations

using an alternative technique. To achieve an equivalent sensitivity by aperture rejection alone would require the construction of an un-economic number of telescopes. Time profiles, either of individual pulses or of the shower front, may be used to differentiate between γ-ray and nucleon progenitors. The latter require measurement of the arrival time of a Cerenkov flash at more than one detector. Background rejection by inter-telescope timing is the subject of chapter five.

Although several research groups have confirmed the existence of a significant unpulsed flux, generally attributed to inverse Compton scattering and synchrotron radiation in the Crab nebula, none have yet matched the sensitivity of the Whipple Collaboration's HRC. The popularity of the Crab nebula and pulsar as a target for VHE γ-ray observations is such that a simple comparison of the results presented at recent International Cosmic Ray Conferences (ICRCs) on this source alone give a clear indication of the current status of atmospheric Cerenkov astronomy in the Northern Hemisphere (see figure 2.3b). The flux from the Crab Nebula was found to be sufficently stable to be the subject of the first measurements of a VHE γ-ray source spectrum by the systematic variation of the selection criteria (and thus of the threshold energy) of a single experiment. At the 23rd ICRC (July, 1993), the measurement of a source spectrum of the form:

$$\varphi\ (>E_{(TeV)}) = (3{\cdot}7\pm0{\cdot}5)10^{-12}(E/5)^{-1.5+/-0.20}\ \ cm^{-2}s^{-1}$$

was reported by the French team operating the THEMISTOCLE array which operates on the fast timing - shower front reconstruction principle. This result was in reasonable agreement (considering the uncertainties in energy calibration) with the differential spectrum:

$$\frac{dN(E)}{dE} = (1{\cdot}48\pm0{\cdot}09\pm0{\cdot}41)10^{-11}(E_{(TeV)})^{-(2.69+/-0.09+/-0.3)}\ cm^{-2}s^{-1}TeV^{-1}$$

presented by the Whipple Collaboration and based upon the imaging technique of cosmic ray background rejection.

research group	epoch	threshold energy (TeV)	technique	exposure (hours)	unpulsed flux seen?	significance (stnd. dev.)	unpulsed flux (photons $cm^{-2}s^{-1}$)	flux pulsed at 33 ms radio period?
University of Michigan (Albuquerque, New Mexico)[1]	1988	0.2	2 x 7 PMT clusters 2-fold coincidence & simple imaging	-	yes	5.8	2×10^{-11}	upper limit 7.6×10^{-13} photons cm^{-2} s^{-1}
Whipple Collaboration (Mount Hopkins, Arizona)[1]	1988 - 1989	0.4	109 pixel camera azwidth cut	30	yes	15.3	7×10^{-11}	no
Tata Institute (Pachmarhi, India)[1]	1987 - 1988	1.1	20 single dishes fast majority logic	72	-	-	-	upper limit 5.6×10^{-12} photons cm^{-2} s^{-1}
University of California Riverside (Albuquerque, New Mexico)[1]	1987	0.6 +/- 0.3	2 single dishes pulse shape selection	2	yes	4.2	$(2.5 +/- 1.3) \times 10^{-11}$	-
Whipple Collaboration (Mount Hopkins, Arizona)[2]	1988 - 1989	0.4	109 pixel camera "supercuts"	30	yes	34.1	-	no
	1989 - 1990			21	yes	24.5	-	no
	1990 - 1991			18	yes	17.6	-	prob. 0.01 in one 29 min. run
THEMISTOCLE (French Pyrennees)[2]	1990 - 1991	3	18 single dishes shower front reconstruction	60	yes	3.5	-	-
HEGRA (La Palma, Canary Islands)[5]	1992 - 1993	2	37 pixel camera	53	yes	4.6	1.5×10^{-11}	-
ACT-2 (Bejing)[3]	1992	3	3 single dishes 3 fold coincidence	155	-	-	-	4×10^{-11} photons cm^{-2} s^{-1} during a 90 min. burst
Tata Institute (Pachmarhi, India)[3]	1992	0.6	12 single dishes fire pattern selection	40	-	-	-	4.3 standard deviation peak on 20 bin phasegram
University of Durham (La Palma, Canary Islands)[3]	1988 - 1989	0.4	3 x 7 PMT clusters 3-fold coincidence	23	-	34.1	-	upper limit 5×10^{-11} photons cm^{-2} s^{-1}
(Narrabri, N.S.W.)[3]	1989 - 1990	3		34	no	24.5	$< 0.3 \times 10^{-11}$	-
(Narrabri, N.S.W.)[3]	1990 - 1991	3		83	-	17.6	-	upper limit 0.1×10^{-11} photons cm^{-2} s^{-1}

Fig. 2.3b: recent results of Atmospheric Cerenkov observations of the Crab pulsar and Nebula.

[1] *Proc. 21st ICRC (Adelaide, 1990), volume 2.*

[2] *Proc. 22nd ICRC (Dublin, 1992), volume 1.*

[3] *Proc. 23rd ICRC (Calgary, 1993), volume 1.*

CHAPTER THREE

The Durham Southern Hemisphere Installation

This chapter consists of a description of the site of the University of Durham Atmospheric Cerenkov Observatory, and of the design and operation of the three telescopes in use in March 1993.

3.1 the site

The greater variety of potential VHE γ-ray sources in the southern skies, particularly along the galactic plane, prompted a move from the Utah site of the Mark I and Mark II telescopes to Australia. The University of Durham Mark III telescope began operation at Bohena Settlement, some 20 km south of Narrabri, New South Wales, in October 1986. This flat forest clearing was the hub of the Sydney University Giant Air Shower Recorder from 1968 to 1979 (Meyhandan et al., 1991). The Anglo Australian Telescope lies 100 km to the south of Bohena Settlement and the Australia Telescope is 20 km to the west. Data from the former suggested that clear skies would be maintained on 180 nights per year on average (Chadwick, 1987). The site co-ordinates (obtained from Global Positioning Satellite measurements) are 30° 28' 20·57 ± 0·54'' S, 149° 39' 36·5 ± 1·01 '' E, and its height above sea level is 257 ± 38 m. At this latitude the hours of darkness per night vary from 8 in the summer months to 12 in July.

3.2 the Mark III telescope

The University of Durham Mark III telescope consists of three paraxially mounted parabolic dishes which make up a total mirrored area of 34 m^2. At the focus of each dish rests a detector package comprising seven 2" diameter photomultiplier tubes (PMTs). In order for a Cerenkov light flash to be recorded as a genuine "event" it must trigger a similar

response from each PMT cluster.

3.2.1 mechanical design

As illustrated in figure 3.2a, each dish is made up of a set of spherical mirrors of 60 cm in diameter. These were formed from polished and anodised thin sheet aluminium of 80 % reflectivity stretched and bonded over lightweight aluminium honeycomb (Chadwick, 1987). Those near the centre of each dish have a focal length, f, of 240 ± 8 cm whilst those at the periphery are of f = 260 ± 8 cm, so that a point source at infinity is brought to an image of approximately 2 cm in diameter.

The framework of the telescope is lightweight aluminium, so the three dishes may be supported by a single bearing. The telescope is driven in altitude and azimuth by two DC servomotors. During normal operation, information from shaft encoders on the telescope mount is relayed to a microcomputer which then displays the actual telescope attitude to an accuracy of 0·09°. This computer re-calculates the target position every 6 s from the celestial co-ordinates of the object under observation, compares this with the actual pointing direction at 0·1 s intervals and supplies power to the motors if correction is required.

3.2.2 the detector packages

Browning and Turver (1977) estimated that such a detector having a 1° field of view would respond to the Cerenkov light from air showers of impact parameter < 50 m. Thus the experiment could be said to have a sensitive area to cosmic γ-rays of ~ 10^4 m^2. The effective aperture of the Mark III telescope was measured, by allowing a star to drift through the field of view of a single 2" PMT at its focus and plotting the rise and decay of the current from the PMT, to be 1·1° FWHM (Brazier, 1991).

Each detector package consists of one PMT at the focus of the dish,

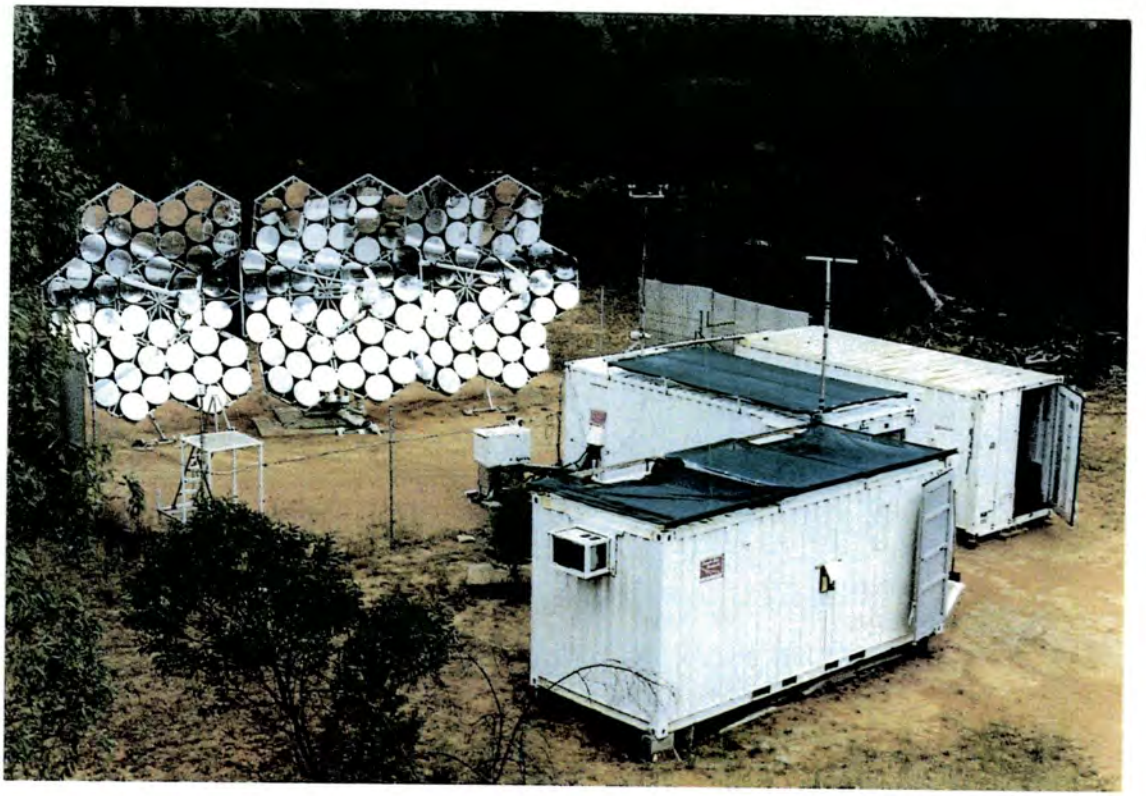

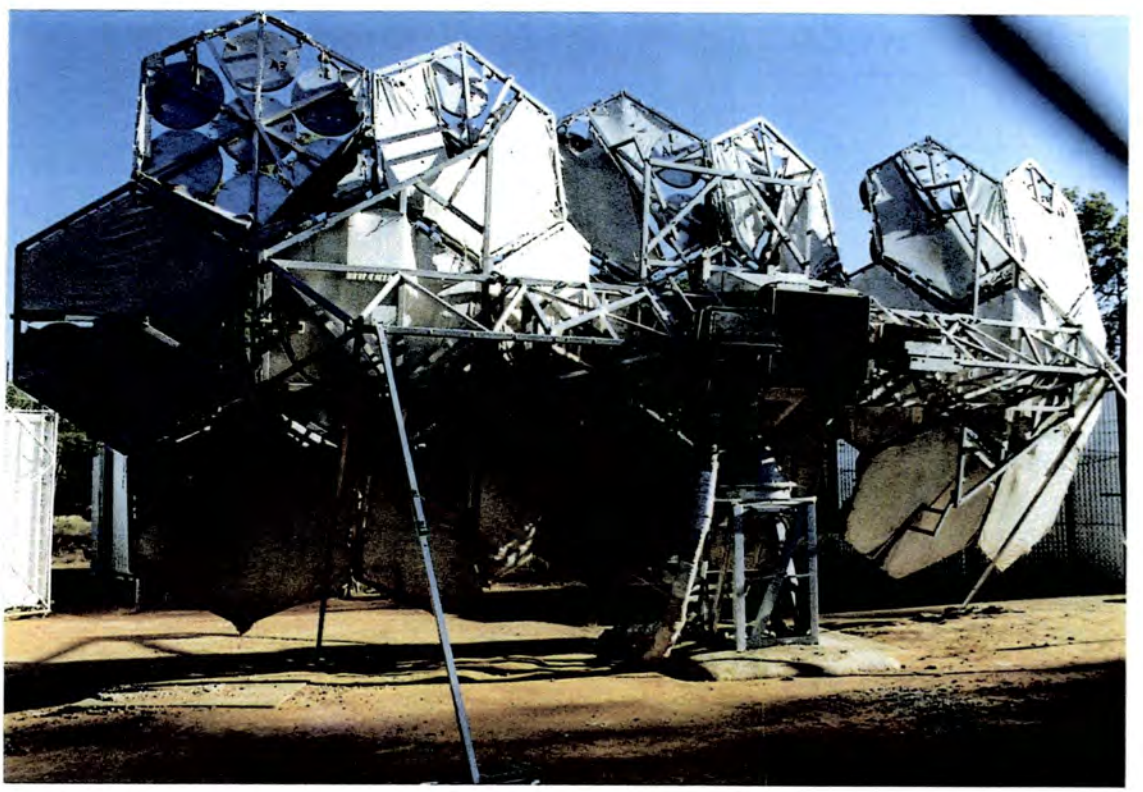

Figure 3.2a : the University of Durham Mark III telescope at Bohena Settlement N.S.W. in March 1993.

surrounded by six others also in the focal plane but slightly off-set from the optic axis. The six "guard ring" PMTs serve to monitor the sky around the target position. Their response to a Cerenkov event which is registered by the central PMT may be used to determine whether the intensity of the light pool was a maximum in the on-source direction. The original separation between the centres of two adjacent PMTs in the focal plane was equivalent to a projected separation on the sky of 2°. However, this spacing was reduced to 1·5° in March 1991 after computer generated simulations showed that this would improve the efficiency of off-axis event recognition. The configuration and the nomenclature of the PMTs within the detector package are given in figure 3.2b.

The PMTs, which were chosen for their fast response (a 2 ns rise time of the order of the duration of a Cerenkov pulse), low intrinsic noise rate and stable gain, are of type RCA 8575. Their sensitivity is greatest at a wavelength of ~ 370 nm which is appropriate to the 300 to 400 nm air Cerenkov spectrum. Under dark sky conditions a typical RCA 8575 will support an anode current of 25 μA and noise rate of 30 kHz when supplied with a electric potential of 1500 V. In order to maintain a constant level of background illumination under varying sky conditions, an LED is positioned at the side of each PMT's photocathode. The anode current of each PMT is regularly compared with a reference current, and the brightness of the corresponding LED is altered in order to ensure that the tube's gain remains within 1 % of its initial value throughout an observation.

3.2.3 modes of operation

For each potential source, a method of observation is chosen which is considered appropriate to the predicted form of its γ-ray flux. These modes of operation are distinguished by the position of the target within the telescope's field of view, which may be systematically varied during the course of an observation.

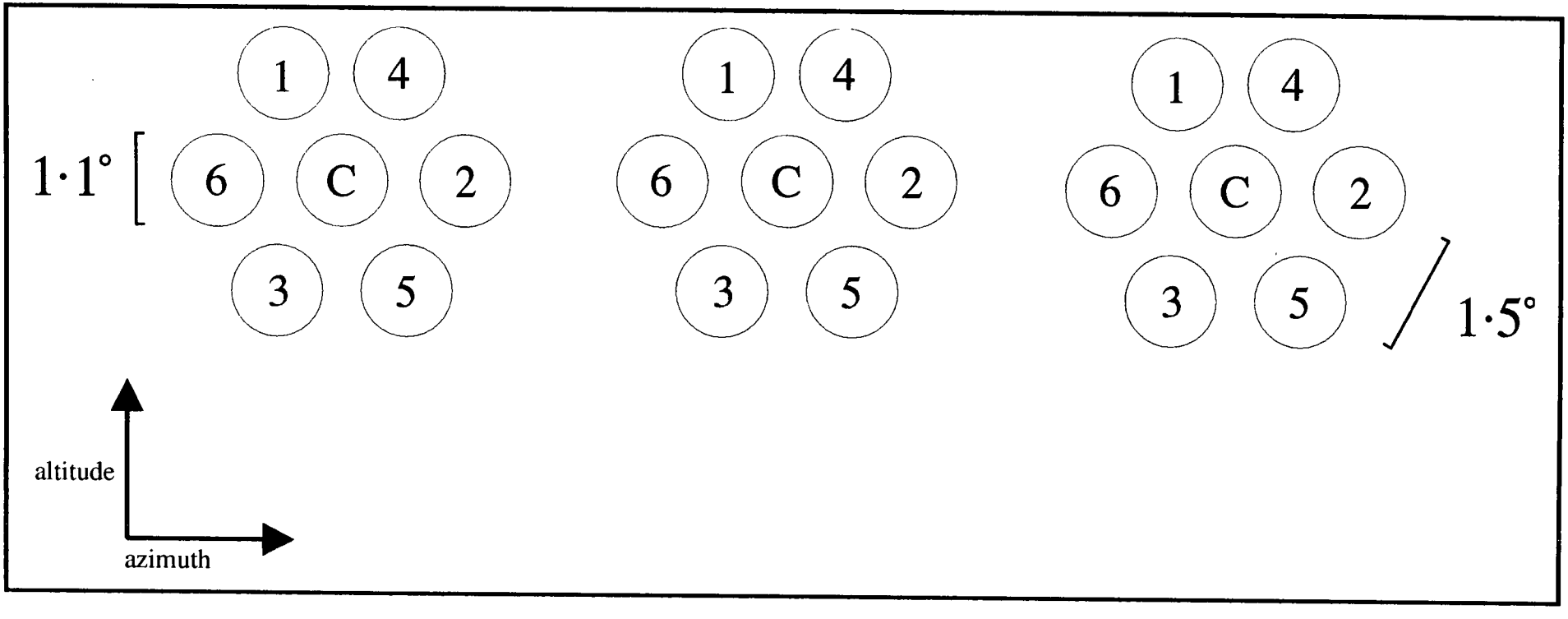

Figure 3.2b : the configuration of the photomultiplier based detector packages of the Mark III telescope. Each grouping of seven PMTs faces a single mirrored dish (the hexagon to hexagon separation is not to scale). Three similarly labelled PMTs make up a single telescope channel. Channel C tubes lie on the optic axis. Channels 1 to 6 are referred to as the off-axis guard ring.

(i) tracking mode

If the candidate source is known to have a characteristic pulse period at other wavelengths, then it is hoped that a VHE γ-ray signal may be identified from a similar time signature. In this case, the telescope pointing follows the path of the object across the sky such that the target remains always within the field of view of the on-axis, central channel. The off-axis guard ring may thus be fully exploited to maximise the signal to noise ratio.

(ii) chopping mode

Where no pulse period is known or expected, a γ-ray source may be detected if it is sufficiently powerful to produce a statistically significant increase in the number of Cerenkov light flashes recorded when the telescope is brought to bear upon it, as opposed to viewing an off-source control region of "empty" sky. As the motor drive to the telescope is sufficient to accelerate it to an azimuthal slew rate of $1^{\circ}\ s^{-1}$ within 10 s (Mannings, 1990), a simple method of tracking the object whilst rotating the telescope such that the central channel alternately views the source direction and then a region of sky 2° in azimuth from this position is possible. This has the advantage that on-source and off-source data are obtained using the same PMTs, thus reducing any instrumental effects. Originally, when the central channel was off-source for two minutes, channel 2 was centred upon the target object and vice versa, therefore the source was in fact monitored throughout. The option was available to combine on-source data from both channels and apply a periodicity test should a time signature be discovered at a later date. However, data from channel 2 were found to have a poor signal to noise ratio due to an incomplete guard ring and hence were seldom analysed for periodicity. It was therefore considered unnecessary to alter the 2°

chopping motion when the PMT separation was reduced to 1·5°. Although the sky conditions are viewed continuously and "chopping" is performed in a strictly azimuthal sense to avoid any variation in the Cerenkov flash count rate with altitude, since the response of the two channels cannot be said to be identical, no attempt is made to observe in this mode unless the sky is uniformly clear of cloud.

(iii) drift scans

The observation of an extended source, such as the galactic centre, may be performed under exceptionally clear sky conditions by simply allowing the object to pass through the field of view of the stationary telescope. The instrument is "parked" at an attitude such that data is collected on an "empty" region of the sky before and after the source performs this transit. Clearly, an increase in the number of Cerenkov events maintained whilst the object was visible would constitute a detection. This mode of observation has been virtually abandoned in favour of the chopping technique, since chopped observations may be curtailed without loss at any stage and the sky conditions in Narrabri are somewhat unpredictable.

3.2.4 signal processing

The process of reduction of the PMT responses to Cerenkov light flashes to permanent data records is summarised below. It has previously been described in detail, by Chadwick (1987) and Mannings (1990).

The raw signals are amplified and then passed simultaneously to the "QT unit" and to a pulse discriminator. The function of the QT unit is to sum the amount of charge received from each PMT within a 30 ns gate time, and to temporarily store this figure in digital form. The pulse discriminator converts the analogue signal to a digital one for further

processing *only* if the pulse it receives exceeds a threshold of 50 mV. Low level noise is therefore excluded at this stage whilst a "true" pulse is forwarded to a digital logic unit.

Given a PMT noise rate of 30 kHz, it would be expected that N separate tubes would fire within a time T purely by chance at a rate $R = N!\ (30 \times 10^3)^N\ T^{(N-1)}$. The digital logic unit registers a three-fold coincidence if a pulse is received from the discriminator for each of the three tubes which make up a single channel (see figure 3.2b) within a 5 ns gate time. Such a three-fold coincidence constitutes an "event". The rate of acceptance of events which occur by chance should not exceed $R \approx 15$ events per hour. If an event occurs then a response is sent to the Coincidence Register and to the Master Trigger.

The Coincidence Register temporarily stores information as to which channel(s) registered an event in the digital logic unit, and displays this "fire pattern" to the observers via a column of 7 LEDs.

The Master Trigger interrupts the background routine of the Logger (a Motorola 68000 based microcomputer) to initiate its data recording subprogram. It also latches the steering and local clock units such that their instantaneous status at the time of event recognition may be read by the Logger in due course. If a second event arrives at the Master Trigger whilst the Logger is "busy" with the first then the Master Trigger has the capacity to read and store its arrival time and that of up to 15 more such "dead time events" until the Logger is ready to receive this information. The Master Trigger may deal with one dead time event per 6 μs. Since *only* the arrival times of these events are eventually recorded, they are of use simply as an indicator of data quality and are generally associated with distant lightning or electronic noise, as opposed to cosmic rays (which are expected to give rise to 1 or 2 events per second).

The Logger reads the anode currents and noise rates of all 21 PMTs and environmental information such as the wind speed and direction, and the

temperature of the detector packages, the mirrors and the signal processing electronics. It broadcasts this information to a series of networked microcomputers for real time display and records it to tape once every minute. This sequence is suspended when an event is flagged by the Master Trigger and the Logger gathers the following information: the 21 values stored in the QT unit, the 6 anode currents of the PMTs forming the central channel and channel 2, the UTC time (to 1 μs), the actual and the target values of the target altitude and azimuth, and the fire pattern stored by the Coincidence Register. These data are formatted and written to magnetic tape and tagged as an "event block" as opposed to a "housekeeping block". Finally, after an elapsed time of 639 μs (Carraminana, 1991), the Logger returns to the Master Trigger, retrieves the arrival times of any dead time events and resets it.

3.3 the Mark IV telescope

3.3.1 history

Relocation of the principal observing site from Dugway to Narrabri left no means of building upon the data already obtained on some well-established γ-ray sources in the Northern Hemisphere. The Mark IV telescope was constructed using technology and materials already to hand with a view to continued monitoring of these few objects. It was operated at the Observatorio del Roque de los Muchachos in the Canary Islands during the summer months (June to October) of 1988 and 1989. This site was then abandoned, due mainly to high winds which made the operation of a free standing telescope difficult. The instrument was transported to the Narrabri site, where it was installed at a distance of approximately 100 m from the Mark III telescope, and began operation there in May 1990.

3.3.2 design

The mounting, steering mechanism and detector packages of the Mark IV telescope are the same in most respects as those of the Mark III, as is the signal processing routine. As shown in figure 3.3, the flux collectors are in the form of three dishes, which are comprised of identical mirror sections, and the two instruments have comparable focal lengths. The total mirrored area of the Mark IV telescope is 18 m^2, its aperture is 0·8°, and its event count rate is 55% of that of the Mark III telescope given the same target position (Brazier, 1991).

The data logging in the Mark IV telescope is performed by a microcomputer which stores the information on a hard disc rather than on magnetic tape. The system dead time is approximately 1 ms (Rayner, 1989).

3.4 The Mark V telescope

The Mark V telescope, which was commissioned in May 1992, has become a test bed for various cosmic ray background rejection techniques. These were listed in Bowden et al. (1991) and are discussed in chapter five.

3.4.1 mechanical design

The Mark V telescope (shown in figure 3.4a) was designed on essentially the same principles as the Mark III and Mark IV instruments. It does, however, benefit from an innovative mirror configuration. Each of its parabolic dishes is made up of twelve mirrored segments which are formed from aluminium honeycomb and an 80% reflective top sheet as "pie slices" so that no light is lost between them. There are three main dishes each of surface area 9·2 m^2 in a Mark III type configuration, and a fourth of area 6 m^2 above these on the axis of symmetry, all have f = 3·4 m and reduce a point source to an effective image size of 0·34° (or 2 cm in the focal plane).

Figure 3.3 : the University of Durham Mark IV telescope at Bohena Settlement N.S.W. in March 1993.

Figure 3.4a : the University of Durham Mark V telescope at Bohena Settlement N.S.W. in March 1993.

The aluminium superstructure supporting the mirrors rests upon an alt-azimuth mount and the whole is steered in a similar fashion to the Mark III telescope.

3.4.2 the detector packages

The "extra" 6 m^2 dish is not intended to contribute to the general Mark V telescope data stream. It is hoped that by using a single wide angle PMT (a RCA 4522 tube with a 5" photocathode) at its focus to study the time structure of individual Cerenkov light pulses, some correlation may be found to exist between the strength and duration of a pulse and its rejection or otherwise, as a genuine, γ-ray generated event, by the "main" instrument.

At the foci of the two outer 9·2 m^2 dishes there are detector packages which resemble those of the Mark III telescope. Each contains a filled hexagon of seven RCA 8575 PMTs. In addition, sufficient space and cabling have been provided for a further three 2" PMTs to be inserted between the tubes which make up the alternative on-source channel when in chopping mode, so that the on-axis channel and channel 2 may both benefit from a full guard ring.

Two detector packages are available for use at the focus of the central dish; one is identical to those used in the outer dishes as described above, the other is an adaptation of the Whipple HRC described in section 2.3.2.

The "camera" (shown in figure 3.4b) comprises 19 closely packed 1" diameter PMTs which act as "pixels" each covering a solid angle on the sky of 0·3°, and an outer ring of 11 RCA 8575 PMTs which each have a field of view of ~ 1·5°. The 1" tubes are of BURLE type C83062E, having a peak response at a wavelength of 400 nm and a rise time of 2·3 ns. They were chosen for the similarity of their response to that of the RCA 8575 tubes (see figure 3.4c). In laboratory tests, when lit by an LED at a level

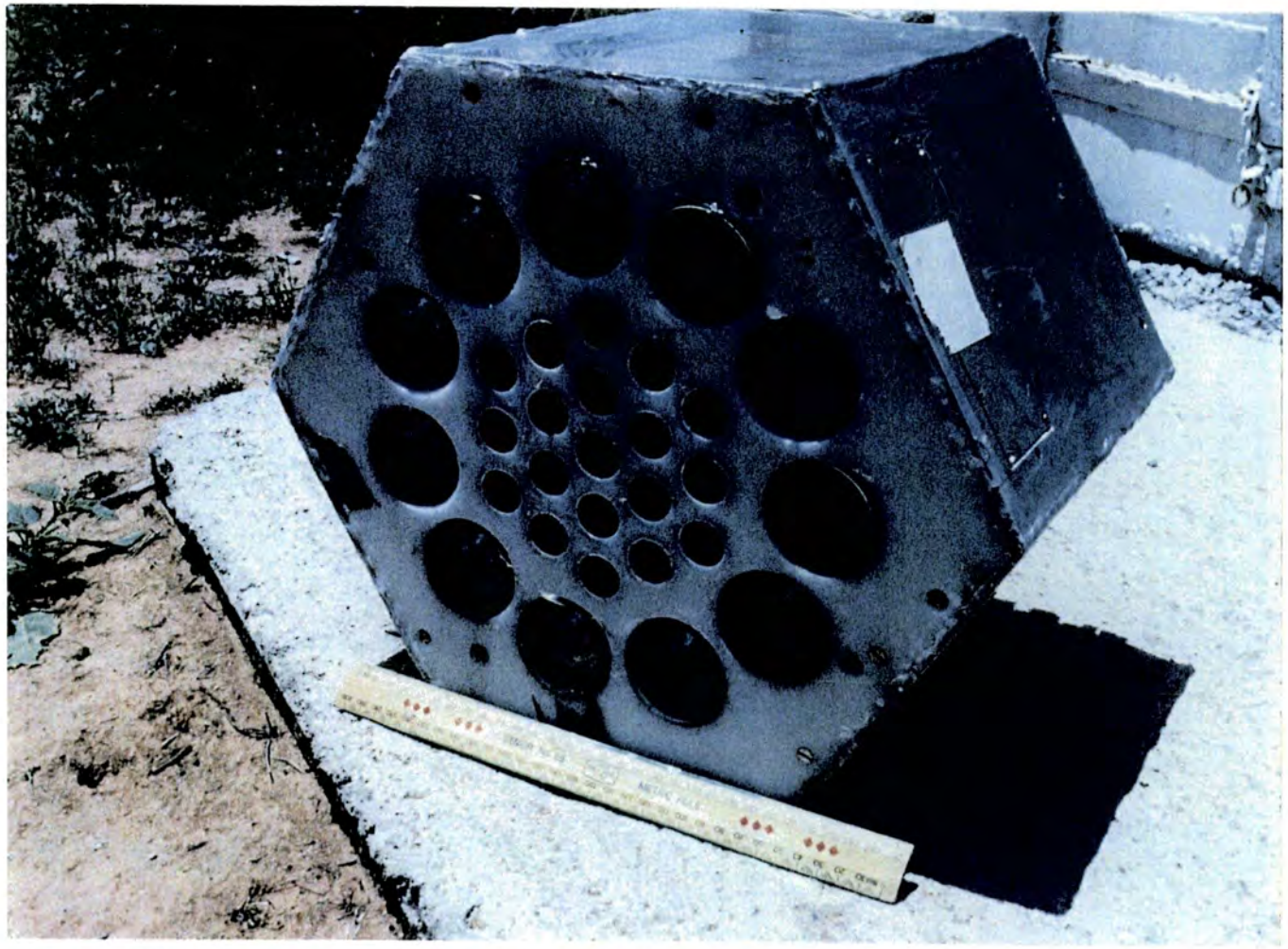

Figure 3.4b : the 30 pixel "camera" which may be placed at the focus of the central dish of the Mark V telescope. It contains nineteen 1" and eleven 2" photomultiplier tubes.

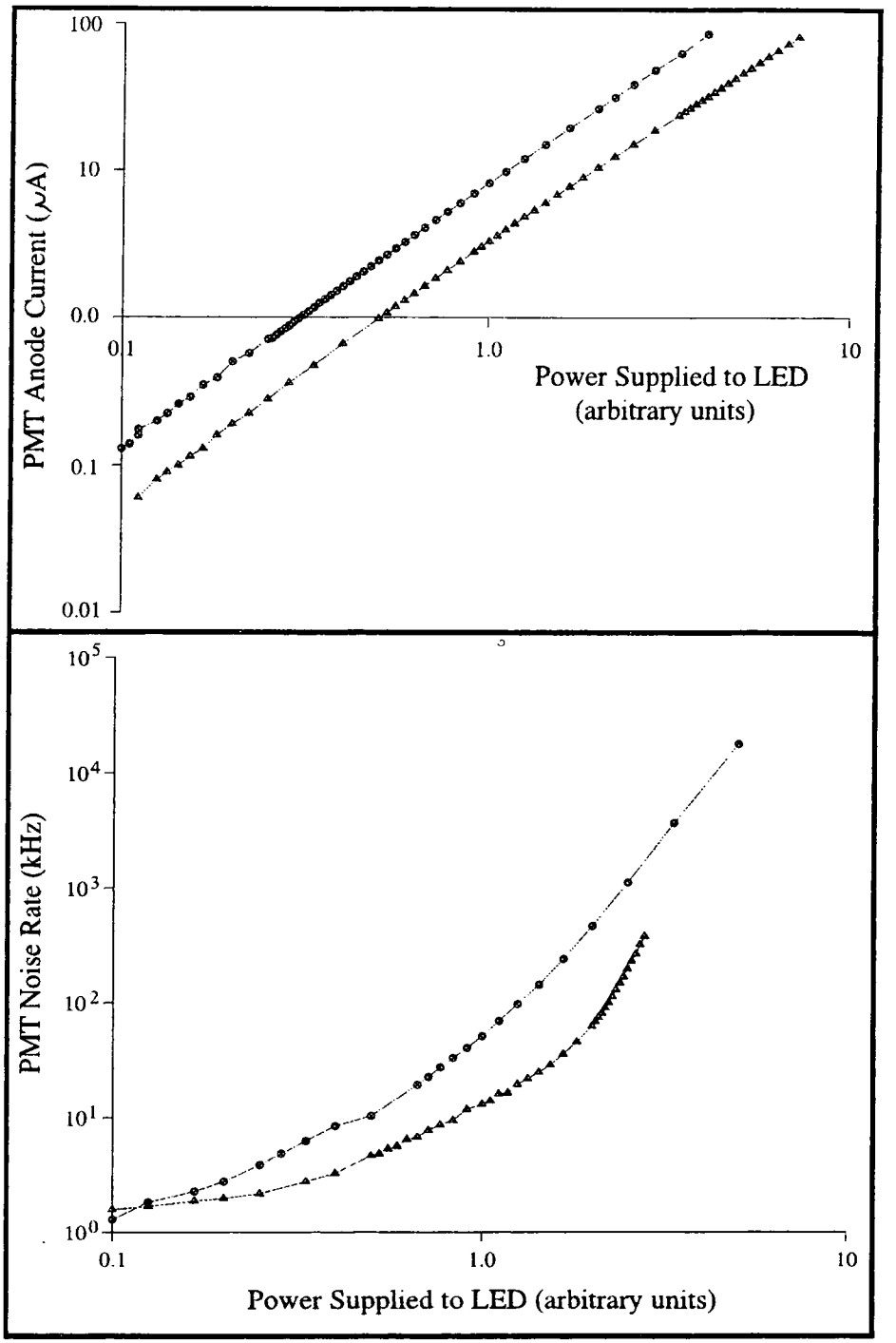

Figure 3.4c : anode current and noise rate characteristics of a RCA 8575 PMT (circles) and of a BURLE C83062E PMT (triangles) given constant supply voltages of approx. 1400 V and 1000 V respectively. The tubes were placed in a light tight container in turn and illuminated by a single LED powered through a variable resistance. The brightness of the night sky is roughly equivalent to 0.9 on the LED power scale.

comparable with the brightness of the night sky in Narrabri (as determined from the behaviour of an RCA 8575 tube), the anode current of the C83062E was found to stabilise only after a 100 minute long warm-up period, during which time it fell by 20% of its final value. After ten 8 hour exposures, the time constant was unchanged but the anode current decay was reduced to 7%. Although this did not compare favourably with the 8 minute, 2% decay curve of a "well-worn" RCA 8575 tube, it was felt that the C83062E tubes would be sufficiently stable after a few months in the field.

During these comparative tests it was found that the addition of a light guide of polished aluminium foil bent about the 1" tube to form a cone having a base of 2" in diameter more than doubled the anode current of the C83062E tube under stable illumination. In September 1992, with this result in mind, tessellating light guides were fitted to those detector packages of the Mark V telescope which contained seven 2" tubes, as shown in figure 3.4d. Thus, a large fraction of the light which would otherwise have fallen between two bare channels is now registered, and the energy threshold of the instrument has been slightly reduced.

3.4.3 signal processing

The PMT signals are electronically amplified by a factor of 10 and passed through a discriminator which is triggered by pulses of 50 mV and above. An event is recorded when a "standard" three fold coincidence occurs with the 7 tube central detector in place, or, when the outer detectors register light in co-located tubes and any combination of the central 19 tubes is lit (with or without a response from the outer guard ring) in the 30 tube camera.

The collection of housekeeping data and the logging routine are performed as for the Mark IV telescope.

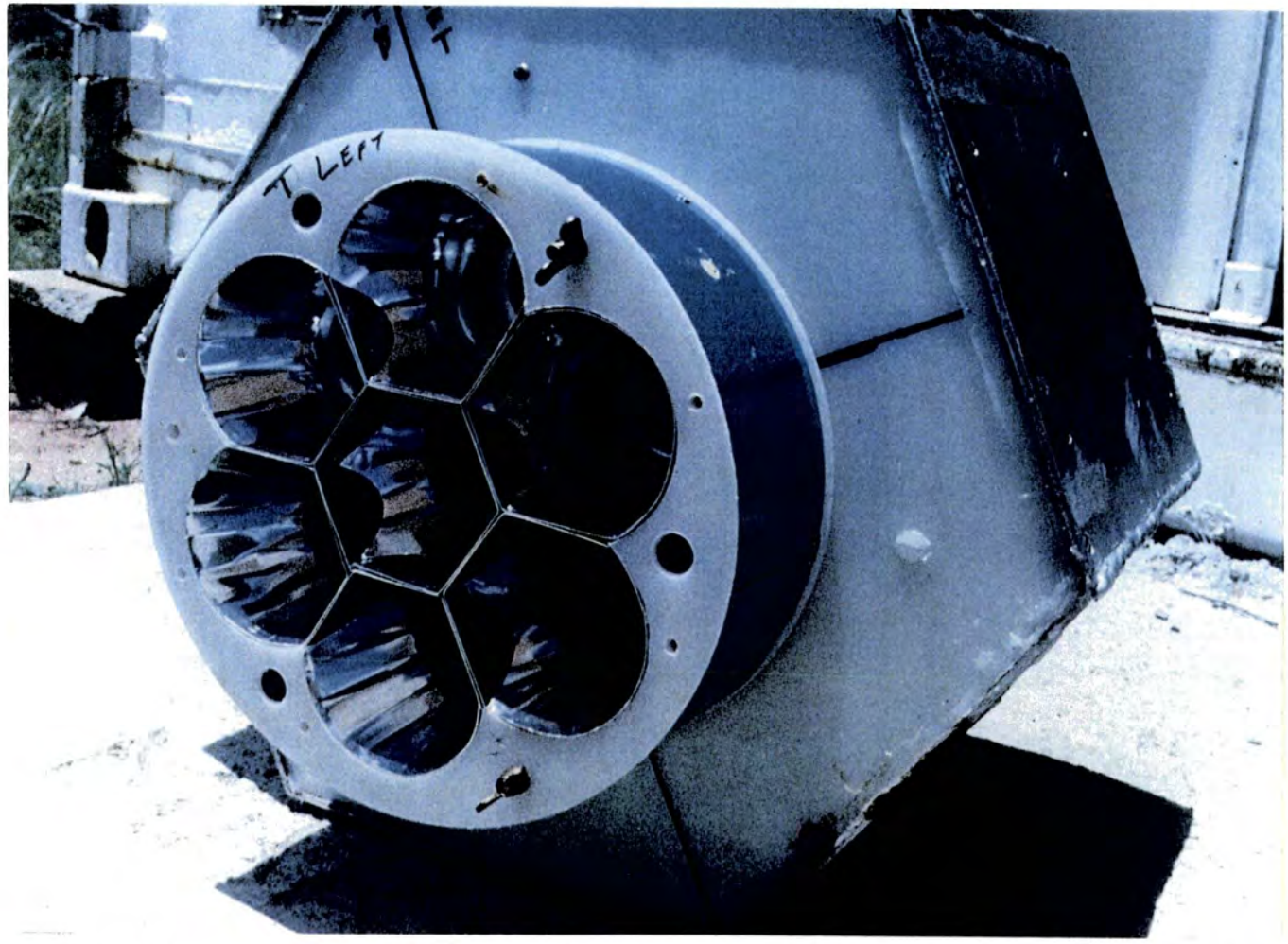

Figure 3.4d : a detector package which is placed at the focus of one of the outer dishes of the Mark V telescope. It contains seven 2" photomultiplier tubes.

3.5 Operation of a three-telescope observatory

The Mark III, Mark IV and Mark V telescopes lie within ~ 100m of each other (see figure 3.5a). Adjacent to each detector there is a control cabin which houses its signal processing and control electronics. The three telescopes operate independently; it is considered safe to alter steering instructions or the power supplied to the PMTs only from the local control room where the effects of such changes may be directly observed. However, the detectors are sufficiently well behaved to allow observers to monitor their behaviour remotely once an observing run has been set in motion.

3.5.1 remote surveillance

During "stable running" the observers retire to a cabin beside the control room of the Mark III telescope. Video signals from the telescope performance display monitors of each detector are passed across the site, along buried cables, to this room. Direct cable links also exist which allow the observers to cut the power to the detector packages and/or the drive motors of each telescope in case of emergency.

3.5.2 absolute timekeeping

A commercial GPS receiver is housed in the Observers' Cabin. Signals from Global Positioning Satellites are triangulated and decoded to give a reading of Coordinated Universal Time (UTC).

The on-site time-base is a Rubidium atomic resonance controlled oscillator and is generally referred to as "the Rubidium clock". The oscillator produces a sinusoidal signal at a frequency of 10 MHz (specified as accurate to one part in 10^{11}), which is then converted to a square wave and divided by 10 to give a 1 MHz output waveform. This 1 MHz standard is compared with the clock units in each telescope's signal processing suite,

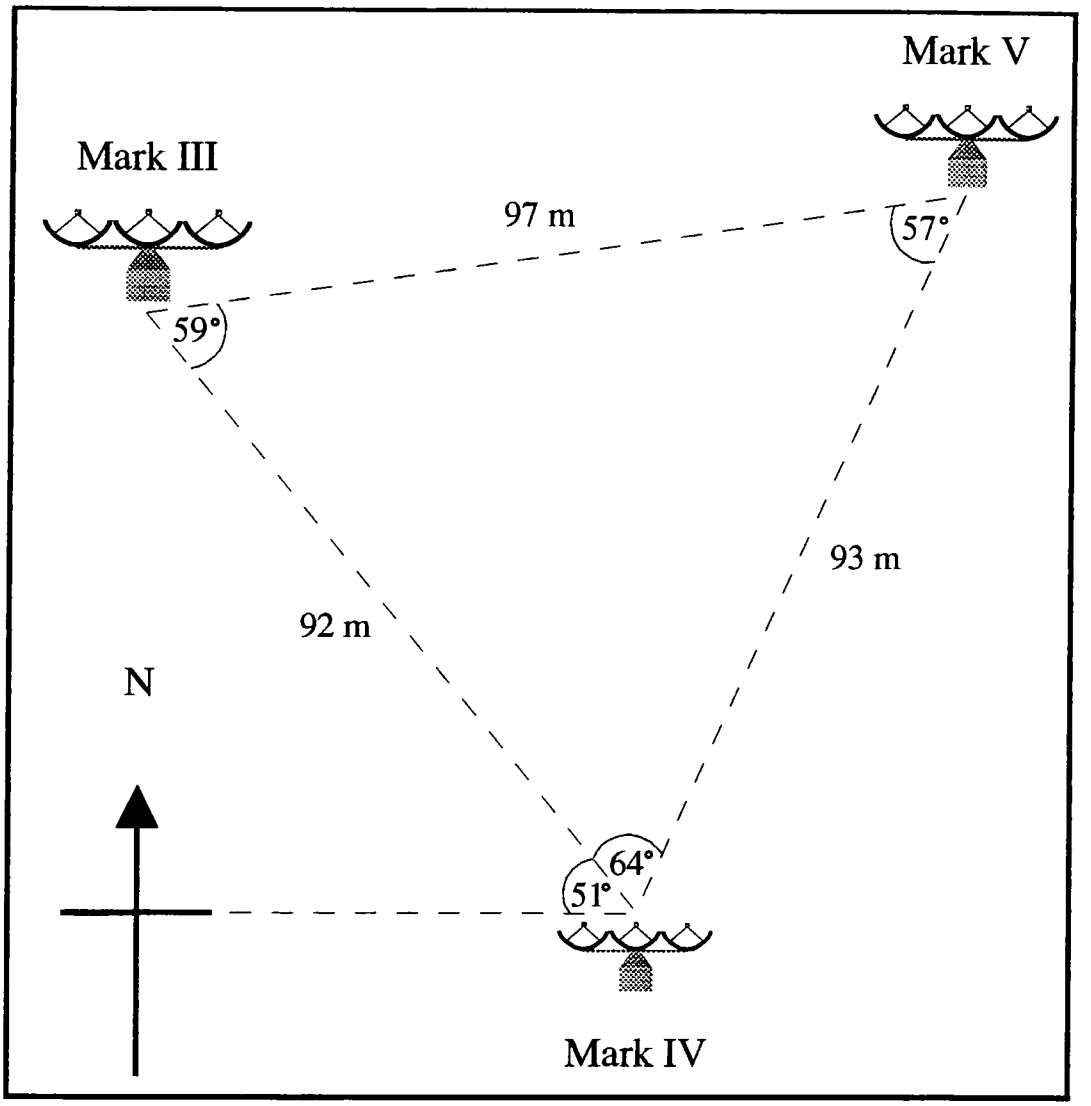

Figure 3.5a : disposition of the three telescopes at Bohena Settlement as surveyed in November 1992. Linear dimensions and bearings (relative to *geomagnetic* north) are accurate to within 3 m and 1° respectively. Telescopes are not shown to scale.

where the Cerenkov event times are recorded relative to each other to an accuracy of 1 μs (Chadwick, 1987).

The Rubidium clock was set to UTC in January 1987 using an off-air signal broadcast from Victoria by the radio station VNG. Synchronisation to a radio signal is far from ideal; the 1 MHz clock output is gated and then released when the leading edge of the tone broadcast on the minute is received, if radio reception is poor then the leading edge is ill-defined. Also, the accuracy attained from a strong signal is limited to that to which the transit time between the radio transmitter and the receiver is known. From 1987 to 1990 this was estimated from the transit delay measured to the Anglo Australian Telescope, such that knowledge of the absolute UTC at Narrabri was limited to within an error of ± 10 ms. In January 1991, a similar Rubidium clock (previously devoted to the Mark IV telescope in the Canary Islands) was taken for comparison to the time standard at the Australia National Radio Observatory. It was then returned to Narrabri and used to measure the actual radio transit time, thus reducing the absolute timing error for data collected after January 1991 to 30 μs (Brazier, 1991).

The absolute time of the telescope clock units is still set by the radio pulse method from the VNG signal (broadcast from Llandilo, New South Wales since January 1989). The GPS system (introduced in April 1992) is used to monitor the behaviour of all on-site clocks, and, in particular, the slip rate of the Rubidium clock, the interpolated value of which is being continuously refined and now stands at 0·0535 ms per day (Rayner, priv. comm.).

3.5.3 performance and environment monitoring

The information displayed in the Observers' Cabin during an observing run falls into three main categories: telescope steering, detector performance and environmental conditions.

(i) steering

The target position and the actual position of each telescope is relayed to the Observer's Cabin together with the instantaneous voltages supplied to the drive motors. A "history" display can also be accessed showing the varying displacement of the actual position from the targeted azimuth or zenith value during the course of the observation. An alarm is displayed if the telescope has not moved over a two minute period.

A high-gain closed-circuit television camera, with a field of view of 25 square degrees, is mounted below the central dish of each instrument such that its optic axis is parallel to that of the telescope. Any stars in the field of view at the start of an observation should gradually rotate about its centre as the target object is tracked across the sky. The camera images provide a means of monitoring the telescopes' steering during an observation which is independent of the guiding computer. The screen position of field stars is also a useful indication as to whether the same point is targeted and attained on each night. Several times a month, the pointing accuracy of the telescopes is assessed by allowing them to track the positions of a selection of low magnitude stars and noting the off-sets of the stellar images from the centre of each of their cameras' fields of view.

(ii) detector performance

Instantaneous values of the anode current and noise rate of every PMT are displayed for each telescope together with the three fold coincidence rate averaged over three minutes (this is updated every minute). Visual alarms are activated when anode currents tend towards a level which may damage the PMTs, when the noise rate becomes excessive (thus generating many "accidental" events) or when the three fold rate is abnormally low. The "history" of each of these commodities may be retrieved for inspection

at any stage during an observation. Of these, the three fold coincidence record (or "on-line" display) is routinely printed out at the end of each observing session and inserted in the log in which observers record their personal comments.

(iii) environmental conditions

The on-line record is a useful indicator of the presence of cloud during an observation. It is complemented by the observers' visual assessment of the cloud cover and sky clarity.

In addition to cloud cover, the formation of ice or condensation can cause a decline in the three fold coincidence rate, as these reduce the effective reflectivity of the telescope mirrors. A BBC microcomputer in the Observers' Cabin displays data from a "weather station" beside the Mark III telescope from which observers may assess the likelihood of "misting" or "icing". This weather station consists of shielded thermistors for measurement of the ambient air temperature, wet and dry bulb thermometers which reflect any change in humidity, a wind vane and an anemometer. No attempt is made to track an object if the wind speed is consistently in excess of 10 kts. If an electrical storm is seen to be approaching, observations are abandoned, and all signal processing and control electronics are isolated from external equipment.

3.5.4 burst confirmation

The possibility that a burst of events recorded by a single telescope is due to electronic noise can never be ruled out entirely. It is therefore desirable when targeting an object which may exhibit brief episodes of γ-ray emission (as evinced by transient behaviour at lower wavelengths) to track the potential source with more than one telescope. An enhancement of the Cerenkov event rate observed by two or more instruments must be due to

some extrinsic factor.

A fine example of just such a "corroborated detection" is the burst of events, of approximately one minute in duration, seen by the Mark III and the Mark IV telescopes whilst both were targeted upon the cataclysmic variable AE Aqr (Bowden et al., 1992). The rate of occurrence of on-source events (in which only the central, on-axis channel exhibits a three fold coincidence) during this observation is shown in figure 3.5b. The brief episode of enhanced activity is self evident in the count rate profiles of both instruments. The ratio of the number of on-source Cerenkov flashes (where events recorded simultaneously by both telescopes are counted as a single flash) to the total number of on-source events (obtained by simple addition of the Mark III and Mark IV count rates) remained at a level of $0{\cdot}8 \pm 0{\cdot}03$ throughout the observation whilst the target zenith angle gradually increased from 30° to 50°. In other words, 20 % of the Cerenkov flashes detected in the target direction were observed by both telescopes.

As a consequence of its smaller mirror area, the Mark IV telescope has a lower characteristic event count rate than the Mark III and Mark V instruments and is therefore the least well-suited of the three to the detection of a weak γ-ray source. For this reason it is generally run "in tandem" with one of the larger instruments as an "independent witness" to any signal which they may detect.

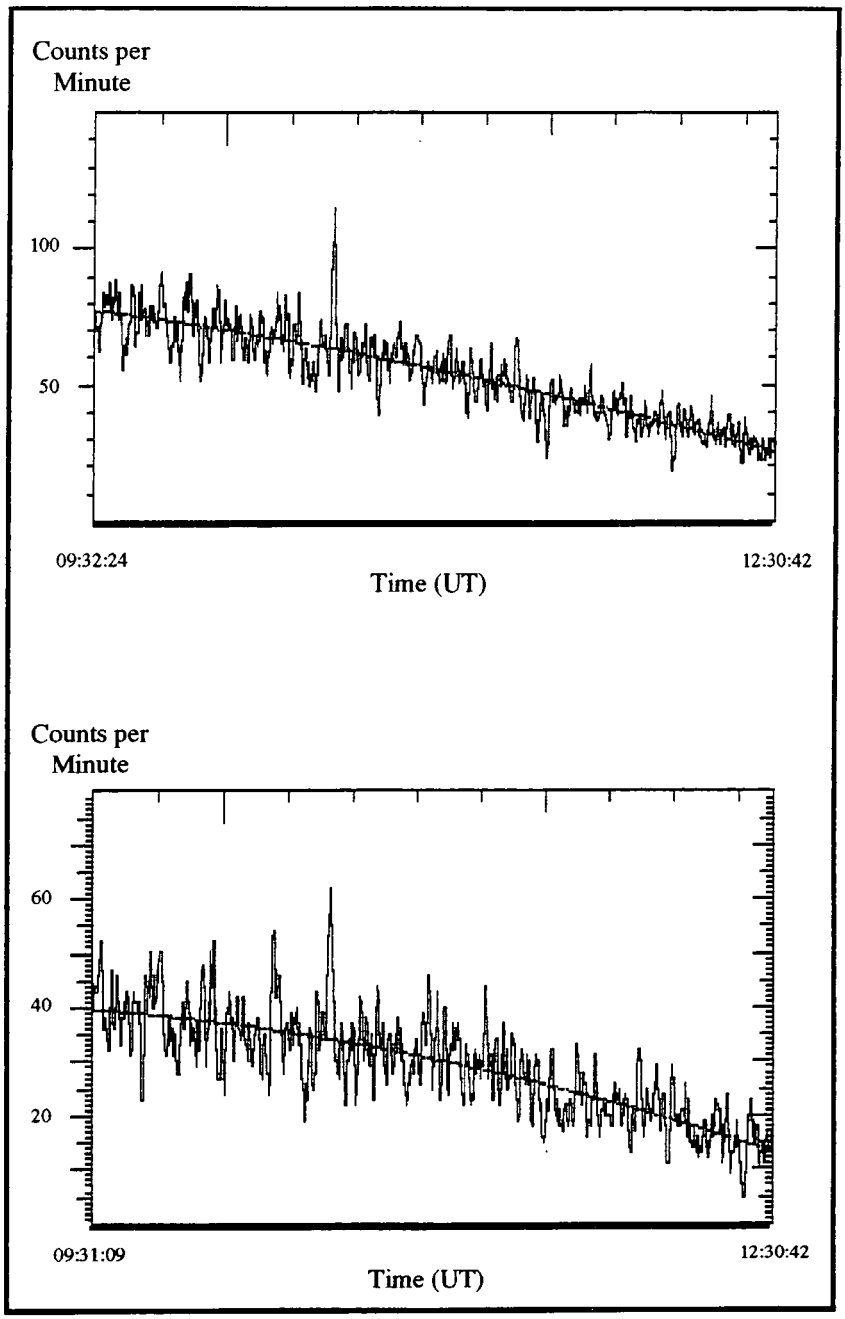

Figure 3.5b : count rate history of the Mark III telescope (top) and the Mark IV telescope (bottom) during an observation of AE Aqr taken on 13/10/1990. Only those on-axis events which did *not* include a response from any guard ring channels are shown. A minute long burst of activity is apparent in the data recorded by both instruments.

CHAPTER FOUR

Data Processing and Analysis Techniques

The routine pre-analysis processing which is applied to all data is described in this chapter, together with the data quality selection criteria and various statistical techniques which have been applied in order to obtain the results detailed in chapters six and seven.

4.1 routine data processing

At the commencement of an observing session, a "run start" file is recorded for each telescope. This file contains the date, weather information, the identity of the observers and their assessment of the sky clarity and telescope serviceability, and a record of the mapping of information to data recording channels.

A separate "source start" file is written at the beginning of each observation, in which is recorded the time and the name and co-ordinates of the target object. Also included are the position of the observing site and the steering offsets which are required to compensate for the non-verticality of the telescope axis.

During an observation, the following information is recorded for each event:

a) the time (to 1 μs resolution)

b) the fire pattern (the contents of the coincidence register)

c) the time integrated charge for each triggered channel

d) the anode currents from the photomultipliers which make up the central channel and channel 2

e) the telescope position and the motor drives' voltages.

At the end of every minute, a meta-data block is recorded containing

weather information, the instantaneous anode currents of all the PMTs, and the number of single-fold responses registered in the preceding second by each scaler counter. The resulting "data file" varies in size between one and five megabytes, according to the length of an observation and the sky clarity. During a typical three week observing period roughly thirty such data files are accumulated per telescope.

Data from the Mark III telescope are written directly on to 68 Mbyte 3M DC600 tape cartridges which are returned to Durham for processing. Data from the Mark IV and Mark V telescopes are recorded on Winchester hard discs during an observation, and are then transferred to 44 Mbyte removable hard discs for transportation. On arrival in Durham, all data are subject to the routine shown in figure 4.1a.

4.1.1 conversion to a format suitable for analysis

The run start, source start and data files are read from tape or disc by an Acorn Archimedes computer. The unformatted data files are sifted in such a way that the part of each event record containing the time, fire pattern and pulse integrals for an event is written to one Fortran data file, whilst the meta-data is written to another "housekeeping" file together with the run start and source start information. The housekeeping data is not referred to, unless an improbable result arises during analysis for which the telescope operating conditions should be examined.

4.1.2 routine corrections to event times

A search for periodicity requires a precise knowledge of the time delay between events. This time signature may be compared with that of the pulsed emission detected by other groups. The recorded Cerenkov flash arrival times must be corrected for any deviation of the local clock from

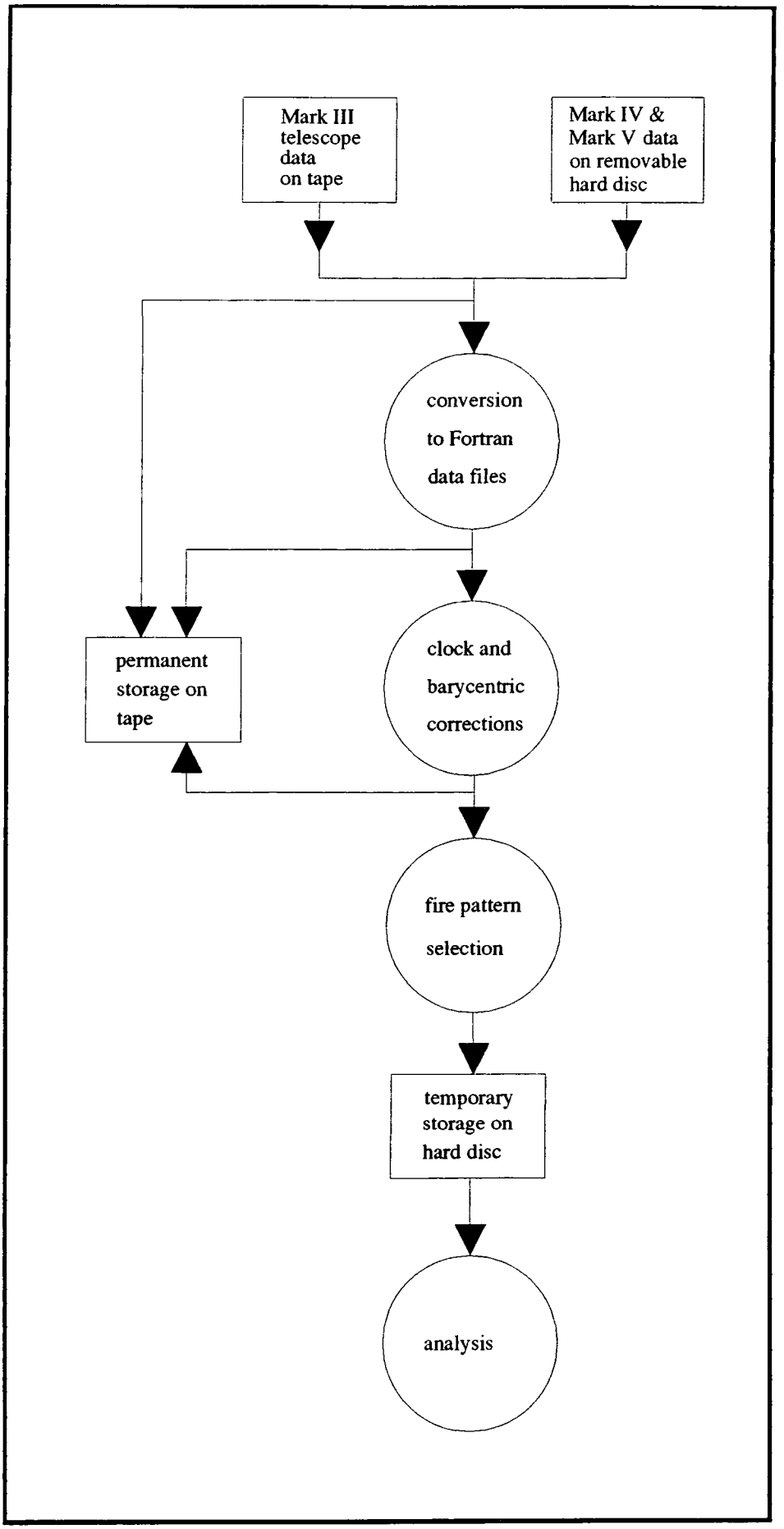

Fig. 4.1a : the pre-analysis data processing routine.

Universal Time and for the Doppler effect due to motion of the telescope relative to the local standard of rest.

(i) clock corrections

Timekeeping at the Bohena Settlement site was described in chapter three. In Durham, event times are corrected individually for the divergence of the Rubidium clock maintained on site from absolute U.T. as registered by the GPS receiver. The appropriate number of leap seconds are added, together with an offset calculated from the continuously monitored Rubidium oscillator "slip rate" (currently - 0·0531 ms per day) and the 2·69 ms delay between the Rubidium clock time and the VNG radio time standard measured in January 1991.

(ii) reduction to the solar system barycentre

A Doppler shift in the frequency of a pulsed γ-ray signal occurs due to the combined motion of the observer about the Earth's axis, the Earth-Moon barycentre and the solar system barycentre. Recorded event times are corrected for the delayed arrival of what is effectively a plane wave, given a source at infinity, due to the offset position of the observer from the local standard of rest (the solar system barycentre). Clearly, from figure 4.1b, this delay is given by:

$$\Delta t = \frac{(\underline{r}_1 + \underline{r}_2 + \underline{r}_3) \cdot \hat{\underline{s}}}{c}$$

where c is the speed of light, $\hat{\underline{s}}$ is a unit vector in the source direction and $\underline{r}_1$, $\underline{r}_2$ and $\underline{r}_3$ lie between the solar system barycentre and the observer, the observer and the Earth's axis and between the Earth's axis and the Earth - Moon barycentre respectively.

Relativistic time dilation is also taken into account, although significant only at millisecond pulsar frequencies. The time between the

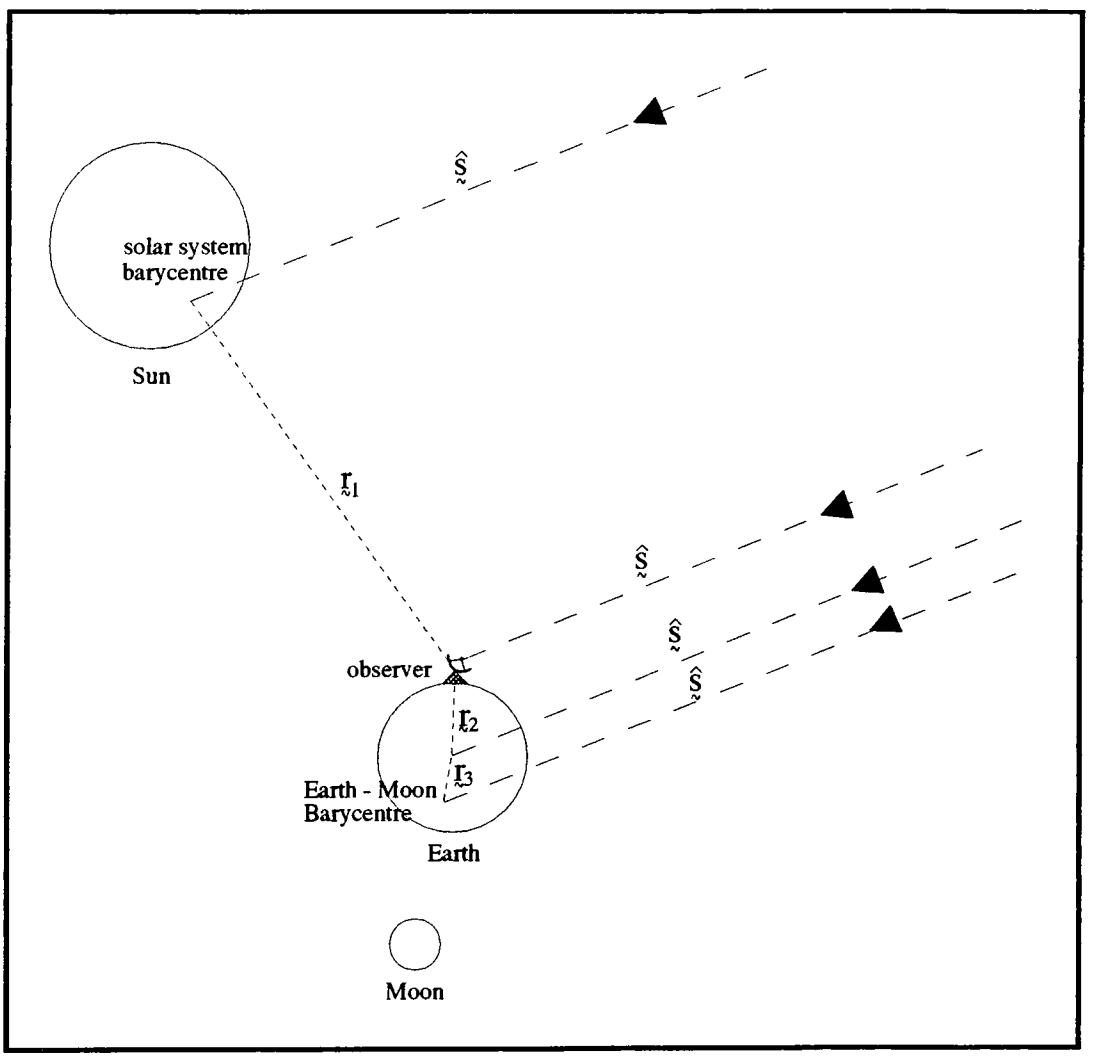

Fig. 4.1b : system geometry for time of flight corrections.

arrival of consecutive γ-rays at the Earth is slightly longer than it would be at a point outside the gravitational potential well of the Sun. This protraction increases towards perihelion.

The magnitudes of these time variations are summarised below (from Mannings, 1990). The relative positions of the Earth, Moon and solar system barycentre which are required in performing these corrections are taken from the JPL DE200 Solar System Ephemeris (Standish, 1982).

source of delay	$\underline{r}_1$	$\underline{r}_2$	$\underline{r}_3$	time dilation
maximum time delay	500 s	40 ms	32 ms	3 ms
recurrence period	1 year	1 day	1 month	1 year

4.1.3 fire pattern selection

Time-corrected files are written which contain all recorded events. To reduce handling time, events which include a response from the central channel are extracted to create smaller files for analysis; these are of 1 Mbyte to 2 Mbytes in length. It is assumed that the γ-ray light pool is centred approximately on the target direction and will not trigger only guard ring photomultiplier tubes. Before this fire pattern "filtering" an average is taken, over all events, of the time-integrated charge from each channel. A pedestal is then subtracted from the integrated charge values recorded for each event. Data taken from a channel which was consistently less responsive than the others will receive a correspondingly smaller adjustment at this stage. This "pedestal correction" is necessary if later analysis requires event selection based not only upon the fire pattern, but also upon the intensity of the Cerenkov flash, as described in chapter five. Filtered, pedestal-corrected events are written to a final "analysis file".

4.1.4 data archives

Analysis files are transferred to one of several 60 Mbyte hard discs for temporary storage. When due for analysis they are copied to 4 Mbyte Acorn Cambridge Workstations running Fortran 77. Permanent backup copies of the data are recorded onto 68 Mbyte 3M DC600 tape at various stages during processing. These include the raw "run start","source start" and data files, the housekeeping and uncorrected data files and the time corrected files containing all events.

4.2 quality control

A graphical record is kept of the windspeed, humidity and ambient temperature during an observation, and also of the temperature of the telescope mirrors, the photomultiplier package and the signal processing electronics. Observers note any anomalies in the detector response or telescope pointing. Steering accuracy is checked every few days by targeting a selection of bright stars and noting their position in the field of view of a co-axially mounted camera. An observation is curtailed if the wind is such that the telescopes may be blown off target. The windspeed at which this occurs varies between 12 and 16 kts and is dependent upon the "sail area" presented and therefore upon the telescope orientation. The telescopes are anchored if the average wind speed is 10 kts or above, to allow for sudden gusts. At Bohena Settlement loss of observing time due to wind is very rare. High winds on La Palma were a significant factor in the decision to relocate the Mk IV telescope.

The count rate may fall simultaneously in all channels due to cloud cover, misting of the telescope mirrors or the subsequent freezing of this condensation.

If the temperature and humidity are such that misting is imminent, then the mirrors are sprayed with detergent before steering to the source

position in order to prevent the formation of light scattering water droplets. During the winter months it is not uncommon for the resulting detergent and water film to freeze. When this occurs the mirrors are sprayed with alcohol. The frost crystals dissolve to form clear ice, but generally reform within half an hour, at which point the observing session is abandoned.

Unless a significant breeze is blowing, the difference between the mirror temperature and the ambient temperature is a good indicator of sky clarity. The presence of cloud is reflected in the fluctuations of the count rate profile. In the event of cloud cover, any attempt to detect unpulsed emission by the comparison of on-source and off-source count rates must be abandoned. The passage of a series of cloud banks across the field of view can introduce periodicities of the order of a few minutes, the higher harmonics of which may produce spurious results if the data is searched for a long-period source. Millisecond pulsars are therefore the preferred target sources if cloud is expected. An example of periodic variation in count rate due to the presence of high cloud is shown in figure 4.2a.

Lightning is quite frequent throughout the summer months. At the approach of an electric storm, observations are abandoned and the control electronics are isolated from each telescope. Distant lightning, which poses no immediate threat to equipment, will prevent the observation of non-periodic sources requiring a constant sky background illumination. Lightning-filled data display a great deal of millisecond periodicity because the atmospheric discharge occurs as a relaxation oscillation on this timescale (Orford, priv. comm.). Since lightning gives rise to tens or hundreds of events in less than a second, whilst the Cerenkov event rate is about one per second, contaminated data is easily recognisable from count rate profiles such as that shown in Figure 4.2b. In the past, data recorded on millisecond pulsars which were found to contain lightning "events" were

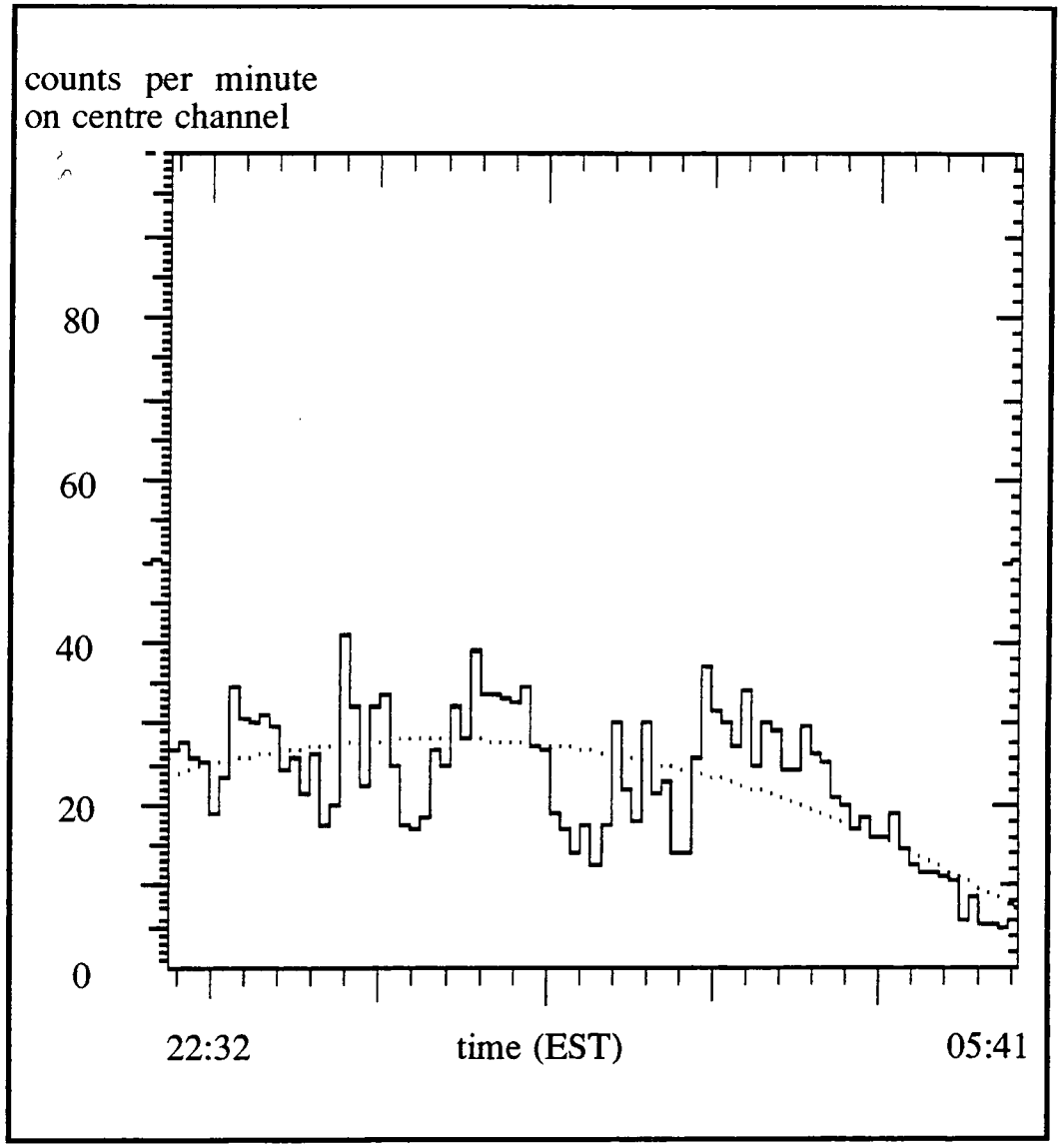

Fig. 4.2a : the on-axis count rate profile, averaged over 300 s bins, of an observation of Sgr X-7 made on 17/06/1991. The object culminated at a zenith angle of 7° at 00:50 EST. The periodic "furrows" are due to the passage of cloud across the field of view.

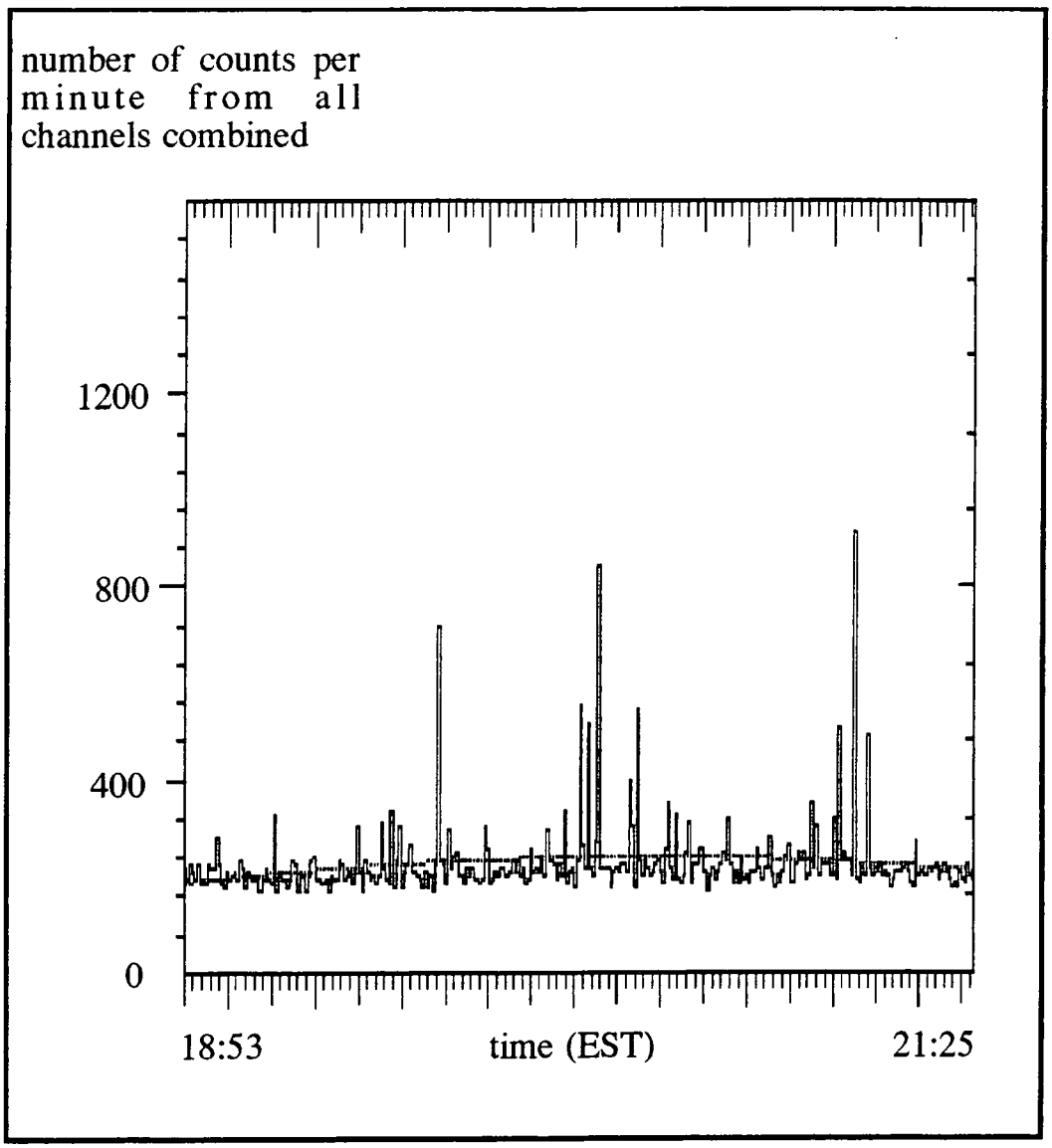

Fig. 4.2b : the all channel count rate profile of an observation of Sgr X-7 made on 23/08/1992. The average count rate is shown for 30 s bins. The spikes are due to lightning episodes which are significant on this time scale.

either rejected entirely or truncated. Today, data need not be "lost" in this manner as lightning features may, with care, be excluded during the final analysis stage, by using the techniques described in the following chapter.

Generally, lightning causes count rate "bursts" in multiple channels. Bursts in the on-source channel alone, which could be due to source activity, are much rarer. Sudden fluctuations in which a scaler counter completely overflows are usually attributed to electronic pick-up. A corresponding burst of dead-time events appears in the raw data file, which will be abnormally large in comparison to the analysis file produced after fire-pattern selection. These events are a clear indication of electronic noise, since the time separation of Cerenkov flashes is much greater than the system dead time of 0.6 ms (Carraminana, 1991).

If a count rate excess is observed which is thought to be characteristic of a genuine burst of γ-rays, then the corresponding housekeeping file is retrieved and the behaviour of the photomultiplier anode currents and single-fold count rates is studied. One such episode was the AE Aquarii burst of 13th October 1990, detected by both the Mk III and Mk IV telescopes, the count rate profiles of which are illustrated in chapter three. Figures 4.2c and 4.2d demonstrate the stability of the anode currents and single-fold noise rate of the on-source and selected off-source channels during this observation.

4.3 analysis techniques

The γ-ray flux from a single astronomical source amounts to only a tiny fraction of the cosmic ray background. Thus, the first task of a VHE γ-ray astronomer is not to estimate a signal strength, but to show that such a signal exists. The following simple hypotheses are formulated:

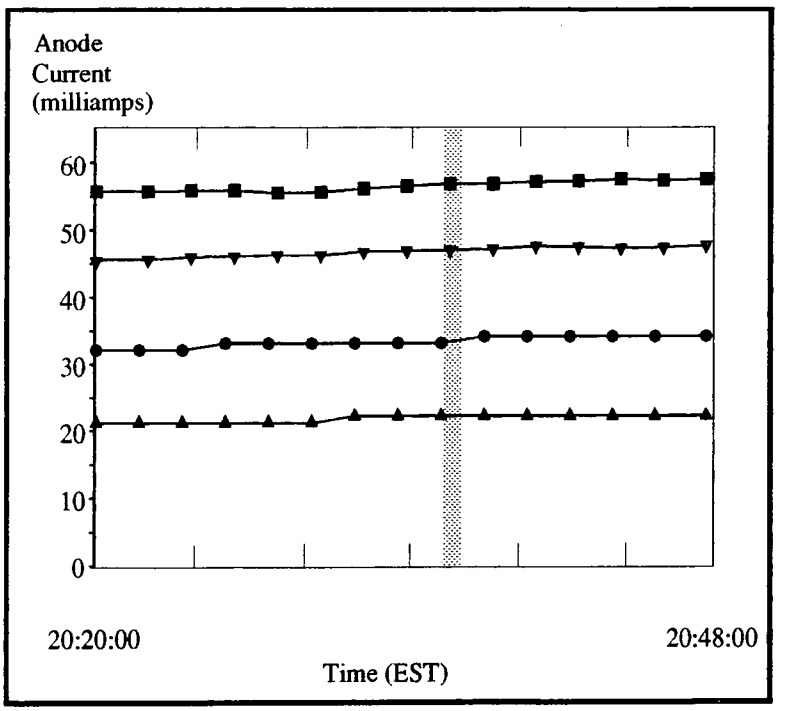

Fig. 4.2c : anode current history.

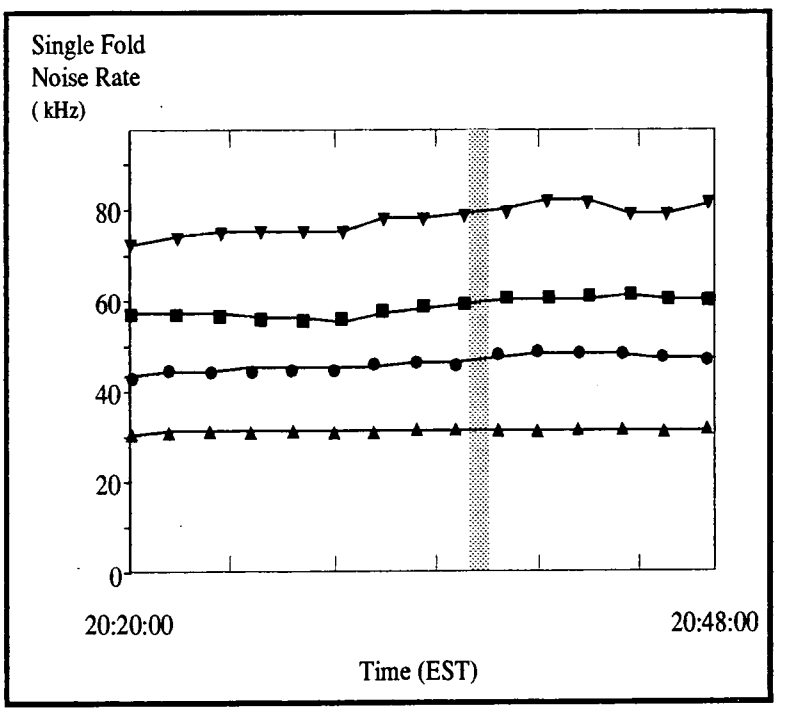

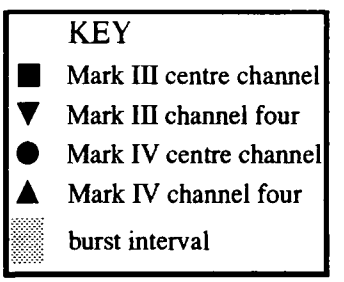

Fig. 4.2d : single fold noise rate history.

On the 13th October 1990, a count rate "burst" was observed simultaneously by the Mark III and Mark IV telescopes. The anode currents and single fold noise rates during the active period are shown here for photomultiplier tubes facing the central dish of each instrument. The gain of the centre channel is stabilised by an LED as described in chapter three, whilst that of channel four is not. The behaviour of the latter therefore gives the best indication of sky clarity.

null hypothesis, H_0: the population sampled consists entirely of the isotropic cosmic ray background

alternative hypothesis, H_1: the population sampled contains an anisotropic γ-ray signal as well as background cosmic rays

A test statistic is used to calculate the probability level at which H_0 may be rejected in favour of H_1. The statistic is chosen which should be the most powerful test, i.e. that least likely to result in wrongful acceptance of H_0, given the nature of the γ-ray emission predicted for a particular target source.

A summary of the data analysis strategy is given in figure 4.3a.

4.3.1 a test for unpulsed emission

The rejection of H_0 is simplified by the presence of a time signature in the data characteristic of the source under observation. If an object is expected to emit a particularly strong γ-ray flux but neither theory nor observations at different wavelengths lead to a reasonable expectation of periodicity at TeV energies, then a valid detection requires there to be a significant excess in the number of Cerenkov events from the source direction when compared to one slightly displaced from it. A data set containing on-source and off-source exposures may be obtained by allowing the target object to pass through the field of view of a stationary detector and comparing the flux whilst it was present to that before and after its passage. An alternative method used by the Whipple group is to track an object for 28 minutes then return to the starting position and track an "empty" field through the same set of alt-azimuth co-ordinates. This technique requires implicit faith in the ability to assess the stability of the electronics and sky conditions over an hour of

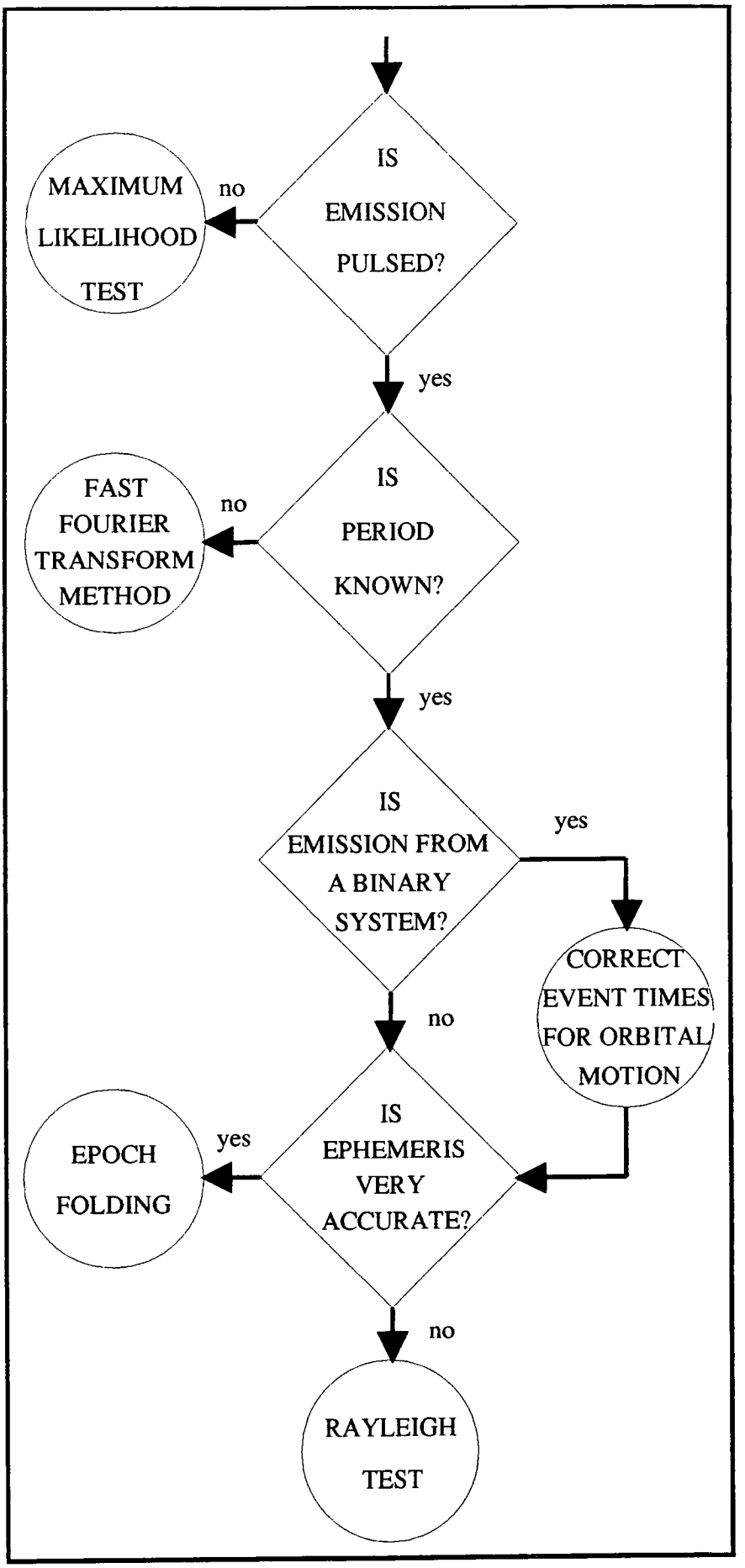

Fig. 4.3a : the data analysis strategy.

observation. The mechanics of the chopping method of observation favoured by the Durham group are described in chapter three.

Macrae (1985) showed that event count rate of a tracking Cerenkov telescope was proportional to $\cos^n(\theta)$ where θ is the zenith angle. Brazier et al. (1989) gave $n \approx 2.3$. Thus, if a chopped observation began near the horizon with a two minute off-source segment, and ended with an on-source segment at the culmination of the source, an excess number of events would be expected in the on-source channel. In fact, observations are generally centred upon the time of culmination, at which the count rate is a maximum, so this effect is less extreme. Before analysis, chopped data files are truncated such that they begin and end in the middle of a centre channel on-source segment and the exposure times on-source and off-source are equivalent.

The null hypothesis that no signal is present is tested by the maximum likelihood method (Gibson et al., 1982a). Given n_{on} observed on-source counts and n_{off} off-source counts, the relative likelihood of the value of n_{on} being a statistical fluctuation from a pure background distribution as opposed to background events plus s events contributed by the targeted source is given by:

$$\lambda = \frac{\max L(n_{on} | S=0)}{\max L(n_{on} | S=s)}$$

where λ is the maximum likelihood ratio.

If in equal time intervals, n_{on} on-source counts and n_{off} off-source counts are collected and the number of events expected from a purely background distribution is B whilst the number of events due to the γ-ray source is S, then assuming that the events are sampled from a Poisson distribution, the probability of obtaining n_{on} events given zero source strength is given by:

$$Pr_1 = Pr(n_{on}|S=0,B) = \frac{B^{n_{on}} \exp(-B)}{n_{on}!}$$

similarly,

$$Pr_2 = Pr(n_{on}|S=s,B) = \frac{(B+S)^{n_{on}} \exp(-(B+S))}{n_{on}!}$$

and

$$Pr_3 = Pr(n_{off}|S=0,B) = Pr(n_{off}|S=s,B) = \frac{B^{n_{off}} \exp(-B)}{n_{off}!}$$

Then

$$Pr(S=0) = Pr_1 Pr_3 = \frac{B^{(n_{on}+n_{off})} \exp(-2B)}{n_{on}!n_{off}!}$$

and

$$Pr(S=s) = Pr_2 Pr_3 = \frac{(B+S)^{n_{on}} B^{n_{off}} \exp(-2(B+S))}{n_{on}!n_{off}!}$$

In order to find the maximum likelihood value of B given no source contribution, the first differential of $Pr(S=0)$ with respect to B is set to zero. This gives $B = (n_{on}+n_{off})/2$. By the same method, if a source is present, $B = n_{on}-s$. By substitution of the appropriate expression for B into those for $Pr(S=0)$ and $Pr(S=s)$, $\max L(n_{on}|S=0)$ and $\max L(n_{on}|S=s)$ are obtained, giving (for s tending to zero):

$$\lambda = \left\{ \frac{n_{on}+n_{off}}{2n_{on}} \right\}^{n_{on}} \left\{ \frac{n_{on}+n_{off}}{2n_{off}} \right\}^{n_{off}} \qquad \text{eqn. 4.3a}$$

If the calculated λ is less than a pre-specified confidence level, then H_0 is rejected in favour of H_1. If this is the case then $s = n_{on}-B$ is the correct maximum likelihood estimate of s, where $B = n_{off}$. The standard error in s may be found by calculating the value of s which would result in the rejection of H_0 at the 68% confidence level.

This "counting heads" method was used to estimate the γ-ray flux from the globular cluster 47 Tucanae in chapter seven.

4.3.2 searching for unknown periodicities

As figure 4.2a graphically demonstrates, brief fluctuations in the event count rate which exceed $\sqrt{B}$ (where B is the expected background rate in events per minute) are not uncommon. It is not inconceivable that a downward fluctuation in the background count rate could coincide with an increase in the fraction of pulsed events. Since the stable weather conditions required to pursue chopped observations occur infrequently, those objects for which a pulse period has not been accurately measured at any wavelength, but which could theoretically be a source of pulsed γ-rays, may be observed in tracking mode. The data is then scanned for signs of a non-uniform distribution of event arrival times, using the fast Fourier transform (FFT) method common to x-ray astronomy. This technique was tailored for use with TeV γ-ray data and described in detail by Carraminana (1991).

Fourier's statement that a function x(t) which, for all values of t, is equivalent to x(t+P) where P is a constant may be described by:

$$x(t) = \sum_k J_k \exp(2\pi i \cdot kt/P)$$

is well known.

This result may be used to examine a series of Cerenkov event times for signs of periodicity, since it holds true in the region (0;T) where T may be the length of an observation. The Fourier series represents an

infinite set of discrete periods, which conform to P=T/k where k is an integer. The difference between successive periods is known as the Fourier interval (F.I.):

$$F.I. = T/k - T/(k+1)$$

$$= \frac{P^2/T}{1 + P/T}$$

This expression may be expanded to a Taylor series. However, for this experiment, P/T is generally small and the approximation $F.I. = P^2/T$ is sufficient. The Fourier coefficient, J_k, is a measure of the strength of the function of period P. It is given by:

$$J_k = 1/n_e \sum_{j=0}^{n_e-1} x(t) \exp(-2\pi i . k t_j / T)$$

where n_e is the number of events forming the time series $\{t_j\}$ (Van der Klis, 1989). A Fortran program was implemented by Carraminana (1991), designed for the 4 Mbyte Acorn Cambridge Workstations used by the Durham group, which could be used to calculate J_k for a wide range of trial frequencies ($\nu_k = 1/P_k$; $\{\nu_k\}$ are known as the Nyquist frequencies). It is possible that periodicity which falls between adjacent Nyquist frequencies may be overlooked. This may be compensated for by also considering J_k at $(k + \delta k)$, where the choice of increments between k and k+1 is limited by the available computing power. Carraminana found that the use of three trials per F.I. was the best compromise between sensitivity and computing time.

Clearly, the number of computations required increases with the chosen trial frequency range and the length of a data file. Analysis of a complete observation would require an excessive amount of disc space, so data files are generally split up into ten minute sections which are analysed

individually. This is hardly practicable for a whole four hour observation, so sections are extracted for analysis which encompass a period of above average on-source activity according to the count rate profile.

The number of trials which this form of analysis entails (of the order of 10^6) is such that significance cannot be claimed for a periodic effect unless it recurs in more than one observation. If the magnitude of an effect is particularly compelling, then a narrow search range may be presented to a data set of several whole observations using one of the trial period specific tests described in the following section. The greatest obstacle to this analysis procedure is the possibility that orbital motion of the emitting region will impose a Doppler shift upon any pulse period. Some allowance must be made for this frequency shift when comparing marginally significant FFT "sightings". Ideally, if the orbital motion of the potential source is well documented, then the orbital phase at which the Doppler shift is a minimum may be targeted. The effects of orbital motion are discussed further in section 4.3.3. Examples of analysis by the FFT method may be found in chapter six. It was also crucial to the study of the x-ray binary 4U1822-37 described in section 7.3.

4.3.3 tests for uniformity of phase

If an ephemeris exists which may be assumed to apply to emission at TeV energies, then a test is chosen which will make the most efficient use of this information. If the ephemeris is old or not particularly accurate, or if there is some doubt as to whether the pulse period will exactly coincide with prediction due to an offset between the sites of emission at the reference wavelength and that of γ-ray production, then the chosen test must be sensitive to a few independent periods to either side of that expected. Data above soft x-ray wavelengths are too sparse (i.e. there are too few photons) for ephemerides to be produced with an acceptable degree of accuracy. Generally, radio or x-ray pulse periods are referred to since

their emission mechanisms are thought to be related to γ-ray production.

The events in a data file are each assigned a phase (between 0 and 1) appropriate to the trial period, P. If the first event occurs at time t_0, then the phase of a subsequent event which arrived at time t_j is given by:

$$\varphi_j = \varphi(t_0) + (t_j - t_0)/P$$

As the first and sometimes the second time derivative of the period is generally significant when comparing data collected over several months, these are included by considering the first few terms in the Taylor expansion:

$$\varphi_j = \varphi(t_0) + (t_j - t_0)\left[\frac{1}{P}\right] - \frac{(t_j - t_0)^2}{2\,!}\left[\frac{\dot{P}}{P^2}\right] + \frac{(t_j - t_0)^3}{3\,!}\left[\frac{2\dot{P}^2}{P^3} - \frac{\ddot{P}}{P^2}\right] + \cdots \quad \text{eqn. 4.3b}$$

Unless the precision of the measurements and the accuracy of the ephemeris are such that the absolute phase of the first event may be calculated, $\varphi(t_0)$ is set equal to zero. It is then not possible to test the goodness of fit of the distribution of Cerenkov arrival times to the shape of a known light curve. However, if the event phases are not random relative to each other then the presence of a γ-ray signal may be inferred. The null hypothesis under test becomes:

H_0 = the event arrival times are randomly distributed in phase

Various "goodness of fit" tests of H_0 have been applied to TeV data. The power of these statistics is dependent upon the shape of the actual γ-ray light curve. The validity of results obtained in this fashion is often called into question because of the difficulty in estimating the number of degrees of freedom which were used in choosing the test statistic.

(i) the Rayleigh test

Having assigned each a phase φ, the Cerenkov events may be represented as a set of vectors, at an angle θ ($= 2\pi\varphi$) to a common reference frame. As no information is considered other than the time of arrival, each event has an equal weighting in the analysis process and therefore all vectors are of unit length. A test for uniformity on a circle may now be applied. Assuming a von Mises distribution, of peak concentration κ symmetric about a direction μ, the "events" are described by the density function:

$$f(\theta) = (2\pi I_0(\kappa))^{-1} \exp(\kappa\cos(\theta-\mu)) \qquad \text{eqn. 4.3c}$$

where I_0 is a normalising parameter (Mardia, 1972). This expression may be reduced, as in section 4.3.1, to give a maximum likelihood ratio:

$$\lambda = \{I_0(\kappa)\}^{n_e} \exp(-n_e \kappa R)$$

where n_e is the number of events. As the maximum likelihood estimate of μ is the sample mean, R is the resultant vector obtained by addition and normalisation over all events from i=1 to n_e:

$$(R)^2 = (n_e^{-1}\Sigma\cos\theta_i)^2 + (n_e^{-1}\Sigma\sin\theta_i)^2 \qquad \text{eqn. 4.3d}$$

When R is small, as is expected given the small signal to noise ratio of TeV γ-ray data, the maximum likelihood value of κ, κ is approximately equal to R. For $n_e > 100$, the power of the test, referred to as the Rayleigh probability, is then given by:

$$\Pr(nR^2 \geq K) = \exp(-K)$$

where $\Pr(nR^2 = K)$ is the chosen confidence level for rejection of H_0. As R is a function of $\sin\theta_i$ and $\cos\theta_i$, which are uncorrelated and both of which have zero mean, nR^2 is distributed as χ^2 with two degrees of freedom (Mardia, 1972).

An analytic description of the probability density function of a noise current was formulated by Rice (1944) in a review of "Mathematical Analysis of Random Noise". His work leads to the following expression for the fractional pulsed signal strength in terms of **R** (de Jager, 1987).

$$S = 2\left[\frac{nR^2-1}{n-1}\right]^{1/2} \pm \left[\frac{2}{n}\right]^{1/2}$$

Clearly, for large n, $S \approx 2R$.

The Rayleigh statistic was originally developed to describe the distribution of amplitudes (J_k) of the Fourier components of noise spectra. Indeed, the results of FFT analysis are generally given in terms of the equivalent Rayleigh probability. The application of the Rayleigh test to TeV data was first suggested by Gibson et al. (1982) and it has since become a standard tool. It is a test for power at a single harmonic. It is not a suitable test for a multimodal distribution, since the contributions of opposing vector "bundles" will cancel. If results at other wavelengths suggest that a single cycle contains two peaks, a pulse and an interpulse, diametrically opposed in phase, the γ-ray data may be presented with a test period of P/2. This course is practicable as the Rayleigh test is, as is apparent from eqn. 4.3b, sensitive to all but the most narrow light curves.

(ii) the Z^2_m test

The Z^2_m test is an extension of the Rayleigh test, which allows the simultaneous summation of the powers of m harmonics of the fundamental frequency. The Z^2_m statistic is a measure of the integrated sum of the squares of the difference between the uniform density value of $f(\theta)$ and the best estimate $F_m(\theta)$. Expansion of equation 4.3c, assuming small κ, shows that under H_0 the expected value of $f(\theta)$ is $1/2\pi$. $F_m(\theta)$ is the summation, over the harmonics given by l = 1 to m, of the expression obtained by the

substitution of 1Θ for θ in equation 4.3b and replacement of κ by the maximum likelihood value R_1 obtained through a similar substitution in equation 4.3d. Thus:

$$Z^2_m = 2\pi n_e \int_0^{2\pi} (F_m(\theta)-1/2\pi)^2 \, d\theta$$

The power of the test is given by $Pr_1 = Pr(>K_1 | H_0)$ and the Rayleigh power is $K_1 = n_e R_1^2$.

This test is most powerful when a single cycle is made up of a series of m oscillations. At present, results at TeV energies are such that the shape of a light curve can never be safely said to be known a priori. Therefore, the Durham group has not yet implemented the Z^2_m test for multiple harmonics, which will tend to smooth out sharp peaks or pass over wide structures given an inappropriate choice of m. Reliance is placed upon the case in which m=1; the Rayleigh test. Although it too suffers from a lack of sensitivity to narrow features, this simple test requires less computing power. A knowledge of the Z^2_m test is needed for the comparison of results presented in this thesis with those obtained in the x-ray to PeV energy range by other observers. These and other likelihood ratio statistics in use in VHE γ-ray astronomy have been well documented by de Jager (1987).

(iii) amendment for a dataset of finite length

The Rayleigh test is based upon Poincare's theorem, which states that the stopping position in a horizontal plane of a needle which is free to rotate about a vertical axis is random, and follows a uniform distribution as the number of revolutions tends to infinity (Mardia, 1972).

When events are ordered according to pulse phase, it must be recalled that it is highly improbable that an observation will span an integer number of pulse cycles. Thus, when vectors are summed, the last few events

may fall at the beginning of a new cycle, causing an excess at an early phase which is an artefact of the observation length, rather than a feature of the source light curve. This end-point error is not significant in a search for millisecond periodicity, since the observation length is always far greater than the trial period and the expected event rate is only one or two per minute. However, it becomes problematic in application of the Rayleigh test to x-ray binary and cataclysmic variable sources which may contain periods of up to 300 s.

A phase assignment test which does not suffer from end-point errors has recently been introduced by Orford (priv. comm.). It is based upon the Central Limit Theorem: if Y_n is the sum of n random variables, μ_n is their mean and σ_n^2 their variance, then the distribution function of the random variable, $(Y_n-\mu_n)/\sigma_n$, approximates to the standard normal distribution function (Conover, 1980). In other words, the distribution of μ_n has a variance equal to that of the sample distribution divided by n. Thus, by measurement of the variance of $\cos\theta_i$ and $\sin\theta_i$ in equation 4.3d and division of their sum by the number of events, a test statistic is obtained. The sine and cosine terms are independent and both follow a standard normal distribution, thus the test statistic is distributed as χ^2 with two degrees of freedom.

(iv) correction for number of trials

Having decided upon a statistical test appropriate to the available knowledge of the source parameters, a period search range must be chosen. The number of independent trials made in a given range from P to $P+\Delta P$ is equivalent to the number of Fourier intervals it encompasses (this is $\approx T\Delta P/P^2$; see section 4.3.2). However, as mentioned in the context of the FFT method, a peak probability may fall between two adjacent independent periods. To allow for this, further trials may be made at periods separated by less than one F.I. The probability for uniformity obtained must then be

multiplied by both the number of independent trials and a further oversampling factor. It has been shown by Monte Carlo simulation that this oversampling factor tends to ~3 as the number of trials in a F.I. increases, at which point it is limited by the finite length of the dataset (de Jager, Swanepoel & Raubenheimer, 1989). Orford (1991) obtained an expression for the oversampling factor based upon a final chance probability given by $1-(1-Pr)^d$, where d is the number of independent trials and Pr is the lowest probability found within a F.I. This analytical treatment supported the results of the Monte Carlo simulations of de Jager, Swanepoel and Raubenheimer. Unless otherwise stated, the Rayleigh probabilities reported in this thesis are those obtained once the number of trials and the oversampling factor have been taken into account.

4.3.4 a test for goodness of fit

If highly accurate timing and a precise ephemeris are available it is unnecessary to test for periodicity slightly removed from the literature value. Given only one trial period, it becomes practicable to order events into phase bins and produce a single histogram. This distribution may be compared with an "ideal" light curve using the simple χ^2 test.

It is clear that if the null hypothesis of section 4.3.3 applies, the events should be uniformly distributed across ξ phase bins, resulting in an expectation value, given large n_e, of $e_i = n_e/\xi$ events per bin. The test statistic is:

$$\chi^2 = \sum_{i=1}^{\xi} (n_i - e_i)^2/e_i \qquad \text{eqn. 4.3e}$$

where n_i is the number of events observed in the ith phase bin (Batschelet, 1981). Although there are ξ degrees of freedom inherent in the assumed noise distribution, the estimation of e_i from a knowledge of the sample size reduces the degrees of freedom of the test statistic to $\xi-1$. H_0 is rejected if χ^2 falls above a chosen confidence level. Many statistical

texts include tabulated critical values of χ^2 and associated probabilities.

Since the sample events represent a Poissonian distribution of discrete phases, rather than a continuous Gaussian distribution for which the test statistic was designed, $n_i \geq 5$ is required for this to be a valid approximation where $Pr(\chi^2) \geq 10^{-3}$. $n_i >> 5$ must be true for $Pr(\chi^2) << 10^{-3}$.

In the calculation of χ^2 the order of the bins is irrelevant and it is merely required that the error in the assigned phase, $\delta\varphi$ be less than $1/\xi$ over the duration of the data set. However, if the behaviour of the target source is well documented, and their arrival times are recorded to sufficient accuracy, events may be assigned an "absolute" phase relative to the reference ephemeris. In equation 4.3b t_0 is replaced by T_0, where T_0 is the ephemeris epoch of pulse phase zero. This gives the added advantage of a visual comparison between the γ-ray histogram and a light curve obtained at a different wavelength. One notable incidence of this was the detection of VHE γ-rays from the Geminga pulsar (Bowden et al., 1993), the significance of which was greatly enhanced by the coincidence of the TeV peak with that in the light curve observed by the EGRET detector aboard the CGRO.

A major disadvantage of the χ^2 test for this use is its lack of sensitivity to broad light curves. There is also a danger that the power of a peak of width $< \xi$ may be divided between two adjacent bins. The test can be best applied to detect objects having a weak signal and short duty cycle (i.e. emitting during only a small fraction of the pulse period). The bias in the sensitivity of χ^2 towards peaks of width $1/\xi$ is seen as an advantage given a good prior estimate of the duty cycle. However, any trial and error optimisation of χ^2 by variation of ξ given no such a priori expectation must be acknowledged, and the number of degrees of freedom thus introduced accounted for. Astronomers frequently resort to "standard" twenty bin light curves in order to avoid misrepresentation. The same proviso applies to χ^2 optimisation by shifting of the phase bin origins.

4.3.5 periodic emission from binary star systems

(i) transformation of event times

In a search for periodic γ-ray emission from cataclysmic variables, x-ray binaries and pulsars in binary systems, allowance must be made for the effect of the orbital motion of the production site upon the pulse frequency.

The terminology necessary to the discussion of this topic is summarised below and in figures 4.3b and 4.3c. Note that for the purpose of this investigation, representation of the orbit has been simplified by the assumption that the eccentricity of the orbit is minimal and that the system consists of a small degenerate primary star and a considerably more massive secondary companion.

Parameter	Interpretation	Alternative Name
i	angle between the orbital plane and the plane perpendicular to the line of sight	inclination
P_{orb}	binary orbital period	
a	semi-major axis	
superior conjunction	episode in which the secondary star lies directly between the primary star and the observer	eclipse or phase 0
descending node	orbital position at which the velocity of the primary star away from the observer is a minimum	phase 0·25
inferior conjunction	episode in which the primary star lies directly between the secondary star and the observer	anti-eclipse or phase 0·5
ascending node	orbital position at which the velocity of the primary star away from the observer is a maximum	phase 0·75
Φ	orbital angular separation of position of primary from its place at superior conjunction	(orbital) phase angle
φ	$\Phi_{(rad)}/2\pi$	(orbital) phase

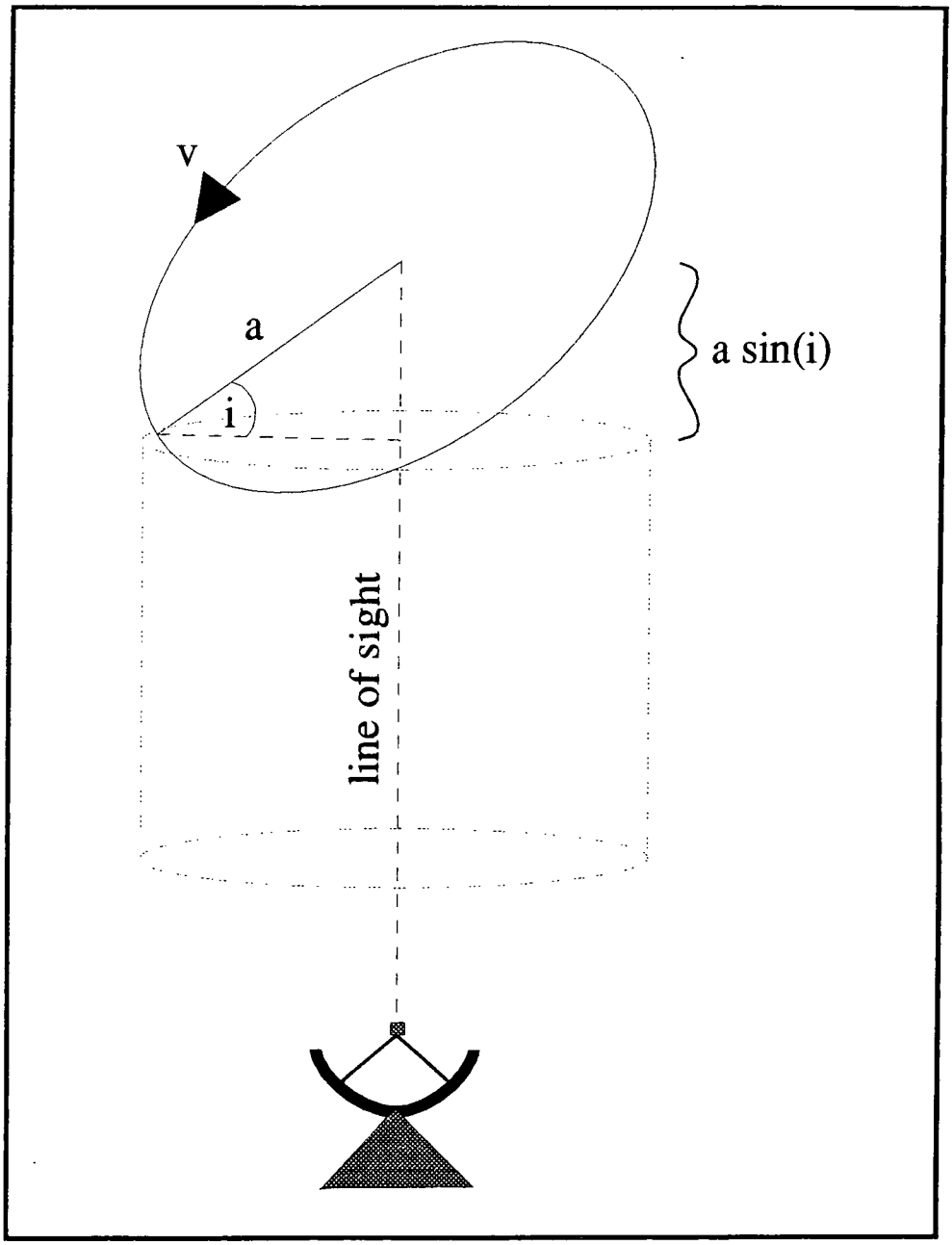

Fig. 4.3b : parameters of an orbit inclined at an angle **i** to the plane of the sky.

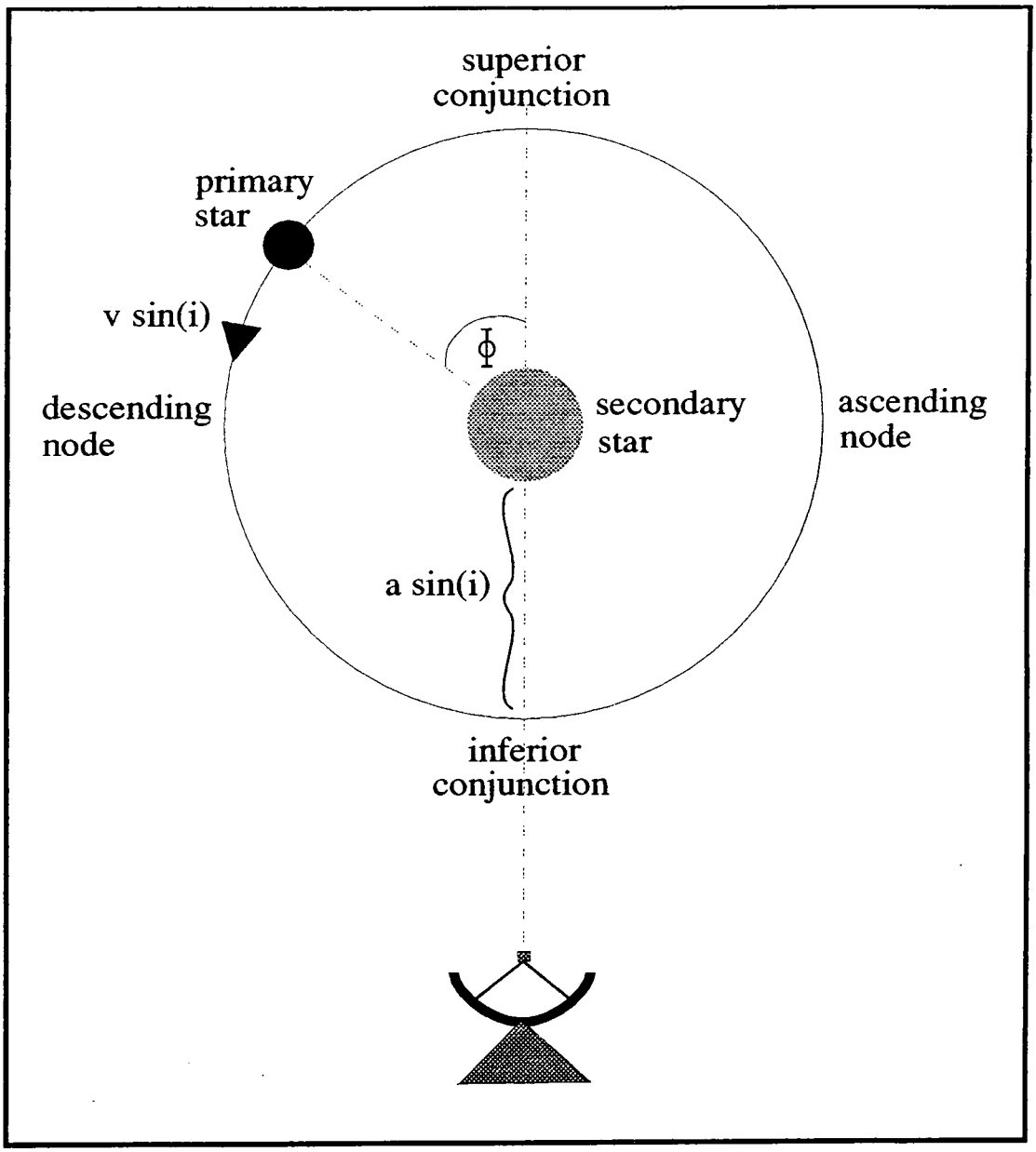

Fig. 4.3c : orbital parameters projected onto a plane perpendicular to the plane of the sky.

It is not possible to quantify all of the parameters descriptive of a distant orbit. The instantaneous velocity of the source, along the line of sight, is measured by the Doppler shift of spectral lines in the radio to x-ray region. It is possible to estimate vsin(i) by fitting a sinsoidal curve to these results, where v is the orbital speed of the primary given by:

$$v = 2\pi a(P_{orb})^{-1}$$

If radiation travelling at the speed of light, c, is emitted at a frequency ν_o by an object moving towards a stationary observer at velocity u, then the Doppler shift in the observed frequency is given by:

$$\nu = \nu_o c(c-u)^{-1}$$

$$\nu = \nu_o \gamma^2 (1 + u/c)$$

If velocities are given in units of c and it is reasonable to assume that $u << c$ and hence $\gamma \approx 1$, then:

$$\nu = \nu_o(1 + u)$$

If v is a fraction β of c, then the line of sight velocity measured by an observer, u, when the emission site is at phase angle Φ is given by $u = \beta\sin(i)\sin(\Phi)$. Therefore, the above expression for v becomes:

$$\nu = \nu_o(1 + \beta\sin(i)\sin(\Phi)) \qquad \text{eqn. 4.3f}$$

Observers find it useful to estimate the coherence time. This is the duration, over which periodicity may be observed, before the Doppler effect is sufficient for the perceived frequency v to change by a Fourier interval to another independent frequency, v', i.e. to cause a pulse phase shift of unity. If an observation is commenced at a time t=0 when the emission region is at Φ_0, then according to equation 4.3f, at a time t, the

observed pulse frequency is:

$$\nu(t) = \nu_o(1 + \beta\sin(i)\sin(\Phi_0 + \Omega t))$$

where Ω is the angular velocity $2\pi/P_{orb}$.

By writing $\sin(\Phi_0 + \Omega t)$ as $\sin(\Phi_0)\cos(\Omega t)-\cos(\Phi_0)\sin(\Omega t)$ and expanding the Ωt terms as power series the following approximation is obtained:

$$\nu(t) = \nu_o\beta\sin(i)\left[\sin(\Phi_0) - \cos(\Phi_0)\Omega t - \frac{\sin(\Phi_0)(\Omega t)^2}{2!} + \frac{\cos(\Phi_0)(\Omega t)^3}{3!} + \cdots\right]$$

Therefore, ignoring terms in Ω^3 and above:

$$\Delta\nu = \nu(t) - \nu(0) \approx \nu_o\beta\sin(i)\left(-\cos(\Phi_0)\Omega t - \sin(\Phi_0)(\Omega t)^2/2\right)$$

Near conjunction, $\Phi_0 \approx 0$ or π, therefore the $\sin(\Phi_0)$ term contributes little to the pulse phase shift (which is equivalent to $\Delta\nu\Delta t$). A pulse phase shift of unity occurs over a time τ_1 where:

$$1 = \Delta\nu\tau_1 = (\nu_o\beta\sin(i)\Omega\tau_1)\tau_1$$

hence,

$$\tau_1 = (\nu_o\beta\sin(i)\Omega)^{-1/2} \qquad \text{eqn. 4.3g}$$

At the descending and ascending nodes, $\Phi_0 \approx \pi/2$ and $3\pi/2$ respectively. The coherence time τ_2 is then given by:

$$1 = \Delta\nu\tau_2 = (\nu_o\beta\sin(i)\Omega^2\tau_2/2)\tau_2$$

hence,

$$\tau_2 = (\nu_o\beta\sin(i)\Omega^2/2)^{-1/3} \qquad \text{eqn. 4.3h}$$

Clearly, $\tau_1 < \tau_2$.

As an example, consider the binary pulsar PSR 1855+09. The pulsar ephemeris of Ryba and Taylor (1991) is presented in chapter seven. From their results it is found that:

$$\nu_o \approx (5{\cdot}362\text{x}10^{-3})^{-1} \text{ Hz}$$

$$\Omega \approx 2\pi/1065067 \text{ rad s}^{-1}$$

$$\beta c = 2\pi a/P_{orb} \quad \text{therefore} \quad \beta\sin(i) = 2\pi a\sin(i)/P_{orb}$$

$$= 2\pi(9{\cdot}23078)/1065067$$

where asin(i) is measured in light seconds. Thus, $\tau_1 \approx 4000$ s whereas $\tau_2 \approx 18{,}000$ s. It should be possible to retrieve a single frequency from a five hour data set centred upon the nodes . However, a coherent signal cannot be expected to last for longer than an hour at conjunction. Since long exposures are required for a significant γ-ray detection, a correction for the Doppler effect by the "focusing" of event times to a common reference is imperative.

The condition for coherent emission is that γ-rays, which originated at a pulse phase $((\nu_o t_o) \bmod 2\pi)$ at the emission site, are perceived as having arrived at the detector at an equivalent phase $((\nu t) \bmod 2\pi)$ i.e. $\nu_o t_o = \nu t$. Returning to equation 4.3f, it is required that:

$$\nu_o t_o = \nu_o(1 + \beta\sin(i)\sin(\Phi))t$$

therefore

$$t_o = t(1 + \beta\sin(i)\sin(\Phi)) \qquad \text{eqn. 4.3i}$$

Hence, in order to retrieve ν_o, each measured event time, t, must be corrected by the factor $(1 + \beta\sin(i)\sin(\Phi))$.

(ii) orbital sampling

The accuracy of an orbital ephemeris may not be sufficient to allow the reconstruction of the predicted periodicity by a single "focussing" operation as described above. It then becomes necessary to choose a search range in terms of either the orbital parameters asin(i) and Φ, or of the equivalent pulse period and its time derivatives.

If it is assumed that a single observation covers only a small fraction of the orbit, such that the Doppler effect acts in one sense only, then the error in arrival time required for a period change of one Fourier interval is given by:

$$(T_2 - T_1 + \delta T)/P = A + 1 \qquad \text{eqn. 4.3j}$$

where T_1 and T_2 are the corrected times of the first and last events in the data set respectively, δT is the error due to incorrect focussing, P is the pulse period and A is a constant equal to $(T_2 - T_1)/P$. An equivalent expression may be written in terms of an error in the trial period:

$$(T_2 - T_1)/(P + \delta P) = A + 1 \qquad \text{eqn. 4.3k}$$

In order to sample in terms of orbital parameters, intervals in asin(i) and Φ are calculated using equation 4.3f. A matrix of these incremented parameters is constructed. The event times are focussed and tested at period P so that each point in the matrix receives a corresponding Rayleigh probability. If evidence of periodicity appears consistently offset from its predicted position by more than one F.I., then it may be inferred that this is the effect of either a systematic error in the ephemeris, or that the site of γ-ray production is slightly removed from that of the emission upon which the ephemeris is based.

Focussing results in correction of the travel time of γ-rays along the observer's line of sight. However, the orbital parameters are varied in a plane perpendicular to this line. The number of independent periods tested

does not directly equate to the number of steps taken in asin(i) and Φ. The number of degrees of freedom expended in orbital sampling are therefore found from simulations, as described in detail by Brazier (1991). Orbital sampling has been applied in the study of PSR 1855+09, the results of which are presented in chapter seven.

In order to avoid uncertainty in the number of degrees of freedom employed, the data may instead be tested using a range of pulse periods and period derivatives. Should the need arise, it is possible to reconstruct the orbital parameters required to cause an observed period shift by equating equations 4.3j and 4.3k.

4.3.6 combining a set of discrete observations

Assuming a Poissonian distribution of events, for an observation of duration T, it can be shown that the fractional error in the number of source counts is proportional to $T^{-1/2}$. It is therefore advantageous to combine multiple observations of a single source in order to obtain the best estimate of, or upper limit to, its signal strength.

The treatment of multiple observations may be approached in one of two ways. If the behaviour of the source is well known, observations may be combined and analysed as a single dataset; alternatively, the results of tests on individual nights may be summed.

(i) retention of relative phase

Given a good ephemeris and sufficiently accurate timing information, it is possible to treat observations separated by a period of several months as a single exposure of length $T = t_n - t_1$, where t_1 and t_n are the start time of the first and the end point of the last observation respectively. This has the obvious advantage that the Fourier interval P^2/T is greatly reduced, thus giving improved period resolution.

Unfortunately, such a dataset will consist of data "windows" interspersed with a series of gaps following a daily, monthly and for observations spanning several years, six-monthly cycle according to the "availability" of the target source. This will have the effect of introducing beat frequencies between these periodicities and the pulse period. It is difficult to distinguish between the fundamental period indicated by a minimum Rayleigh probability and its aliases. The correlation between Rayleigh vectors at the beat induced alias periods and the fundamental is not well understood.

(ii) aggregate probability from individual datasets

It is often the case that either clock drift or the period derivatives and "glitching" behaviour of a source prevent the amalgamation of observations as described above. The accumulated uncertainty in event times over a year may equate to a significant fraction of the trial period, particularly in the case of millisecond pulsars. In order to benefit from the size of the dataset, the Rayleigh test is applied to each observation separately and the probabilities of uniformity are combined. Since this requires that all data is sampled at the same trial periods, the test range applied to all datafiles is chosen to be a multiple of the F.I. of the shortest observation. If at a test period P_i a Rayleigh probability of Pr_j is obtained from each of n observations then, according to Eadie et al. (1971), the logarithmic sum, C_i, constructed as:

$$C_i = -2\ln \prod_{j=1}^{n} Pr_j(P_i) \qquad \text{eqn. 4.31}$$

is distributed as χ^2 with 2n degrees of freedom. Thus the power of the test (the probability of *correctly* rejecting the null hypothesis given C_i) is given by:

$$Pr(H_0) = Pr(\chi^2 > C_i)$$

4.4 calculation of flux and flux limits

In the drive to constrain models of γ-ray production sites and mechanisms, atmospheric Cerenkov data may provide more information than a simple rejection or otherwise of H_0.

From a knowledge of the cosmic ray integral energy spectrum, the flux of cosmic ray events incident within the collecting area of a telescope may be calculated. A comparison may then be made between the observed event count rate and that expected for the relevant aperture. The cosmic ray energy at which observation and prediction converge is taken to be the threshold energy of the atmospheric Cerenkov telescope, E_{thresh}. Primary particles of energy $< E_{thresh}$ are not detected.

In fact, the cosmic ray spectrum is such that the total number of particles above an energy E is proportional to $E^{-1.6}$ (Khrenov, 1993). A simple estimation of the observed γ-ray flux may therefore be made, from the actual cosmic ray flux at E_{thresh} and the ratio of the number of γ-ray-like events in the source direction to the number of apparently nucleon-induced events. A count rate excess of one percent in the on-source channel is thus equivalent to a γ-ray flux of $\varphi_{1\%}$ given by:

$$\varphi_{1\%} = 0{\cdot}01 \times \varphi_{cr}(E_{thresh}) \times A \times \theta$$

where φ_{cr} is the cosmic ray flux in $cm^{-2}s^{-1}sterad^{-1}$, A is the flux collecting area and θ is the telescope aperture in steradians. The effective sensitive area, A, is estimated from simulations which predict the maximum telescope - air shower core separation at which the Cerenkov flash will trigger the on-source channel. The Durham group has quantified this impact parameter to be ~50 m, giving a value of A of approximately 1000 m^2. For convenience, a quantity $\varphi_{100\%} = 100 \times \varphi_{1\%}$ will also be used in the following discussion.

At present, the comparison of flux measurements from different atmospheric Cerenkov experiments is complicated by varied methods of

presentation. It is to be hoped that, as simulations become increasingly detailed, a consensus will be reached within the observing community as to a standard model for the calculation of telescope sensitivity.

4.4.1 method of flux estimation

Given an estimate of $\varphi_{1\%}$, the γ-ray flux is estimated in a manner appropriate to the form of analysis used to reject H_0.

(i) unpulsed emission

This provides the simplest method of flux estimation. For a long exposure the event distribution approximates to a Gaussian. The excess number of on-source counts may therefore be described in terms of an equivalent number of standard deviations, $n\sigma$, in the off-source count total, n_{off}. The excess flux is then given by:

$$\varphi = n\sigma/n_{off} \times \varphi_{100\%}$$

If H_0 has not been rejected, then it is possible to estimate the minimum source flux which would have resulted in the rejection of H_0 at the 3σ level by:

$$\varphi_{(3\sigma)} = 3\sigma/n_{off} \times \varphi_{100\%} \qquad \text{eqn. 4.4a}$$

(ii) the Rayleigh test

The magnitude of the Rayleigh vector **R** is a measure of the ratio of pulsed to unpulsed events, since, according to de Jager (1987), the expectation value of the fractional pulsed signal strength is 2R, the pulsed flux is given by:

$$\varphi = \varphi_{100\%} \times 2R \qquad \text{eqn. 4.4b}$$

The probability of obtaining a result outside 3σ of the mean, equivalent to the area under the standard normal curve, is approximately $1{\cdot}3\text{x}10^{-3}$ (Walpole, 1982). By equating this to the Rayleigh probability, Pr, **R** can be evaluated as:

$$Pr = \exp(-NR^2)$$

therefore,

$$R = (-1/N(\ln 1{\cdot}3\text{x}10^{-3}))^{1/2}$$

Thus the flux limit is given by:

$$\varphi_{(3\sigma)} = \varphi_{100\%} \times 2N^{-1/2}(-\ln 1{\cdot}3\text{x}10^{-3})^{1/2} \qquad \text{eqn. 4.4c}$$

where N is the total number of events.

(iii) the χ^2 test for goodness of fit

If the duty cycle of pulsed emission is narrow and extremely well known, then it is possible to divide epoch folded data into a number of phase bins, n, such that all γ-ray emission should appear in one bin. If the dataset contains N events in all, then the expectation value for the number of events in a phase bin is N/n. If a total of δ γ-ray events are detected and are contained within a single bin, then in that bin the observed frequency will be $(N-\delta)/n + \delta$, whilst in the other n-1 bins, on average there will be only $(N-\delta)/n$ events. By substitution into equation 3.5e, the following expression for χ^2 is obtained:

$$\chi^2 = \frac{n}{N}\left[\left\{\frac{N-\delta}{n} + \delta - \frac{N}{n}\right\}^2 + (n-1)\left\{\frac{N-\delta}{n} - \frac{N}{n}\right\}^2\right]$$

which simplifies to:

$$\chi^2 = \frac{\delta^2}{N}(n-1)$$

The fraction of pulsed events, δ/N, may be obtained from the above expression given N and the value of χ^2 with (n-1) degrees of freedom. In order to obtain a 3σ flux limit, the tabulated value of $\chi^2_{(n-1)}$ is found which corresponds to a probability of 1.3×10^{-3}.

For a "standard" twenty bin light curve, if a 5% duty cycle were assumed, a 3σ detection would result in a value of χ^2 with nineteen degrees of freedom of 42·75. The fraction of pulsed events is then found from:

$$\frac{\delta}{N} = N^{-1/2} \left[\frac{\chi^2}{n-1} \right]^{1/2} = 1{\cdot}5\ N^{-1/2}$$

and the 3σ flux limit is:

$$\varphi_{(3\sigma)} = \varphi_{100\%} \times 1{\cdot}5 \times N^{-1/2} \qquad \text{eqn. 4.4d}$$

4.4.2 flux limits from the Durham database

By extrapolation from the characteristics of the early Dugway instruments, E_{thresh} was found to be 250 GeV for the Mark III telescope (Brazier et al., 1989). This result was then scaled to a value of 400 GeV for the Mark IV telescope, which had the same aperture as the Mark III but a smaller mirror area. These values are based upon the count rate at the zenith. E_{thresh} varies systematically during an observation as the cosmic ray flux is zenith angle dependent; the count rate falls as the telescopes track towards the horizon. At a zenith angle of 45° the threshold energies of the Mark III and Mark IV detectors become roughly 450 GeV and 600 GeV respectively. These quantities are not definitive for all Bohena Settlement observations because both telescopes have been subject to continual improvements in design. In fact, by 1991 the Mark III telescope's cosmic ray count rate had increased to 200% of its 1986 value. Fluxes are generally calculated from observations spanning several years. The early

telescope sensitivities must be assumed in combining recent and archival data, so that such estimates are conservative.

The threshold energy of the Mark V telescope has not yet been quantified, as since its commissioning it has been used primarily as a test bed for the imaging technique.

For the Mark III detector, assuming a flux of cosmic ray protons of 2×10^{-5} $cm^{-2} s^{-1} str^{-1}$ and a field of view of $3 \cdot 3 \times 10^{-4}$ str, a 1% excess in the on-source channel would correspond to an excess flux of γ-rays of energy $\geq$ 250 GeV of:

$$\varphi_{1\%} = 2 \times 10^{-5} \times 3.3 \times 10^{-4} \times 0.01\% = 6.6 \times 10^{-11} \text{ cm}^{-2} \text{ s}^{-1}$$

At a zenith angle of 45°, where E_{thresh} rises to 450 GeV, $\varphi_{1\%}$ becomes approximately 8×10^{-10} cm^{-2} s^{-1}.

Flux estimates obtained at m separate epochs were combined for twenty five objects in the Durham database using the expression:

$$\varphi_{tot} = \left[(1/m) \sum_{j=1}^{m} \varphi_j^2 \right]^{1/2} \qquad \text{eqn. 4.4e}$$

and were given in Bowden et al. (1991).

It should be noted that the accuracy of Atmospheric Cerenkov flux limits is never likely to exceed a factor of two, the sophistication of air-shower simulations notwithstanding, because of the variations in threshold energy caused by frequent changes in sky clarity.

CHAPTER FIVE

Signal to Noise Enhancement Techniques

The development of particle showers in the atmosphere is described in this chapter. Emphasis is placed upon features which may be used to distinguish cascades triggered by cosmic ray protons from those due to γ-rays, with a view to improving the signal to noise ratio of atmospheric Cerenkov data. Various methods for the rejection of proton induced "events" are reviewed. A case study is presented in which the arrival time of a Cerenkov flash at multiple telescopes is used to determine its point of origin.

5.1 the distribution of Cerenkov photons

5.1.1 air shower propagation

The galactic cosmic ray flux consists of protons, α particles, a small fraction of heavier nuclei (and the products of their collisional fragmentation), electrons and γ-rays. These are released during stellar evolution and undergo shock acceleration or interact with magnetic fields to attain a mean energy of 10^9 eV (Silberberg, Tsao & Letaw, 1993). In the TeV region, the number density of this approximately isotropic flux of fast particles falls off according to a power law of the form N = a constant x $E^{-1.6}$ (Khrenov, 1993) such that 2 x 10^{-5} particles cm^{-2} s^{-1} str^{-1} of energy $E \geq 250$ GeV are incident at the Earth. The proton fraction increases with the energy per nucleon (Dyakonov et al., 1993) and is dominant at $E \approx 10^{12}$ eV (Protheroe, 1977).

On close encounter with an atomic nucleus, a VHE γ-ray can interact to form an electron - positron pair ($e^- e^+$) whilst the energy-momentum four vector remains invariant (the same in all inertial frames) through electro-

magnetic photon-to-neucleon coupling. The daughter particles, each carrying almost half of their parent's total energy, may emit γ-rays in the form of bremsstrahlung radiation as they pass close by further nuclei. The radiation length for e^-e^+ pair production, X_o, is 37·2 g cm^{-2} and that of the bremsstrahlung mechanism is similar (Rao & Sinha, 1988). This is of the order of $\frac{1}{28}$ times the column depth of the Earth's atmosphere. Thus, a cosmic ray photon can produce an e^-e^+ pair near the top of the atmosphere and each daughter particle will go on to produce bremsstrahlung γ-rays which undergo pair production in turn. A cascade of energetic particles (or Extensive Air Shower) will develop via this cyclical process which will continue to branch out until the electrons and positrons lose energy more rapidly to nearby atoms (through ionisation) than as bremsstrahlung radiation. In air, ionisation becomes the dominant loss mechanism at particle energies of 84 MeV and below (Carraminana, 1991).

A cosmic ray proton can undergo strong interactions, on colliding with atomic nuclei in the atmosphere, to produce neutral and charged pions. Neutral pions decay into γ-rays which then succumb to e^-e^+ pair production to form an electro-magnetic cascade as outlined above. The still-energetic proton may move on to produce more pions at another interaction centre. A proton of energy E_{p+} GeV can produce up to $(E_{p+})^{1/4}$ pions per nuclear collision. A resume of the pion decay products is given below (data taken from Griffiths, 1987):

particle	lifetime (s)	prob. of decay above ground	principal decay product
π^+ or π^-	2·6 x 10^{-8}	high	$\mu^+ + \nu_\mu$ or $\mu^- + \nu_\mu$
π^o	8·7 x 10^{-17}	very high	$\gamma + \gamma$
μ^+ or μ^-	2·2 x 10^{-6}	low	$e^+ + \nu_e + \nu_\mu$ or $e^- + \nu_e + \nu_\mu$
ν or ν	stable	zero	none

Figure 5.1a consists of a schematic representation of the development of γ-ray initiated and proton initiated air showers (it does not illustrate the relative abundances of the component particles or their spatial separation). For convenience, the former will be referred to here as "electro-magnetic cascades" and the latter as "hadronic cascades", although it should be noted that proton initiated cascades do generate γ-rays which give rise to electro-magnetic sub-showers.

5.1.2 air shower morphology

In an electro-magnetic cascade, the γ-ray is annihilated in the act of creation of an e^+e^- pair and approximate equipartition of its energy between the two daughter particles occurs. In a hadronic cascade, a single component may carry a disproportionate amount of energy away from an interaction site. The mean free path of a proton in the atmosphere is of the order of double the bremsstrahlung radiation length. The "opening angle" between the path of an incident proton and that of a pion which it generates is greater than the angle of divergence of a newly created e^+e^- pair (Rao & Sinha, 1988). These facts conspire to give hadronic air showers a wide spread and a random "clumpiness" when compared to the narrow lateral distribution of particles in electro-magnetic cascades. This is illustrated by increasingly complex Monte Carlo simulations (see, for example, Kertzman & Sembroski, 1991). It is the atmospheric Coulomb scattering of the e^+e^- component of electro-magnetic cascades which determines their lateral extent.

According to Rao and Sinha (1988), the number of particles in an electro-magnetic cascade is greatest at a depth δ_{em} in the atmosphere given by:

$$\delta_{em} = X_o \left[\ln \left[\frac{E_o}{E_t} \right] - 0{\cdot}5 \right] \qquad \text{eqn. 5.1a}$$

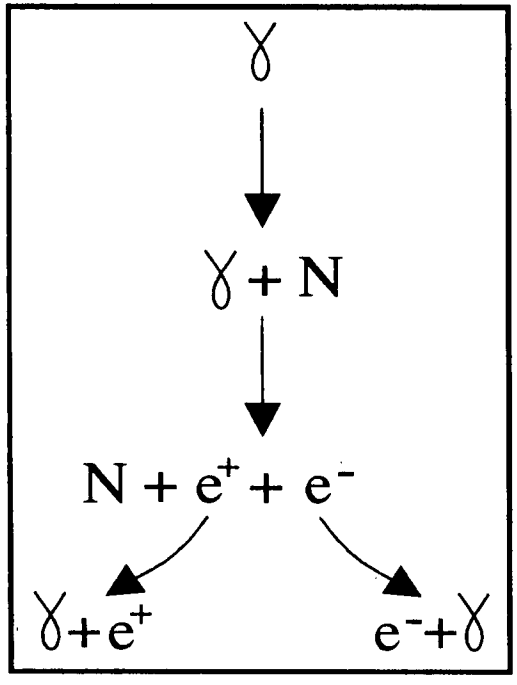

Figure 5.1a : the development of an electro-magnetic cascade (above) and of a hadronic cascade (right) in the Earth's atmosphere. The curved arrows indicate episodes of bremsstrahlung radiation. N represents the nucleus of an atom of the air and N* are the fragments of this remaining after a particle - particle collision.

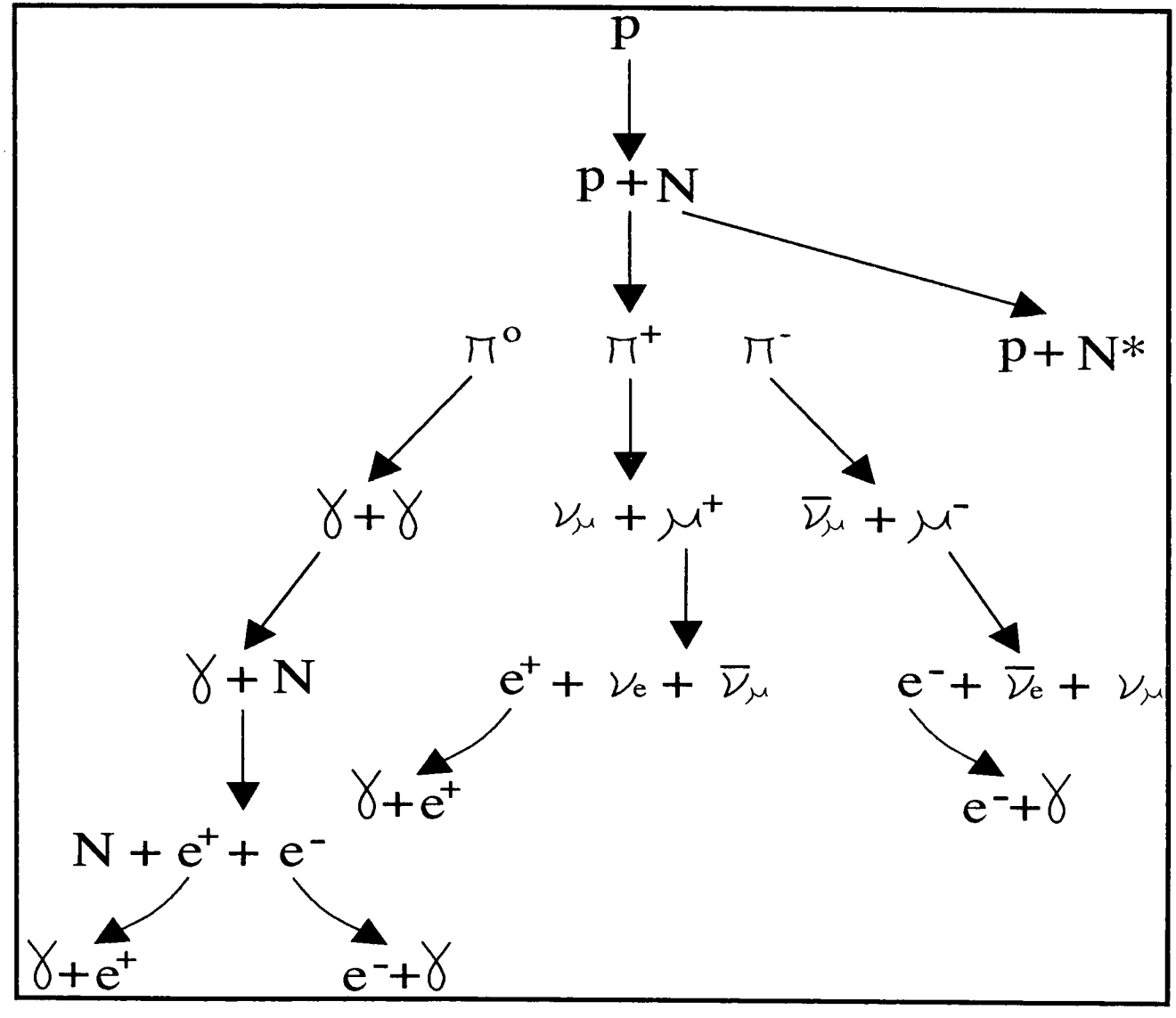

where X_o is the radiation length for pair production, E_o is the energy of the primary particle and E_t is the energy of a single particle at this depth. These authors also quote the following expression for a hadronic cascade adapted from Gaisser and Hillas (1977):

$$\delta_h = 0{\cdot}51\ \lambda\ \ln\left[\frac{E_o}{E_t}\right] \qquad \text{eqn. 5.1b}$$

where $\lambda = 70$ g cm^{-2}.

The column depth (in g cm^{-2}) may be converted to an equivalent height above sea level (in metres) using the expression:

$$h_{max} = (6740 + 2{\cdot}5\delta)\ \ln(1030/\delta) \qquad \text{eqn. 5.1c}$$

When $E_t \leq 84$ MeV, ionisation of the surrounding medium becomes the dominant energy loss mechanism for e^+ and e^-, and the particle flux ceases to multiply. By putting $E_t = 84$ MeV and $E_o = 250$ GeV in equations 5.1a and 5.1b it is found that $\delta_{em} = 279$ g cm^{-2} and $\delta_h = 286$ g cm^{-2}, giving equivalent heights a.s.l. of shower maximum of $h_{em} \approx 9{\cdot}7$ km and $h_h \approx 9.6$ km. The column depth at the University of Durham Observatory at Bohena Settlement, ~260 m a.s.l., is 1001·5 g cm^{-2}.

5.1.3 the Cerenkov flash

(i) the light pool

The energy spectra and nuclear composition of cosmic rays incident at Earth are well-documented for particles having energies of the order of 1 to 100 TeV per nucleon. In an excellent review of the field, Khrenov (1992) summarises the results obtained from balloon borne calorimetric detectors flown by the Japanese-American-Cooperative Emulsion Experiment and by two satellite experiments run by Moscow State University originally presented

at ICRCs in 1990 and 1992. The charge dependence of ionisation losses and Cerenkov radiation was used to determine atomic number, whilst the optical density of tracks left in x-ray film or grain counting in layers of nuclear emulsion interleaved with an absorber (e.g. lead) provided a measure of the energy of the primary particle. The University of Chicago Cosmic Ray Nuclei Experiment, flown on Spacelab-2 in 1985, successfully used gas Cerenkov detectors to measure particle energy and plastic scintillators to determine particle charge in the 1 GeV/amu to 1 TeV/amu region.

The Larmor radius of a proton of energy 10^{15} eV passing through the ~3μG galactic magnetic field is of the order of 0·3 pc. Charged VHE cosmic ray particles therefore follow twisted paths and cannot be traced to their points of origin (e.g. the Crab nebula at a distance of ~1 kpc). The astronomy of discrete VHE cosmic ray sources is therefore largely based on the detection of high energy photons. The flux of VHE γ-rays expected from individual objects is so low when compared with the overall background count rate that large area detectors are required. These are of necessity operated at ground-level. As VHE γ-rays give up their energy to electron-photon cascades in the atmosphere, detections are based upon optical...

emission, in the form of Cerenkov radiation from the air shower particles themselves and as the fluorescent light (of wavelength 300 nm to 430 nm) emitted by relaxing atmospheric Nitrogen molecules excited by their passage. The fluorescent light yield does not vary greatly with atmospheric depth. As the density of N_2 rises so does the likelihood that the process will be quenched through molecular collisions. The intensity of fluorescent light therefore mirrors the development of the particle cascade (Protheroe, 1982). The fluorescent radiation is isotropic, whereas the direction of emission of Cerenkov light is restricted to a narrow cone about the shower axis. The photon density at a detector due to Nitrogen fluorescence exceeds that of Cerenkov light only for showers which have an impact parameter > 500 m and are therefore viewed "side-on".

The number of Cerenkov photons emitted (which is proportional to track length) per unit column density by a particle of a given energy does not vary greatly with atmospheric depth, and it is therefore reasonable to assume that most of them originated from the height of the shower maximum. To a first approximation it is expected that the distribution on the ground of Cerenkov photons created at a height, h, by a vertically incident shower, will be a circle of radius $h\theta$ where θ is the Cerenkov angle given by equation 2.1a. As the inclination of the shower axis increases so does the ellipticity of this Cerenkov ring. Since the atmospheric refractive index increases with decreasing height, giving an associated narrowing of the Cerenkov angle, the product $h\theta$ takes a value of between 110 m and 145 m for photons produced in the range $7 \text{ km} < h < 20 \text{ km}$ (Hillas, 1982). Near the base of a shower, the angles at which the low energy particles are scattered on collision with air molecules etc. exceed θ, and the Cerenkov ring is therefore blurred. In hadronic cascades, the electro-magnetic component which gives rise to Cerenkov emission develops at a greater atmospheric depth than in a similarly energetic γ-ray initiated shower. As a consequence, the lateral distribution of Cerenkov light at the ground is

due principally to the transverse momentum with which the neutral pions are endowed at birth, rather than to the Coulomb scattering of their daughter particles.

A fraction of the Cerenkov light from the shower's core will be redistributed isotropically through Rayleigh scattering and aerosol scattering at low altitudes.

The electro-magnetic component of a hadronic cascade, which gives rise to its Cerenkov signal, receives only a fraction of the energy of the primary particle. In order to yield the same Cerenkov flux as a 1 TeV primary γ-ray, a cosmic ray proton would require approximately twice as much energy (Rao & Sinha, 1988).

Numerous investigators have extended the Monte Carlo technique of air shower simulation to model the distribution of Cerenkov photons. For example, Krys, Krys and Wasilewski (1991) have shown, by this method, that the intensity of Cerenkov light is sharply peaked about the axis of a hadronic cascade and rapidly declines with increasing perpendicular distance from it, whereas the Cerenkov flux from an electro-magnetic cascade is evenly distributed within the radius $h\theta$ and only falls off beyond the Cerenkov ring. This distinction is marked at a primary energy of 1·2 TeV but the $h\theta$ shoulder is not significant at $E_o \geq 10$ TeV. Figure 5.1b, which illustrates this lateral Cerenkov light distribution has been adapted from their Figure 6. Patterson and Hillas (1983) noted that the lateral distribution of the intensity of Cerenkov light becomes steeper as the energy of the primary particle increases and/or the zenith angle is decreased.

(ii) the time profile

The expected duration of a Cerenkov light pulse at a ground level detector can be estimated from the following simple "point emission model". It is assumed that the radiating particles travel along a vertical shower

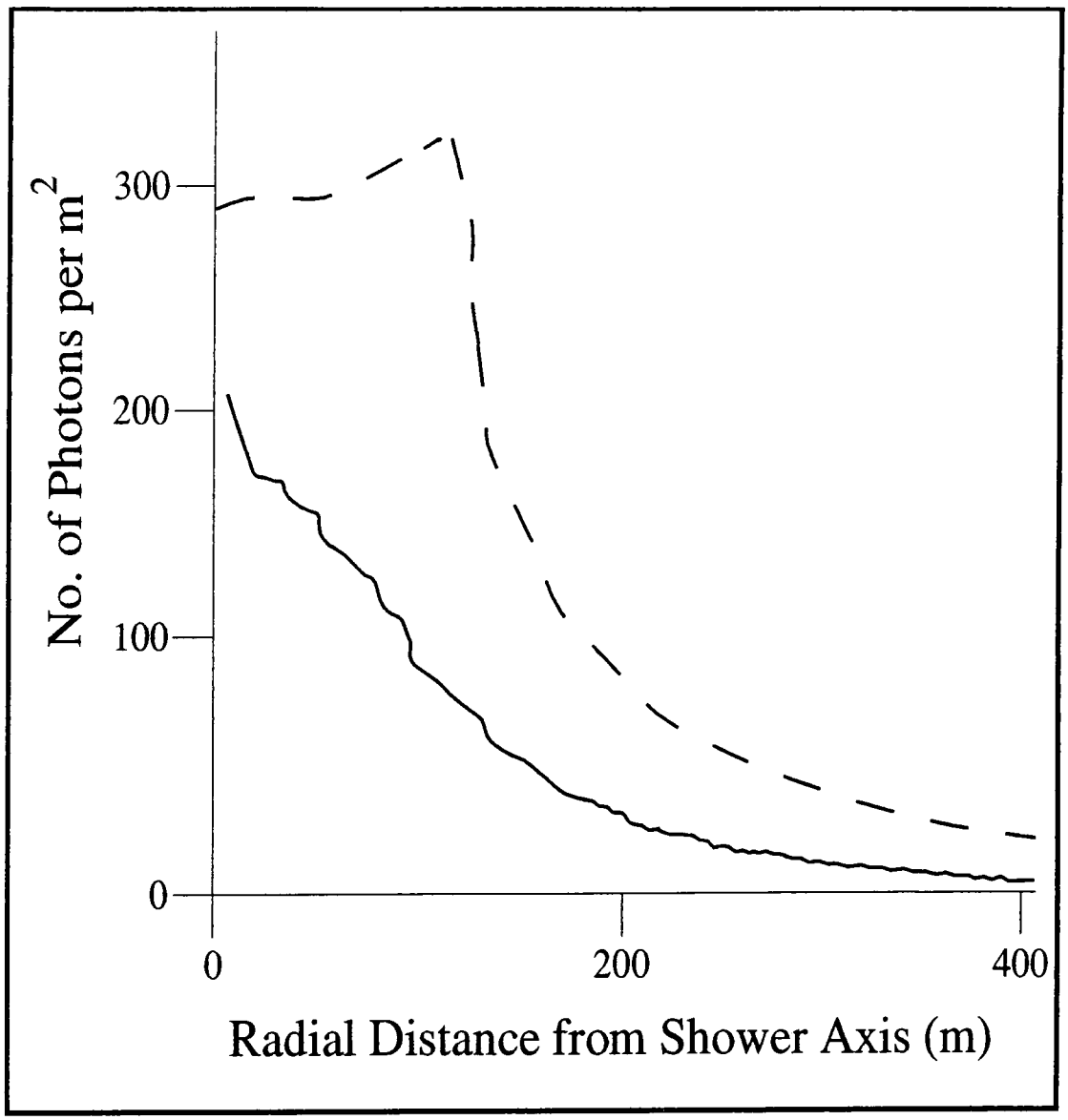

Figure 5.1b : the lateral distribution of Cerenkov light from air showers initiated by a proton (unbroken line) and a photon (dashed line) both of energy 1.2 TeV, as viewed at an atmospheric depth of 940 g cm^{-2} (adapted from Krys, Krys & Wasilewski, 1991).

axis at a velocity which approximates to the speed of light in vacuo, and that photons arriving at the ground within a given time interval were emitted from a well-defined range of altitude. The instantaneous intensity of Cerenkov light received by a detector reflects the maturity of the cascade at its depth of origin. The mapping of a pulse of Cerenkov light of a few tens of nanoseconds duration onto a shower track several kilometers in length is shown in figure 5.1c.

Hillas (1982) noted that the above construction was not adequate within the Cerenkov ring, where the light travel time from A to D in figure 5.1c exceeds the combined particle plus light travel time from A to D via B or C. In this case the mapping is reversed.

Antonov et al. (1991) used Monte Carlo simulations of 10 TeV electromagnetic cascades to model the relationship between the time taken for a Cerenkov pulse to reach half of its maximum height at a detector and the shower impact parameter, d. Figure 5.1d (adapted from their figure 2) shows that the increasing pulse rise time becomes significant for showers viewed at large zenith angles, Z° ($Z^\circ \approx 90^\circ - \tan^{-1}(h_{em}/d)$).

According to Protheroe (1982), the contribution of scattered light to the width of the Cerenkov pulse is independent of the impact parameter. This is because the separation of scattering centres radially distributed about the shower axis exceeds the particle track length within a $2{\cdot}5^\circ$ field of view. The scattered light becomes the dominant component of the Cerenkov flux only at large zenith angles (this may lead to over-estimation of δ_{em} for a highly inclined cascade).

Tumer, Hammond, Zych and MacCallum (1990) found, from Monte Carlo simulations, that the irregular distribution of energy between daughter particles during the growth of a hadronic shower could lead to the development of "large scale fluctuations or jets". The path length, to a ground-based detector, for Cerenkov light emitted by these jets of charged particles could differ from the expected distribution by a few metres,

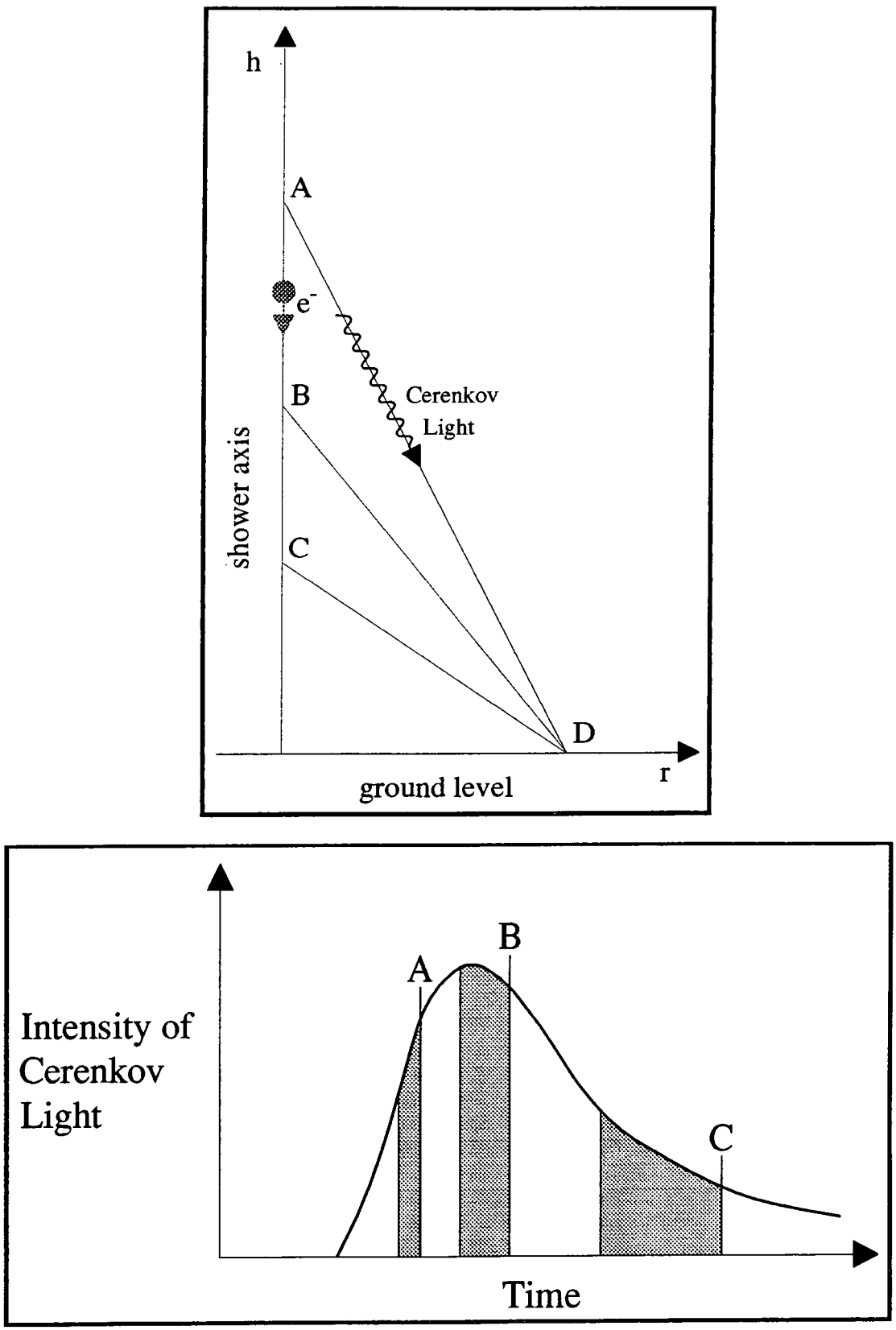

Figure 5.1c : the relationship between the height (h) at which light is emitted from a particle cascade (above) and its contribution to the time profile of the Cerenkov flash at a detector (D) at a radial distance r from the shower axis (below), as depicted by Hillas (1982).

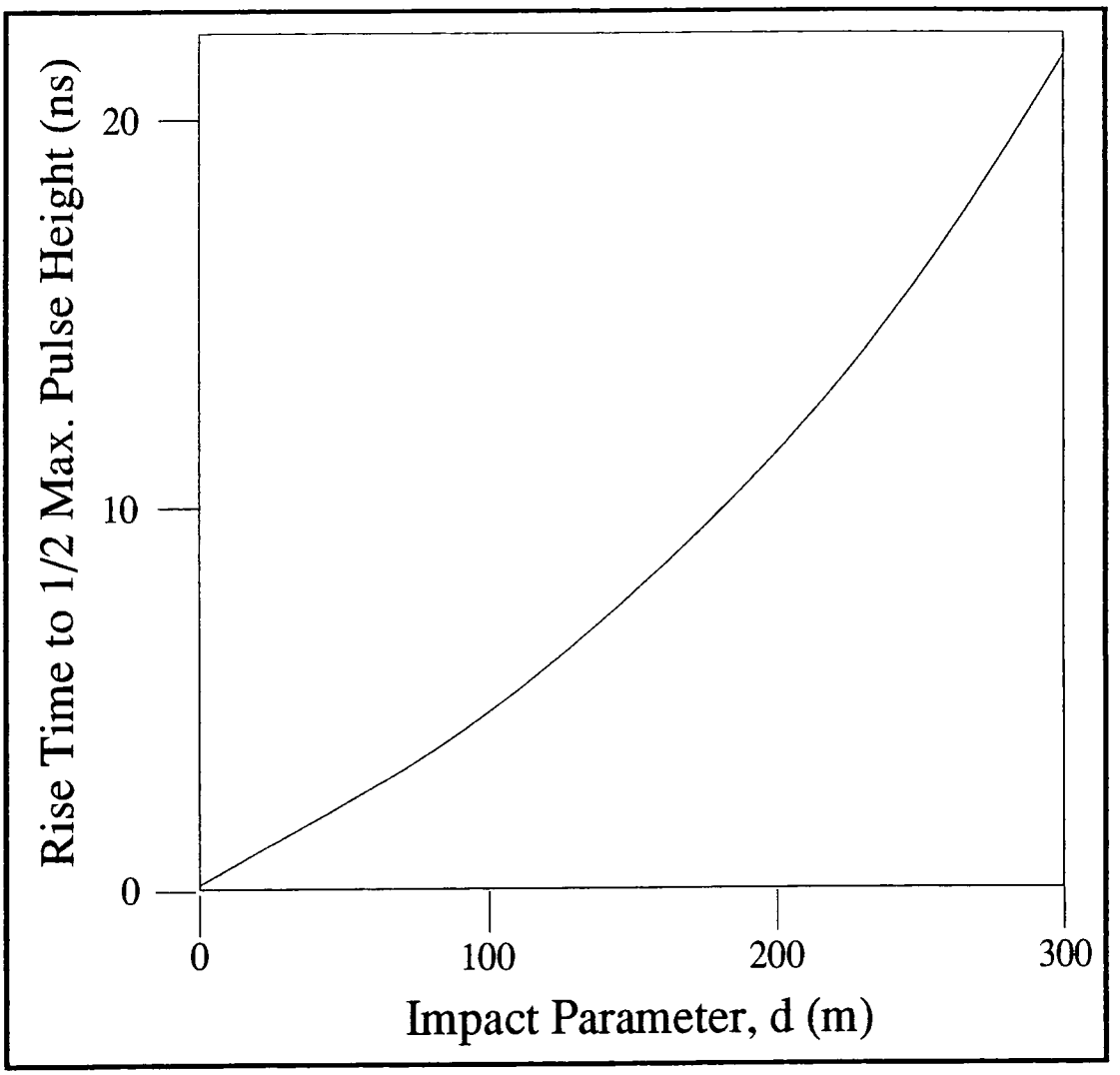

Figure 5.1d : mean delay in Cerenkov pulse arrival time at a detector at a horizontal distance d from the projected axis of an air shower initiated by a gamma ray of energy 10 TeV (after Antonov et al.,1991).

leading to a disparity in arrival time of the order of a few nanoseconds. As a result, these authors predict that hadronic cascades will exhibit "kinks" in the tails of their Cerenkov pulse profiles, as distinct from the smooth curves of γ-ray initiated showers (as shown in figure 5.1e). A drift scan observation of the Crab nebula was taken using two detectors of the mirror plus single photomultiplier tube "light bucket" type. A coincident response from the two PMTs triggered a fast oscilloscope, which displayed their output signals so that the pulse waveforms could be recorded on video tape. Tumer, Hammond, White and Zych (1990) reported that, by visual inspection, 8% of the ~ 3200 pulses obtained were concluded to be of the unstructured γ-ray type, leading to a detection of unpulsed emission from the Crab nebula significant at the 4·2 standard deviation level. Attractive as this result may seem, this method of discriminating between hadronic and purely electro-magnetic showers is inexpedient as, at present, it is labour intensive and is based upon the subjective decisions of the observers.

5.2 techniques of γ-ray signal enhancement

In order to distinguish point sources of VHE γ-rays against the isotropic cosmic ray background, Atmospheric Cerenkov astronomers must either exploit the fundamental differences between γ-ray initiated air showers and hadronic cascades, or rely upon the detection of enhanced activity from the direction of the target object. Such considerations have already been touched upon in section 2.3. Here, some methods of improving the signal to noise ratio of the University of Durham telescopes invoked in chapters six and seven are examined in greater detail.

5.2.1 a test of aperture rejection

The University of Durham Mark III and Mark IV telescopes are narrow aperture instruments. The rejection of background cosmic ray events is

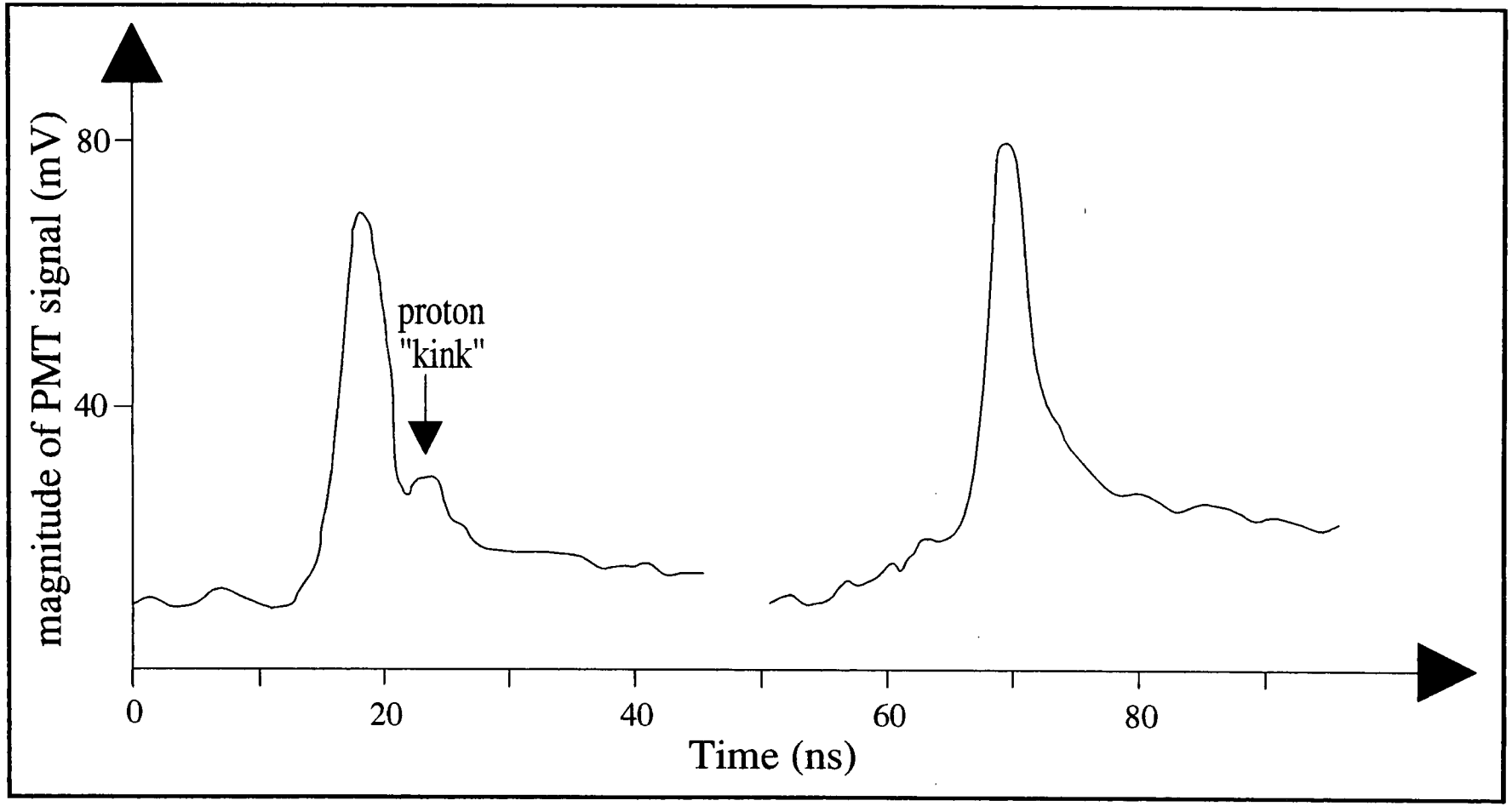

Figure 5.1e : typical Cerenkov pulse time profiles. The "kink" in the trailing edge of the left hand peak is indicative of a late arriving sub-cascade in a hadronic air shower, whilst the smooth profile on the right is a "candidate photon event" according to Tumer, Hammond, Zych and Maccallum (1990).

performed solely on the basis of the arrival direction of their Cerenkov flashes. Only the light from air showers incident from the sky within 1·5° of the position of the targeted object is recorded. Generally, any flashes which trigger a response from one or more of the off-axis guard ring channels are considered not to have come from the point source direction. This includes those "multi-fold" events in which the pulse heights recorded by several channels including the *central* one have exceeded the pre-determined 50 mV hardware threshold.

When the projected tube to tube separation in the Mark III telescope detector packages was 2° on the sky, between 40% and 50% of the events in which the central channel had been triggered included a response from an off-axis channel. When the tube separation was reduced to 1·5° in March 1991, this figure was increased by ~10 %.

In 1990, simulations were carried out from which it was inferred that γ-ray induced air showers from the on-axis direction would result in a high incidence of flashes triggering the central channel plus one other (commonly referred to as "spoke 2-fold events"). These are often routinely rejected together with the randomly incident Cerenkov light from hadronic cascades. To summarise, a fire pattern such as that labelled (i) in figure 5.2a is accepted for analysis, pattern (ii) *could* be due to a γ-ray primary from the source, whilst (iii) and (iv) are attributed to the cosmic ray background.

In order to investigate the prediction that "spoke" 2-folds could contribute to the γ-ray signal, the ratio of the frequency of occurrence of pattern (ii) type events to that of pattern (i) events was calculated for a selection of observations, during some of which the pulse signature of a point source was manifest. Data collected on the eclipsing X-ray binary Centaurus X-3 as it passed from orbital phase 0·7 to phase 0·85 (with respect to X-ray eclipse), were chosen for analysis. Evidence for emission at the object's 4·8 s pulse period had been found in three datafiles

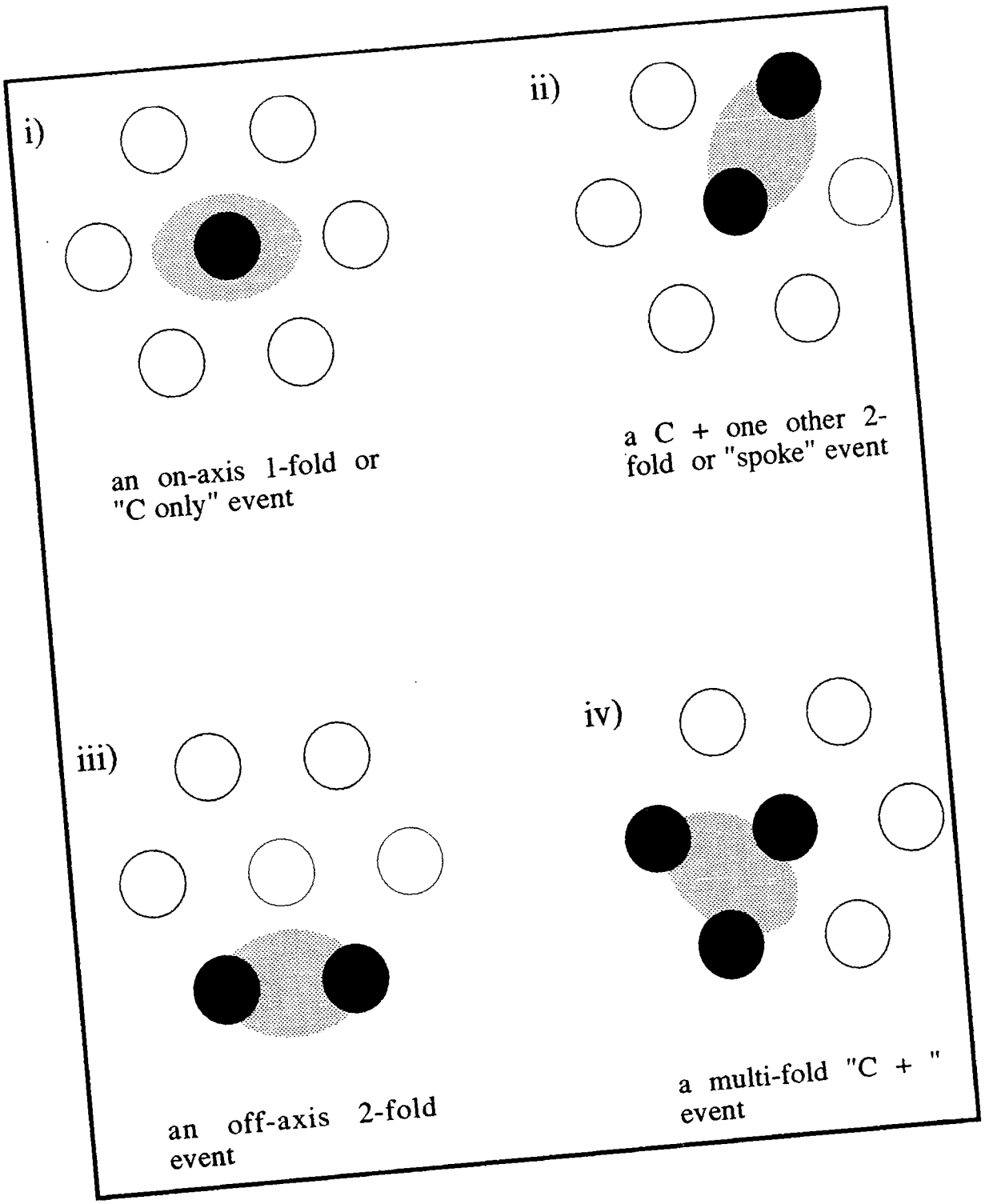

Figure 5.2a : common telescope fire patterns. The 5 mV discrimination threshold is exceeded in the channels shaded black (above) as their three constituent photomultipliers respond to similarly oriented Cerenkov images (shaded grey) at each dish.

confined to this part of the orbit (Brazier, 1991, 75). The above fire pattern ratio has been plotted, versus the mean zenith angle of each of 25 observations, in figure 5.2b. Up until 18/06/1987, the off-source monitoring system consisted only of channels 1,2 and 3 (see figure 3.2b). It was only after this date that channels 4,5 and 6 were incorporated to form the current guard ring. Points relating to data collected before June 1987 are ringed in figure 5.2b. Each datum has been classified, according to the weather summary in the observer's written log, as having been recorded under below average (cloud cover), average (no cloud, moderate sky clarity) or above average (clear skies) weather conditions. From figure 5.2b it can be seen that:

1) The introduction of channels 4,5 and 6 resulted in a decrease in the "spoke" 2-fold fraction. It is clear that a significant proportion of the events attributed to spoke 2-folds in the early three off-axis channel system were, in fact, large off-source events, such as that in figure 5.2a(iv). The full guard ring is therefore performing as desired.

2) Sky clarity does not have a systematic effect upon the "spoke" 2-fold fraction.

3) The "date-stamped observations" thought to contain a γ-ray signal do not include a disproportionate number of events recorded by the central channel only. A large deviation from the norm would be surprising, given that the number of pulsed events is not expected to exceed ~1% of the cosmic ray background count rate in this system.

There is some slight indication that the "spoke" 2-fold fraction falls off with increasing zenith angle. Since the altitude of the target object is not a linear function of time and the observations were of varying duration, the zenith angle values in figure 5.2b are only approximate.

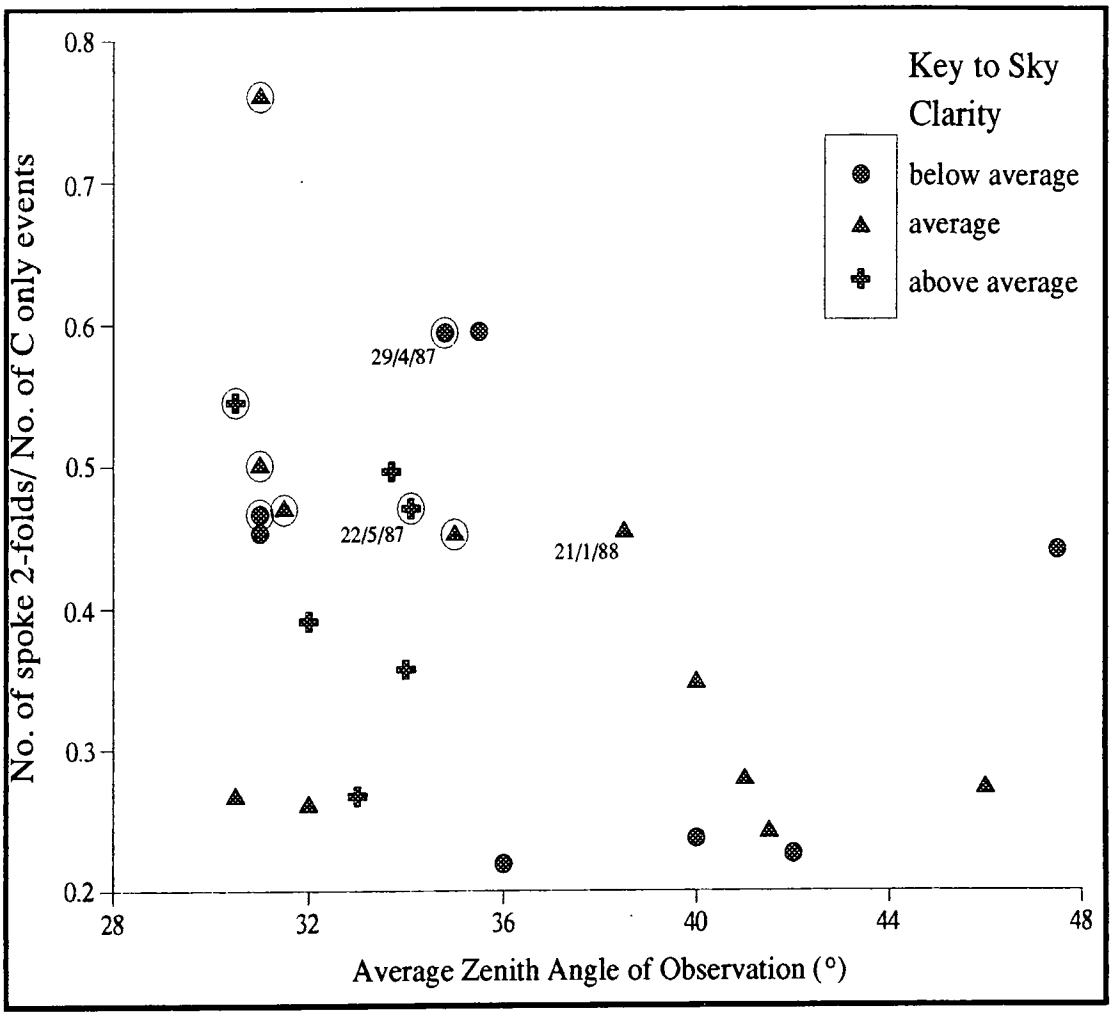

Figure 5.2b : the ratio of "spoke" 2-fold events to events triggering the central channel only, plotted versus the mean zenith angle for 25 observations of Cen X-3 taken with the Mark III telescope. Points corresponding to data obtained before channels 4,5 and 6 were incorporated into the guard ring in June 1987 are circled. The three individually labelled points correspond to those datafiles in which the Cen X-3 pulse period has been identified.

Air showers initiated by primary particles of the same energy will maximise after having traversed equivalent depths, regardless of their angle of incidence to the top of the atmosphere. Cascade maxima which appear low in the sky will therefore lie at a greater distance from a detector than those of smaller zenith angles. This being the case, Cerenkov flashes arriving from large zenith angles will tend to form increasingly narrow elliptical images at the detector, and will be less likely to trigger both the on-axis channel *and* the guard ring as a consequence. This effect, together with the atmospheric attenuation of the light flash along a lengthening path from the shower maximum to the detector, result in an effective increase in the threshold energy of the instrument as it tracks a celestial object from its culmination down towards the horizon.

Brazier (1991, 58) showed that in a single datafile, as the target zenith angle fell from 20° to 40°, the ratio of the number of events triggering the central channel only to those including the central channel and *any* guard ring response increased from 0·51 to 0·67.

With the advent of the AE Aquarii "burst" (cited in sections 3.5.4 and 4.2) came the opportunity of assessing the "spoke" 2-fold fraction for a sample known to be rich in γ-rays. Figure 5.2c illustrates the increase in the ratio of the frequency of "spoke" type events to that of 2-fold events of any orientation during the burst. Also shown is the ratio of the frequency of C only events to that of 1-fold events recorded on any channel. The most prominent peak indicates that a fraction of the γ-ray signal took the form of "spoke 2-fold events". Further evidence to suggest that the γ-ray triggered events were not confined to the central channel was presented by Bowden et al. (1992), who found that data taken on AE Aquarii did not respond well to the pulse integral threshold selection technique described overleaf.

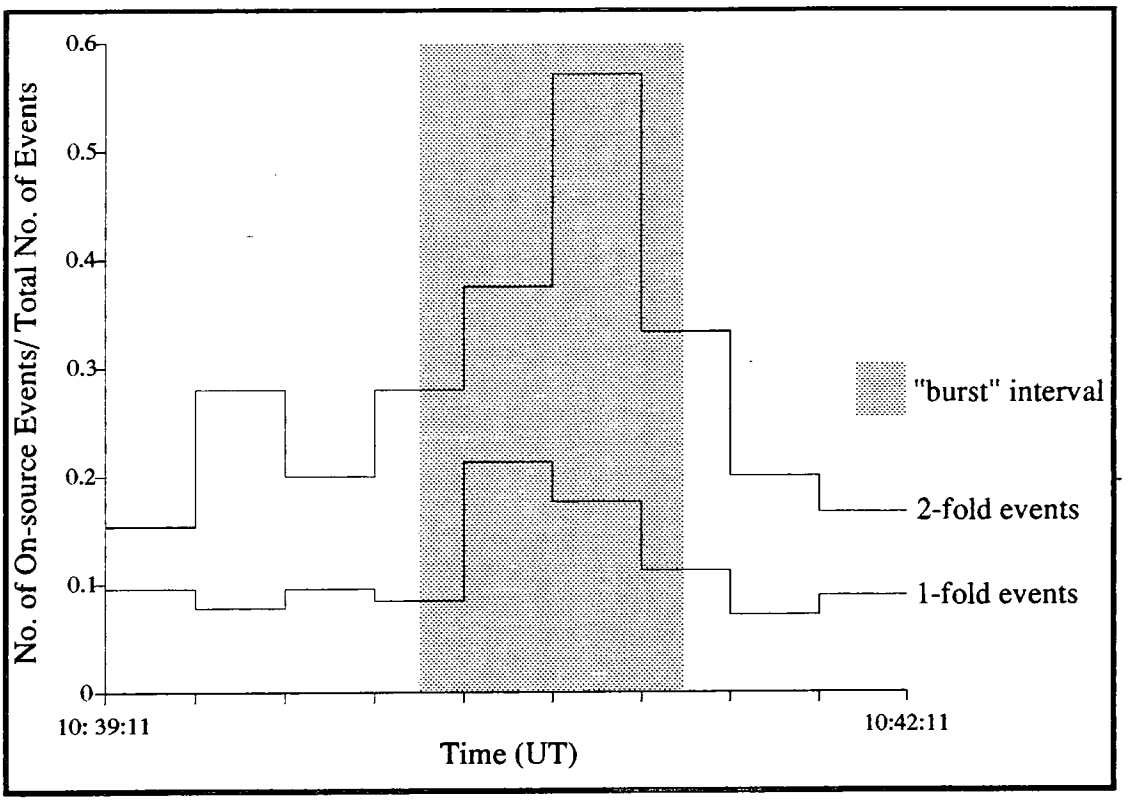

Figure 5.2c : the ratio of "spoke" 2-fold events to the total number of events triggering any combination of two channels, during the burst of activity from AE Aquarii detected on 13/10/1990. The number of events triggering the central on-source channel only is also shown, as a fraction of the total number of 1-fold events recorded.

5.2.2 pulse integral threshold selection

The efficiency of the aperture rejection method of background noise discrimination is limited by its rigid selection criterion which does not make use of all the available information. Any light flash which causes the voltage of three tubes forming a guard ring channel to rise above 50 mV is considered to have fallen off-axis. As a result, an unusually energetic primary particle arriving from the on-axis direction will be summarily discounted if the extended air shower which it creates is large enough to trigger one or more of the guard ring channels, as well as the central one. Conversely, small, off-axis showers may *just* trigger an on-axis response and fail to fire what may be a marginally less sensitive guard ring channel.

The pulse integral threshold selection technique was developed by Brazier (1991) to make use of the information on the heights of the Cerenkov pulses arising in each photomultiplier tube (the QT readout described in section 3.2.4), which was already documented as a quality control measure. At the fire pattern selection stage of the data processing routine (see section 4.1.3), an option has been introduced which allows events in which the central channel took part to be selected on the basis of the pulse height recorded on the guard ring channels *relative* to the intensity of the on-axis response.

The pulse integrals are digitised and recorded as bits. The "QT spectra" (histograms of the number of Cerenkov pulses reaching a given time-integrated charge threshold for each individual PMT) are unimodal and may therefore be normalised to allow for the differing gains of the tubes, by adding or subtracting a pedestal so that the modal pulse sizes coincide. The normalised pulse integrals from the three tubes forming a single channel are averaged. The relative amplitudes of these mean pulse integrals are a direct measure of the fraction of an air shower's light falling on one particular channel as opposed to any other. As such, they can be used

to determine the direction of propagation of the cascade regardless of its size.

Pulse integral selection is generally applied in conjunction with the aperture rejection technique. Brazier (1991) found that once events including a guard ring response were excluded from the dataset, those remaining were almost all due to light flashes falling upon either the central channel alone, or upon the central channel, which had been triggered, plus *one* other which had failed to reach the 50 mV discrimination threshold. She therefore formulated the following rejection criterion:

Accept event if:

{each off-axis pulse height} x $\kappa\%$ $\leq$ on-axis pulse height

where κ is the chosen threshold percentage (normally of the order of 35 to 45).

As this selection is not performed in real time and is not a "hard-wired" feature of the recording electronics, it is commonly referred to as a "soft cut". Since the spectral hardness ratios of celestial γ-ray sources vary, the value of κ is chosen to be that which maximises the significance of the first detection of the object under investigation. Unfortunately, statistically significant results are not yet easily reproducible in this field. A value of κ may therefore be selected on the basis of a single, strong, rogue effect, attributable either to noise or to atypical behaviour of the target source, so that its application to further data may mask a genuine, weak signal.

The number of degrees of freedom used in perfecting the soft cut criterion for a given dataset must be included in the assessment of the statistical significance of any result.

5.3 the inter-telescope timing experiment

The University of Durham telescopes at Bohena Settlement lie at the apices of a triangle of side ~100 m (see figure 3.5a). Given the lateral distribution of Cerenkov light shown in figure 5.1b, it is therefore reasonable to assume that a single air shower from a common target direction may trigger a response from all three telescopes. Bowden et al. (1992) reported that, of the total number of events recorded during simultaneous observation of an object using the Mark III and Mark IV detectors, 25% had a common origin. It has been suggested that the ~1° angular resolution which these instruments share could be improved, without further reduction of their sensitive area (and a consequent increase in threshold energy), if the time of arrival of a light flash at each could be accurately measured. A calculation of the parallax of the point of origin of the Cerenkov light could then be performed over an ~100 m baseline.

The ASGAT telescope situated in the French Pyrennes is run on a similar principle. It consists of a set of seven Cerenkov light buckets at the centre and apices of a hexagon of side 100 m (Basiuk et al., 1991). When four or more detectors register a Cerenkov flash, a trigger pulse is generated. The time at which each device registered a response relative to the time of arrival of the trigger pulse is recorded. At the analysis stage, the direction of propagation of the Cerenkov light front is "reconstructed", in a similar fashion to that of the particle flux arriving at an extensive air shower array (see section 1.4.2(ii)). Basiuk et al. (1989) pointed out that one advantage of fast timing over the imaging technique practised by the Whipple Collaboration (mentioned in section 2.3.1(iii)) was that the field of view of the telescope could exceed the desired angular resolution, thus allowing the cosmic ray background event rate to be continuously recorded.

It was noted that the introduction of inter-telescope timing measurements would necessitate no significant additions or alterations to

the instruments already operational at Bohena Settlement. A short feasibility study was therefore set in motion, with a view to assessing the suitability of fast timing selection as an additional means to the rejection of cosmic ray background events.

5.3.1 projected time delays

The intention was to determine the point of origin of a Cerenkov flash, from a knowledge of the altitude and azimuth to which a single, "prime" telescope was pointing, and an estimate of the atmospheric depth of the parent air shower's maximum. The Mark V telescope was chosen as the reference point for these observations, as the recorded pointing direction could be modified to include information as to where the light pool was situated in the field of view of the 30 pixel camera. Given the co-ordinates of the two other telescopes relative to the Mark V, the path length to each from the shower maximum may be estimated from the simple geometrical construction shown in figure 5.3a. The relative time of arrival of Cerenkov light, from a single origin, at each telescope should reflect the radial distance, r, of the corresponding shower maximum from the projected target direction. Showers having r greater than a preset threshold value would be assumed to be due to the background flux of cosmic rays.

The atmospheric depth of the maxima of showers initiated by a γ-ray signal from the target object will vary according to the hardness of the source spectrum. Some trial values of the energy of the primary particle, E_o, were input to equations 5.1a and 5.1b in order to determine the characteristic depth of shower maximum, δ_{max}, and the corresponding difference in light travel time, Δt (assuming a refractive index of ~1·0), from the shower maximum to two detectors 260 m a.s.l. at a horizontal separation of 100 m. Given a value of δ_{max}, if it is assumed that the axis of the air shower in question is perpendicular to the ground, then the

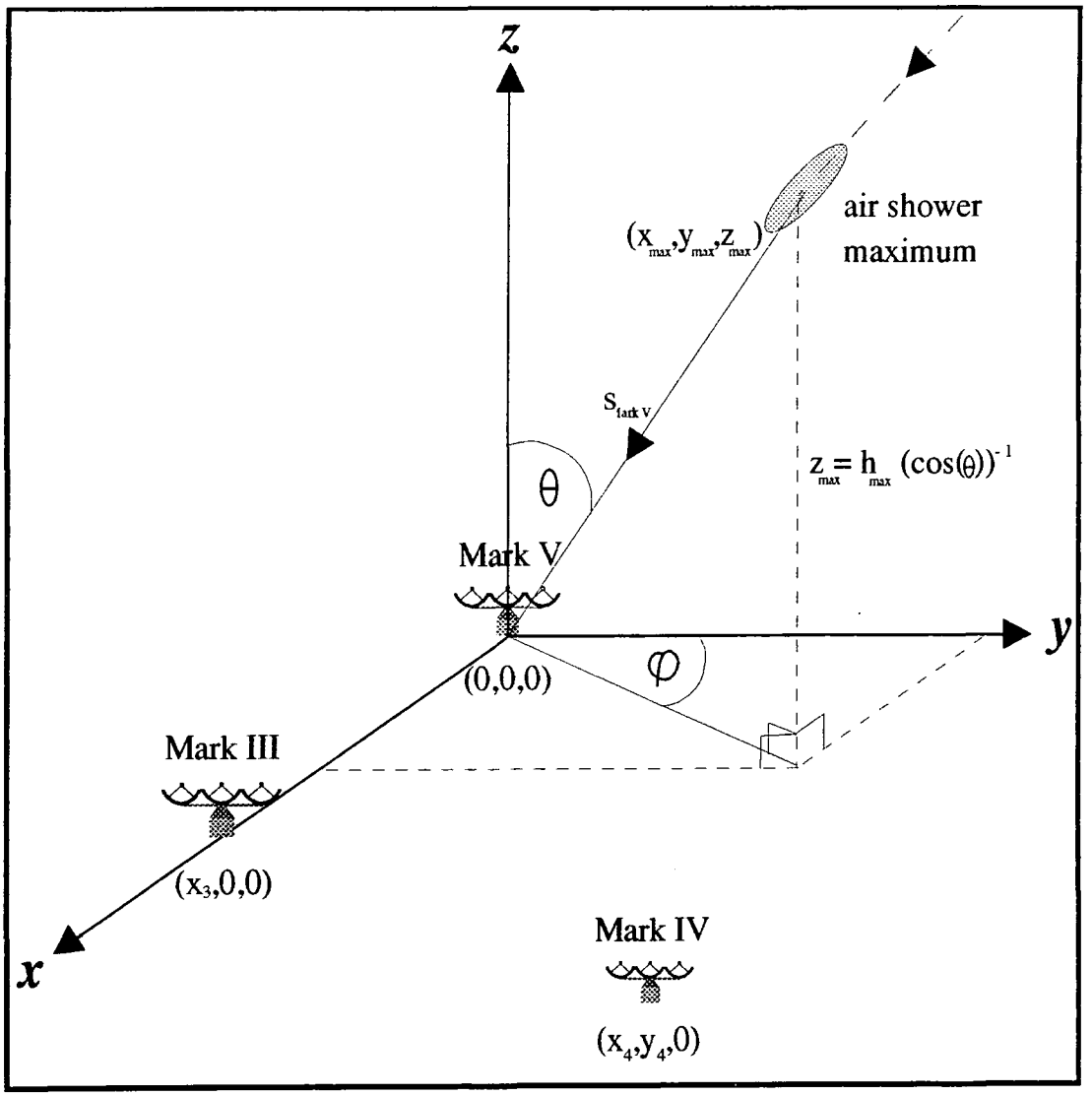

Figure 5.3a : the co-ordinate system upon which approximate calculations of the light travel time, from the maximum of an air shower to each detector, have been based. The length of the vector s_{MarkV} may be found given the attitude of the Mark V telescope (in terms of the azimuth and zenith angles shown above) and the expected height of the shower maximum, h_{max} given by equations 5.1a (or 5.1b) and 5.1c.

height of the shower maximum a.s.l., z_{max}, is equivalent to h_{max} in equation 5.1c. If the shower is incident at a zenith angle θ, then $z_{max} = h_{max}/\cos(\theta)$. From figure 5.3a, it can be seen that if the transmission vector from the point of origin of the light flash to telescope N is given by:

$$\mathbf{s}_N = \begin{bmatrix} x_{max} \\ y_{max} \\ z_{max} \end{bmatrix} - \begin{bmatrix} x_N \\ y_N \\ z_N \end{bmatrix}$$

then

$$\Delta t_{a,b} = c^{-1} \left[\left| (\mathbf{s}_N \cdot \mathbf{s}_N)^{1/2} \right|_{N=a} - \left| (\mathbf{s}_N \cdot \mathbf{s}_N)^{1/2} \right|_{N=b} \right] \qquad \text{eqn. 5.3a}$$

For ease of calculation, the detectors were assumed to lie along the x axis in figure 5.3a, with the shower maximum in the x-z plane, such that $x_{max} = z_{max} \tan(\theta)$ and $y_{max} = 0$. As can be seen from the following table, $\Delta t_{a,b}$ does not vary by more than 1 ns for shower maxima which lie along the projected target direction, at a given zenith angle, over a range of atmospheric depths.

E_o (TeV)	Primary Particle	Zenith Angle (°)	h_{max} (km)	$\Delta t_{a,b}$ (ns)
0·25	γ	65	9·7	302.66
0·25	γ	20	9·7	115.23
0·25	p^+	65	9·6	302·66
0·5	p+	65	9·0	302·70
1·0	γ	65	8·6	302·73
10	γ	65	7·0	302.87
10	γ	20	7·0	115.72

Hillas (1982) stated that 0·00767 ns should be added to the travel time of Cerenkov photons for every g cm^{-2} of path length traversed, in order to allow for the change in refractive index with atmospheric depth. Thus, a vertically incident photon may pass from a height of 9·7 km a.s.l. to 7·0 km a.s.l in [(9·7 - 7·0)/c + *1.05*] ns, where c is the speed of light in vacuo in units of km/ns. This correction does not bring the dependency of $\Delta t_{a,b}$ upon z_{max} alone to a detectable level.

As shown schematically in figure 5.3b, at infinity, the on-source field of view of a pair of University of Durham type telescopes approximates to a cone of half angle 0·5°. Protheroe and Patterson (1984) give a more detailed interpretation of the effective cross-section of two such detectors, and note that the most probable location for a light flash seen by both is midway between the two. If the telescopes and the shower maximum are again assumed to lie in the x-z plane then the path difference (s_a - s_b) in figure 5.3b is ≈ 190 m giving $\Delta t_{a,b}$ ≈ 625 ns for a light flash at the edge of the field of view. Clearly, $\Delta t_{a,b}$ = 0 for an on-axis shower at the zenith.

In conclusion, the expected delay in arrival time, $\Delta t_{a,b}$, of Cerenkov light triggered by a genuine γ-ray signal may be estimated quite simply from the telescopes' attitude, as it is not highly dependent upon E_o. A Cerenkov flash offset from the source direction by 0·5° may exceed the predicted value of $\Delta t_{a,b}$ by several tenths of a microsecond.

5.3.2 method of inter-telescope time delay measurement

A four channel time to digital converter (TDC) unit was installed in the control cabin of the Mark V telescope. When the Mark V Master Trigger unit registered an event, a "start pulse" was sent to the TDC. Channels 0 and 2 were wired to receive a "stop pulse" from the Master Trigger of the Mark III telescope whilst channels 1 and 3 were connected to the Mark IV telescope Master Trigger. The scaler counters which make up each channel

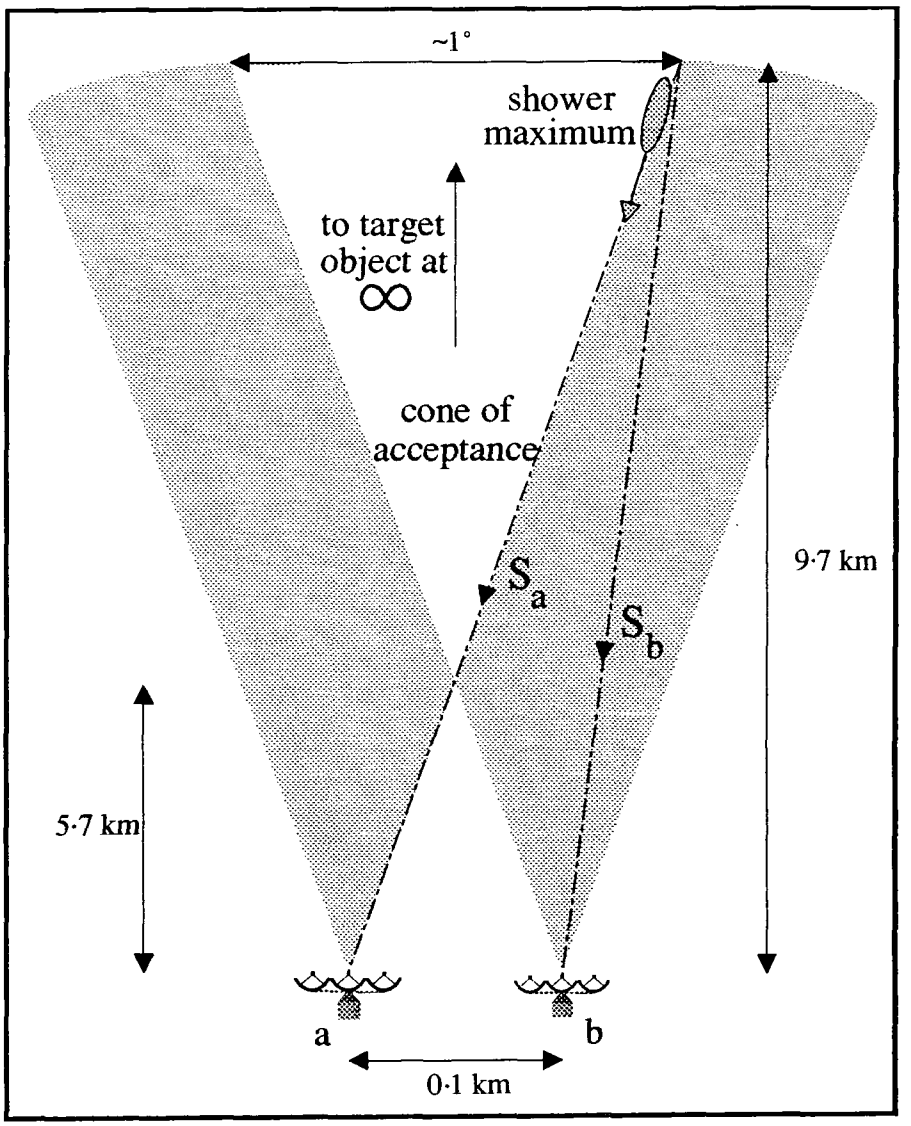

Figure 5.3b : the field of view of two University of Durham type telescopes, which approximates to a cone of half angle 0·5° at infinity (not to scale). The position of an air shower maximum which is *just* observed by both instruments is shown, at a height approximately characteristic of a 250 GeV gamma ray. The difference in path length, s_a - s_b, could be used to discriminate between gamma-ray initiated showers from the target direction, and those due to the cosmic ray background which lie at the edge of the field of view as shown here. In the above scenario, the Cerenkov light pool from the shower maximum would trigger detector a some 600 ns after having reached detector b.

continue to increment until either a stop signal arrives, indicating that the appropriate secondary telescope has registered an event, or a reset signal is sent out by the Mark V Master Trigger. The final value registered by each TDC channel is read out (in bits) by the Mark V telescope's Logger unit and incorporated into the data block (including the fire pattern, QTs and relative arrival time) recorded for the Mark V telescope event. This process is summarised schematically in figure 5.3c.

The start pulse is passed through a delay unit between the Mark V Master Trigger and the TDC, in order to *partially* compensate for the 550 ns taken by the stop signals to travel across the site from the Mark III and Mark IV telescopes. A delay of ~ 270 ns is employed, such that a light flash arriving at the Mark V telescope ~ 300 ns *after* it has reached one of the other detectors starts the TDC just before the stop pulse arrives. Each TDC channel can count from 0 to ~500 ns. A 0 to ~1000 ns range is achieved for both secondary telescopes by delaying the start pulse to two of the channels (2 and 3) by a further 500 ns. The results of the calibration of the TDC unit, performed in situ by delivering start and stop signals from pulse generators via variable delays whilst viewing both pulses on an oscilloscope, are shown in figure 5.3d.

5.3.3 data analysis and results

In Durham, eight trial datafiles (listed in figure 5.3e), were submitted to a BASIC program which performed the following routine. For each event record which included a Mark V - Mark III and/or Mark V - Mark IV time delay measurement of magnitude < 1200 bits, the pointing direction registered by the Mark V telescope's shaft encoders was combined with the telescope to telescope distances presented in figure 3.5a, to give expected values of $\Delta t_{v,III}$ and $\Delta t_{v,IV}$. A value of h_{max} of 9 km was assumed, since most events detected are triggered by primary particles having an energy close to the threshold energy of the telescopes (~250 GeV for a

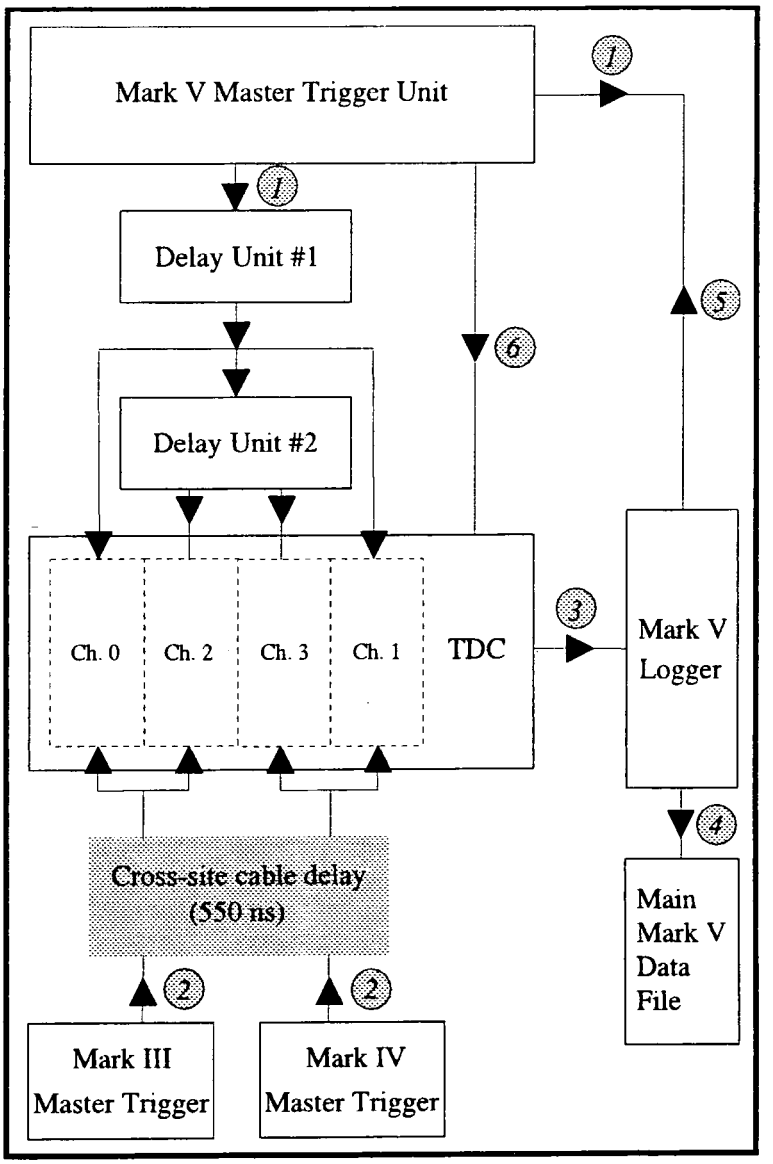

Figure 5.3c : the inter-telescope time delay measurement procedure.

1. The Mark V telescope Master Trigger registers an event and sends a "start pulse" to the Mark V Logger and to the Time to Digital Converter.
2. The Mark III and Mark IV telescopes register events triggered by the same light pool and send "stop pulses" to the TDC.
3. The TDC response is read by the Mark V Logger.
4. The Logger records the timing information to disc within the main data stream.
5. The Logger resets the Master Trigger once the event record is complete.
6. The Master Trigger resets the TDC.

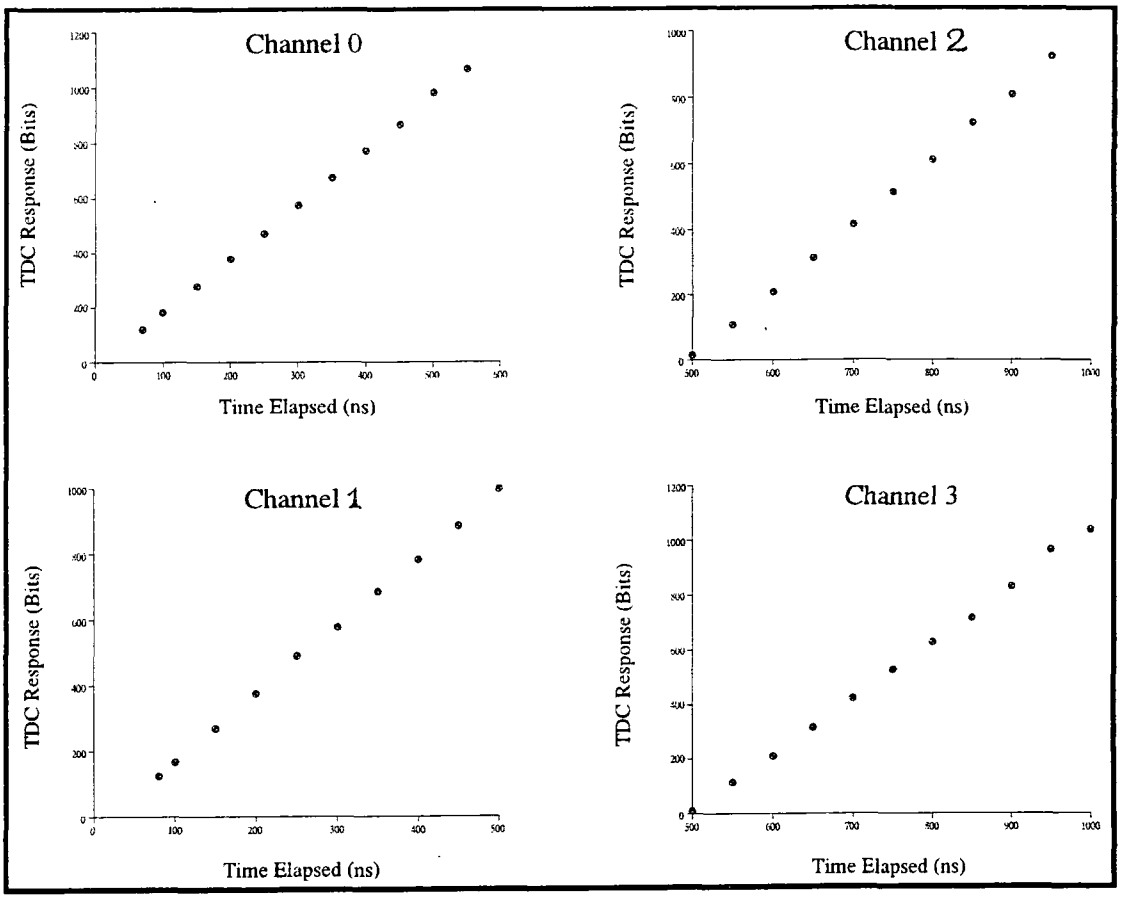

Figure 5.3d : the response curves of the four channels of the time to digital converter (TDC). Start and stop signals were supplied to the TDC unit by Pulse Generators. The actual time elapsed between the arrival of the start and stop pulses was measured by viewing them on an oscilloscope. The response of channels 2 and 3 was retarded by approximately 500 ns relative to channels 0 and 1, by passing the start pulse to the former via an extra cable delay.

γ-ray and 500 GeV for a proton) due to the inverse relationship between the cosmic ray number density and particle energy. The known cable delays were added to obtain the time delays which should actually have been registered by the TDC, denoted Δt_3 and Δt_4. Δt_3 and Δt_4 were plotted versus the appropriate TDC reading (ΔTDC_N in bits) for each event in a single observation. A regression line of the form $\Delta TDC_N = a(\Delta t_N) + b$ was fitted to the resulting scatter chart by the method of least squares described by Walpole (1982, 348).

Those events which lay within 20 bits of the line of regression for a given telescope were selected and saved to "clean" datafiles, which amounted to approximately 40 % of the original dataset.

The clean datafiles were re-submitted to the above program, so that regression lines could be fitted to the data from which rogue points had been excluded. The gradients of the regression lines were very similar from one observation to the next (see figure 5.3e), and were in good agreement with the pre-determined TDC characteristics shown in figure 5.3d. There was a correlation between the intercept at the ΔTDC_N axis and the targeted source. Since the zenith angle of each object was restricted to between approximately 45° and 55° throughout, the variable offsets must be attributed to the fact that the initial target azimuth was -20° for AE Aquarii and SMC X-1, whilst observations of Geminga were commenced at an azimuth of -200°. This behaviour, due to errors in the calculation of Δt_3 and Δt_4, is to be expected given the low accuracy with which the positions of the three telescopes are known.

A technique has been developed for selecting events recorded by the Mark V telescope which arrive at this detector within the expected time interval calculated from equation 5.3a. Do events which lie close to expectation differ from the rest in any parameter, other than their time of arrival, which may identify this well-behaved sample as γ-ray rich? The following questions were formulated. Is the measured value of ΔTDC_N related

Date (UT)	Target Source	Total No. of events		No. of events within 20 bits		Intercept at TDC axis, b (bits)		Gradient of Line, a (bits/ns)	
		Mark III / V	Mark IV / V	Mark III / V	Mark IV / V	Mark III / V	Mark IV / V	Mark III / V	Mark IV / V
22/10/1992	AE Aquarii	4428	3984	1524	1370	1078	1239	1.86	1.62
22/10/1992	Geminga	2151	1264	668	383	1043	1451	2.24	0.69
25/10/1992	SMC X-1	6582	3950	3306	1488	1253	787	1.93	1.33
25/10/1992	Geminga	2690	2093	1022	1009	1071	1384	2.15	1.00
26/10/1992	SMC X-1	3001	2633	1048	1315	1064	823	2.12	1.54
26/10/1992	Geminga	2315	1868	1030	783	1050	1396	2.18	0.97
27/10/1992	SMC X-1	1772	1601	524	777	1238	789	1.68	1.32
27/10/1992	Geminga	1133	914	239	266	999	1397	2.47	0.93

Figure 5.3e : the November 1992 inter-telescope timing dataset. The coefficients of linear fits to plots of the actual TDC output (in bits) versus the expected time delay (in ns) between the Mark V telescope and the Mark III and Mark IV detectors are shown, together with the number of events which lie within 20 bits of this line.

to:

1) The position of the Cerenkov image in the field of view of the Mark V telescope's 30 pixel camera?

2) The lateral spread of the Cerenkov image at the detector package as evinced by the PMT fire pattern?

3) The intensity of the light flash (given by the pulse integrals recorded for each tube)?

Two subsets of data were extracted from each of three observations chosen because their ΔTDC_N versus Δt_N plots were well behaved. One "good" subset contained events less than 5 bits above or below the line of regression $\Delta TDC_3 = a(\Delta t_3) + b$, and the other "bad" selection included events which lay further than 65 bits from it. The position of the centroid of the image of each light flash at the Mark V camera was estimated from the pulse integral values recorded for the 30 PMTs. This is shown relative to the centre of the field of view (in arbitrary units), for the good and bad data extracts from each observation, in figure 5.3f(i to iii). The good data appear to be more tightly clustered about the centre of the field of view at (0,0) than are the bad events. This suggests that the good timing selection has excluded Cerenkov images lying far off-axis. More data is required to produce a conclusive result.

The calculated position of the centroid of the 30 pixel camera's image is highly dependent upon the accuracy to which the PMT pulse integrals are normalised. Therefore, the effect of the timing selection was also compared with the fire pattern of the six channel guard ring, provided by the two outer detector packages of the Mark V telescope, which forms the basis of the aperture rejection technique of section 5.2.1. Sample events, which lay within a given ΔTDC_N range of each line of regression were extracted from the Mark V telescope datafile. The ratio of the number of events including

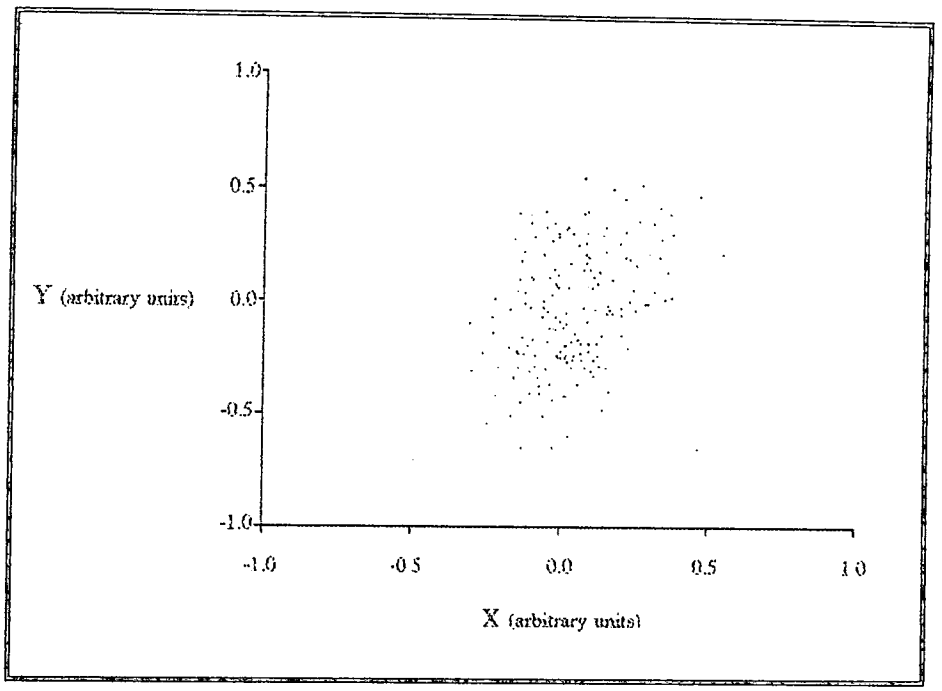

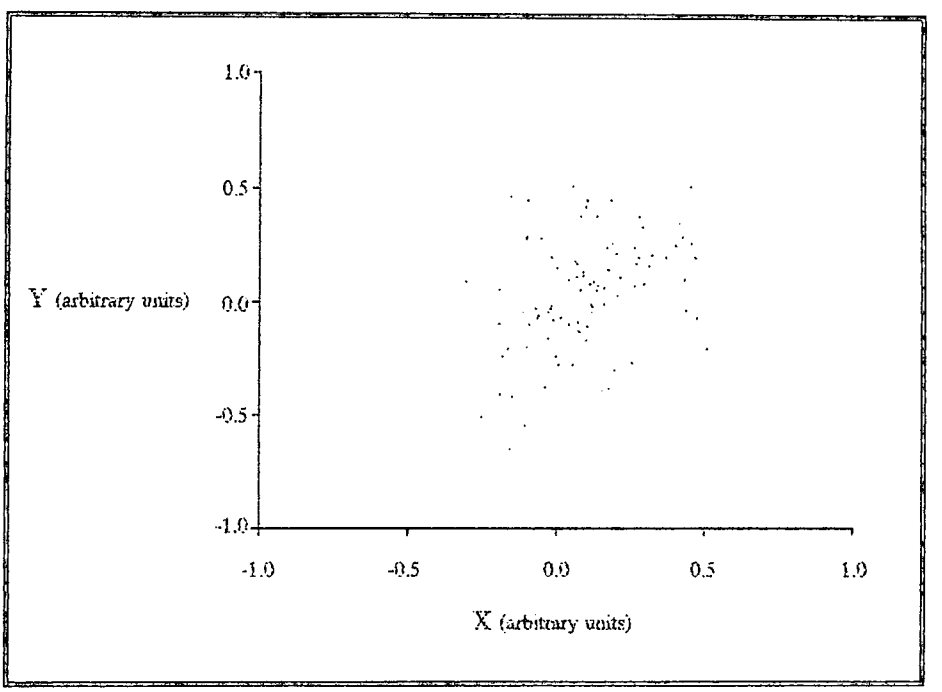

Figure 5.3f(i) : the position of the centroid of each Cerenkov image at the Mark V telescope's 30 pixel camera, in terms of orthogonal vectors X and Y measured from the centre of the field of view, for events recorded on 25/10/1992 during an observation of SMC X-1. Only those points which lay within 5 bits of the Mark V/ Mark III regression line (top) or further than 65 bits from it (bottom) are shown. Each plot was produced from 184 selected events.

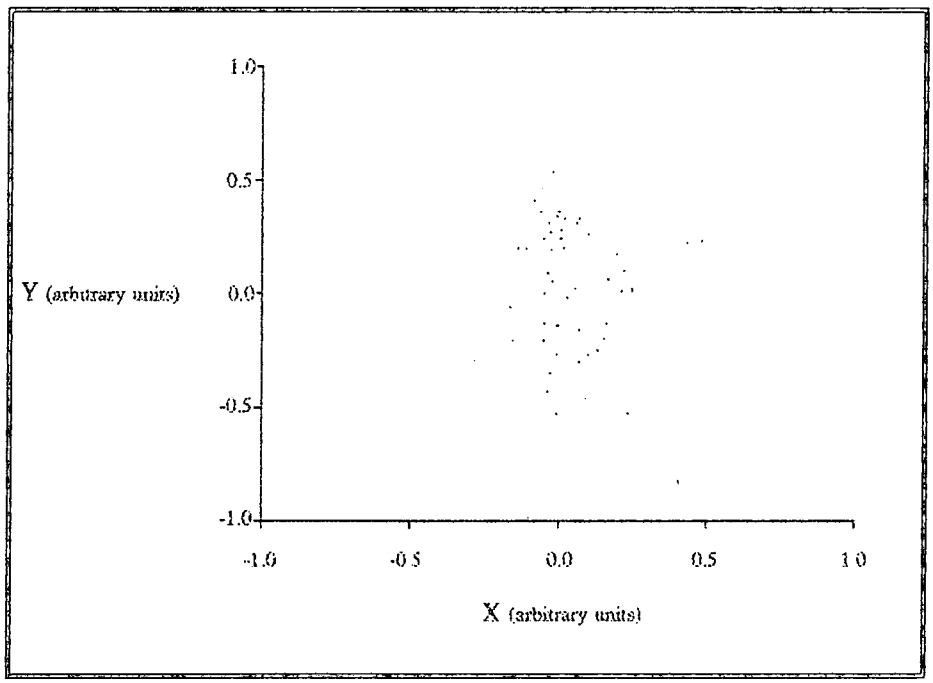

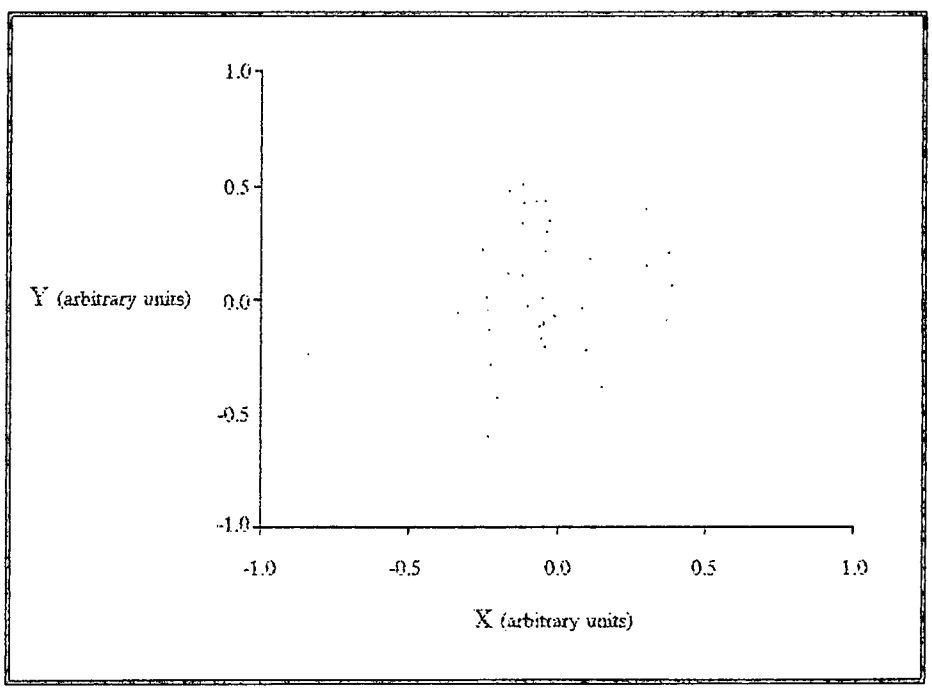

Figure 5.3f(ii) : the position of the centroid of each Cerenkov image at the Mark V telescope's 30 pixel camera, in terms of orthogonal vectors X and Y measured from the centre of the field of view, for events recorded on 25/10/1992 during an observation of Geminga. Only events which lay within 5 bits of the Mark V/ Mark III regression line (top) or further than 65 bits from it (bottom) are shown. Each plot was produced from 58 selected events.

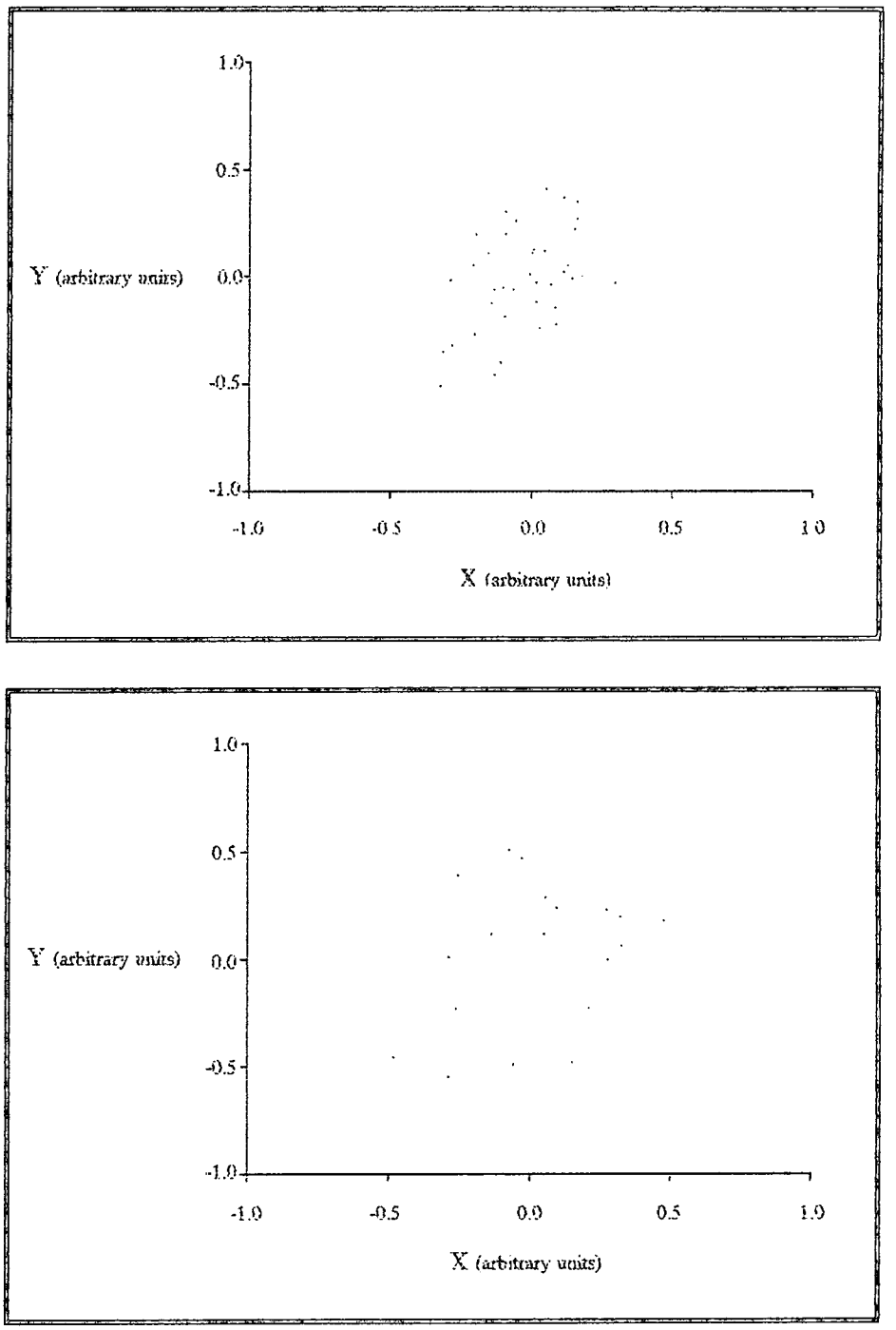

Figure 5.3f(iii) : the position of the centroid of each Cerenkov image at the Mark V telescope's 30 pixel camera, in terms of orthogonal vectors X and Y measured from the centre of the field of view, for events recorded on 26/10/1992 during an observation of Geminga. Only events which lay within 5 bits of the Mark V/ Mark III regression line (top) or further than 65 bits from it (bottom) are shown. Each plot was produced from 49 selected events.

a response from the central channel ("C+" events) to the total number of events selected was calculated. The datafile recorded on 25/10/1992 during a tracked observation of Geminga was chosen for analysis because the line of regression fitted to its ΔTDC_N versus Δt plot most closely resembled that of the "clean" file extracted from it. The results of this investigation are presented in figure 5.3g. The fraction of off-source events increased as the time delay selection criterion was relaxed.

It was thought that the Cerenkov light from events rejected as due to off-axis cosmic rays, on the basis of a large deviation from the $\Delta TDC_N = a(\Delta t_N) + b$ regression line, would be less evenly distributed between two or more detectors than that from the target direction. Figure 5.1b illustrates that the number of Cerenkov photons from a hadronic cascade is approximately halved at a radial distance from the shower axis equivalent to the ~100 m separation of the Mark III and Mark V telescopes, whilst that from γ-ray cascade is evenly distributed over this range. To test the above hypothesis, two subsets of data, the first containing events within 0·5 bits of the $\Delta TDC_3 = a(\Delta t_3) + b$ regression line and the second events lying outside the 35 bit range, were extracted from each of four Mark V telescope datafiles. These extract files and the four contemporary Mark III telescope datasets from consecutive observations of SMC X-1 and Geminga taken on 25/10/1992 and 26/10/1992 were converted to standard analysis format as per section 4.1.1. No correction was made to the event times to convert them to solar system barycentric time.

The Mark V telescope datafiles and the corresponding Mark III telescope data were submitted to a BASIC program which compared the absolute times recorded for the series of events registered by each detector. Paired events (one from each telescope) which occurred within ~100 ms of each other were assumed to have been triggered by the same light pool and were re-recorded to a new "matched" file. The matched files contained the pulse integral values recorded by the central channel of the

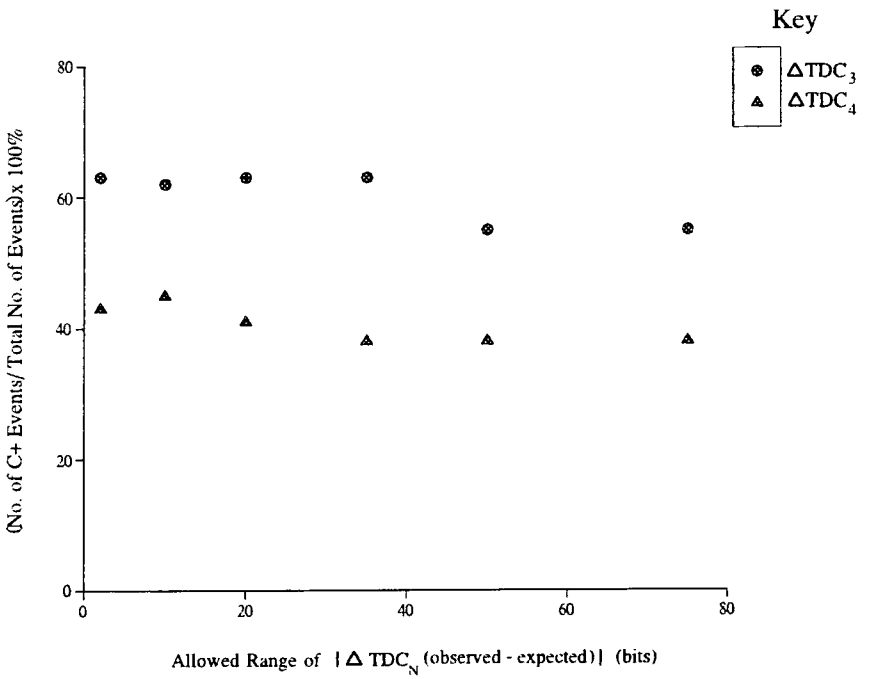

Allowed Range of ΔTDCN (observed - expected)	No. of Mark V/III events included in extract file	No. of Mark V/IV events included in extract file
0 to 2	105	153
0 to 10	694	561
0 to 20	1061	1047
all	2690	2093

Figure 5.3g : the relationship between the percentage of events in a data extract which include a response from the central channel of the Mark V telescope and the proximity to the regression line required for inclusion in the sample.

Mark III telescope and by each of the inner nineteen 1" tubes in the Mark V telescope camera. The average response of the 19 Mark V telescope PMTs (QT5) was plotted against that of the Mark III telescope central channel (QT3) for each event registered by both detectors. A linear fit was performed to the distribution obtained from each observation, again using the method of least squares. To provide a simple comparator of the amount of scatter in $QT3_j$ about the line of regression, $\Delta QT3_j$, for "good" and "bad" data extracts from the same observation, the following expression was evaluated for each:

$$\xi = n^{-1} \sum_{j=1}^{j=n} (\Delta QT3_j)^2 ((\Delta QT3_j)^2 + (\Delta QT5_j)^2)^{-1/2}$$

where n is the total number of events in the extract and event j lies at a perpendicular distance of $\frac{(\Delta QT3_j)\ (\Delta QT5_j)}{((\Delta QT3_j)^2 + (\Delta QT5_j)^2)^{1/2}}$ from the line of regression of the form QT5 = a(QT3) + b.

QT5 and QT3 are recorded in bits from the telescopes' QT units (see section 3.2.4). Since the responses of the two systems are not identical, ξ, which is tabulated below, is given in arbitrary units.

The time taken for an output pulse from a PMT to exceed the 50 mV trigger level at the QT unit will vary slightly according to its magnitude. Cerenkov pulses of all sizes approximately conform to the profile shown in figure 5.1c. The response time of a charge to time converter which is triggered by the leading edge of such a pulse will therefore decrease with increasing pulse height. A greater value of ΔTDC_3 is therefore to be expected for Cerenkov flashes which are brighter at one telescope than at the other as compared to those for which QT5 = QT3. Since the overall rise time of each QT unit is of the order of 2 ns, approximately equivalent to the 1 bit ΔTDC_N resolution available, this instrumental effect should not dominate any apparent QT5/QT3 - ΔTDC_3(observed - expected) relationship.

Date (UT)	Target Source	|Obs.-Exp.| ΔTDC3 (bits)	No. of Events	ξ
25/10/1992	SMC X-1	< 10	212	36
25/10/1992	SMC X-1	> 35	175	94
25/10/1992	Geminga	< 10	52	20
25/10/1992	Geminga	> 35	53	94
26/10/1992	SMC X-1	< 10	90	32
26/10/1992	SMC X-1	> 35	76	21
26/10/1992	Geminga	< 10	42	25
26/10/1992	Geminga	> 35	45	39

The above values of ξ indicate that some events which do not conform to the expected distribution of arrival times also give rise to anomalously large pulse integrals at one detector relative to those at another.

5.3.4 conclusions and recommendations

A method of measuring the relative time of arrival of a Cerenkov flash at each telescope has been established at Bohena Settlement. The results of initial trials have shown qualitatively that, as predicted, these timing measurements bear some relation to the intensity, lateral spread and position of Cerenkov images at the detector packages. The configuration of these photomultiplier arrays is based principally upon the results of computer generated shower simulations. The actual relationship between the relative times of arrival of a Cerenkov flash at multiple detectors and the intensity and lateral distribution of the light pool is not well-determined. Until reproducible detections of celestial objects are obtained, preferably from sources which exhibit an identifying γ-ray pulse signature, it will not be possible to say for certain what are the true characteristics of a γ-ray initiated flash (as opposed to that from a hadronic cascade). More inter-telescope timing data, ideally containing a

well-documented γ-ray signal is required.

Inter-telescope timing measurements are important as information is gathered which may be used to refine theoretical models of air shower propagation which, for individual events, is not dependent upon the choice of tube configuration. Narrowing the cone of acceptance of an atmospheric Cerenkov telescope by performing a time-of-arrival based event selection is a way of increasing the fraction of γ-ray initiated events retained for analysis without making assumptions as to the finer features of the Cerenkov images. Attempts to calibrate the inter-telescope timing apparatus have shown that a more accurate survey of the Bohena Settlement site is required. This measurement, which will probably be performed in the next year during trials of the stereo imaging technique mentioned in chapter eight, should simplify the data processing routine and support an estimate of the angular resolution which may eventually be achieved by inter-telescope timing.

It is too early to comment upon the true worth of either inter-telescope timing or of the stereo imaging technique as methods of cosmic ray background rejection as both are still in the early stages of their development. If, as simulations suggest, the positions of light flashes in the multiple PMT cameras' fields of view are better correlated with the relative times of arrival for γ-ray primaries than for hadronic showers, then the parallel development of imaging criteria and accurate inter-telescope timing may lead to a robust, hybrid technique of cosmic ray background event rejection. The application of an initial "timing cut" could greatly reduce the volume of data to which the complex imaging selection must be applied.

CHAPTER SIX

Cataclysmic Variables as Sources of VHE γ-rays

In this chapter, the case for including Cataclysmic Variables in the category of potential γ-ray sources is reviewed. Observations of Cataclysmic Variables by the atmospheric Cerenkov technique are documented including detailed results of the analysis of data taken on three such systems by the Durham group.

6.1 an introduction to Cataclysmic Variables

The history of Cataclysmic Variable (CV) studies has been recounted by Payne-Gaposchkin (1977) who was in part responsible for this nomenclature. These "stars" were subject to sudden brief episodes of high luminosity reminiscent of supernovae. Unlike supernovae they were seen to recover from this explosive activity, hence the term "cataclysmic" which whilst it describes a great outflow of energy does not necessarily imply finality.

It has been shown, principally through radial velocity measurements at optical and ultraviolet wavelengths, that all CVs are close binary systems the peculiar properties of which are due to the transfer of mass from a late-type star to a white dwarf. It is the great abundance and proximity of these objects relative to other probable particle acceleration sites which encourages atmospheric Cerenkov astronomers to include them in a search for VHE γ-rays. The presence or otherwise of γ-ray emission could prove decisive in the choice between the quite detailed models of these nearby systems which have already been formed through extensive studies at other wavelengths.

6.1.1 the formation of degenerate stars

X-ray binary systems (XRBs), which are similar in geometry to CVs

except that the degenerate component is a neutron star rather than a white dwarf, have been established as γ-ray sources. The relative abundances of CVs and XRBs may be largely attributed to the conditions required for degenerate star formation.

When nuclear burning ceases, a star of mass less than four times that of the Sun will collapse to form a white dwarf of 0.01 solar radii. The white dwarf cannot exceed the Chandrasekhar mass limit of 1.4 solar masses, at which electron degeneracy pressure just balances self-gravitation. A neutron star, $^{1}/_{1000}$ th of the size of a white dwarf and having up to three times its mass, is formed in the collapse of giant stars of between 4 and 10 solar masses. The birthrate and number density of white dwarfs and neutron stars given in the following table are taken from Shapiro & Teukolsky (1983) as are the typical stellar surface gravitational potentials of importance to any accretion mechanism.

stellar type	$g_{surface}$ ($J\ kg^{-1}\ /\ c^2$)	galactic birthrate (yr^{-1})	number density (pc^{-3})
white dwarf	$\approx 10^{-4}$	0·16	$1{\cdot}5\times10^{-2}$
neutron star	$\approx 10^{-1}$	0·021	$2{\cdot}0\times10^{-3}$

The ratio of white dwarf to neutron star number densities is echoed in Ritter's "Catalogue of Cataclysmic Binaries, Low-mass X-ray Binaries and Related Objects" (Ritter, 1990) in which 168 cataclysmic variables are listed beside only 36 low-mass x-ray binaries. Note also that the dissociation of a binary system is more likely to occur when one component collapses to form a neutron star than it is at the birth of a white dwarf.

Polarimetric and spectroscopic observations of isolated white dwarfs have revealed surface magnetic field strengths, B_S, of up to 5×10^{8} G (Lasota, Hameury & King, 1989). The average flux strength of these objects is therefore within an order of magnitude of that attributed to neutron

stars, for which $B_s \approx 10^{12}$ G, since magnetic flux = $\pi r^2 B_s$, where r is the stellar radius. A common originating mechanism may therefore be inferred for the magnetic fields of both stellar types. Theory suggests that these fields are formed in the convective carbon burning cores of parent stars before their collapse. It follows therefrom that the white dwarf population, formed from less massive progenitors than neutron stars, contains a correspondingly smaller fraction of strongly magnetised bodies, as is indeed seen to be the case (Angel, 1978). However, it is reasonable to assume that at least a few CVs can support the magnetic field related particle acceleration mechanisms which are thought to engender γ-ray emission in x-ray binary systems.

6.1.2 the cataclysmic variable population

CVs were originally classified in terms of the frequency of occurrence of their "eruptions" and the associated increase in visual magnitude. This scheme is summarised in the table overleaf (after Robinson, 1976). The novalike variables, although never seen to erupt, are included in the cataclysmic variable "genus" as their spectra are very similar to the post-eruption classical novae.

Since the introduction of this terminology, both observers and theoreticians have found it increasingly useful to identify CVs in terms of the strength of the white dwarf's magnetic field, since this factor is significant in determining the geometry of the system and its emission spectrum. To this end, two sub-divisions of novalike systems have been introduced; "AM Her type" or "polar" objects in which the presence of a strongly magnetised white dwarf is irrefutable given the strength of polarisation in their optical output, and "DQ Her type" or "intermediate polar" systems in which the white dwarf magnetic field is not directly quantifiable in this manner because of obscuration by intervening material, but may be inferred from the total power output of the system.

class	amplitude (mag.)	recurrence time	est. energy release per outburst (ergs)
novalike (NL)	_	never seen to erupt	_
classical novae (N)	9 – >14	one eruption	10^{44} - 10^{45} +
recurrent novae (RN)	7 – 9	10 – 100 years	10^{43} - 10^{44}
dwarf novae (DN)	2 – 6	10 – 500 days	10^{38} - 10^{39}

For comparison of the absolute luminosities of the various CV classes, in order to make an assessment of relative accretion rates etc., distance determination is required. Individual CVs do not always return to the same minimum luminosity between outbursts. Attempts to estimate the mean minimum light absolute magnitude for such complex systems are unlikely to result in the construction of an accurate distance scale. Few CVs are within the range of parallax measurements. White dwarfs, having reduced radii, cool by radiating principally at ultraviolet wavelengths (Liebert, 1980); thus in the infrared region the non-degenerate secondary star is predominant. Bailey (1981) has shown that measurements of the colour of the secondary star and its apparent surface brightness may be combined with a knowledge of the binary orbital period in order to form a distance estimate.

Given an approximate distance, it is possible to calculate the total energy output during a nova outburst episode. Cordova and Mason (1983) state that between 10^{38} and 10^{39} ergs are emitted during a dwarf nova outburst whilst classical novae may release more than 10^{44} ergs. They also remark that for a given dwarf nova, the energy of such an outburst is proportional to the time taken to return to minimum light, Δt. This relaxation time is also a function of the binary orbital period. Such behaviour supports a model in which Δt is the time taken to empty a disc of accreted material surrounding the white dwarf, the size of which is limited by the orbital geometry.

6.2 mass transfer in binary systems

An excellent review of spectroscopic and photometric observations of CVs has been given by Warner (1976). In some systems, spectroscopy has revealed two sets of Doppler shifted emission lines, the first simply representative of the binary's orbital motion, and the second due to rapid rotation of an emission region near to the white dwarf. Variations in visual magnitude are dominated by a "hump", present throughout approximately half of the orbital cycle, the principle component of which is a continuum source upon which emission lines of hydrogen, helium and calcium are imposed (Robinson, 1976). These phenomena are best described by models in which the CV light curve is dominated by emission from accreting material surrounding the white dwarf which is regularly eclipsed by the donor companion star.

Many CVs have been identified as strong EUV and soft x-ray sources. Their power in this region is indicative of mass transfer from the secondary to the compact primary. The gravitational potential energy of infalling matter is given up during rapid deceleration at or near the surface of the white dwarf. This energy is principally re-emitted as blackbody radiation of characteristic temperatures of $\geq 10^5$ K, whereas the effective temperatures of most isolated white dwarfs lie in the range 5000 to 50,000 K (Angel, 1978).

Subsequent photon-electron scattering at the stellar surface is expected to give rise to an upward force upon further incoming particles, through Coulombic interactions between scattered electrons and this proton rich material. The surface luminosity cannot exceed the Eddington limit at which this outward radiation pressure balances the attractive gravitational force. A simple test of the mass transfer assertion is therefore to look for such a cut off in the source spectrum. This argument may be applied to x-ray binary systems. These display effective blackbody temperatures of up to 10^7 K consistent with accretion onto a neutron star.

Shapiro and Teukolsky (1983) noted that the x-ray sources of known distance observed by the Uhuru satellite conformed to this cut off behaviour. A derivation of the Eddington limit may be found in Longair (1981).

6.2.1 stellar wind accretion

The simplest scenario for mass transfer in a binary system consisting of a degenerate primary and a main sequence or red giant companion star, is one in which the gravitational attraction of the former enables it to trap a passing fraction of the latter's stellar wind. This phenomenon is illustrated in figure 6.2a (after Shapiro & Teukolsky, 1983).

A particle of mass m will be swept up by the primary, of mass M_p, if the relative wind velocity, v, does not exceed the escape velocity imposed by the star's gravity at the distance of their closest approach, r_{ca}, i.e. if the kinetic energy of the particle, $^1/_2 mv^2$, is less than its gravitational potential energy $GM_p m/r_{ca}$. The interaction cross-section is thus given by:

$$\sigma = \pi\, r_{ca}^2 = \pi\, (2GM_p/v^2)^2$$

$$\sigma = \pi \left[\frac{2\ GM_p}{v_{orb}^2 + v_{wind}^2} \right]^2$$

where it is assumed that the degenerate star follows a circular path of radius a, with an instantaneous velocity v_{orb} in the inertial frame of the system, centred upon the massive secondary, from which a wind is emitted radially having velocity v_{wind}. The accretion rate, dM_p/dt, as a function of the secondary's total mass loss rate, dM_s/dt, is described by:

$$\frac{dM_p}{dt} = \frac{dM_s}{dt} \left[\frac{\sigma}{4\ \pi a^2} \right]$$

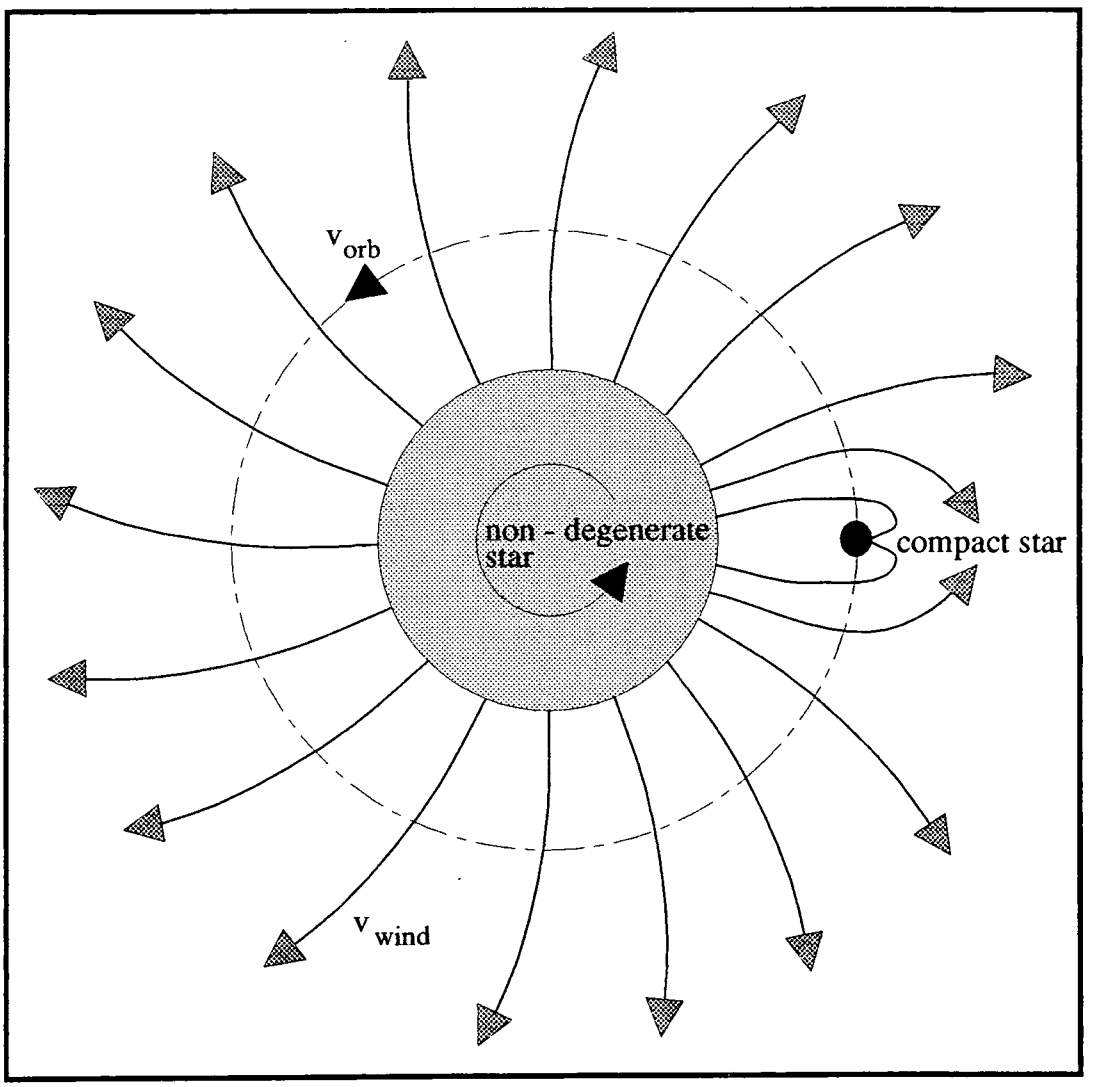

Fig. 6.2a : mass transfer from the secondary star to the primary via a stellar wind.

This expression assumes that dM_s/dt is uniform over the donor's surface. However, if the rotation of the secondary is synchronous with the orbital period, feedback may occur; a unique area of the secondary is thus exposed to radiation from the primary, the mass outflow from this point is then enhanced as a consequence of this preferential heating.

Shapiro and Teukolsky (1983) state that dM_p/dt is typically 0.1% or less of dM_s/dt for accretion onto a degenerate star. Assuming a loss rate of 10^{-6} solar masses per year for an upper main sequence companion, $dM_p/dt \approx 10^{13}$ kg s^{-1}. If the surface gravity of a white dwarf given in section 6.1.1 is assumed, the accretion power is approximately 10^{26} W or 10^{33} erg s^{-1}. This simple model of radial infall is unable to account for the observed steady state luminosity of the brightest CVs. For example, the novalike object AM Her has been seen to emit consistently at a rate of $\geq 10^{34}$ erg s^{-1} (Tuohy, Mason, Garmire & Lamb, 1981). Also, some other mechanism must be invoked in order to account for the "outburst" phenomenon.

6.2.2 mass transfer by Roche lobe overflow

The un-trapped stellar wind carries angular momentum out of the system. In addition to this particle ejection, gravitational radiation is emitted. Gravitational waves set up as the stars distort their surroundings carry away energy and momentum. Thus, the binary orbit gradually shrinks. It is not uncommon for the secondary star to be seen to be rotating synchronously with the orbital period. Tidal interactions between the two components promote both this co-rotation and a circular orbit. Linkage of the secondary's magnetic field to its stellar wind, which tends to be swept back as shown in figure 6.2a, may assist tidal forces by contributing a retarding torque (Eggleton, 1976).

For a binary system in which the companion star is in synchronous rotation with the orbiting compact primary, lines of gravitational

equipotential may be drawn about the two as in figure 6.2b (also after Shapiro & Teukolsky, 1983). The innermost shared equipotential surface is the boundary of the "Roche lobes". The saddle point on this surface on the line of centres of the two stars is known as the inner Lagrangian point, L_1. Clearly, the dimensions of a Roche lobe are limited by the size of the orbit, and thus may be inferred from radial velocity measurements.

As the orbit tightens, L_1 approaches the surface of the secondary. This star expands to fill its Roche lobe and gas pressure causes a stream of material to flow from its surface, through L_1, and into the sphere of influence of the primary. This method of mass transfer is known as "Roche lobe overflow", and is the dominant mass expulsion mechanism in such systems (Petterson, 1983).

Roche lobe overflow is most likely to be initiated by the evolution of the secondary. The growth of the helium core of a low mass giant star coincides with the expansion of its outer hydrogen burning shell. The luminosity and radius of the star increase, driving the mass transfer mechanism. As mass and momentum are redistributed within the system, the orbit gradually widens such that the expanding donor remains contained within its Roche lobe (van den Heuvel, 1987). The validity of parameters, such as the stellar wind contribution to mass transfer, estimated on the assumption that the behaviour of the secondary is comparable to that of isolated stars in the same spectral class is doubtful. This is because large-scale mass transfer can modify the secondary's effective surface temperature, whilst its synchronous rotation may relieve some of its internal hydrostatic pressure causing a reduction in luminosity (Cordova & Mason, 1983).

The "eruptions" of some CVs may be attributed to brief episodes of mass accretion by this mechanism. According to Bath (1976), mass loss from the donor should result in the recombination of ionized material beneath its photosphere. The energy thus released promotes further mass ejection.

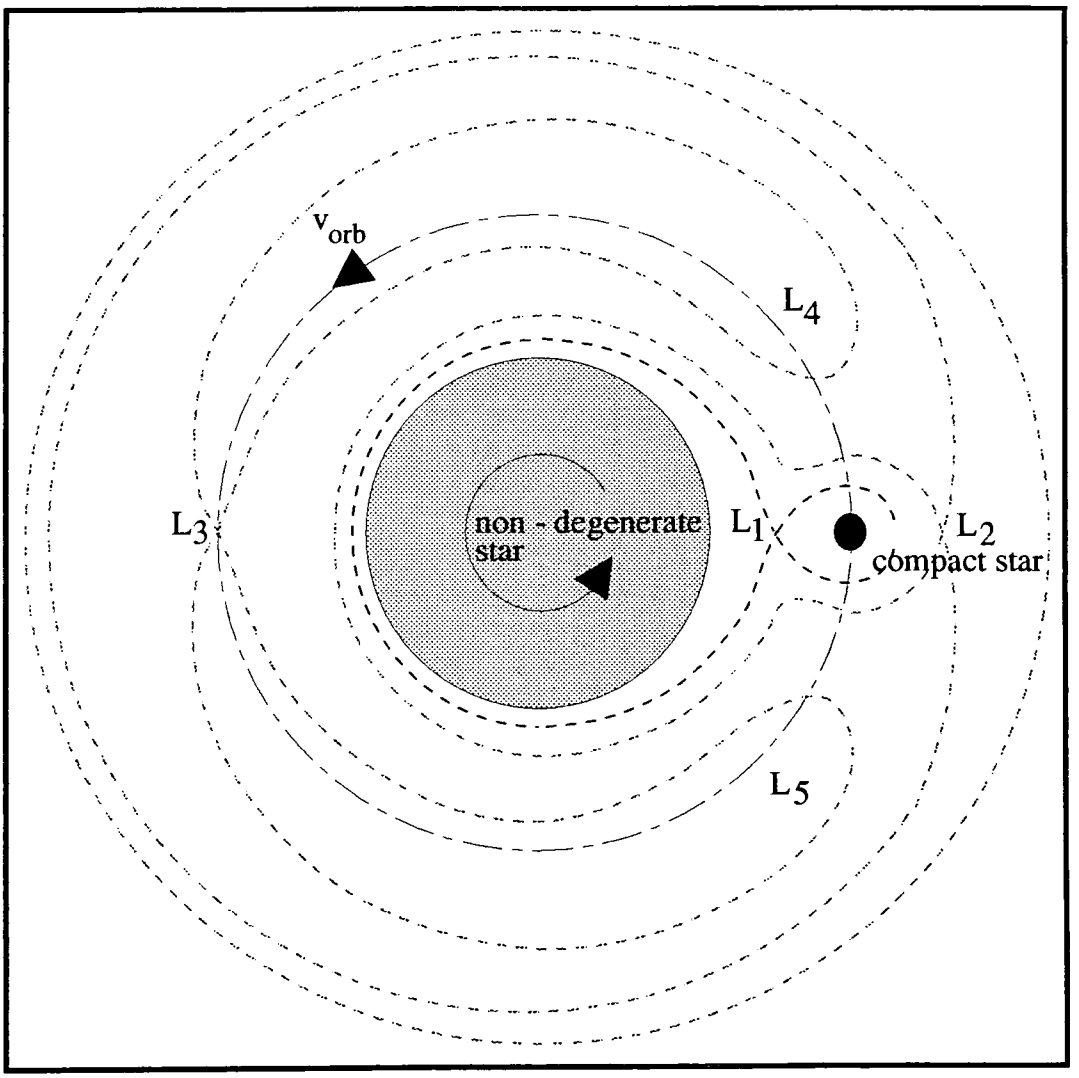

Fig. 6.2b : gravitational equipotentials in a binary system where the mass of the secondary star exceeds that of the primary. L_1 to L_5 are Lagrangian points.

If this balance is disturbed, the stellar envelope falls away from the Roche surface until its luminosity is restored by energy transport from the hydrogen burning interior. The recovery period for contact and thence Roche lobe overflow to be re-established is of the order of 10 to 200 days, comparable with the recurrence time of dwarf nova outbursts.

Recurrent novae have been found to contain, almost exclusively, secondary stars which have evolved from the main sequence onto the giant branch of the Hertzsprung-Russell diagram. Given the short orbital periods of these binaries and the stellar radii, mass transfer by Roche lobe overflow is almost a certainty (Warner, 1976). Where accretion is apparently a continuous process, a fraction of the gravitational potential energy released by matter falling onto the primary may be stored in a disc or column, until it can contribute to a large amplitude eruption.

6.2.3 production of accretion columns and discs

(i) disc formation

Although the material accreted from the stellar wind has some angular momentum with respect to the compact star, this is not sufficient to prevent its quasi-radial infall (Shapiro & Teukolsky, 1983). Equating expressions for the gravitational and centripetal forces involved gives an estimate of the minimum angular velocity, ω_{min}, required to prevent direct radial infall: $\omega_{min} \approx (GM_p/r_{min})^{1/2}$, where r_{min} is the shortest distance from the centre of mass of the primary at which a stable orbit may be maintained. This distance is equivalent to the stellar radius of a non-magnetic white dwarf and may extend to the magnetospheric boundary of others (Petterson, 1983).

The angular velocity of material ejected from the inner Lagrangian point during Roche lobe overflow generally exceeds ω_{min}. Initially, the motion of the plasma stream is perpendicular to that of the orbiting

primary. During mass transfer the primary moves on from this target position. On close approach, the plasma is deflected towards the compact star and is thrown into an orbit, the ellipticity of which is rapidly reduced through thermal energy losses. Whilst most of the matter in the resulting annulus drifts towards r_{min}, thus reducing the stored energy, a small fraction is spun outwards so that angular momentum is conserved (Petterson, 1983). This expansion will continue until mass at the inner surface falls within r_{min}, so that gradual accretion onto the star itself begins, and the outer material is near enough to L_1 to return some of its angular momentum to binary orbital motion, via tidal interaction. Incoming particles which experience a sufficiently strong shock on contact with this extended layer may carry away excess angular momentum, as they are ejected from the disc region and fall back to the secondary star or leave the system through L_2 (see figure 6.2b). Viscous stress tends to damp random motions perpendicular to the orbital plane, thus a thin disc of material is formed about the primary. Note that this disc need not lie in the compact star's equatorial plane, unless the compact star's axis of rotation is aligned with that of the binary orbit.

Clearly, this disc accretion does not lend itself to simple calculations of expected luminosity output such as those followed for wind accretion in section 6.2.1. An upper limit may be placed upon the actual rate at which mass reaches the compact star by equating its Eddington luminosity to the power released through gravitational energy loss:

$$L_{Edd} \approx \frac{GM_p}{r_p} \times \frac{dM_p}{dt}$$

where r_p is the radius of the primary star. However, it should be noted that the Eddington limit may not hold in such turbulent systems.

Mass transfer via Roche lobe overflow into an accretion disc is illustrated schematically in figure 6.2c. Angel (1978) predicts that, in a

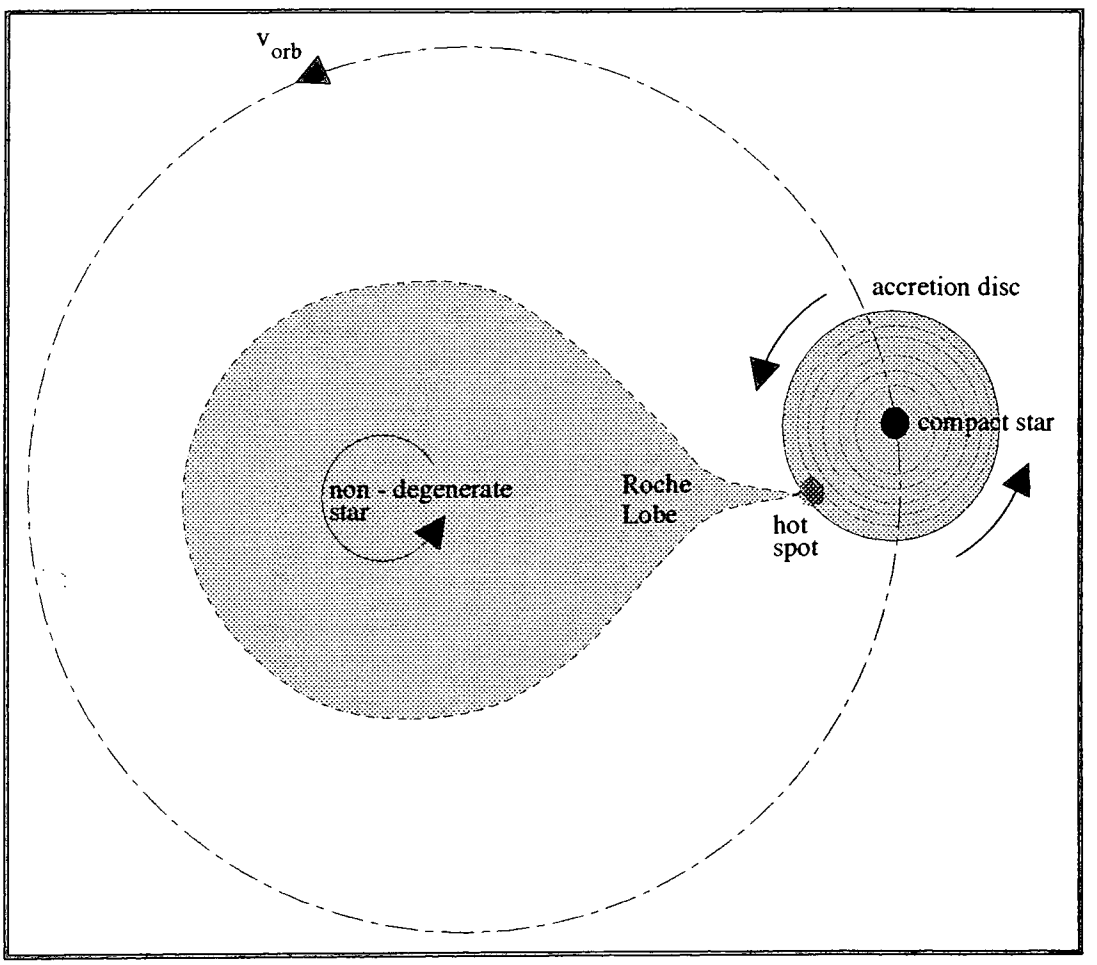

Fig. 6.2c : mass transfer via Roche lobe overflow from the secondary star to an accretion disc.

non-magnetic CV system, wherein a low mass companion donates material to the compact star at a rate of $dM_p/dt \approx 10^{-8}$ solar masses per year across a distance of a $\approx 10^{11}$ cm, an accretion disc may be formed of radius $\approx 10^9$ cm (that is of the order of one to ten times the radius of a white dwarf).

Observational evidence of the presence of accretion discs in CVs is plentiful. Unless the secondary star in the system is a giant, the optical spectrum is dominated by emission in the vicinity of the white dwarf. The geometry of this region is constrained by the symmetry of the emission line broadening, which is generally indicative of a narrow accretion disc rather than an amorphous cloud (Robinson, 1976). The "hump" in many light curves is attributed to a hot spot on the edge of the disc where it meets the plasma stream. In inclined systems, this shocked region, a strong source of continuum emission, is easily obscured because of its small relative size, hence its ~ 50% duty cycle.

(ii) accretion in a strong magnetic field

The presence of intense magnetic fields is manifest in some CVs, through the circular and linear polarisation of their optical emission, and the failure of line spectra to coincide with those predicted from models from which magnetic field effects are omitted. It was noted in section 6.1.1 that isolated white dwarfs may retain magnetic fields of up to 5×10^8 G in strength. However, studies of the AM Her type systems, which exhibit the strongest optical polarisation of all CVs, have revealed line profiles typical of Zeeman splitting and cyclotron emission which place the strengths of the magnetic fields within all but a few in the 20 to 30 MG region (Lasota, Hameury & King, 1989). These authors postulate that magnetic field strengths of $> 4 \times 10^7$ G give rise to a loss of angular momentum due to magnetic braking which results in catastrophic expansion of the orbit and negates any further large-scale mass transfer between the white dwarf and its companion.

The degenerate primary's magnetic field must be expected to have an effect upon the accretion flow of ionised material. At a distance r_A from the centroid of the compact star's magnetic dipole, the energy density inherent in the magnetic field is equivalent to that of the accreting material. r_A is known as the Alfvén radius. Ionised matter which lies inside r_A is forced to flow along the magnetic field lines. If the radial distance from the centre of the primary within which a particle may co-rotate with it, r_c, is much greater than r_A, the magnetic field cannot prevent the formation of an accretion disc (Angel, 1978).

A fundamental difference which has been observed between polar and intermediate polar systems is that the light curves of the latter class of objects generally show coherent pulsed emission. These frequencies, of the order of 0.01 to 0.1 Hz never exceed the maximum spin frequency for a rigid rotating white dwarf, and tend to include a time derivative consistent with the expected "spin-up" of such a body as angular momentum is gained through accretion. Hence, intermediate polars, in common with x-ray binaries, are assumed to contain a rapidly rotating degenerate star. No such behaviour is observed in polar CVs. It is therefore assumed that some mechanism exists in polar systems which is capable of producing a torque strong enough to combat the accretion driven "spin-up" effect, and to dissipate any angular momentum intrinsic to the white dwarf before the onset of mass transfer.

One braking mechanism sufficiently powerful to bring the white dwarf to co-rotate with the binary period is magnetic interaction between the star and its companion. For this to occur, the white dwarf's field must extend as far as the secondary. The condition $r_c >> r_A$ is almost certainly broken therefore, and it is to be expected that polar CVs will show no sign of an accretion disc. Instead, material must be funnelled along the magnetic field lines directly onto the primary's surface. The gravitational energy of matter falling towards the compact star's magnetic poles (or pole depending upon the inclination of the stellar dipole) in a field guided

accretion column does not suffer degradation to thermal wavelengths as it would within a disc. A shock front is set up in the column several white dwarf radii (r_{wd}) above the star's surface, through which matter passes and then continues its descent at subsonic velocities. The gravitational energy of the slowed material is then released via bremsstrahlung radiation in the hard x-ray region. This mechanism may be quenched within one r_{wd} of the stellar surface if $B_s \geq 10^7$ G, through cyclotron losses which give rise to optical and U.V. emission as the base of the column becomes optically thick (Rees, 1989).

6.2.4 observational implications

The optical properties of polars, intermediate polars and dwarf novae may now be explained in terms of the geometry of their accretion flow. The polarised light can escape from polar (or AM Her type) systems as they are powered by pseudo radial accretion. This polarisation is obscured by the accretion disc, with its characteristic Doppler shifted emission lines, in many intermediate polar (or DQ Her type) systems. If a partial accretion disc exists which is disrupted by the magnetic field where $r_c \geq r_A$, variations in mass transfer rate, possibly due to instability in the outer envelope of the donor star, may provoke shifts between disc accretion and pseudo radial infall, which could be the basis of some dwarf novae eruptions (Cordova & Mason, 1983). The outbursts of dwarf novae are attributed to an increase in the luminosity of the accretion disc, as Doppler shifted hydrogen absorption lines indicate that the excess emission is associated with the orbiting primary rather than the non-degenerate secondary, whilst the decay from maximum light occurs too rapidly to be linked to the cooling of the white dwarf itself. The energy release in classical nova eruptions is so great that they are thought to be due to thermonuclear runaway in the envelope of the white dwarf. Conversely, the delay between recurrent novae outbursts is reminiscent of the recovery

timescale of the late-type companion (Robinson, 1976).

6.3 VHE γ-ray emission mechanisms

Disc accretion and accretion column configurations have been described which fit adequately with observations of CVs taken across the spectrum from radio to x-ray wavelengths. Can these models accommodate any of the γ-ray emission mechanisms detailed in chapter one? If so, will the position of the emission sites allow γ-rays to escape from the CV system and reach the Earth?

6.3.1 curvature radiation

Usov (1988) applied the model of a rapidly rotating magnetised sphere, frequently cited in the description of γ-ray production by pulsars, to forecast very high energy emission from white dwarfs. His argument, valid for white dwarf magnetic fields in the range 10^6 to 10^8 G and rotation periods of the order of 10 to 100 s may be summarised as follows. The rotation of the magnetised star generates an electric field, **E**, having a non-zero component along the field lines of the magnetic dipole. Where the resultant force upon particles of charge ne at the stellar surface, neE, exceeds the star's gravitational attraction, they escape to form a magnetosphere. At a little distance from the white dwarf, **E** is screened by these charged particles, except in those regions where the cloud is penetrated by the magnetic field lines. Here electrons flowing out from the star are accelerated to relativistic speeds along the field lines and may emit curvature radiation in the γ-ray region (see figure 6.3a). The Lorentz factor of an accelerated electron is given by:

$$\gamma \approx 6\times10^{6}\left[\frac{B_p R^3}{10^{34}\ \mathrm{Gcm^3}}\right]\left[\frac{P}{10\ \mathrm{s}}\right]^{-5/2}\left[(r/R)^{1/2}-1\right] \qquad \text{eqn. 6.3a}$$

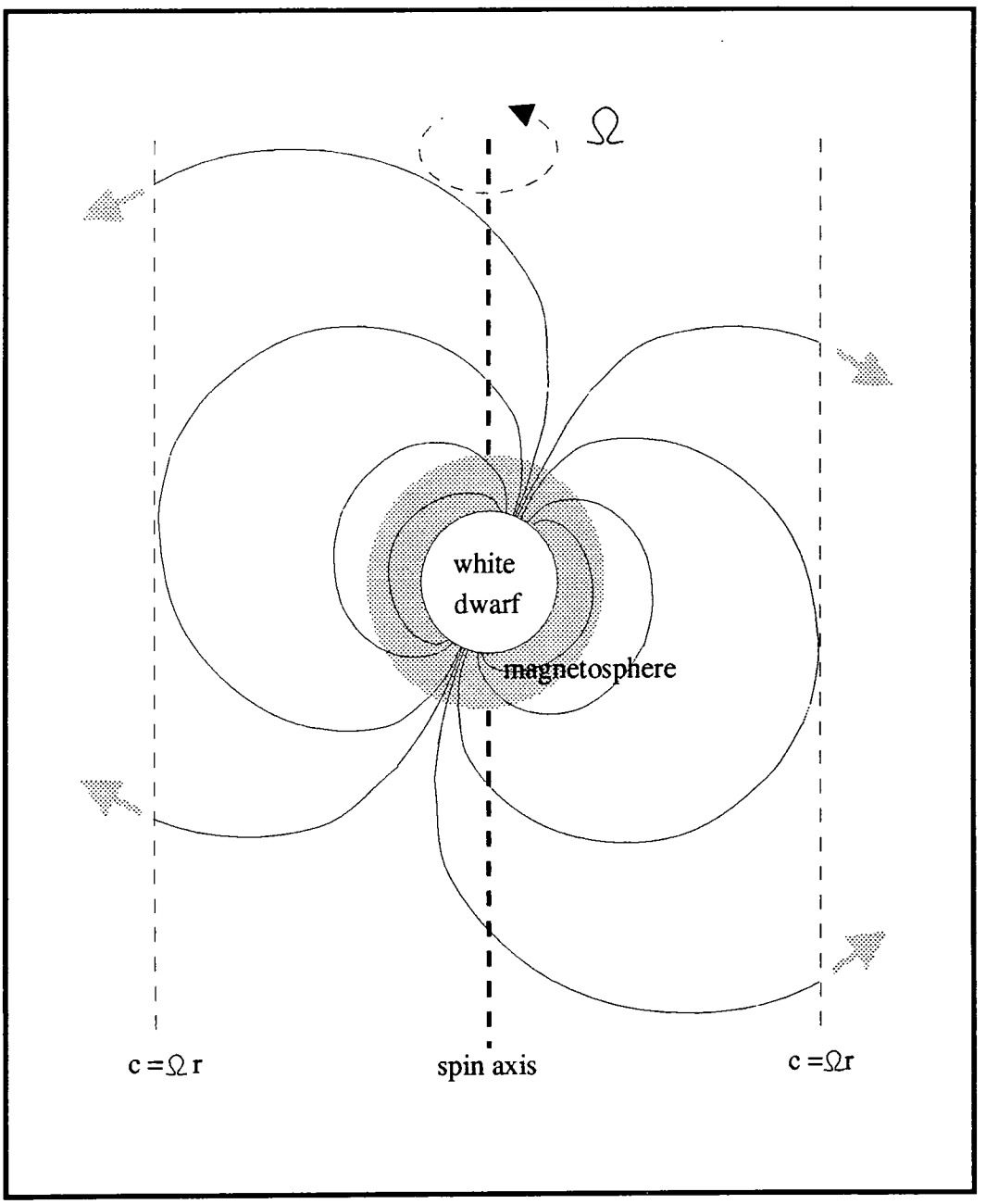

Fig. 6.3a : disposition of the magnetic field within the light cylinder of a white dwarf.

where B_pR^3 is the magnetic moment of the white dwarf of radius R, P is its rotation period and r is the radial distance to the electron. The mean energy per quantum of curvature radiation is then:

$$\varepsilon = \frac{3}{2}\,\frac{hc\gamma^3}{2\pi R_c} \qquad \text{eqn. 6.3b}$$

where R_c is the radius of curvature of the magnetic field lines, given approximately by $(cr/\Omega)^{1/2}$ where Ω is the star's angular velocity in rad s^{-1}.

It has been stated that the greatest white dwarf magnetic field strength which can be supported in a CV system is of the order of 4 x 10^7 G (Lasota, Hameury & King, 1989). Referring again to the CV catalogue of Ritter (1990), the most rapid coherent period observed and attributable to white dwarf spin is that of the intermediate polar WZ Sge at 28 s. If r is allowed to equal the radius of curvature of the last closed field line within the light cylinder ($r = c/\Omega$), then according to Usov, equations 6.3a and 6.3b combine to give:

$$\varepsilon \approx 10^7 \left[\frac{B_pR^3}{10^{34}\ \mathrm{Gcm^3}}\right]^3 \left[\frac{P}{10\ \mathrm{s}}\right]^{-7} \mathrm{eV} \qquad \text{eqn. 6.3c}$$

Thus ε for a white dwarf of $B_p = 4\times10^7$ G, $R = 10^9$ cm and P = 28 s is 0·5 MeV, whereas to obtain a flux at the 250 GeV threshold of the Mark III telescope would require $P \approx 4$ s. For comparison, 250 GeV emission from a neutron star of $B_p = 10^{12}$ G and $R = 10^6$ cm would require $P \approx 45$ ms.

This model was developed to describe an isolated white dwarf. It is of limited use in the discussion of very high energy CV emission, as those CV bound white dwarfs having the strongest magnetic fields are rapidly slowed to rotate synchronously with the binary orbital period.

6.3.2 accretion driven γ-ray production

In chapter one, it was noted that of the few objects confirmed as sources of VHE γ-rays, most are in fact x-ray binaries. Many mechanisms for γ-ray emission in these accretion driven, neutron star primary - non-degenerate secondary systems have been put forward since their detection. Hillas (1987) emphasised the fact that no single mechanism is able to account for the full range of γ-ray energies and time dependencies already observed from such systems. Chanmugam and Brecher (1985) chose to include CVs in their assessment of a model in which high energy emission from binary systems is powered by accretion rather than the rotation of a degenerate star, and found that CVs were indeed capable of producing γ-rays at ultra high energies. Some accretion driven γ-ray production models, reviewed in detail by Carraminana (1991) with reference to x-ray binary systems, are considered here in the context of CVs.

It is generally assumed that the VHE γ-rays which are observed from systems whose luminosity is maintained by mass accretion are the result of particle - particle encounters. An efficient production mechanism would encompass the acceleration of particles in the vicinity of the primary, where most of the gravitational energy of accreting material is released, and their subsequent escape and collision with target material at some distance from the compact star, where the γ-rays produced in these encounters do not decay by pair production induced by a strong magnetic field. The most promising methods by which fast particles may be obtained are summarised below.

(i) first order Fermi acceleration

Consider a shock wave propagating through a plasma with a velocity greater than the Alfvén speed in the medium. Some of the particles which lie in the path of the shock may pass through the shock front, gain kinetic

energy from the material behind it, then re-cross it bringing excess energy into the pre-shock region (Longair, 1981). This process, first proposed by Fermi (1949), is driven by the reflection of charged particles off "magnetic mirrors"; the anisotropic flow of high energy particles on either side of the front causes magnetic wave disturbances with which charged particles spiralling along field lines resonate and are reflected (Hillas & Johnson, 1990). As the shock front progresses, the kinetic energy stored in the gas ahead of the shock increases and the gas particles reach higher and higher velocities. Shock accelerated relativistic charged particles may go on to produce γ-rays through interactions with a local magnetic field or with other particles, or simply by decay as outlined in section 1.2.

Cataclysmic Variable systems provide a host of potential sites for the shock acceleration process, the most obvious being the base of an accretion column. Kazanas and Ellison (1986) were amongst the first to suggest that the kinetic energy of infalling plasma might be converted into the energy of ultra-relativistic particles by diffusive shock acceleration near the surface of a degenerate star. Hillas & Johnson (1990) raised the objection that within the Alfvén radius of such a star, the energy density of the magnetic field (W_{mag}) should greatly exceed that of the accreting material (W_{gas}), as by definition, at r_A $W_{gas} = W_{mag}$, but their radial dependencies combine such that the ratio (W_{gas}/W_{mag}) is proportional to $r^{5/2}$. If $W_{gas} << W_{mag}$ then the material cannot deform the field to provide "magnetic mirrors" and Fermi acceleration does not take place. According to Chanmugam & Brecher (1985), the Alfvén radius is given by:

$$r_A = 1{\cdot}8\times10^{8}\ B_{12}^{4/7}\ R_6^{10/7}\ (M/M_{sun})^{1/7}\ L_{38}^{-2/7}\ \text{cm} \qquad \text{eqn. 6.3d}$$

where (M/M_{sun}) is the mass of the degenerate star in solar mass units, B_{12} is its surface magnetic field strength in units of 10^{12} G, R_6 is the stellar radius in units of 10^6 cm and L_{38} is the total accretion luminosity in units of 10^{38}erg s^{-1}. These authors cite as an example the intermediate

polar V1223 Sgr, having an accretion luminosity of 5×10^{34} erg s^{-1} and containing a compact star of magnetic field strength 10^6 G. If a one solar mass white dwarf is assumed of radius $r_{wd} = 5 \times 10^8$ cm, then from the above expression, $r_A \approx 8 r_{wd}$. Significant particle acceleration by the first order Fermi mechanism is therefore unlikely to occur at or near the white dwarf surface in this system. By the same argument, this mechanism should be inefficient in the vicinity of the compact star in all magnetic CVs, and also in the accretion columns of polar systems, as although Angel (1978) states that shocks may occur at many white dwarf radii from the primary in such a column, the suspension of disc accretion indicates that r_A extends almost to L_1.

Harding (1990) gives an approximate expression for the energy, ε_p, which may be attained via first order Fermi acceleration by a proton within a plasma, the particle energy density of which exceeds the local magnetic pressure. She assumes that the time spent within the acceleration region is a function of the particle velocity and is not dominated by synchrotron radiation energy losses; thus ε_p is an upper limit and is given by:

$$\varepsilon_p \approx e \, (u_1/c) \, B \, R_s$$

where u_1 is the velocity of the as yet un-shocked plasma and R_s is the radius of the shock region (assumed spherical). u_1 may be estimated for material falling on to a white dwarf by equating gravitational energy loss to the total kinetic energy. Using the gravitational field strength given in section 6.1.1, it is found that for a proton near the primary's surface, $u_1 \approx 0{\cdot}01$ c. If it is assumed that for the shock to lie outside r_A, $B \leq 10^5$ G and, optimistically, that the shocked region may cover up to 1/10000 th of the white dwarf surface such that $R_s \approx 10^7$ cm, then $\varepsilon_p \approx 10$ GeV. Katz & Smith (1988) estimate that for a neutron star, the bundle of open field lines along which accreting matter may flow should cover 1/1000 th of the stellar surface). If $r_A << r_{wd}$, then an oblique

shock will occur in the boundary layer where the accretion disc meets the stellar surface. Kirk & Heavens (1990) have shown that the angle between the magnetic field and the shock normal has little effect upon the spectral index of the accelerated particles for plasma velocities of 0.01c and below. It is not inconceivable therefore that fast particles can be obtained through this mechanism, in systems where $r_A \leq r_{wd}$, which then collide with material at some distance from the star, perhaps undergo further Fermi acceleration, and produce γ-rays.

Belvedere (1989) noted that the acceleration of non-thermal particles some distance from the white dwarf might account for the observed time delay between the optical and radio outbursts of dwarf novae.

One mechanism to which the offset of a site of very high energy emission from the position of a compact stellar "engine" may be attributed is given by the co-rotating jet model, reviewed by Kiraly & Meszaros (1988). Accreting matter guided towards a stellar polar cap is contained within an accretion funnel by the pressure of the dipolar magnetic field. If the radiation pressure at the column base exceeds this magnetic pressure, material may flow back up through the low matter density core of the column. A jet is formed which may undergo shock acceleration or γ-ray production through nuclear interactions when it encounters a cloud of material at the source of the column, near r_A. There is no observational evidence for the formation of such jets in CVs comparable to the radio emission representative of jets in some x-ray binary systems. It is assumed that the surface magnetic field strengths and accretion rates are insufficient to maintain a radiation pressure in excess of that due to bulk infall.

Another means by which a shock might be maintained at some distance from a compact star, through ejection of matter at its surface, is by the generation of a pulsar wind. Rotation of a strong dipolar magnetic field can cause charged particle outflow from the surface of a degenerate star. A

shock front may form where this "pulsar wind" impinges upon the companion star's magnetosphere/atmosphere or its stellar wind. According to Harding (1990), a standing shock front may be maintained by the repulsion of accreting material in systems where the spin period of the compact star, P, conforms to the condition:

$$P < 31\text{ms}\ (B_{12})^{4/7}\ (dM/dt_{18})^{-2/7}$$

where B_{12} is the surface magnetic field of the compact star in units of 10^{12} G and dM/dt_{18} is the would-be mass accretion rate in units of 10^{18} g s^{-1}. Taking as an example the mass transfer rate of $2x10^{-7}$ solar masses per year observed in the CV DQ Her and magnetic field strength of 10^{7} G (Robinson, 1976), it becomes immediately apparent that this mechanism is not suited to CV systems as a spin period of the order of 1/100 th of a millisecond is required by the above inequality.

(ii) plasma turbulence

Where an accretion process is underway, plasma turbulence is inevitable. The bulk motion of accreting material can propagate disturbances throughout the charged-particle filled magnetosphere surrounding the compact star. As a result of the random motions of the plasma in the region of a magnetic field, fluctuating electric fields are induced. Chaotic scattering of the charged particles on encounters with these transient fields can result in a net acceleration, despite the seemingly non-systematic pattern of accelerating and decelerating events (Fermi, 1949). This mechanism is referred to as second order Fermi acceleration, as its power is proportional not to the relative velocity of the particle and the scattering centre (as a fraction of c) as in the first order Fermi mechanism, but to the square of this factor, thus second-order Fermi acceleration is the slower process of the two (Longair, 1981).

Katz & Smith (1988) proposed that protons accelerated by this

mechanism along the closed magnetic field lines of neutron stars could give rise to γ-rays of energies in excess of 10^{15} eV. They emphasised the fact that the relatively low particle density in the magnetosphere, compared with that of an accretion column, greatly reduces the magnitude of Coulomb frictional and collisional energy losses, which tend to counteract first order Fermi acceleration in the latter region. The energy gain is limited instead by the synchrotron loss mechanism. Harding (1990) gives an upper limit to the energy gain of a proton accelerated by this mechanism, $\varepsilon_p{}^{max}$, which is based upon the assumption that particles escape when their gyroradius about the magnetic field lines exceeds the scale size, R, of the acceleration region:

$$\varepsilon_p{}^{max} \approx e\ B\ R$$

where B is the local magnetic field strength (at radius r, $B_{(r)} \equiv B_{wd}(r_{wd}/r)^3$). Thus for the CV V1223 Sgr for which $r_A \approx 8\ r_{wd}$ as previously calculated, a proton at r_A might be expected to achieve an energy of 20 GeV if R is taken to be of the order of 10^7 cm as in part (i) of this section.

Irregularities in the flow of accreting plasma can also lead to particle acceleration through magnetic reconnection. Bulk motions near the boundary of two distinct flux regions, where the magnetosphere of a compact star meets an accretion disc for instance, can distort the local magnetic field to the extent that oppositely directed field lines are brought together. At this point a neutral sheet is formed across which a difference in electrical potential may accelerate charged particles. Wang (1986) states that boundary perturbations result in plasma vortices which expand until their kinetic energy is similar to that retained by the magnetic field i.e.:

$$\rho\bar{v}^2 \approx B^2/4\pi$$

where ρ is the plasma mass density and $(\bar{v}^2)^{1/2}$ is the root mean square

velocity of its circular motion. Loops will form in the magnetic field such that reconnection occurs at the edges of the vortices. The rate of reconnection is dependent upon the Alfvén speed in the medium given by:

$$v_A = \frac{B}{(4\pi\rho)^{1/2}} \approx (\bar{v}^2)^{1/2}$$

An electric field E = v_A x B may be formed. According to Wang (1986), the energy which may be attained by a proton via vortex induced magnetic reconnection in the magnetosphere of an accreting neutron star may be estimated from:

$$\varepsilon_p = 10^{14} \left[\frac{(v^2)^{1/2}}{v_{ffA}}\right] \left[\frac{B}{B_A}\right] \left[\frac{\delta}{r_A}\right] L_{37}^{5/7} B_{12}^{-3/7} R_6^{-4/7} M^{1/7} \quad eV$$

where M is the mass of the degenerate star in solar mass units, R_6 is its radius in units of 10^6 cm, B_{12} is its surface magnetic field strength in units of 10^{12} G and L_{37} is the total accretion luminosity in units of 10^{37} erg s^{-1}. δ is a measure of the scale of the magnetic field loops. v_{ffA} is the free-fall velocity of accreting material at r_A. Thus, at r_A, if the bracketed terms tend to unity, for a CV of the dimensions of V1223 Sgr it is found that $\varepsilon_p \approx 20$ TeV. It is the opinion of Wang (1986) that this mechanism can account for the observation of γ-rays of energies in excess of 10^{15} eV from the x-ray binaries Vela X-1 and Cyg X-3.

It is interesting to note that CVs have already been observationally identified as sites of large scale magnetic reconnection. The light curves of dwarf novae from optical to x-ray wavelengths have been found to exhibit quasi-periodic oscillations (QPOs) coherent over of the order of ten cycles, the period stability of which suggest an origin in the rotation or "vertical" oscillations of the accretion disc. Patterson (1981) referred to these phenomena as "dwarf nova oscillations" (DNO) in order to distinguish

between them and the more erratic QPOs presumed to be the signature of mass accretion in all CVs. Tajima & Gilden (1987) considered magnetic reconnection within the accretion disc to be the driving mechanism of these DNO, the period stability being guaranteed by the occurrence of reconnection at a preferred disc radius. If the angular velocity of the disc is not matched to that of the white dwarf, then it is to be expected that lines of the stellar magnetic field coupled to the disc plasma become twisted in the azimuthal direction. According to the above authors, some shearing of the field lines and reconnection will occur on every rotation. This may continue for weeks until the field curvature is so great that further "winding" is balanced by radial diffusion, which is in turn governed by the viscosity of the disc and thus by the accretion rate.

(iii) dynamo models

It was mentioned at the beginning of this discussion of accretion driven acceleration that Chanmugam & Brecher (1985) have identified a method by which ultra high energy particles may possibly be produced within CVs. Theirs is a mechanism of the type referred to as a "star-disc dynamo" model, in which, as the name implies, a differentially rotating, ionised accretion disc is an essential feature.

The dipolar magnetic field of the degenerate star is threaded through the accretion disc, where it is assumed, for the purposes of this calculation, to be effectively anchored. If the accretion disc lies in the equatorial plane of the white dwarf of mass M_{wd}, radius r_{wd} and surface magnetic field strength B_{wd}, whose rotation and magnetic axes are aligned, then the magnitude of the magnetic field component which is perpendicular to the disc at a radial distance r from the rotation axis is proportional to $r^{-1/2}$, and so may be written as $B_{z(r)} = C_B r^{-1/2}$, where C_B is a constant. An electric field is induced by the rotation of B_z, which is given by $E_{r(r)} = B_{z(r)} \times v_{K(r)}/c$, where $v_{K(r)}$ is Keplerian velocity of the rotating

disc of magnitude $v_{K(r)} = (GM_{wd}/r)^{1/2}$. The size of the potential difference which may thus be attained is limited by the physical extent of the disc. If $r_A < r_{wd}$ then it is reasonable to assume that the inner boundary of the disc lies near r_A, whilst an upper limit to the outer radius may be inferred from measurements of the orbital parameters. The difference in electrical potential across the disc between the edge closest to the compact star and a point at radius r and is then given by:

$$V_{(r)} = - \int_{r_A}^{r > r_A} E \cdot dr$$

thus

$$V_{(r)} = - \int_{r_A}^{r > r_A} \left[\left(C_B r^{-1/2} \right) \times \left(c^{-1} (GM_{wd}/r)^{1/2} \right) \right] \cdot dr$$

hence

$$V_{(r)} = - \frac{C_B (GM_{wd})^{1/2}}{c} \ln \left(\frac{r}{r_A} \right)$$

If it is assumed that $B_{z(r)} \approx B_{wd}(r_{wd}/r)^3$ near the Alfven radius, then $C_B = B_{z(r)}\, r^{1/2} = B_{wd}\, r_{wd}^3\, r_A^{-5/2}$ and the greatest potential difference which may be achieved is given by:

$$V_{max} = - \frac{(GM_{wd})^{1/2}}{c} \frac{B_{wd} r_{wd}^3}{r_A^{5/2}} \ln \left(\frac{r_{out}}{r_A} \right)$$

where r_{out} denotes the edge of the disc furthest from the white dwarf. For the intermediate polar V1223 Sgr cited as an example in part (i) of this

section, Chanmugam & Brecher (1985) found $V_{max} \approx 3x10^{13}$ V. According to these authors, as charged particles rotate with the disc, they experience a force due to their passage through this radial electric field. The acceleration provided may be sufficient to produce two oppositely directed, charge-separated particle beams perpendicular to the disc plane. The combined power output of this outflow current being given by $L_{part} \approx 2\zeta cV^2$, where ζ is an efficiency factor limited by the allowed accretion luminosity.

Two obstacles to fast particle production by this mechanism are firstly, that any radial plasma flow may reduce the magnitude of the potential difference developed and secondly, that acceleration is presumed to take place within the disc from which particles must therefore escape without energy loss through thermalisation.

Cheng & Ruderman (1991) have put forward a model in which particle acceleration may occur in regions above and below an accretion disc. Their argument may be interpreted as follows.

If a system is assumed wherein a charged magnetosphere and a rigid accretion disc co-rotate with a degenerate star, at angular velocity Ω, then $\mathbf{E} = (\Omega \times \mathbf{r}/c) \times \mathbf{B}$ throughout. The charge density is then given by $\rho = \nabla \cdot \mathbf{E}/4\pi$, and it is found that the magnetosphere is divided into oppositely charged regions by "null surfaces" where $\Omega \cdot \mathbf{B} = 0$. Now, if the inner edge of the disc, at r_0, is allowed to rotate at a velocity Ω_d which exceeds that of the star, Ω_s, the magnetosphere is parted along the null surfaces to form plasma deficient gaps as shown in figure 6.3b. In the magnetosphere, $\mathbf{E} \cdot \mathbf{B} = 0$, but it has a finite value in the gap. The potential difference across the gap, V_{gap}, must therefore be balanced by those within the star and disc, as the interval C to D in the path A to F in figure 6.3b prohibits the flow of current around this circuit.

Ω_d may be a function of r such that it exceeds Ω_s close to the star at r_0 but is less than Ω_s at the periphery of the disc. A gap will open in the

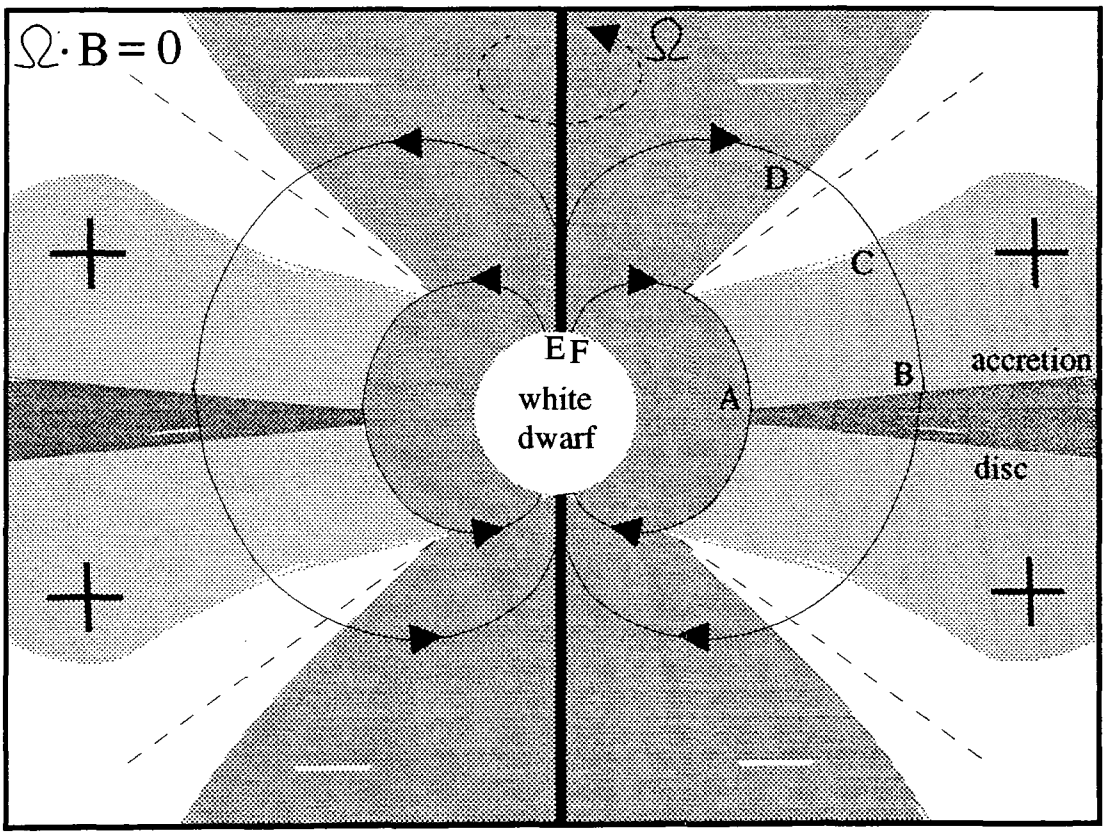

Fig. 6.3b : charge separation and the formation of vacuum gaps in the vicinity of a magnetised white dwarf and a rapidly rotating accretion disc.

magnetosphere above the region where $\Omega_M > \Omega_S$, and may or may not close before it extends to r_{out} depending upon the proximity of r_{out} to the star - disc co-rotation radius r_{co}. V_{gap} reaches a maximum in the gap region which is linked by the dipolar magnetic field to the disc at r_{co}. For Keplerian rotation, r_{co} is given by:

$$r_{co} = (GM/\Omega^2)^{1/3} \qquad \text{eqn. 6.3e}$$

where M is the mass of the central rotator and Ω is its angular velocity. For the CV V1223 Sgr, $\Omega \approx 0.008$ rad s^{-1}, thus $r_{co} \approx 10^{10}$ cm.

In practice, the maximum electromotive force which may be developed is limited by the "spin-up" impulse of accreting material, which opposes the retarding electromagnetic torque upon the disc.

According to Cheng & Ruderman (1991), the gap potential at radius r cm from the stellar centre is given by:

$$V_{gap(r)} = 4\times10^{14}\ B_S\ M_S^{1/2}\ R_S^{3} \left[\frac{10^8\,\text{cm}}{r_0}\right]^{5/2} \left[1 - \left[\frac{r_0}{r}\right]^{5/2}\right] \text{V}$$

where M_S, R_S and B_S are respectively the mass (in solar mass units), radius (in units of 10^6cm) and surface magnetic field strength (in units of 10^{12}G) of the degenerate star and r_0 is in cm. For the parameters of V1223 Sgr, if $r_0 \approx r_A$, then according to the above expression, the maximum gap potential, at $r = r_{co}$, is approximately 5×10^{12} V.

A large particle flux may be accelerated across the gap provided that the flow of positive and negative charges is balanced. Gap accelerated electrons and positrons may boost the x-rays prevalent near the star-disc boundary to γ-ray energies via inverse Compton scattering. However, the power of e^+/e^- γ-ray production is limited by curvature radiation. An ion beam, directed from the gap towards the disc, may give birth to a narrow cone of γ-rays as a product of the decay of neutral pions created through the collision of fast protons with disc material.

6.3.3 encounters with matter

(i) γ-ray production

Collisions between accelerated protons and other protons or nuclei in the vicinity can result in the emission of neutral and/or charged pions, as described in chapter one. The lifetime of a neutral pion is $\approx 10^{-16}$ s, and, fortunately for γ-ray astronomers, its principal decay mode is: $\pi^o \rightarrow \gamma + \gamma$ (Griffiths, 1987). The cosmic γ-ray spectrum above 100 MeV is well matched by that predicted purely for π^o decay (Longair, 1981) and it is this "photo-meson mechanism" which is generally assumed to produce the VHE γ-rays observed from discrete galactic sources. Balashov, Korotkikh & Moskalenko (1990) have investigated a photo-nuclear production mechanism, in which relativistic nuclei absorb soft photons and the resulting fragments release their excitation energy as γ-rays. These authors find that the mean energy of photonuclear produced γ-rays is in the 1 to 10 MeV region.

In their discussion of static gap acceleration, Cheng & Ruderman (1991) suggested that if the x-ray flux in the magnetospheric gap was high, a beam of neutrons might be obtained through the photo-nuclear disintegration of fast protons according to:

$$\underset{\text{x-ray}}{\gamma} + p^+ \rightarrow n + \pi^+$$

This neutron beam could leave the acceleration region, without energy loss to the electromagnetic field, and power the photo-meson mechanism elsewhere.

The cross-section for neutral pion production, $\sigma(E)$, is of the order of the geometric size of the nucleon, and has been found experimentally for proton energies above 2 GeV to be $\approx 2.7 \times 10^{-26}$ cm^2 (Lang, 1986). For a proton rich target therefore, a column density of $\kappa_o \approx 62$ g cm^{-2} is

required. If the column density of the target medium, κ, is $>> \kappa_o$, the π^o decay γ-rays will not leave it, but will form e^+e^- pairs, so that any γ-rays detected from this region are the products of an electron - photon cascade. The mean energy of escaping photons will then be given by:

$$\bar{\varepsilon} = \varepsilon_o \exp(-\kappa/\kappa_o)$$

where ε_o is the energy of the primary γ-ray (Carraminana, 1991). The process of conversion of the energy of a fast proton to that of π^o decay γ-rays is approximately 10% efficient (Lang, 1986). According to the above expression, in the limit $\kappa \geq \kappa_o$ the production of free γ-rays of energy 250 GeV therefore requires a proton energy in excess of 6 TeV.

(ii) particle - particle collision sites

A stream of fast particles accelerated in the region of the compact star may impact upon accreting matter or, if charged, may be steered towards a collision with the non-degenerate companion.

Cheng & Ruderman (1989) considered the interaction of a gap accelerated particle beam with an accretion disc in an axisymmetric rotator. They expect that a particle stream guided by the dipole field lines will pass through the disc in such a way as to generate γ-rays emitted parallel to the disc's axis of rotation. In the event of $r_A \geq r_{wd}$ the thickness of the disc in this direction is such that fast protons will become trapped within it and may give rise to an enhanced neutron flux. Since the flow of neutrons is not restricted to the direction of the magnetic field lines, they may run parallel to the disc surface, thus encountering sufficient material to cause π^o production in a region from which γ-rays may escape. In this situation, γ-ray emission would be confined to the plane of the disc. It should therefore be possible to test this theory by observation of eclipsing binary systems and particularly to CVs as their geometry has been closely studied at longer wavelengths. Cheng

et al. (1990) suggest that large fluctuations in the x-ray flux from disc supporting systems are coincident with the temporary thinning of localised areas of the disc, and that these "windows" may promote γ-ray outbursts.

If disruption of the disc results in the dissociation of clumps of material, due to turbulence at the inner edge for example, then QPOs might be observed as a result of γ-ray production in this tenuous, drifting, yet still rotating material.

Some other potential targets for particle beam dumping are shown in figure 6.3c (after Hillas, 1987). These include the area where the plasma stream from the inner Lagrangian point, L_1 (see figure 6.2b) broadens near the edge of a disc during Roche lobe overflow, the atmosphere of the companion star and the compact star's accretion wake (to which the stellar wind of the companion is gravitationally focussed). The density of any accretion wake may be determined from periodic variations in the magnitude of line-of-sight extinction. In his work on the magnetic steering of charged particle beams in x-ray binaries, Mannings (1992) found that an accretion wake target was consistent with the orbital dependency of VHE γ-ray emission from Vela X-1 observed by the Durham group. He also suggested that bursts of VHE γ-rays observed during the eclipse of the neutron star in Vela X-1 could be due to the interaction of a curved charged particle beam with the limb of its supergiant companion. Clearly, the extent of these target areas is highly dependent upon the evolutionary state of the secondary star. Young stars maintain the strongest stellar winds, whilst giants obviously provide the greatest beam dump target area. No CV has yet been found to contain a non-degenerate star of spectral type earlier than F (Ritter, 1990). Those short period systems in which the spectral type of the secondary cannot be distinguished are necessarily incapable of containing a giant star within their restricted orbit (Robinson, 1976).

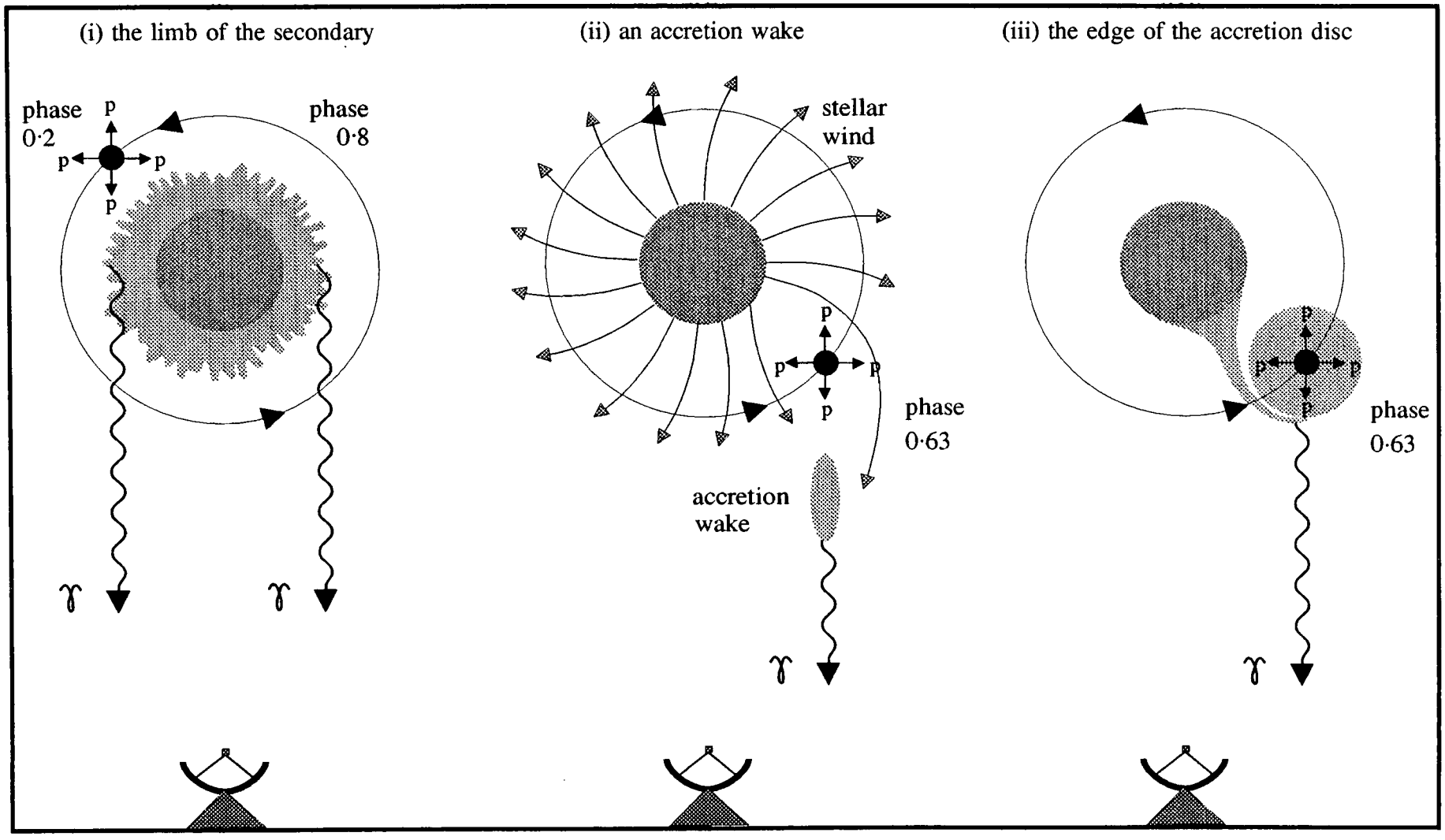

Fig. 6.3c : targets for particle beam dumping and the phases of their passage through an observer's line of sight.

6.3.4 loss mechanisms

(i) synchrotron emission

In discussing their plasma turbulence model, Katz & Smith (1988) consider that synchrotron radiation may be the most significant factor in limiting the energy of accelerated protons.

Synchrotron emission was introduced as a contributory factor to the cosmic γ-ray spectrum in chapter one, where it was however noted that synchrotron radiation itself can provide only a small fraction of the observed flux at TeV energies.

A charged particle of mass m and charge q flowing through the dipolar magnetic field of a degenerate star follows a helical path having a magnetic field line as its axis. The gyration frequency of this motion is given by: $w_B = qB/\gamma mc$, where B is the strength of the local magnetic field and γ is the Lorentz factor. The acceleration of the particle, $a = \omega_B v^{\perp}$, where $v^{\perp}$ is the velocity of the particle perpendicular to the field, causes it to radiate a power spectrum which extends to the critical frequency $\omega_c = 3/2\ \gamma^3\ \omega_B \sin\alpha$, where α is the angle between the particle beam direction and that of the magnetic field (Rybicki & Lightman, 1979). Clearly, the maximum radiation frequency is obtained for $\alpha = 90^\circ$, when $v^{\perp} = \beta c$. Thus, the maximum synchrotron photon energy which might be obtained, $E_{max} = (h/2\pi)\ \omega_c$, is given by:

$$E_{max} = \frac{3\ \gamma^2\ h\ q\ B}{4\ \pi\ m\ c}$$

Using the above equation, for $B = 10^6$ G, it is found that for the particle energies of ~10 TeV required to produce 250 GeV γ-rays, an electron would emit synchrotron photons of energy ~20 keV, whilst the radiation of a fast proton would be entirely negligible because of its greater rest mass. The rate of energy loss of such an electron, W, may be

estimated using Larmor's formula:

$$W = \frac{2\ q^2\ a^2}{3\ c^3}$$

By setting $a = \beta\ c\ \omega_c$, it is found that for the electron, $W_{max} = 0{\cdot}45$ TeV s^{-1}. Therefore, a mechanism capable of producing VHE γ-rays near the surface of a magnetic white dwarf or similar body via fast particle collisions must do so as a result of the acceleration of protons or heavier ions.

(ii) absorption by pair production

A γ-ray may interact with a real or virtual photon to form an electron - positron pair. This pair production process is the dominant absorption mechanism for photons of energy greater than a few MeV.

By conserving energy and momentum in the centre of mass frame, it is found that the energy required of a γ-ray for pair production to result from a "head-on" collision between it and a photon of energy hv is given by:

$$E = \frac{(m_e\ c^2)^2}{h\ \nu_{min}}$$

where m_e is the rest mass of an electron.

The annihilation between γ-rays and the virtual photons of a magnetic field was described in detail by Erber (1966). This process has a significant effect in the vicinity of a neutron star of surface field strength $> 10^9$ G, but is negligible at the field strengths of CV bound white dwarfs. Usov (1988) noted this as an advantage of his white dwarf pulsar model over neutron star pulsars.

For pair production to occur through the interaction of γ-rays and the abundant soft x-ray photons in the accretion column or disc of a CV, the

above equation dictates that γ-ray energies of the order of 60 MeV are required. Few γ-rays will survive in this region. Sites which may support π^o production *and* permit VHE γ-rays to escape are few, hence degradation of the γ-ray flux through electron - photon cascades is to be expected.

Carraminana (1991) has shown that the effect of absorption by pair production in a black-body accretion disc target is to produce a gap in the γ-ray spectrum. This gap lies between the energy at which annihilation commences between γ-rays and thermal x-rays and that at which the interaction cross-section is sufficiently small for a significant fraction of the γ-rays to escape. Carraminana found that the γ-ray flux at energies below 800 TeV should be strongly absorbed in the x-ray binary Sco X-1, unless it is produced at several stellar radii from the neutron star or is strictly perpendicular to the plane of the disc. A rough estimate, by this method, of the energy gap for a system of the parameters of the CV V1223 Sgr suggests that disc absorption should suppress γ-ray emission in the 0·3 MeV to 3·5 TeV range. Absorption by pair production is less significant in CVs than in XRBs because of the lower accretion luminosity of the former.

6.3.5 the γ-ray light curve

To summarise, particles of sufficiently high energy to produce π^o decay γ-rays in the vicinity of an accreting white dwarf may be obtained through plasma turbulence and magnetic reconnection or by a star-disc dynamo type mechanism. The π^o production may occur in an accretion disc or column and in the atmosphere of the non-degenerate secondary.

A γ-ray flux exhibiting no pulse structure could be attributed to plasma turbulence driven second order Fermi acceleration in the white dwarf magnetosphere. If magnetic reconnection of the dipolar field is expected then a search for a γ-ray DNO signature near the white dwarf rotation period might prove worthwhile.

Cheng and Ruderman (1991) predicted that a γ-ray flux due to acceleration across a magnetospheric gap would be modulated at the white dwarf spin period, as emission occurs where the fast particle beam encounters a "window" in the rotating accretion disc of an appropriate density. The radial motion of such windows through a disc may account for the observed one part in 10^3 difference between the x-ray and short term γ-ray pulse periods determined for some x-ray binaries e.g. Her X-1 (Slane & Fry, 1989). The magnitude of the period shift is governed by the radial dependence of the azimuthal velocity of the particle beam and the time of flight to the observer, and by the curvature of the magnetic field lines which the fast particles follow (Cheng & Ruderman, 1989). These authors also suggest that when a neutron beam is produced in the gap through photo-nuclear disintegration it will intersect the accretion disc at a different point to the charged particle beam, giving rise to an inter-pulse.

Particle acceleration through magnetic reconnection may be confirmed through a search for DNO at γ-ray energies in dwarf novae. If γ-ray periodicity is observed from intermediate polar systems then some beaming mechanism must be at work. It may then be possible to determine the role of fast neutrons in γ-ray production through analysis of the pulse structure and the depth of the γ-ray eclipse. Bursts of γ-ray activity might be expected to coincide with an increased luminosity at other wavelengths in systems where disc accretion is excluded, due to plasma turbulence or a sudden density increase near the base of an accretion column resulting in fast particle ejection.

6.4 the Durham cataclysmic variable survey

The University of Durham group observed four CVs over the period October 1990 to November 1991. Of these target objects two, AE Aquarii and H0253+193, are intermediate polar systems, EF Eridani is a polar CV and VW Hydri is of DN type.

6.4.1 AE Aquarii, an intermediate polar system

AE Aqr is a novalike CV of intermediate polar type. It consists of a 0·9 M_{sun} mass white dwarf and a 0·7 M_{sun} K5 type secondary in a 9·88 hour orbit of inclination 58° (Ritter, 1990) and is a well established soft x-ray source.

Bastian, Dulk and Chanmugam (1988) studied AE Aqr at four radio frequencies and found evidence for flare activity. This emission was attributed to the synchrotron radiation generated by relativistic electrons accelerated at some distance from the surface magnetic field, of strength $\sim 10^5$ G, of the white dwarf. The flare phenomenon was assumed to be related to the disruption of an accretion disc by sporadic mass transfer. Pulsations were observed at a fundamental frequency of ~ 0·03 Hz and at its first harmonic. The above authors drew parallels between the morphology of the AE Aqr radio emission and that of the x-ray binary Cyg X-3 in quiescence, and suggested that AE Aqr could prove to be a "low-power analogue to Cyg X-3" visible in VHE γ-rays.

(i) the Potchefstroom report

The University of Potchefstroom (S.A.) group have observed eight CVs using the atmospheric Cerenkov technique, of which three have shown some evidence of VHE γ-ray emission. These are AO Psc (an intermediate polar) and UZ For (a polar), both of which require further observation and analysis (Meintjes et al., 1992) and AE Aqr (de Jager et al., 1990).

The Potchefstroom dataset includes 93 observations of AE Aqr made from 1988 to 1991 at an average threshold energy of 2·4 TeV. The data were searched for the 30·23 mHz variability characteristic of the optical flux during quiescence, which is believed to represent a beat period between the rotation of the white dwarf and the orbital motion (Robinson, Shafter & Balachandran, 1991), and at QPO frequencies of 29·94 mHz and 30·04 mHz which may be due to decomposition of the fundamental by one F.I. (de Jager et al., 1990). None of these trial frequencies appeared to occur at a non-statistical level in the dataset taken as a whole, although each was observed above the background noise in some individual observations. Through simultaneous photometric observations of the optical spectrum it was established that optical flares lasting for minutes or hours were coincident with VHE γ-ray emission events and displayed the same pulse frequency on at least one occasion. De Jager & Meintjes (1992) suggest that these optical bursts are associated with dynamic activity in the white dwarf magnetosphere, which may induce large electric fields and thence particle acceleration. They note that the observed flare rise times are of the order of the time taken for a clump of accreting material to traverse the magnetospheric depth $r_A - r_{wd}$, and that power at the first harmonic may be indicative of oblique rotation of the white dwarf, the pulse and inter-pulse being due to different magnetic poles.

(ii) the Durham observations

The Potchefstroom designation of AE Aqr as a TeV γ-ray emitter was confirmed by the Durham group, following observation of the burst activity which was used in chapter three to illustrate the advantages of multiple telescope source coverage. The results obtained from observations made in October 1990 and between August and October of the following year are given in detail in Bowden et al. (1991a) and (1992). The data were Rayleigh tested at the fundamental optical pulse period of 33 s and its first

harmonic. The 34 observations, made using the Mark III and/or Mark IV telescopes, contained no evidence of activity at the fundamental period either individually or when combined with and without the retention of relative phase information (see section 4.3.6). However, a probability of chance occurrence of 0·017 was obtained for periodicity at the first harmonic ($P \approx 16{\cdot}54$ s) from the incoherently combined dataset once degrees of freedom were accounted for. This result was not enhanced by the performance of a "software cut" as described in section 5.2.2. It is therefore concluded that AE Aqr's γ-ray spectrum is "hard" i.e. that the signal consists of a higher proportion of large Cerenkov flashes than does the cosmic ray background.

The burst of 13th October 1990, which occurred at orbital phase 0·17 and was of one minute duration, displayed this 16·54 s periodicity. The probability of chance occurrence of the burst, which amounted to a count rate excess of 75% of the two-telescope cosmic ray background count rate, was $7{\cdot}4 \times 10^{-11}$. The event excess at the Mark III detector alone corresponded to a peak flux of $1{\cdot}6 \times 10^{33}$ erg s^{-1} at a threshold energy $\geq$ 350 GeV at the targeted zenith angle of ~35°. Hardness ratios were calculated for the central channel of the Mark III telescope (as per section 6.4.2(iii)) in order to describe the spectrum of Cerenkov flash sizes recorded before, during and after the burst episode; these were found to be 1·78, 1·20 and 1·77 respectively. The increase in the proportion of large Cerenkov flashes coincident with the on-source event excess and the stability of the PMTs' anode currents and noise rates (shown in figures 4.2c and 4.2d) suggest that an authentic γ-ray burst was witnessed.

6.4.2 H0253+193, an intermediate polar system

(i) background information

H0253+193 appeared first as an unidentified x-ray source in the HEAO

A-2 survey. It coincided with a point source of thermal bremsstrahlung radiation in the 2 to 10 keV band in data from the Einstein observatory (Halpern & Patterson, 1987). Epoch folding of x-ray data taken on this object using the Ginga satellite revealed a double peaked pulse profile (Takano et al., 1989) of period 206·1 ± 0·2 s in data from July 1987 increasing to 206·3 ± 0·1 s in January 1989. The nature of this x-ray pulsator was not immediately apparent owing to optical obscuration by a molecular cloud (MBM 12) which lies on the line of sight at a distance of 65 pc (Koyama et al., 1991). Patterson and Halpern (1990) felt that the x-ray spectra were reminiscent of an intermediate polar CV, coincidentally aligned with an unrelated gas cloud. The binary nature of the system was firmly established following the discovery by Kamata, Tawara & Koyama (1991) of x-ray eclipses recurring at 6·06 hour intervals, for which:

$$JD_{\substack{mid-\\eclipse}} = 2,447,751{\cdot}56036\ (\pm\ 0.00012) + 0{\cdot}25265\ (\pm\ 0{\cdot}00003)\ E$$

where 0·25265 days = P_{orb} and E is the number of cycles elapsed since this measurement. The system was confirmed as a CV through the infrared measurements of Zuckerman, Becklin, McLean & Patterson (1992). They found infrared minima concurrent with the time of x-ray eclipse, which suggests that the light curve at these wavelengths is dominated by activity in the Roche lobe filling region of a non-degenerate secondary. If the secondary star in this close binary is assumed to conform to a main-sequence mass-radius relationship, then, according to the same authors, its apparent magnitude places it at a distance of 200 pc. Thus, the observed x-ray flux is consistent with a luminosity of $2x10^{32}$ erg s^{-1} which is more compatible with that of a white dwarf system than with that of a x-ray binary. The x-ray eclipse duration implies an emitting region of angular extent similar to that of a white dwarf. The hard x-ray flux and absorption intrinsic to the source are typical of intermediate polar systems.

(ii) the dataset

Of the fifteen to twenty CV systems which display intermediate polar type characteristics, H0253+193 was found to be conveniently situated such that its observation would not preclude that of a well-established target source. Data was taken on this object in "tracking mode" during the October and November observing sessions of 1991. At its culmination, around midnight, H0253+193 reached a zenith angle of only ~51°, hence the energy thresholds of the Mark IV and Mark III telescopes must be assumed to have been in the region of 600 GeV and 450 GeV respectively. The duration of each observation and the prevailing sky condition is listed in figure 6.4a.

(iii) analysis and results

The event times were corrected to the solar system barycentre using the position given by Koyama et al. (1991). The errors in the ephemeris of Kamata, Tawara & Koyama (1991) are such that the absolute orbital phase of the Durham observations (made two years after the ephemeris epoch) cannot be stated. If the size of the H0253+193 system is assumed to be similar to that of AE Aqr, having a projected semi-major axis of ~2·4 lt s, then no allowance need be made for the effect of orbital motion upon pulse arrival times in order to recover 206 s periodicity from a four hour observation.

The observations were filtered to produce 20 data files containing Cerenkov events which triggered only the central channel. Of these, 16 were divided into 60 s segments as a test for burst activity similar to that observed from AE Aqr (Bowden et al., 1992). An expectation value for the number of events in each bin was obtained by assuming a Poissonian distribution with a time varying mean given by a parabolic fit to the observed count rate (which varies with zenith angle) according to the method of Carraminana (priv. comm.). The remaining 4 datasets were too sparse (owing to adverse weather conditions) to allow estimation of the

date (UT)	duration (min.)	telescope	sky clarity
01/10/1991	117	IV	v. good
02/10/1991	180	IV	v. good
05/10/1991	154	IV	poor
06/10/1991	129	IV	poor
09/10/1991	210	IV	v. good
10/10/1991	150	IV	v. good
11/10/1991	150	IV	v. good
12/10/1991	195	IV	v. good
13/10/1991	159	IV	v. good
14/10/1991	215	IV	v. good
31/10/1991	165	III	poor
01/11/1991	120	III	v. good
02/11/1991	120	III	good
03/11/1991	121	III	v. poor
04/11/1991	132	III	excellent
05/11/1991	124	III	excellent
06/11/1991	153	III	v. poor
07/11/1991	120	III	excellent
08/11/1991	120	III	v. good
11/11/1991	90	III	poor

Fig. 6.4a : the H0253 + 193 dataset.

statistical significance of any count rate variations. A peak count rate of 4 standard deviations above the expectation value occurred in data collected on 07/11/1991. The excess appeared to be contained within one 60 s bin as illustrated in fig. 6.4b(i). This was the only peak far above the 3 standard deviation level in the H0253+193 dataset. It was established that this activity was confined to the source direction, by returning to the data file containing all recorded events and applying the same treatment to those triggering a single guard ring channel. The count rate profiles of channel 1 and channel 5 are shown in figures 6.4b(ii) and (iii). These channels are diametrically opposed in the detector package. The gain of channel 1 is regulated by a LED feedback circuit whilst that of channel 5 may vary with sky brightness. Close inspection of the data records revealed a spate of events including a response from the central channel lasting for approximately 70 s, centered upon a period from 13:27:29 U.T. to 13:27:36 U.T. during which 2 events arrived per second. This is not the sudden avalanche behaviour associated with electronic noise. In an attempt to determine whether these "burst events" were due to γ-ray primaries rather than nucleon showers, their number spectrum was plotted as a function of the time integrated charge (QT) of each averaged over the three on-source photomultiplier tubes, and compared with the spectra of events during two 700 s sections of data, one ending 100 s before and one beginning 100 s after "mid-burst". These spectra, illustrated in figure 6.4c, appear well-behaved, and there is some indication that the burst event spectrum (middle plot) is rather less concave than the near exponential distributions of the "before and after" data. In order to quantify this deviation, the fraction of events lying below an arbitrarily chosen boundary level (in this case 32 units on the x axis QT scale) was calculated for each data segment. This "hardness ratio" was found to be 2·16 for events before the burst, 1·52 during the burst and 2·03 after it, thus it is clear that the proportion of large Cerenkov light

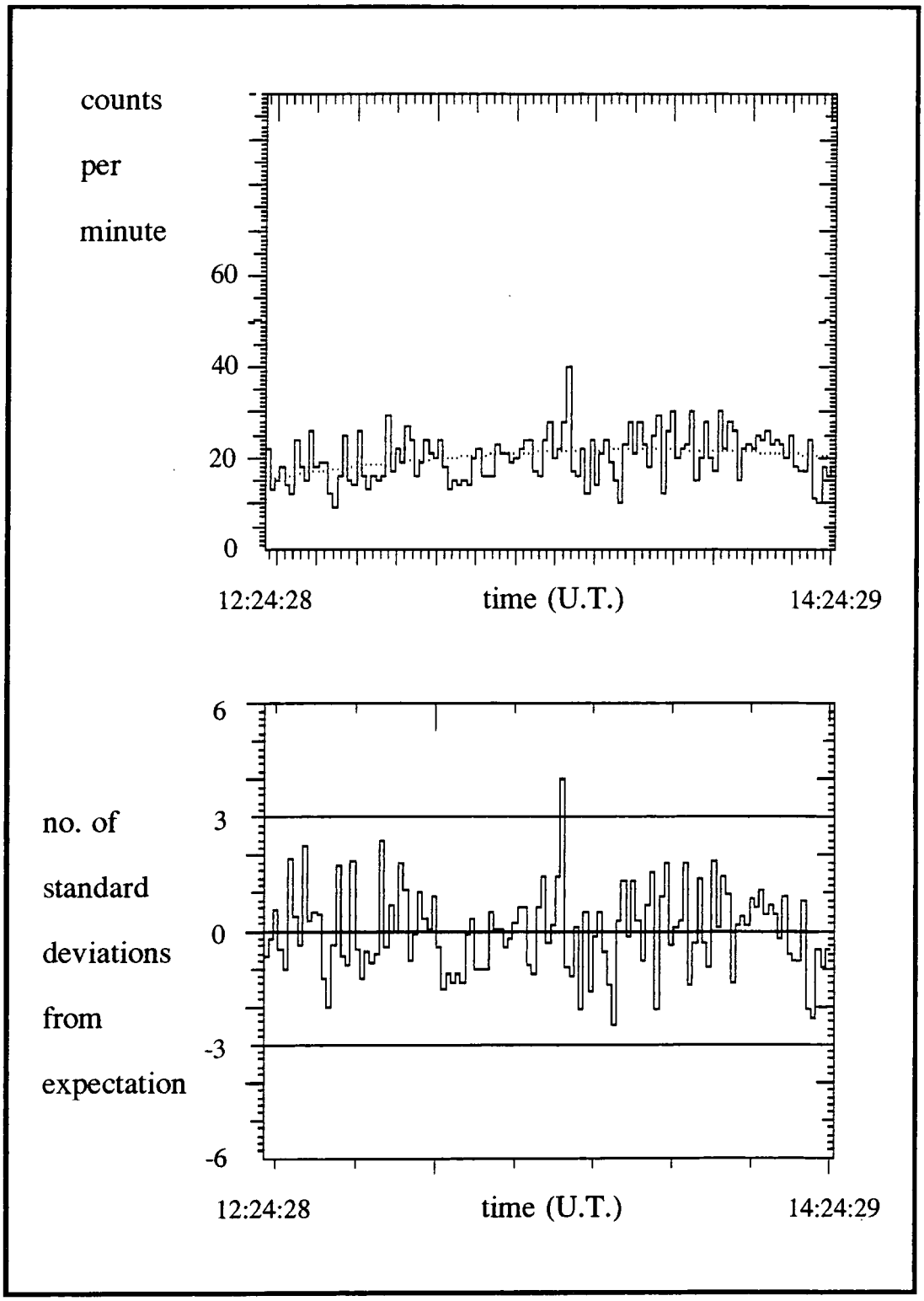

Fig. 6.4b(i) : count rate during the observation of H0253+193 made on 07/11/1991 (Cerenkov events triggering the central channel only).

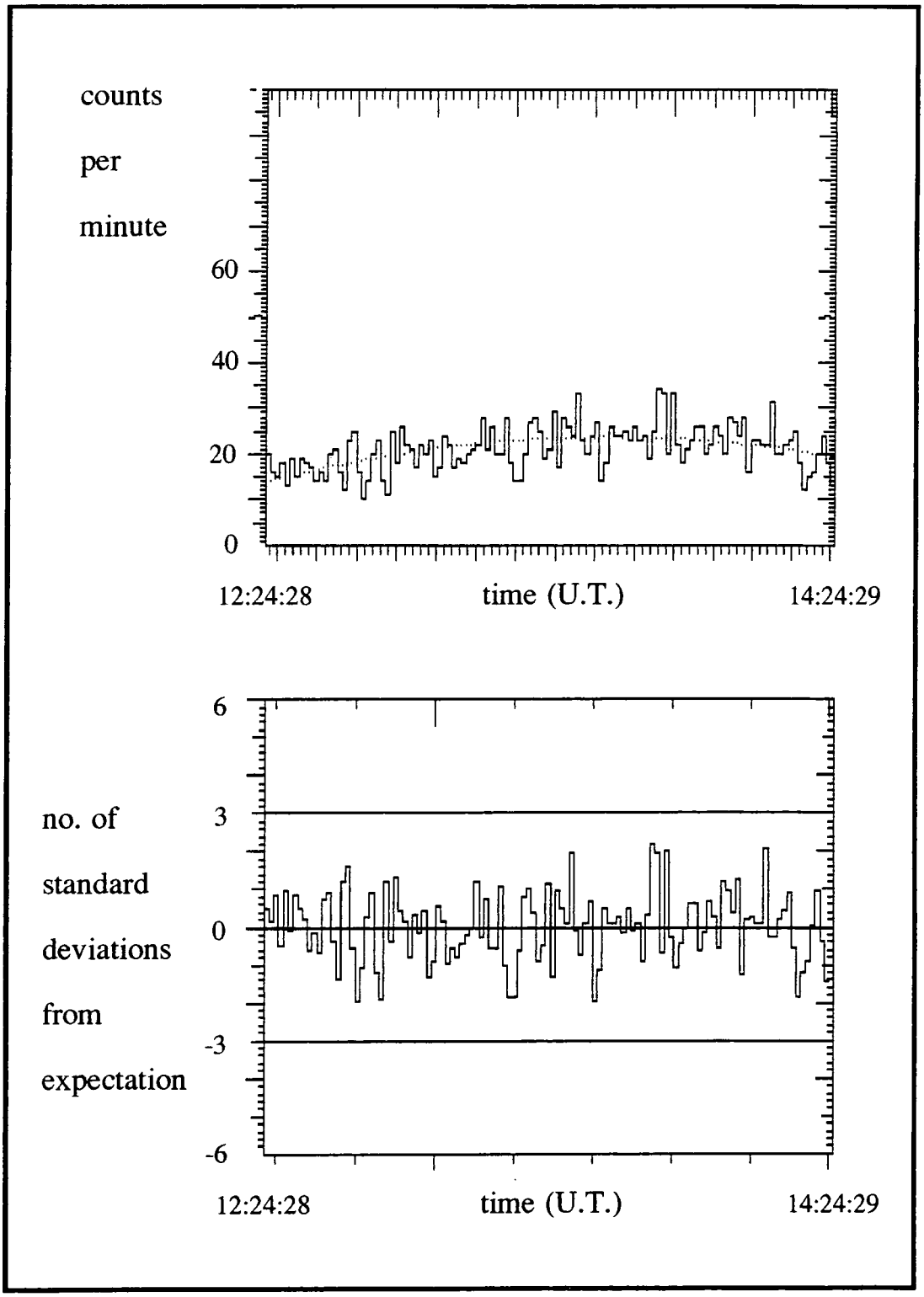

Fig. 6.4b(ii) : count rate during the observation of H0253+193 made on 07/11/1991 (Cerenkov events triggering channel 1 only).

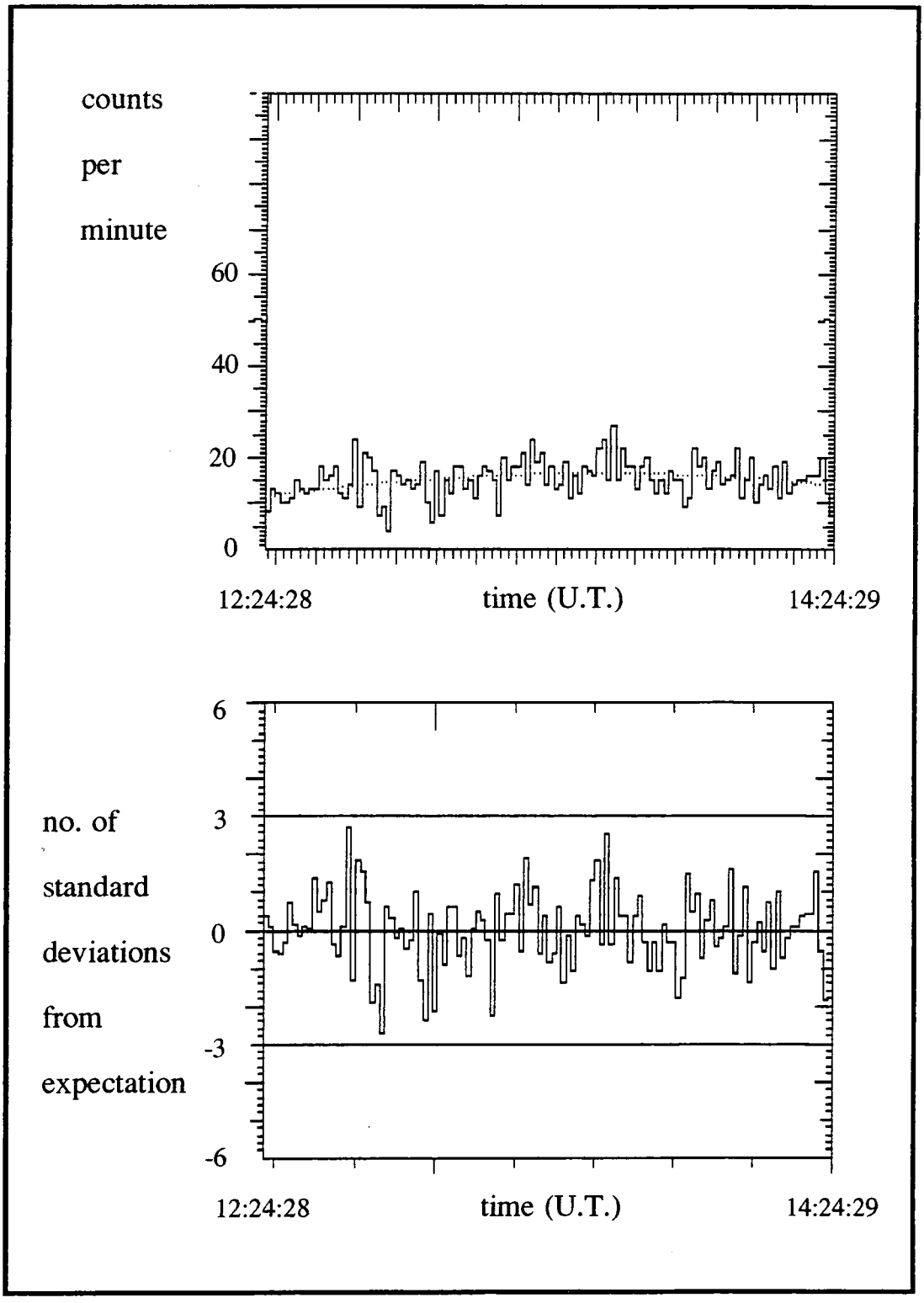

Fig. 6.4b(iii) : count rate during the observation of H0253+193 made on 07/11/1991 (Cerenkov events triggering channel 5 only).

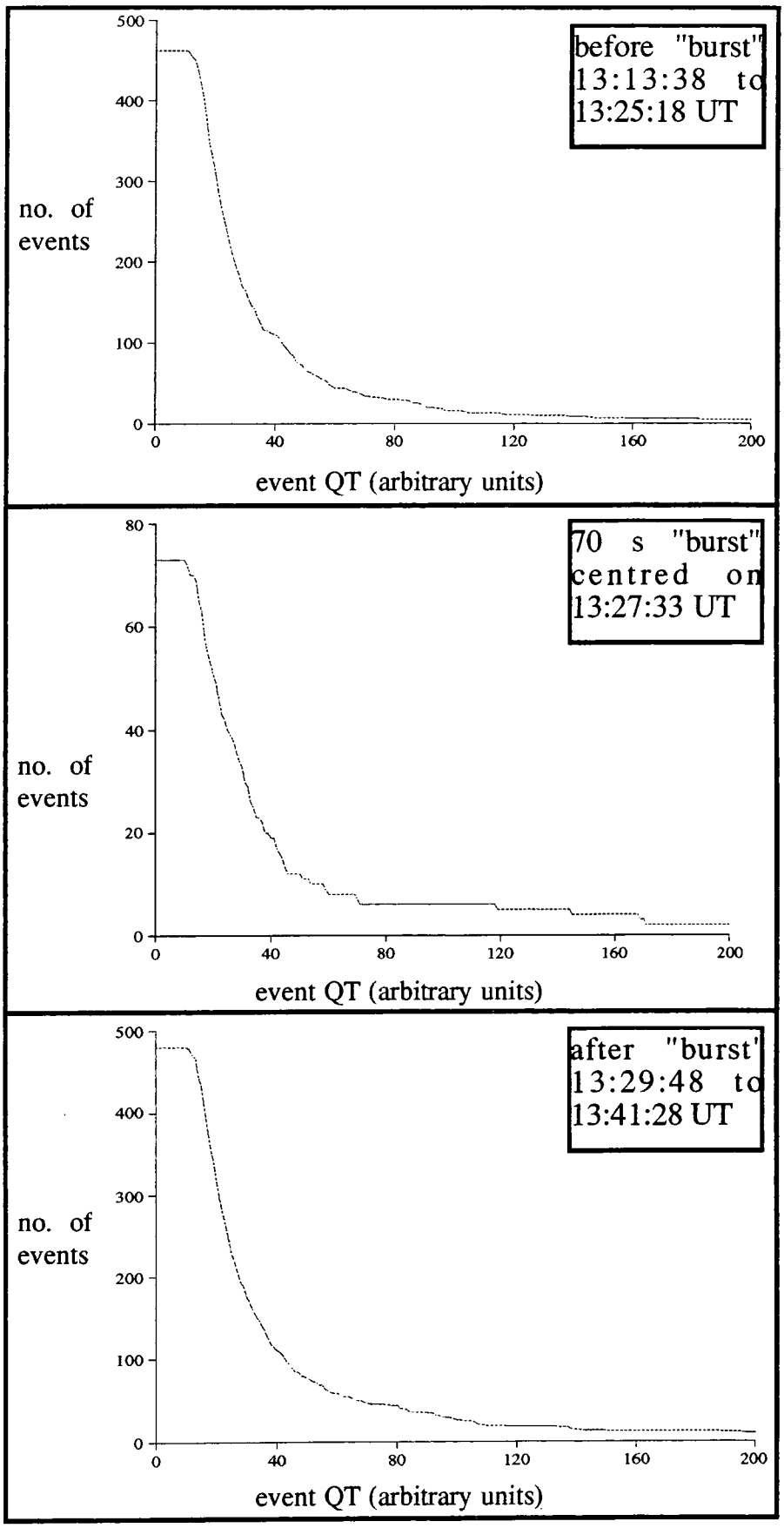

Fig. 6.4c : central channel integral QT spectra.

flashes was enhanced during the burst episode. In other words, the burst events are drawn from a source spectrum which is flatter than that of the cosmic ray background.

Having obtained some slight evidence of burst activity, the 20 observation dataset was searched for periodicity using the test for uniformity of phase described in section 4.3.3(iii). Unfortunately, the length of the x-ray pulse period was such that the preferential selection for analysis of a small section of data at or near the time of the 07/11/1991 was not justified. Each filtered "centre only" data file was analysed for periodicity in the range 150 s to 250 s in the expectation of γ-ray emission at or near the 206 s period reported by Takano et al. (1989). The period having the least probability of occurrence by chance is noted for each observation in figure 6.4d(i). Three trials were allowed per Fourier interval ($\approx$ 6 s for a two hour observation). The tabulated probability values have been corrected for the number of trials employed. Since the above authors found that the x-ray pulse profile is double-peaked, the pulse and inter-pulse being separated by 180°, the period search procedure was repeated over the range 70 s to 120 s, to check for a γ-ray signal at the first harmonic as was discovered in the analogous case of AE Aqr (see figure 6.4d(ii)).

No trace was found of periodicity at the x-ray pulse period or at its first harmonic. However, on inspection of figure 6.4d(i), it will be noted that the peak period of ~162 s present on the night of "known activity" of 07/11/1991 recurs within one F.I. on three other occasions in the November dataset. Since three of these four observations are effectively of the same length, although varying greatly in the event totals, it might be assumed that this "coincidence" was an artefact of the analysis procedure. If this 162 s periodicity is attributable to events such as those present in the 07/11/1991 burst, then its significance should be reduced in a subset of data selected on the basis of having low QT values. Figure 6.4e(i) shows

date (UT)	telescope	channel 0 event total	peak period (s)	prob. of chance
01/10/1991	IV	740	156.4	0.55
02/10/1991	IV	1015	222.4	0.39
05/10/1991	IV	1356	177.1	0.27
06/10/1991	IV	563	150.0	0.95
09/10/1991	IV	1748	248.7	0.59
10/10/1991	IV	1942	160.7	0.082
11/10/1991	IV	1971	179.9	0.081
12/10/1991	IV	1989	215.3	0.054
13/10/1991	IV	1908	154.7	0.67
14/10/1991	IV	2851	153.9	0.018
31/10/1991	III	1336	162.9	0.092
01/11/1991	III	2048	162.7	0.0067
02/11/1991	III	1418	184.2	0.60
03/11/1991	III	377	162.1	0.0064
04/11/1991	III	2858	210.0	0.061
05/11/1991	III	2624	150.0	0.11
06/11/1991	III	640	246.2	0.0038
07/11/1991	III	2421	162.2	0.053
08/11/1991	III	1959	169.6	0.38
11/11/1991	III	669	184.3	0.024

Fig. 6.4d(i) : H0253 + 193 period search in the range 150 s to 250 s.

date (UT)	telescope	channel 0 event total	peak period (s)	prob. of chance
01/10/1991	IV	740	77.44	0.086
02/10/1991	IV	1015	94.65	0.49
05/10/1991	IV	1356	97.76	0.97
06/10/1991	IV	563	99.48	0.29
09/10/1991	IV	1748	114.2	0.29
10/10/1991	IV	1942	84.40	0.58
11/10/1991	IV	1971	84.95	0.14
12/10/1991	IV	1989	89.03	0.57
13/10/1991	IV	1908	101.1	0.80
14/10/1991	IV	2851	82.04	0.025
31/10/1991	III	1336	75.92	0.087
01/11/1991	III	2048	81.25	0.53
02/11/1991	III	1418	82.71	0.39
03/11/1991	III	377	72.31	0.45
04/11/1991	III	2858	77.16	0.29
05/11/1991	III	2624	91.65	0.027
06/11/1991	III	640	118.1	0.11
07/11/1991	III	2421	113.3	0.79
08/11/1991	III	1959	86.92	0.35
11/11/1991	III	669	109.8	0.21

Fig. 6.4d(ii) : H0253 + 193 period search in the range 70 s to 120 s.

the overall chance probability of periodicity in the range 150 s to 250 s calculated for all central channel only Mark III telescope events by combining the results from individual data files without the retention of relative phase information (as in section 4.3.6(ii)). Note that the y axis values have *not* been corrected for degrees of freedom; once the number of trials is accounted for the probability of the peak period of 162·7 s is reduced to $2{\cdot}5 \times 10^{-5}$. Figure 6.4e(ii) is the counterpart of 6.4e(i) for those events which not only triggered the central channel alone, but also did not deposit a charge in one of the guard-ring channels in excess of 45% of the value attained in the on-source channel. As predicted, this "soft cut" has greatly diminished the peak at 162 s. It is interesting to note the recovery of a peak period of 210 s in figure 6.4e(ii), which lies within one F.I. of the x-ray period but is not statistically significant. When the October Mark IV telescope data were merged in a similar fashion, no significant periodicity was observed in the 150 s to 250 s range either before or after a 45% soft cut selection.

(iv) summary

The only evidence of "burst" activity in the HO253+193 dataset, on a timescale similar to the 6 standard deviation, 60 s burst from AE Aqr reported by Bowden et al. (1991a), is one 70 s episode representing a 4 standard deviation excess above the background count rate. Since HO253+193 was not the subject of dual telescope observations the significance of any count rate deviation is limited as an instrumental origin cannot be entirely ruled out. However, the stability of the detector and of the observing conditions are well documented, whilst the time integrated charge profiles suggest that the excess events were of above average energy for the observation in question.

There was no evidence of pulsation at the 206 s x-ray period or at its first harmonic. A 162 s pulse period was present on more than one occasion

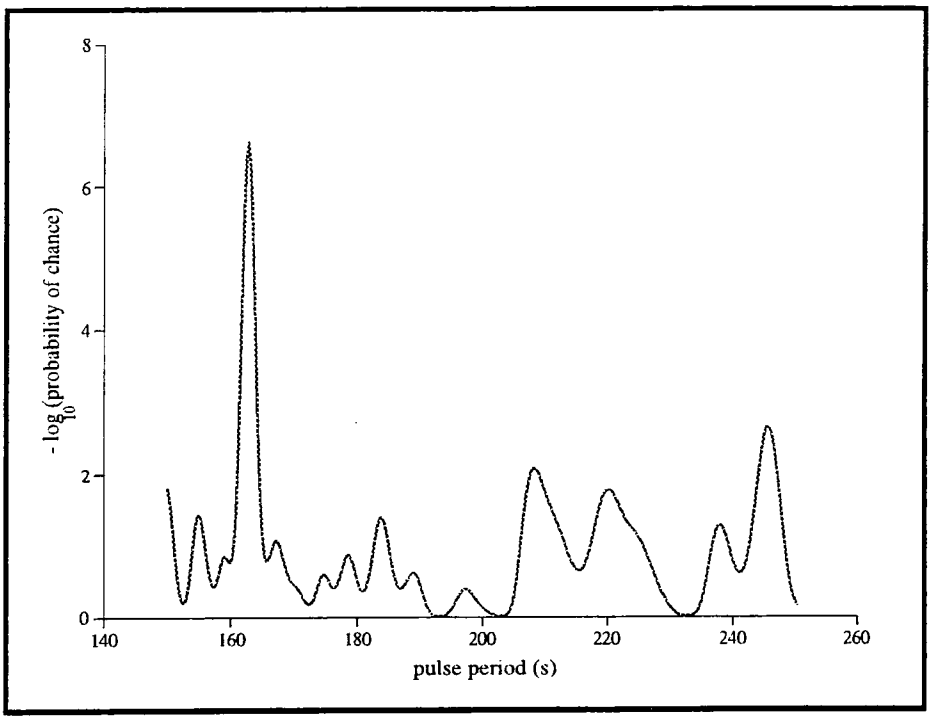

Fig. 6.4e(i) : probability of periodicity in the range 150 s to 250 s in the Mark III telescope dataset (central channel only = 16350 events).

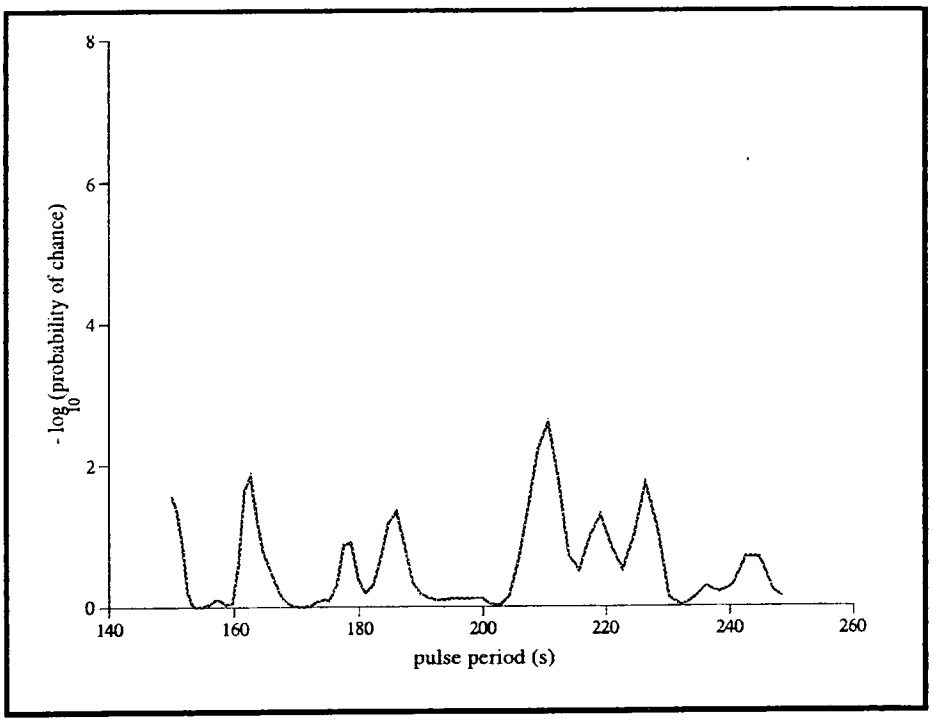

Fig. 6.4e(ii) : probability of periodicity in the range 150 s to 250 s in the Mark III telescope dataset (central channel only, "soft cut" at 45% threshold = 5893 events).

and was found to occur in the Mark III telescope dataset as a whole at a chance probability of ~ 10^{-5}. If this periodicity is of a truly astronomical origin, then it may be attributed to γ-ray production in accreting material rotating more rapidly than the hot x-ray source assumed to lie at or near the white dwarf's surface. If the approximation $r_A \approx 8\ r_{wd}$ calculated for the intermediate polar V1223 Sge using equation 6.3d is applicable to H0253+193 then, according to equation 6.3e, the co-rotation radius will lie just outside the Alfvén radius. A differentially rotating accretion disc may therefore be maintained, where $\Omega_d > \Omega_s$, and provide a site for the re-processing of fast particles.

If the integral cosmic ray energy spectrum is assumed to follow an $E^{-1.6}$ power law, then following the method of section 4.4.2, the 1% flux limit, $\varphi_{1\%}$, is approximately equal to $2{\cdot}6 \times 10^{-11}$ cm^{-2} s^{-1} at E $\geq$ 450 GeV. The peak period in figure 6·4e(i) corresponds to a Rayleigh vector of magnitude 0·03, giving a flux of $7{\cdot}8 \times 10^{-11}$ cm^{-2} s^{-1}, which reduces to a minimum luminosity of $2{\cdot}7 \times 10^{32}$ erg s^{-1} if the source distance of 200 pc assumed by Zukerman, Becklin, McLean and Patterson (1992) is applied. This is strikingly similar to the 2×10^{32} erg s^{-1} measured by these authors for emission in the 2 to 20 keV band, and is therefore not entirely unreasonable.

One point which should be noted is that made by Meintjes et al. (1992), that caution must be employed when assessing the significance of any periodicity of the order of 100 s or more found in VHE γ-ray data, because "the counting statistics are low".

6.4.3 EF Eridani, a polar system

(i) background information

The second Ariel catalogue x-ray source 2A 0311-227 was found to have an optical counterpart exhibiting CV characteristics. The discovery of an

81·02 min period in the optical light curve and of the strong circular polarisation associated with cyclotron emission confirmed its status as a polar system (Williams et al., 1979). Of the 17 or so positively identified polar CVs, only AM Her is brighter and indeed it is not possible to say which of these two systems has the greatest intrinsic luminosity, since the secondary star of the EF Eri system has not yet been identified, making distance determination difficult. Both EF Eri and AM Her appeared as strong hard x-ray emitters in data from the Einstein Observatory, but it is the spectrum of EF Eri which most closely resembles that predicted from simple models, hence Beuermann, Stella and Patterson (1987) refer to this system as "the textbook example" of polar CVs. Seifert, Ostreicher, Wunner and Ruder (1987) interpreted a strong optical polarisation feature of EF Eri as being due to hydrogen emission spectra in a region of magnetic field strength ~ 1·5 MG. This must lie at 1 to 2 r_{wd} above the white dwarf surface if a typical B_{wd} of 30 MG is assumed, and therefore this interpretation is in good agreement with accretion column models. The dipole field strength B_{wd} has not been directly measured, but the above authors also report a lower limit given by a hydrogen absorption feature indicative of a 10 MG field region.

As with all polar CVs, the rotation of the primary is synchronous with the orbital period. EF Eri is of particular interest to γ-ray astronomers since it exhibits a well-established quasi-periodic pulsation at x-ray wavelengths, the presence of which would greatly increase the significance of a weak γ-ray flux detection. These six-minute pulsations have been shown to be present at all wavelengths from 0·05 to 700 nm. Patterson, Williams and Hiltner (1981) observed a mean x-ray period of 5·6 ± 0·2 minutes and excess power extending between 4 and 7 minutes. Since radiation at all wavelengths is dependent upon the accretion rate in some way, it seems reasonable to suppose that the QPOs are due to modulation of the accretion flow. The above authors consider the two most viable driving mechanisms to

be the radial pulsation of an accretion disc and relaxation oscillations in a shocked accretion column. They suggest that although a full accretion disc is prohibited by polar CV models a narrow ring of material may be allowed to exist such that the consequent disruption of the magnetic field is not widespread and synchronicity is maintained. The mass accretion rate onto the white dwarf will vary as the inner edge of this ring regularly grazes the magnetosphere. Alternatively, radiation pressure at the base of an accretion column which is slow to dissipate may temporarily halt the downward matter flow, so that flux variations occur on a timescale typical of that required for plasma at the top of the column to free-fall to the white dwarf surface and restore this pressure balance. Note that these authors find that six minutes corresponds to a free-fall distance equivalent to approximately half the Roche lobe radius of a one solar mass white dwarf primary.

(ii) the dataset

EF Eri was the target of both the Mark III and the Mark IV telescopes during eight nights in November 1990. In addition to these simultaneous observations, data was collected using the Mark IV telescope alone in November 1991. All observations were made in tracking mode when the object was near its culmination at a zenith angle of -8°, hence the Mark III and Mark IV telescope threshold energies were in the region of 250 GeV and 450 GeV respectively. The EF Eri dataset is catalogued in figure 6.4f.

(iii) analysis and results

The correction of event arrival times to the solar system barycentre was performed according to the source position given by Ritter (1990). Routine filtration was carried out in order to obtain 23 individual data files, each containing only those events which triggered the central

date (UT)	duration (min.)	telescope	sky clarity
07/11/1990	32	III	excellent
08/11/1990	142	IV	v. good
09/11/1990	77	III & IV	v. good
14/11/1990	144	III & IV	excellent
16/11/1990	150	III	poor
17/11/1990	120	III & IV	excellent
18/11/1990	120	III & IV	poor
19/11/1990	77	III & IV	excellent
20/11/1990	162	III & IV	excellent
21/11/1990	122	III & IV	excellent
01/11/1991	131	IV	excellent
05/11/1991	124	IV	v. good
06/11/1991	150	IV	v. poor
07/11/1991	130	IV	excellent
08/11/1991	125	IV	v. good
11/11/1991	89	IV	v. poor

Fig. 6.4f : the EF Eridani dataset.

channel alone of the appropriate detector. Since no rapid white dwarf rotation period is documented or indeed expected, a search was carried out for QPOs. The power at frequencies in the range 0·2 mHz to 0·3 kHz, as represented by the magnitude of their Fourier coefficients, was calculated for each data file using the Fast Fourier Transform method described in section 4.3.2. No evidence was found of any periodicity in the 4 to 7 minute (~ 4 to 2 mHz) region apparent in the x-ray data of Patterson, Williams and Hiltner (1981), even before the number of degrees of freedom expended by the application of such a wide search range was considered. In fact, the spectra appeared indistinguishable from that of random noise.

The data were examined for burst activity by splitting each observation into bins of width 42 s in order to produce count rate profiles similar to those in figure 6.4b(i). No bin was found to contain an excess event count lying much further than three standard deviations from the expectation value. A visual inspection of the 23 separate light curves did not reveal any periodicity at the 5·6 minute (≡ 8 bin) level.

It was considered that, given the small zenith angle throughout these observations, the on-source event count rate should be large compared with the magnitude of the statistical fluctuations therein, and the construction of a γ-ray orbital light curve might thus be worthwhile. Four nights from the 1990 dataset were chosen, during which the weather conditions were recorded as excellent and a full orbital period of EF Eri was covered by both telescopes. In order to assess the significance of systematic variations in count rate with zenith angle, parabolic fits were made to the number of events arriving in a 240 s "window" slid through each observation in four steps. The count rate profiles derived from data from the more sensitive Mark III telescope are shown in figure 6.4g. It is clear from these plots that the influence of what is, in all cases, a gradual decrease in zenith angle of $\leq 20^\circ$ is easily overborne by variations in the number of Cerenkov events due to changing atmospheric conditions and random

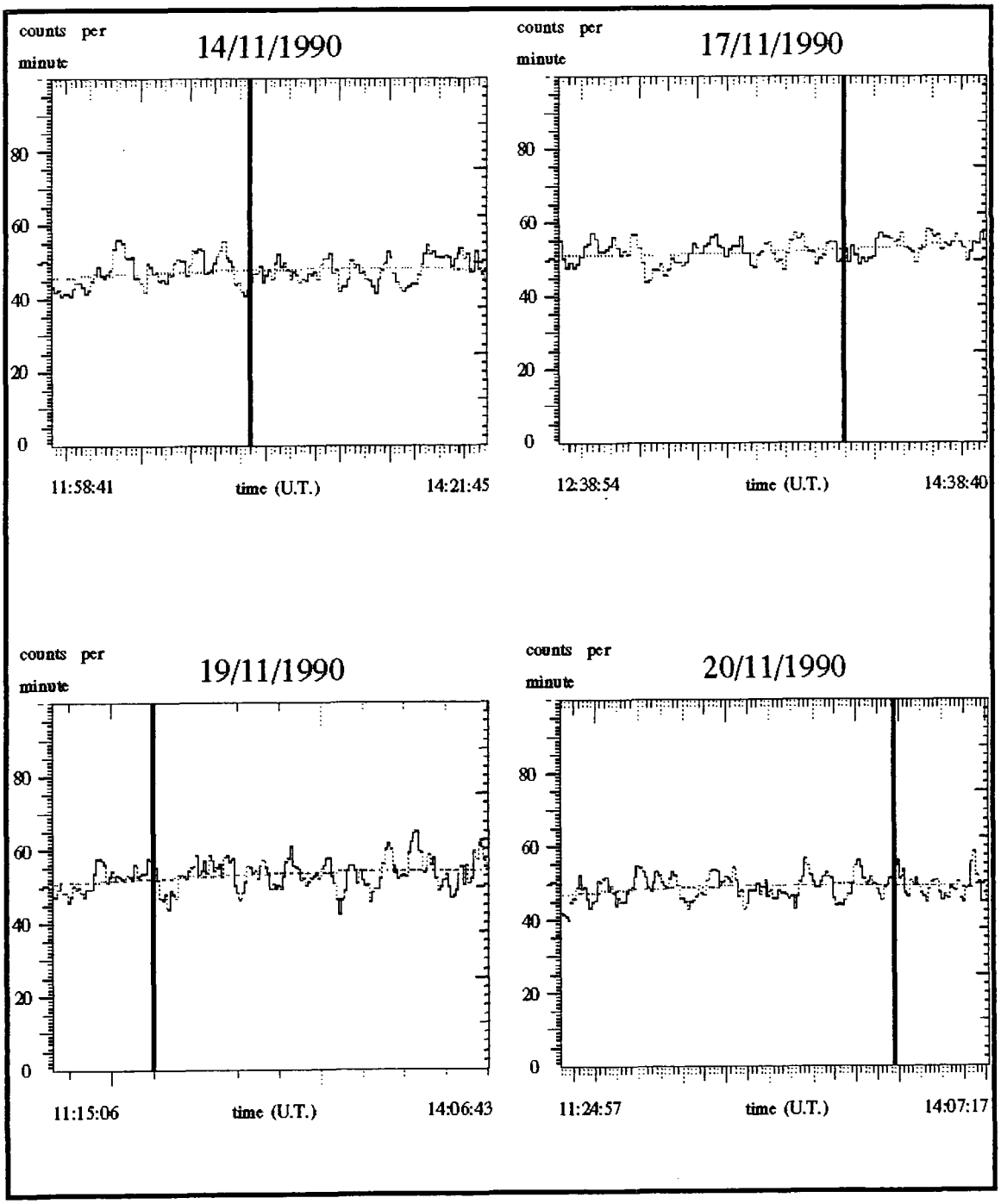

Fig. 6.4g : count rate throughout four Mark III telescope observations of EF Eridani (Cerenkov events triggering the central channel only). Vertical bars denote the time of x-ray eclipse.

statistical effects. The point of x-ray eclipse indicated for each observation was determined from the infra-red ephemeris of Bailey, Hough, Gatley and Axon (1983), as Beuerman, Stella and Patterson (1987) have shown eclipse to be simultaneous in both wavelength regions. The point of mid-eclipse will be referred to here as phase 0 of the 81·02*min* orbit. Data segments running from one occurrence of orbital phase 0·25 to the next were extracted from the observations of 14/11/1990, 17/11/1990 and 20/11/1990, and from phase 0·75 to 0·75 + 1 from the observation of 19/11/1990. These segments were subdivided into 36 orbital phase bins for ease of calculation and the number of events occurring within each bin was totalled. The results obtained from the four separate observing sessions were combined to give the mean number of events expected at a given orbital phase for each telescope, thus nullifying at least some of the random count rate fluctuations. The number of events per 135 s bin were normalised to give the mean count rate per minute shown in figure 6.4h. It was hoped that by producing one light curve per instrument, a trend discovered in data from the Mark III telescope might be confirmed as a non-instrumental effect by a similar response from the less sensitive Mark IV instrument. To assist in this discrimination, the same treatment was applied to events in the original Mark III telescope data files which triggered a response from a single off-source guard ring channel (channels 1 and 5 were chosen as in the analysis of the burst from H0253+193). For completeness, a curve was also produced for those events from the Mark III telescope which met the "soft cut" criterion that the charge collected by the guard ring channels should not exceed 45% of that in the central one, although the corresponding reduction in the total number of events considered increased the apparent significance of statistical fluctuations.

It is clear that the light curves displayed in figure 6.4h show no evidence of a dependency of the on-source count rate upon the orbital phase of EF Eridani.

Fig. 6.4h : orbital light curves of EF Eridani, averaged over four orbital periods, from data collected on the 14th, 17th, 19th and 20th of November 1990. Events which triggered the central channel only are plotted for the Mark IV telescope and for the Mark III telescope before and after data selection on the basis of Cerenkov light flash intensity. Also shown is the concurrent response of two off-source guard ring channels of the Mark III instrument.

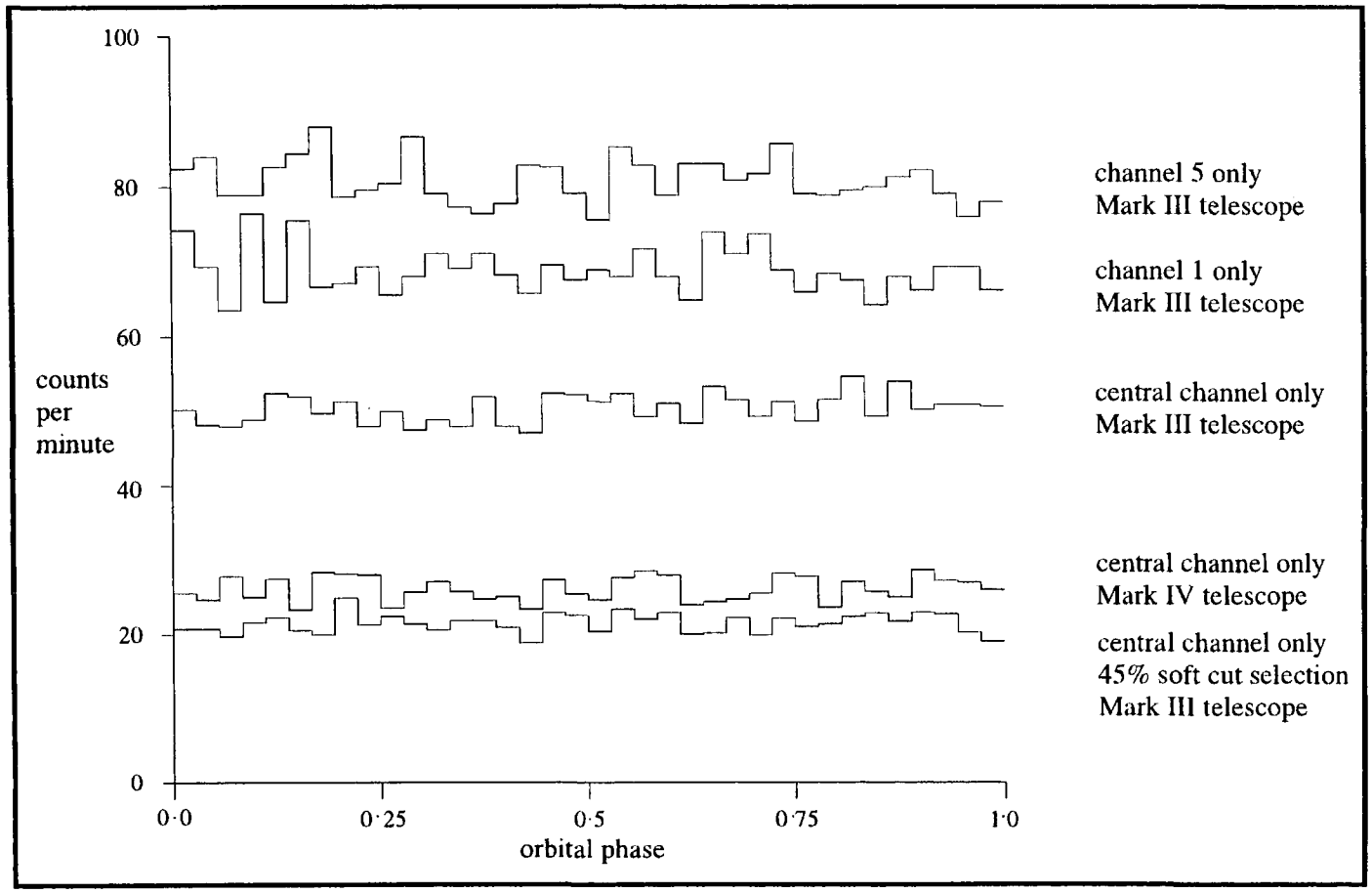

(iv) summary

Although, as an accreting system, EF Eri has the potential to exhibit burst activity as a result of mass transfer instabilities, it is by no means certain that γ-rays would have a role in this energy release. In fact, the 5·6 minute modulation of the x-ray flux suggests that the accretion flow is well regulated. No evidence of bursts of γ-rays or of periodicity on the timescale of a few minutes has been found in the Durham dataset.

Since the white dwarf rotates synchronously with the orbital period, its dipolar field should not be wound about its spin axis, therefore no regular large scale magnetic reconnection is expected. Star-disc dynamo mechanisms of particle acceleration are also inapplicable, and QPOs associated with a disc target for γ-ray production are neither expected nor observed.

Fast particle production might occur through plasma turbulence in the magnetosphere, and power a γ-ray flux modulated at the orbital period in accordance with the occasional availability of a target medium for π^{o} production, such as the limb of the companion star. Since it is assumed that the x-ray eclipse observed by Beuermann, Stella and Patterson (1987), already shallow at an energy of 10 keV, is due to obscuration of a hot region near the white dwarf surface by a thin accretion column, no such γ-ray eclipse is expected. This γ-ray flux might even be enhanced at this orbital phase as this column crosses the line of sight to the compact star providing a target for π^{o} production. No such orbital dependency of the Cerenkov flash count rate has been detected. It would be extremely unwise to draw any conclusions as to the nature of the EF Eri system from this result. It is to be hoped that this might eventually be possible through observations spanning more than one orbital period per session taken over a period of several months. At present, the best possible course to follow in pursuit of the detection of EF Eri at TeV energies would be to carry out a

series of observations in "chopping" mode, in order to establish the presence or otherwise of a count rate excess in the direction of this object.

6.4.4 VW Hydri, a dwarf nova

(i) background information

VW Hyi is a dwarf nova which undergoes "normal" outbursts lasting for 3 to 5 days and recurring on average every 27 days and "superoutbursts" which are brighter than normal ones by approximately one magnitude in the visual region, last for 10 to 14 days and occur once every 179 days (Pringle et al., 1987). Almost 1 in 5 dwarf novae exhibit this duality and are referred to as SU Uma type systems. VW Hyi is the brightest CV of this sub-group (a distance estimate of 90 pc was provided by Bailey, (1981)). It has an orbital period of 0·07427 days and an inclination of about 60° (Schoembs & Vogt, 1981). The spectrophotometry of Bath, Pringle and Whelan (1980) revealed continuum spectra consistent with the presence of an accretion disc. Haefner, Schoembs and Vogt (1979) suggested that "VW Hyi should be considered as an exemplary case for many, if not all dwarf novae". As such, VW Hyi was the object of a coordinated observing campaign spanning several months in 1984 covering the spectrum from optical to x-ray wavelengths (Pringle et al., 1987).

VW Hyi has proved to be an abundant source of QPOs. These range from the 413 s optical modulation observed by Warner and Brickhill (1978) on a single night during a normal maximum to the 14·06 s soft x-ray oscillations at superoutburst reported by van der Woerd et al. (1987). These authors applied the Fast Fourier transform technique to data collected by the Low Energy telescope aboard the EXOSAT observatory during superoutburst, normal outburst and quiescence. They found evidence of periodicity in the range 13 to 15 seconds on four occasions, coincident with superoutburst episodes.

They point out firstly that there are too few detections to justify the assumption that these QPOs are present *only* in superoutburst activity and secondly that the quiescent x-ray spectrum of VW Hyi is harder than the outburst spectrum.

Haefner, Schoembs and Vogt (1979) stated that the optical QPOs of VW Hyi converging upon period P conformed to the expression $\Delta P/P \leq 0{\cdot}01$, such that period stability was maintained for no longer than an hour or two. Their results are in good agreement with those of Robinson and Warner (1984) who discovered a period of 253 s having a coherence time of between 3 and 15 cycles during a three hour photometric observation. A 23·6 s periodicity was present alongside this 253 s signal, which led these authors to suggest that more than one oscillation mechanism was at work.

Outbursts may be caused by either a variation in the mass transfer rate from the secondary star, or by instability in the accretion disc. X-ray emission is thought to arise in the boundary region between the inner edge of the accretion disc and the surface of the white dwarf, where most of the kinetic energy of accretion is given up (van der Woerd et al., 1987). The x-ray flux in the 1 to 6 keV band observed in EXOSAT data throughout quiescence indicates that accretion is continuous, although, according to van der Woerd and Heise (1987), somewhat "erratic". Broadening of the accretion disc during outburst has been observed in some eclipsing SU Uma type dwarf novae. The above authors suggest that this boundary layer also becomes optically thick, hence the decrease in the x-ray hardness ratio at this stage of the emission cycle. Soft x-ray emitting "hot spots" may be generated in the boundary layer through the channelling of energy transport (via electron conduction) by transient magnetic fields.
Van der Woerd et al. (1987) consider the redistribution of angular momentum, and the differential rotation of this layer, to be the cause of the drifts in period of soft x-ray QPOs. These authors also judge that the coherence of the x-ray periodicity which they observe could not be attained

by disc dynamo generated magnetic fields, but require instead the presence of a weak white dwarf dipolar field.

(ii) the dataset

Observations of VW Hyi were made using the Mark III and Mark IV telescopes in tandem on three occasions in November 1990, some 30 days after the supermaximum of 5th October 1990 reported by Harrison (1990). Data was collected in tracking mode at and near the culmination of the object at a zenith angle of 41°. At least one 107 s orbit was covered during each observing session, as is apparent from figure 6.4i.

(iii) analysis and results

The event arrival times were corrected to the solar system barycentre in accordance with the position given by Ritter (1990).

The initial approach to simultaneous observations is to scan the data for on-source burst activity detected by both telescopes, such as that seen during the observation of AE Aqr on 13th October 1990 (Bowden et al., 1992). No similar excess was discovered in this dataset. The data were in fact very well behaved, in that no peak above three standard deviations from expectation appeared when the events triggering the central channel only were assigned to 60 s bins, in the manner described in section 6.4.2(iii).

In order to search for periodicity of the order of tens of seconds, potentially coherent over about an hour, the data files from the 10th and the 13th of November were halved, whilst that from the 11th of November was quartered. The resulting sixteen - one hour long sub-sets of data were analysed separately by the Fast Fourier Transform technique of section 4.3.2., over the range 30 mHz to 2 Hz. No above expectation power was observed anywhere in this region. In particular, there was no evidence of

date (UT)	duration (min.)	telescope	sky clarity
10/11/1990	127	III	poor
10/11/1990	95	IV	poor
11/11/1990	246	III	excellent
11/11/1990	239	IV	excellent
13/11/1990	120	III	v. good
13/11/1990	120	IV	v. good

Fig. 6.4i : the VW Hydri dataset.

any of the QPO periods previously observed at lower wavelengths.

It was concluded that the size and quality of the dataset was not sufficient to justify the construction of an "orbital light curve" such as that produced for EF Eri. The inclination of the VW Hyi system is such that the periodic obscuration or revelation of a γ-ray production site due to orbital motion is improbable.

(iv) summary

No burst activity was observed from VW Hyi. This is not surprising since most energy is released in regular superoutbursts, rather than during apparently random episodes of enhanced accretion as is seen to occur in novalike CVs. It is doubtful as to whether a γ-ray flux would coincide with enhanced activity at longer wavelengths i.e. during outburst, or that the thickening of the disc region during rapid mass transfer would in fact have the effect of suppressing VHE γ-ray emission, through the absorption of potential γ-ray progenitor particles. Given the surprisingly well regulated superoutburst recurrence time and the ten day active period, it should be possible, in due course, to target such an event within the limited duty cycle of a ground-based Cerenkov telescope.

No QPOs were detected in the period range indicated by x-ray observers. Since most previous periodic γ-ray flux detections have been obtained through the accumulation of a weak signal over many months of observation, this is hardly surprising. Although the continued absence of a γ-ray flux would in no way invalidate the magnetic instability QPO generation mechanism of van der Woerd et al. (1987), γ-ray production would certainly suggest the existence of magnetic fields, the random orientation of which might account for the otherwise prohibitively low level of polarisation reported by Schoembs and Vogt (1980).

6.5 conclusions

Of the particle acceleration mechanisms reviewed in section 6.3, within CVs only magnetic reconnection and star-disc dynamos are likely to produce particles having energies in the TeV region. The dipolar magnetic fields of dwarf novae are too weak to support a reconnection driven VHE particle flux, whilst polar CVs do not contain accretion discs. Plasma turbulence and the first order Fermi mechanism may contribute a flux of γ-rays having energies in the tens of GeV region. However, these photons will be susceptible to absorption by pair production and lie below the current 250 GeV threshold energy of the Mark III telescope.

The redistribution of accreting material within a polar CV system may momentarily disrupt the synchronisation of the orbital motion and the white dwarf rotation, thus allowing magnetic reconnection to take place. A brief burst of γ-rays may be observed as a result. No evidence of burst activity was found within the EF Eri dataset listed in figure 6.4f. None of the particle acceleration mechanisms presented here could cause polar CVs to emit a steady VHE γ-ray flux. Therefore, any QPOs detected at lower energies are unlikely to be present throughout an atmospheric Cerenkov dataset. The detection of orbital phase dependent emission would require that magnetic reconnection regularly coincided with a favourable alignment of the particle acceleration site and a material target for γ-ray production. A reproducible, asymmetric γ-ray orbital light curve would reveal valuable information as to the physical processes occurring within such a system. An attempt to construct an orbital light curve for EF Eri served to highlight the difficulty of obtaining atmospheric Cerenkov observations of more than an hour in duration under stable weather conditions. At present, CVs of this class do not appear to be appropriate targets for observation by the atmospheric Cerenkov technique.

Dwarf novae may be found to emit γ-rays on a more regular basis than polar CVs, via some form of star-disc dynamo mechanism. However, the

characteristic dwarf novae oscillations observed in the x-ray region are again only quasi-periodic. At best, DNO may remain coherent for a few tens of minutes so that, if present, such a pulse signature is unlikely to be statistically significant in sparse VHE γ-ray data. Indeed, a null result was obtained when atmospheric Cerenkov data taken on the brightest SU Uma type dwarf nova, VW Hyi, was searched for periodicity using the FFT technique (see section 4.3.2). Since only 8 hours of data of variable quality was analysed, this result should not be seen as conclusive. Targeted observations made over two weeks whilst VW Hyi is in superoutburst could prove worthwhile. The epochs of these active periods are easily predictable from optical data. Since star-disc dynamo mechanisms for γ-ray production entail beams of fast particles, the non-detection of VW Hyi could be attributed to the misalignment of any particle beam with Earth. It is interesting to note that the orbital inclination of the VW Hyi system is within 2° of that of the intermediate polar CV AE Aqr, which *has* been seen to emit VHE γ-rays.

Intermediate polars are the most promising CV targets for atmospheric Cerenkov astronomers. This verdict is not only based upon the detections of AE Aqr reported in section 6.4.1, but also follows from the γ-ray emission models considered in section 6.3. The rotation period of the white dwarf has been measured for many intermediate polars. A pulse signature of this type may be identified using the standard Rayleigh test described in section 4.3.3(iii), which introduces far fewer degrees of freedom than the FFT method required to search for QPOs, and is therefore more likely to uncover a statistically significant signal. The dipolar magnetic fields of intermediate polar bound white dwarfs, which are of the order of 10^5 G in strength, may make star-disc dynamo mechanisms for particle acceleration more efficient in these systems than in dwarf novae (where B_{wd} is negligible). It has been suggested that some intermediate polar systems may alternate between disc accretion and mass transfer via an accretion column

or some combination of the two. This restructuring may give rise to bursts of VHE γ-ray emission powered by magnetic reconnection. The detection of VHE γ-rays from intermediate polars could clarify current understanding as to the nature of these systems, wherein the optical depth of accreting material obscures the central powerhouse from view at longer wavelengths. Analysis of the H0253+193 dataset recorded using the Mark III telescope revealed one potential γ-ray burst episode. This was similar to that seen from AE Aqr in October 1990, although rather less prominent and lacking confirmation from the Mark IV instrument which was not in use. Although no evidence was found of the 206 s pulsation seen in the x-ray spectrum of H0253+193, a 162 s periodicity was discovered, which was present during several observations. An extension of the H0253+193 dataset is recommended.

CHAPTER SEVEN

VHE γ-rays in the Vicinity of Neutron Stars

This chapter contains a short description of x-ray binary systems, drawing upon the similarity between these and Cataclysmic Variables. Mechanisms for γ-ray emission from millisecond pulsars are also considered here, as these objects may be produced through the redistribution of momentum within low mass x-ray binaries. The results of a search for neutron star associated VHE γ-ray emission from various systems are presented.

7.1 x-ray binaries

X-ray binaries are the products of stellar evolution within massive close binary systems in which the primary star has a mass, M_p, in excess of 12 M_{sun}. When this body undergoes gravitational collapse to form a neutron star, the associated supernova explosion will not disrupt the system if the non-degenerate secondary star has a mass $M_s \geq 0{\cdot}3\ M_p$ (van den Heuvel, 1976). In this scenario, the system will remain dormant until such time as the secondary star itself evolves to the supergiant stage, initiating bulk mass transfer to the compact primary via a strong stellar wind, to form a high mass x-ray binary (HMXB). The life span of the x-ray emitting stage is estimated to be 10^4 to 10^5 years in HMXBs (Mannings, 1990).

In the case $M_s < 0{\cdot}3\ M_p$, it is rare for the two stars to remain gravitationally bound after the supernova event. It is generally accepted that those systems which do survive the explosion are the precursors of low mass x-ray binaries (LMXBs). The detection of roughly equivalent numbers of HMXBs and LMXBs in spite of their differing lifetimes is consistent, having allowed for selection effects, with a rate of HMXB production in excess of that of LMXBs, and hence with the close binary - supernova formation

hypothesis.

An alternative mechanism for LMXB formation was proposed by Gursky (1976). He suggested that mass transfer onto a white dwarf could cause it to exceed its Chandrasekhar limit and undergo collapse to form a neutron star. Thus some Cataclysmic Variables may be LMXB progenitors (see also Labay, Garcia, Canal & Isern, 1989).

In LMXBs, the secondary star, from which matter is transferred to the neutron star via Roche lobe overfow (see section 6.2.2), is either a main sequence star of A type or later or a white dwarf (White, 1989). At optical wavelengths, the light from the system is dominated by a disc surrounding the neutron star heated by an accretion powered x-ray flux. Conversely, the optical spectra of HMXB systems are attributed to the early O or B type companion stars. The time elapsed between neutron star formation and the onset of x-ray emission is of the order of 100 times greater for systems which require a low mass secondary star to evolve to fill its Roche lobe than for HMXBs. It has been suggested by Podsiadlowski (1991) that irradiation of the companion's surface by x-rays generated by mass accretion onto the neutron star can induce further expansion of the secondary. As the stellar envelope of the irradiated companion expands in order to attain a thermal equilibrium, the binary orbit widens. The expected increase in orbital period is of the order of that observed in the LMXBs Cyg X-3 and Sgr X-7. The above author predicts that unless magnetic braking, gravitational radiation or some other mechanism can support the accretion flow, an abrupt cut-off of the mass transfer will occur when the irradiating flux falls below a critical level. This model limits the lifetime of LMXBs in which the secondary is a main sequence star to $\sim 10^8$ yr as opposed to only $\sim 10^6$ yr for those containing subgiants.

A recent reassessment of the galactic LMXB distribution by Naylor and Podsiadlowski (1993) confirmed the existence of two distinct classes of LMXB (outside globular clusters). By ordering a sample of 36 LMXBs

according to the magnitude of their x-ray flux in the Ariel V sky survey, these authors found that the ten most luminous sources lay in the direction of the Galactic bulge, and that their large mass transfer rates might therefore be due to evolution driven expansion of the secondary star, in accordance with their association with an old stellar population. The rest of the sample were scattered in longitude and assumed to be related to the Galactic disc, their distance above and below it being consistent with an age of 10^7 to 10^8 yr, given the initial impulse of an asymmetric supernova explosion and subsequent travel time out of the plane of the disc.

Accretion discs and columns form in LMXBs, subject to those constraints which were discussed in the context of CVs in the previous chapter. Similarly, the particle acceleration mechanisms considered in chapter six are generally applicable and many are rather more powerful in LMXB systems than in CVs, since the degenerate star in the former typically supports a magnetic field of $\sim 10^9$ G (Carraminana, 1991). In addition to star - disc dynamo interactions (section 6.3.2(iii)) and the various forms of shock acceleration appropriate to CVs, fast particles may be ejected from the vicinity of an accreting neutron star towards targets suitable for π^o production (such as those in figure 6.3c) in the form of jets, which are formed where gas pressure at the neutron star surface is sufficient to repel in-falling material, which then rebounds and is channelled outwards along the open magnetic field lines (Quenby & Lieu, 1989) or as a pulsar wind.

7.2 an introduction to pulsars

In this chapter, case studies of a LMXB which could potentially support a fast pulsar, of a pulsar within a binary system which exhibits no signs of on-going accretion and of an isolated pulsar are presented.

A simple division may be made between neutron stars whose emission, regularly pulsed at the stellar rotation frequency, is powered simply by

the gradual loss of the kinetic energy with which they are formed and those which are driven by matter accretion from a companion star. The strong magnetic fields and rapid rotation of the former support charged particle acceleration which results in a large flux at radio wavelengths, hence the term "radio pulsars". Any radio emission from the latter is quenched through the interaction of the accelerated ions with in-falling material. Thus the pulsed output of these systems is dominated by x-rays produced through cyclotron radiation in the accretion flow, and they are said to contain "x-ray pulsars".

7.2.1 x-ray pulsars

The conservation of angular momentum during the collapse of its progenitor should endow a newborn neutron star with a spin period of the order of 0·01 s (Henrichs, 1983). This estimate is consistent with the observed rapid rotation of the young pulsars associated with the Crab and Vela supernova remnants. However, the coherent x-ray pulsations attributed to rotating neutron stars in x-ray binary systems lie in the region 0·07 s to 800 s. It is reasonable to assume that the relaxation time of the binary following its explosive disruption is such that the neutron star rotation will have slowed considerably (through radiative energy losses) before the onset of mass transfer. Of the 30 or so known x-ray pulsars, most exhibit a long term *decrease* in period or "spin-up". In many cases, this spin-up rate varies in an apparently random fashion, which is indicative of the transfer of angular momentum from the companion star to the degenerate primary via episodic mass accretion. It is noticeable that those systems in which an accretion disc has been optically identified tend to exhibit the shortest x-ray pulse periods. Rappaport and Joss (1983) report a slight positive correlation between pulse periods and binary orbital periods. If it is assumed that the initiation of mass transfer is coincident with a reduction in orbital separation, then slow pulsars which have not yet been "spun-up"

by accretion should reside in wide, long period binaries, whilst rapidly rotating pulsars should be restricted to close binary systems. If the theory of Podsiadlowski (1991) is correct, then this effect may be partially counter-balanced by the irradiation driven expansion of the secondary, and therefore of the orbit, during accretion.

7.2.2 radio pulsars

In contrast to x-ray pulsars, a systematic *lengthening* of the pulse period is a characteristic of radio pulsars. If the magnetic flux of the parent is conserved on neutron star formation, then the degenerate star may acquire a magnetic dipole field strength of the order of 10^{12} G, which will decay over a timescale of $\sim 10^{6}$ yr (Shapiro & Teukolsky, 1983, 281). Thus the "spin-down" of isolated pulsars is attributable to electro-magnetic braking (Kirk & Trumper, 1983). Only ~1 % of all radio pulsars (of which over 400 have been catalogued) are incorporated in binary systems (Henrichs, 1983). Since it is thought that the stellar wind of the companion star may smother the radio emission of newborn pulsars, these few examples may be the remnants of x-ray pulsars which were "spun-up" in systems within which the mass transfer "engine" has since been exhausted. The magnetic fields of these "recycled pulsars" are generally thought to have decayed over time to lie in the range 10^{8} to 10^{10} G, the consequent reduction in the effectiveness of magnetic braking allowing them to maintain periods between 1 and 33 ms for some time after the withdrawal of the accretion torque (Chiang & Romani, 1992). These rapid rotators in non-interacting binary systems are frequently referred to as "millisecond pulsars". These objects are not to be confused with those which, owing to their relative youth, lie at the short period end of the tens of milliseconds to tens of seconds range typical of isolated pulsars.

(i) braking mechanisms

In the magnetic dipole model of Gunn and Ostriker (1969), a neutron star of radius R, having a magnetic dipole moment $\mathbf{m}$, is assumed to rotate in vacuo at a frequency Ω. If the magnitude of the stellar magnetic field at its pole is B_p, then $|\mathbf{m}| = B_p R^3/2$ (Lorrain & Corson, 1970). If $\mathbf{m}$ is inclined at an angle, α, to the rotation axis, then the star is an "oblique rotator", and, when the object is viewed from a distance, the magnetic moment is seen to vary with time. According to Shapiro and Teukolsky (1983, 278), magnetic dipole radiation is therefore emitted at rate given by:

$$\frac{dE}{dt} = - \frac{2}{3\ c^3} \left| \frac{d^2\mathbf{m}}{dt^2} \right|^2$$

In addition, slight deformation of the neutron star to form a rotating, homogeneous ellipsoid could support energy loss through gravitational radiation according to $dE_g/dt = I\Omega(d\Omega/dt)$, where I is the moment of inertia of the body.

If the neutron star is an "aligned rotator" i.e. if $\alpha = 180°$, then a dense magnetosphere may be formed as electric fields tangential to it remove electrons from the stellar surface (as in figure 6.3a). Within the neutron star's light cylinder the magnetic field is dipolar, yet outside the co-rotation radius it forms an outgoing-wave. Plasma escaping along the open magnetic field lines can carry angular momentum away from the star. Shapiro and Teukolsky (1983) report that the outward energy flux at the dipole field - open field boundary, approximately given by the integral over the surface of the star of the Poynting vector E x H, is equivalent to that estimated for dipole radiation in the oblique rotator scenario.

The braking index, n, of a pulsar experiencing deceleration, as a result of electro-magnetic and gravitational torque slowing the pulsar's rotation to its spin frequency, ν, is given by:

$$n = -\nu \frac{d^2\nu}{dt^2} \left[\frac{d\nu}{dt}\right]^{-2}$$

The above authors state that for purely magnetic braking, $n \approx 3$, whereas by gravitational radiation alone, $n \approx 5$, and that n has been measured as 3·43 for the Crab pulsar.

The characteristic age of an isolated pulsar is defined as: $T \equiv -(\nu\ (d\nu/dt)^{-1})$. Its actual age at the time of measurement is given by:

$$t = -\left[\frac{\nu}{(n-1)\ \frac{d\nu}{dt}}\right] \left[1 - \left[\frac{\nu}{\nu_i}\right]\right]$$

where ν_i is its initial rotational frequency (Cordes & Helfand, 1980).

A power law braking inclusive of both magnetic and gravitational effects is required to reconstruct the age of the Crab pulsar known from its association with the supernova of AD 1054 (Thorsett, 1992).

The spin-down of isolated pulsars, which is in general extremely uniform, may occasionally be interrupted by a brief episode during which a fractional increase in rotational frequency of between 10^{-8} and 10^{-10} occurs in less than a day, followed by a gradual exponential decay back to its "pre-glitch" value (Cordes & Helfand, 1980). The timescale for this recovery varies from a few hours to a couple of years (Link, Epstein & Van Riper, 1992). These "glitch" episodes may be attributed to changes in the ellipticity of the neutron star's crust, in response to a decrease in the centripetal force requirement, or to sporadic linkage between the differentially rotating crust and the star's fluid interior (Lyne & Graham-Smith, 1990).

The maximum power output of a rotation driven pulsar may be estimated from its kinetic energy; $E_{KE} = {}^1/_2\ I\ \Omega^2$, hence $dE_{KE}/dt = I\Omega(d\Omega/dt)$. If $I \approx 3\times10^{45}$ g cm^2, then for isolated pulsars, dE_{KE}/dt lies in the range

10^{32} to 10^{36} erg s^{-1} (Brazier, 1991).

(ii) VHE γ-ray production

Usov (1983) states that "for a neutron star to be a radio pulsar, electron - positron pairs should be present in its magnetosphere". The pulsed radio flux is highly polarised and consistent with cyclotron radiation from magnetospheric particles following the open magnetic field lines. The width of the radio beam constrains the emission site to a region above the magnetic pole of the neutron star (Lyne & Graham-Smith, 1990).

In the polar cap model of Ruderman and Sutherland (1975), electrons may escape from the surface of the neutron star, but the positive ions (principally iron nuclei), which make up the star's solid outer crust, remain bound. A charge depleted gap is formed above the polar cap (which is defined as that area of the neutron star surface bounded by those magnetic dipole field lines which are tangential to the velocity of light cylinder). Electrons are accelerated along the magnetic field lines as they pass through this gap, and emit curvature radiation by the mechanism described in section 6.3.1. Photons of curvature radiation having sufficient energy to do so may undergo pair production, and so add to the charged particle flux.

In the Ruderman and Sutherland (1975) model, the strength of the electric field through which polar gap accelerated particles pass is given by $E = 2\ \Omega\ h\ B_p$, where h is the height to which the gap extends above the stellar surface. Excess power at radio wavelengths is evidence of the acceleration of particles to energies sufficient to support enhancement of the particle flux through pair production. According to Usov (1983), the maximum energy at which photons may escape from the gap without degradation to an electron - positron pair is given by:

$$\varepsilon \leq 10^{10}\ r^2\ P\ B^{-1}\ eV$$

where P is the neutron star spin period (in seconds), B is the magnetic field strength at closest approach to the stellar surface (in units of 10^{12} G) and r is the radial distance from the stellar centre (in units of 10^{6} cm). Using this model, the above author found that 1 % of the total energy loss rate of the 1·5 ms pulsar PSR 1937+214 should be in the form of γ-rays, having a maximum energy per photon of 10^{11} eV.

It might be expected that charged particles which impact upon the polar cap would heat the surface of the neutron star and so produce a strong x-ray flux. No such x-ray emission is observed.

Cheng, Ho and Ruderman (1986) speculated that fast particle acceleration may occur in regions near the velocity of light cylinder, thus the "missing" x-ray flux problem is averted. "Outer gaps" are formed as charge separation occurs within the rotating magnetosphere, in much the same manner as described in section 6.3.2(iii) in the context of a disc supporting system. In the opinion of these authors, curvature radiation and inverse Compton scattering of low energy photons off particles accelerated in these extended gaps (positioned as shown in figure 7.2) could power a flux of γ-rays in the 10^{12} eV region.

Chiang and Romani (1992) endeavoured to reproduce the pulse structures observed in emission from the Crab and Vela pulsars at radio and optical wavelengths using simulations based upon the two models above, in order to test the applicability of the polar cap and of the outer gap configurations. They concluded that whilst the polar cap model correctly describes the observed γ-ray spectrum, the pulse morphologies may only be retrieved by application of the outer gap assumption, although these profiles are still far from perfect.

The above authors noted that of the pulsar population, millisecond pulsars, having relatively low field strengths and narrow light cylinders, would be expected to be the least sensitive to the choice between the polar cap and outer gap emission regions. For millisecond pulsars, where the

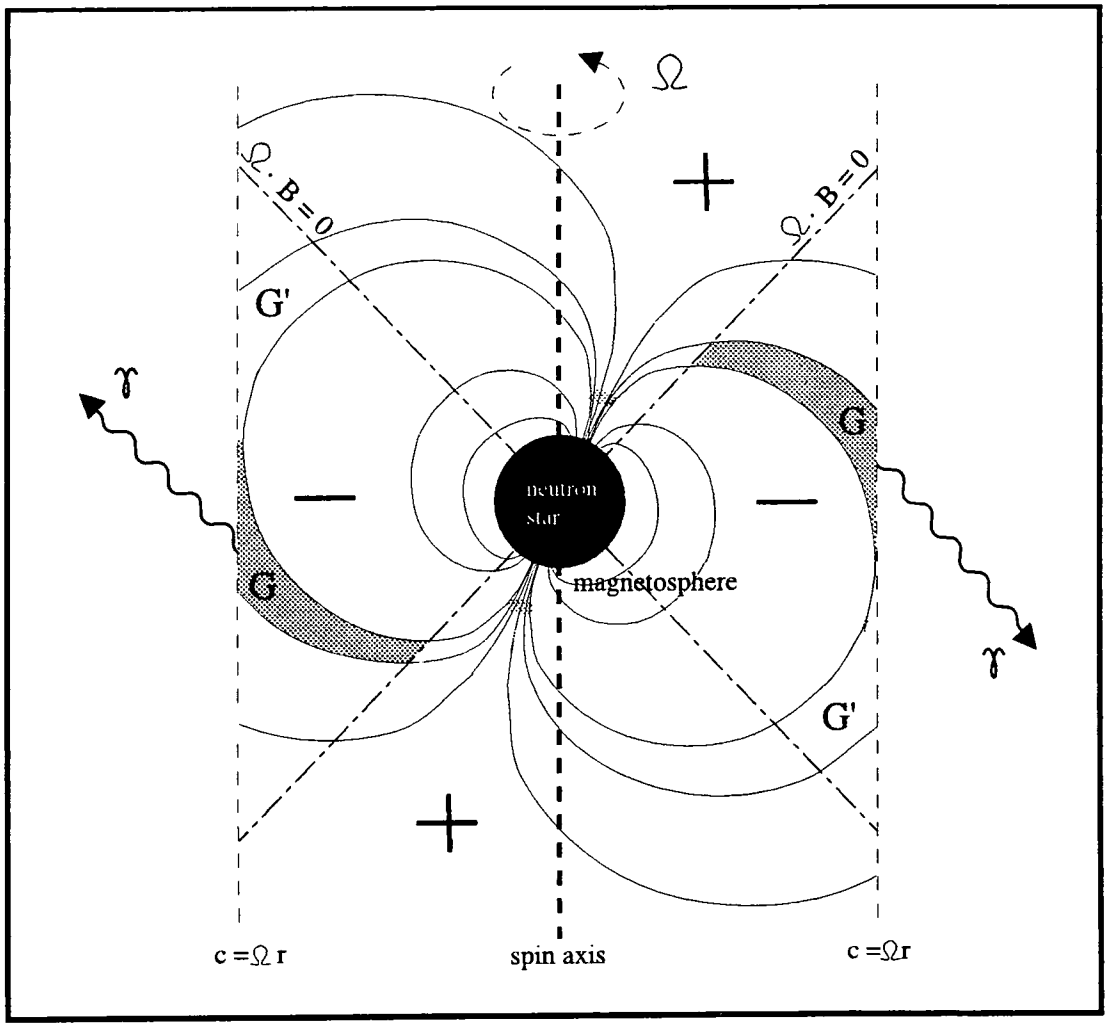

Figure 7.2 : geometry of the outer gaps in a pulsar magnetosphere (after Cheng, Ho and Ruderman, 1986). The particle flux from the gap regions labelled G is expected to suppress the formation of less extensive vacuum gaps in the regions labelled G' .

radius of curvature of the outermost, unbroken magnetic field line is small and synchrotron losses are negligible, they found that the flux of γ-rays above 10 MeV should follow the relation:

$$F \approx 3{\cdot}5 \times 10^{33} P^{-1.4} B^{0.95} \text{ erg s}^{-1}$$

as opposed to:

$$F \approx 6{\cdot}4 \times 10^{32} P^{-2.2} B^{1.1} \text{ erg s}^{-1}$$

for isolated pulsars.

The above "standard model" of millisecond pulsar evolution has recently been called into question as a result of the discovery, by Bell, Bailes and Bessell (1993), of a cool white dwarf companion to the nearby 5·75 ms pulsar J0437-4715. The characteristic age of this pulsar, as evinced by its spin-down rate, is less than the time which must have elapsed since white dwarf formation for the companion's temperature to have fallen to its current value. By implication, if accretion driven spin up of the pulsar ceased on the collapse of the giant, mass donating companion, then the time-averaged rate of decay of the pulsar magnetic field must be considerably less than that previously assumed. If this is the case, then the recycling of slow pulsars need not be considered a ubiquitous requirement for binary millisecond pulsar formation. Kulkarni & Thorsett (1993) summarised the problems attached to the assumption that LMXBs are the progenitors of millisecond pulsars. They stated that not only did the abundance of millisecond pulsars greatly exceed that of LMXBs, but that, referring to LMXBs, "considerable effort has uncovered no evidence for millisecond pulsations from any of them".

An opportunity exists here for γ-ray astronomers to make a significant contribution towards the determination of the origins of millisecond pulsars, possibly through further confirmation of the presence of a 12·6 ms TeV γ-ray pulsar in the LMXB Cyg X-3 reported by Chadwick et al. (1985). A

fraction of the pulsed flux from such an object, perhaps absorbed or scattered at longer wavelengths by the accreting material necessary to the spin up mechanism, may be detected in the form of energetic γ-rays.

7.3 Sgr X-7, a low mass x-ray binary

7.3.1 background information

Sgr X-7, which appeared in the 4th Uhuru catalogue as 4U1822-37, was optically identified as a stellar binary by Griffiths et al. (1978). Its luminosity in the x-ray region exceeds its combined optical and UV output, which is indicative of the presence of a neutron star rather than of a white dwarf (Mason & Cordova, 1982).

Mason et al. (1980) identified a 5·57 hour modulation in the optical light curve with occultation by an accretion disc and noted that this eclipse was "morphologically similar" to that of the x-ray binary Cyg X-3. They attributed optical dimming between phases 0·66 and 0·91 of the orbital cycle to absorption in a stream of accreting material. White and Holt (1982) noted only a partial eclipse in the 2 to 60 keV range, which led them to suggest that x-rays from a central compact source were being scattered by an ionised corona lying above and below the accretion disc. Such a corona might form through the evaporation of material from the disc surface, which would require its illumination by a compact x-ray source radiating close to its Eddington limit where the total x-ray luminosity $\geq 10^{37}$ erg s^{-1}. UV data in the 160 nm region lent weight to the x-ray corona hypothesis; a minimum was observed around orbital phase 0·8, suggestive of the obscuration of a small emission site near the inner edge of an accretion disc by a bulge at the disc's periphery (Mason & Cordova, 1982a). This modulation was present in neither x-rays nor in optical light, as is consistent with x-ray emission above the plane of the disc and an optical contribution from its outer edge. By assuming a black body spectrum for the

inner and outer edges of this "wall" of accreting material, Mason and Cordova (1982) estimated the distance to Sgr X-7 to be 2·5 kpc. From their model, these authors inferred an inclination of the binary orbit to the line of sight of between 76° and 84°.

Mason et al. (1980) searched for periodicity in the range 0·2 to 50 Hz in white light from Sgr X-7. They found that the optical output was in fact remarkably uniform and devoid of flickering. Hellier, Mason and Rees Williams (1992) conducted a "pulsar search" in data collected in the 1 to 30 keV range using the Ginga satellite. They found no evidence from their Fourier analysis of periodic or quasi-periodic oscillations. It should be noted that their sample consisted of a single 45 minute exposure, taken during the brightest part of the x-ray cycle (orbital phases 0·3 to 0·5).

7.3.2 the dataset

Several authors have remarked upon the similarities between Sgr X-7 and the x-ray binary Cyg X-3. A 12·59 ms pulse period was discovered by the Durham group in data taken on Cyg X-3 at the Dugway site in 1983 (Chadwick et al., 1985, Bowden et al., 1992a). Viewed from Bohena Settlement, Cyg X-3 rises no higher than 20° above the horizon, where the Cerenkov event count rate is poor, thus Sgr X-7 became an attractive target for southern hemisphere observations. At culmination, Sgr X-7 reaches a zenith angle of 6° during the month of August, and may therefore be observed near the minimum 250 GeV threshold energy of the Mark III telescope.

Sgr X-7 was targeted for a brief spell in August 1987, but was soon supplanted in the observing schedule by SN 1987A. It was the article by Podsiadlowski (1991) (see section 7.1) which prompted the retrieval and analysis of the 1987 dataset.

Observations have since been made on a further 61 occasions and these are catalogued in figure 7.3a. The tabulated orbital phase is that of the mid-point of each observation, calculated with respect to the time of x-ray

date (UT)	duration (min.)	telescope	sky clarity	orbital phase
15/08/1987	262	III	good	0.73
19/08/1987	251	III	v. poor	0.00
20/08/1987	150	III	good	0.46
21/08/1987	138	III	v. good	0.35
22/08/1987	83	III	v. good	0.51
23/08/1987	295	III	good	0.14
10/06/1991	107	IV	v. poor	0.42
11/06/1991	333	IV	v. good	0.73
12/06/1991	67	IV	v. poor	0.97
13/06/1991	222	IV	v. good	0.38
14/06/1991	406	IV	good	0.87
15/06/1991	372	IV	good	0.26
16/06/1991	419	IV	good	0.49
17/06/1991	429	III	good	0.78
17/06/1991	415	IV	good	0.81
18/06/1991	341	III	poor	0.14
18/06/1991	342	IV	poor	0.18
19/06/1991	309	III	poor	0.58
19/06/1991	288	IV	poor	0.62
20/06/1991	222	III	v. poor	0.93
20/06/1991	207	IV	v. poor	0.96
03/07/1991	22	III	good	0.43
04/07/1991	276	III	poor	0.09
05/07/1991	248	III	v. good	0.39
06/07/1991	258	III	v. good	0.70
07/07/1991	263	III	good	0.99
07/07/1991	260	IV	good	0.03
10/07/1991	83	III	v. poor	0.71
10/07/1991	320	IV	v. poor	0.10
11/07/1991	189	III	v. poor	0.20
11/07/1991	210	IV	v. poor	0.25
12/07/1991	227	III	good	0.50
12/07/1991	235	IV	good	0.53
13/07/1991	154	III	poor	0.93
13/07/1991	184	IV	poor	0.00
14/07/1991	140	III	good	0.17
14/07/1991	162	IV	good	0.12
15/07/1991	144	III	good	0.62
15/07/1991	141	IV	good	0.60

Figure 7.3a : the Sgr X-7 dataset.

date (UT)	duration (min.)	telescope	sky clarity	orbital phase
31/07/1991	59	III	good	0.45
01/08/1991	180	III	poor	0.74
01/08/1991	130	IV	poor	0.88
02/08/1991	252	III	excellent	0.62
02/08/1991	246	IV	excellent	0.60
03/08/1991	175	III	v. poor	0.45
03/08/1991	190	IV	v. poor	0.74
04/08/1991	240	III	poor	0.88
04/08/1991	186	IV	poor	0.11
06/08/1991	41	III	excellent	0.14
06/08/1991	205	IV	excellent	0.33
07/08/1991	206	III	excellent	0.40
07/08/1991	208	IV	excellent	0.65
08/08/1991	215	III	excellent	0.61
08/08/1991	218	IV	excellent	0.98
09/08/1991	208	III	excellent	0.27
09/08/1991	110	IV	excellent	0.55
10/08/1991	212	III	excellent	0.46
10/08/1991	118	IV	excellent	0.37
11/08/1991	208	III	excellent	0.81
11/08/1991	105	IV	excellent	0.70
12/08/1991	221	III	excellent	0.16
12/08/1991	97	IV	excellent	0.02
31/08/1991	141	III	v. good	0.87
01/09/1991	85	III	v. good	0.72
02/09/1991	218	III	v. good	0.64
03/09/1991	144	III	v. good	0.79
04/09/1991	105	III	v. good	0.78
05/09/1991	96	III	v. good	0.82
06/09/1991	197	IV	v. good	0.94
08/09/1991	115	III	poor	0.71
09/09/1991	168	IV	poor	0.78
10/09/1991	121	IV	poor	0.11
11/09/1991	114	III	v. poor	0.73
12/09/1991	56	III	v. good	0.78
18/08/1992	111	III	v. good	0.84
19/08/1992	240	III	v. good	0.11
20/08/1992	121	III	v. good	0.25
20/08/1992	205	V	v. good	0.61

Figure 7.3a cont. : the Sgr X-7 dataset.

date (UT)	duration (min.)	telescope	sky clarity	orbital phase
21/08/1992	127	III	v. good	0.55
21/08/1992	113	V	v. good	0.11
22/08/1992	126	III	excellent	0.87
22/08/1992	216	V	excellent	0.26
23/08/1992	152	III	good	0.21
23/08/1992	241	V	good	0.45
24/08/1992	116	III	excellent	0.50
24/08/1992	206	V	excellent	0.79
25/08/1992	122	III	excellent	0.81
25/08/1992	227	V	excellent	0.13
26/08/1992	68	V	poor	0.48
19/09/1992	117	III	poor	0.72
19/09/1992	103	IV	poor	0.80
19/09/1992	51	V	poor	0.66
20/09/1992	203	III	v. good	0.00
20/09/1992	169	IV	v. good	0.03
20/09/1992	172	V	v. good	0.00
22/09/1992	88	III	good	0.84
22/09/1992	58	IV	good	0.86
23/09/1992	194	III	poor	0.90
23/09/1992	193	IV	poor	0.92
25/09/1992	59	III	v. good	0.81
25/09/1992	90	IV	v. good	0.77
26/09/1992	140	IV	v. good	0.78

Figure 7.3a cont. : the Sgr X-7 dataset.

eclipse according to the quadratic ephemeris of Hellier, Mason, Smale and Kilkenny (1990). All data were collected whilst the telescopes were in tracking mode.

7.3.3 analysis and results

(i) the August 1987 data

The length and quality of the dataset were considered insufficient to allow a search for modulation at the 5.57 hour binary orbital period. The data were scanned for a burst of on-source events, of a few minutes duration, suitable for analysis over a range of frequencies by the fast Fourier transform method. Since Cyg X-3 had previously been found to exhibit 7 minute long spells of enhanced γ-ray emission (Chadwick et al., 1985), the count rate of events triggering the central channel alone was averaged over a 420 s "bin" which was slid through each data file in seven steps. The observation made on 19/08/1987 was excluded from this burst search, as were the last hour of data taken on 15/08/87 and the first hour of that from 23/08/87, on the grounds that cloud cover was noted by the observers. Only one candidate "active period" was found, the peak count rate occurring at 12:04:57 UT on 15/08/1987, as illustrated in figure 7.3b. It is clear from this figure that the peak is only slightly in excess of three standard deviations from the expectation value of the parabolic fit. No concurrent count rate excess appeared in the off-source channels. When the QT spectra were compared, as per the method of section 6.4.2(iii), no significant difference between the magnitude of Cerenkov light flashes arriving before, during and after the peak.

A FFT periodicity search was applied to 800 s of data centred upon the peak of figure 7.3b. Again, events which triggered the central channel only were chosen, hence the width of the allowed time bin was relaxed in order to increase the number of events analysed from 324 to 537. In the range

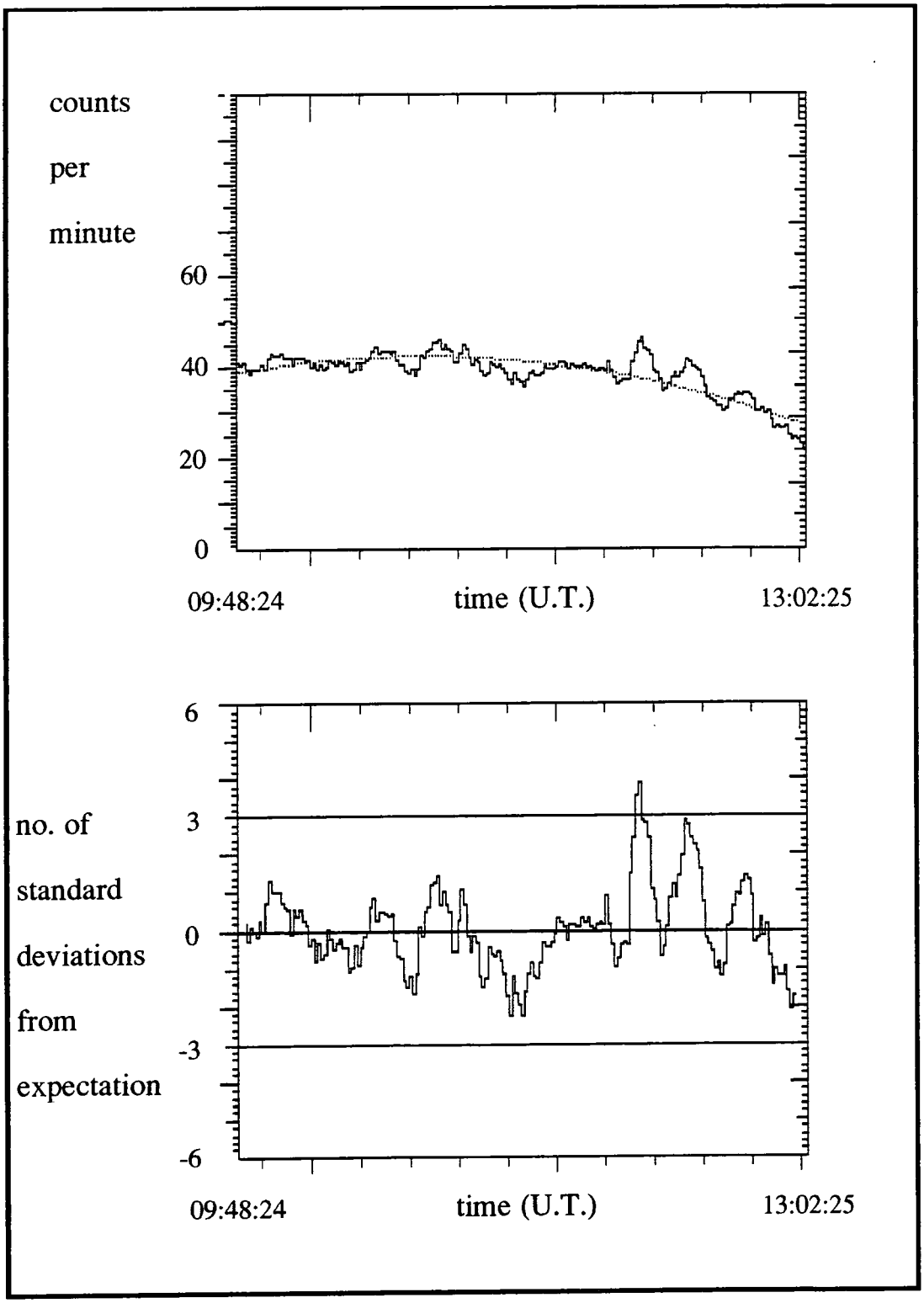

Fig. 7.3b : count rate during the observation of Sgr X-7 made on 15/08/1987 (Cerenkov events triggering central channel only).

$0{\cdot}33 \times 10^{3}$ to $0{\cdot}13 \times 10^{-2}$ Hz, one peak emerged above expectation at a frequency of ~ 34·7 Hz (≡ 28·795 ms), as shown in figure 7.3c. Once the number of degrees of freedom expended in this search were taken into account, this result was found to be statistically insignificant. It was decided to apply a test for uniformity of phase over a narrow search range centred upon this trial period to data covering the same orbital phase of Sgr X-7 as the "burst". This phase, φ_b, was calculated using the x-ray ephemeris of Hellier, Mason, Smale and Kilkenny (1990) given below:

$$JD = T_o + E\,P + E^2\,c$$

$$T_o = 2445615{\cdot}30961(15)$$

$$P = 0.232108782(65)$$

$$c = (2{\cdot}54 \pm 0{\cdot}67) \times 10^{-11}$$

$$P/(dP/dt) = (2{\cdot}9 \pm 0{\cdot}8) \times 10^{6}\ \text{yr}$$

from which $\varphi_b = 0{\cdot}798$.

Orbital phase 0·8 was covered by the observations taken on 19/08/1987 and 23/08/87. In the former this phase coincided with a break in the cloud cover, whilst the count rate was particularly low on the latter occasion. Two 800 s data extracts centred upon these two occurrences of φ_b, were selected and filtered to remove events which triggered any channel other than the central one. The Rayleigh test, (described in section 4.3.3(i)), was applied to search for periodicity in this data over the range 28·78 to 28·81 ms. A null result was obtained for the data collected on 23/08/1987. However, a peak period having a probability of chance occurrence of 0·02 was present in the data from 19/08/1987. Whilst this was not in itself remarkable, application of the same test to the 800 s extract from 15/08/1987 revealed that the periodicity observed in these datasets lay well within one Fourier interval ($\equiv P_{pulse}^2/800s \approx 1\ \mu s$) of each other i.e. they were effectively the same. The resultant periodograms are shown in figures 7.3d(i) and (ii); it should be noted that the y axis values are

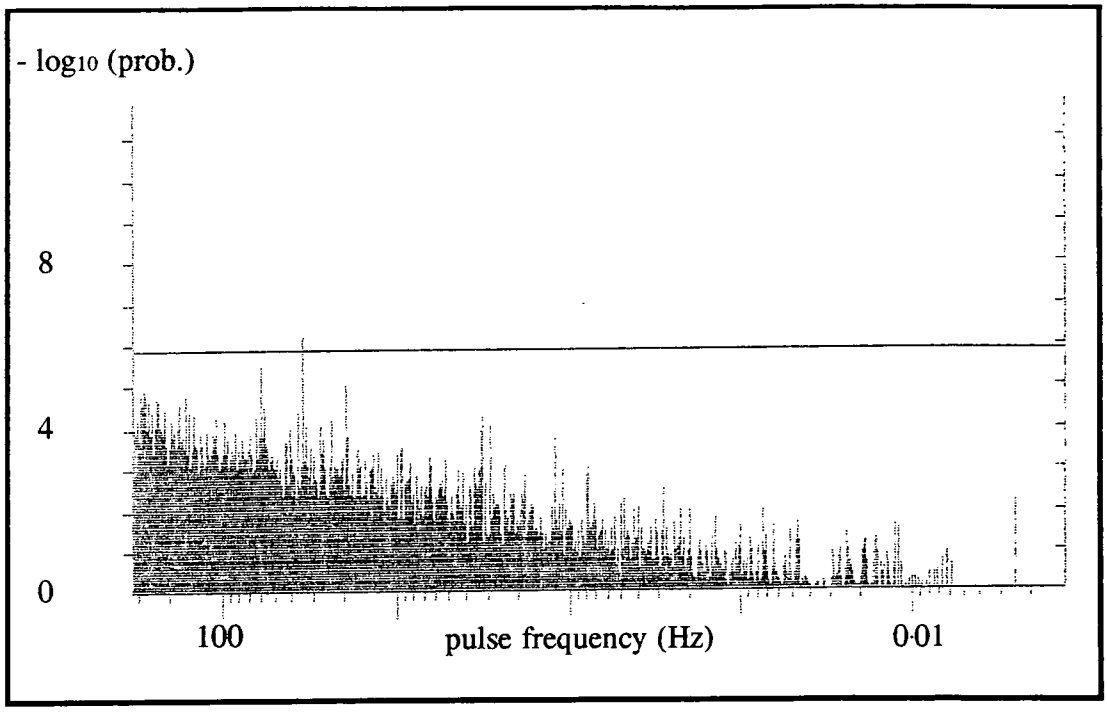

Fig. 7.3c : raw probability of chance occurrence of periodicity in the frequency range 330 Hz to 0.013 Hz in the Mark III telescope dataset of 15/08/1987 (events which triggered the central channel only), calculated using the Fast Fourier Transform method of Carraminana (1991).

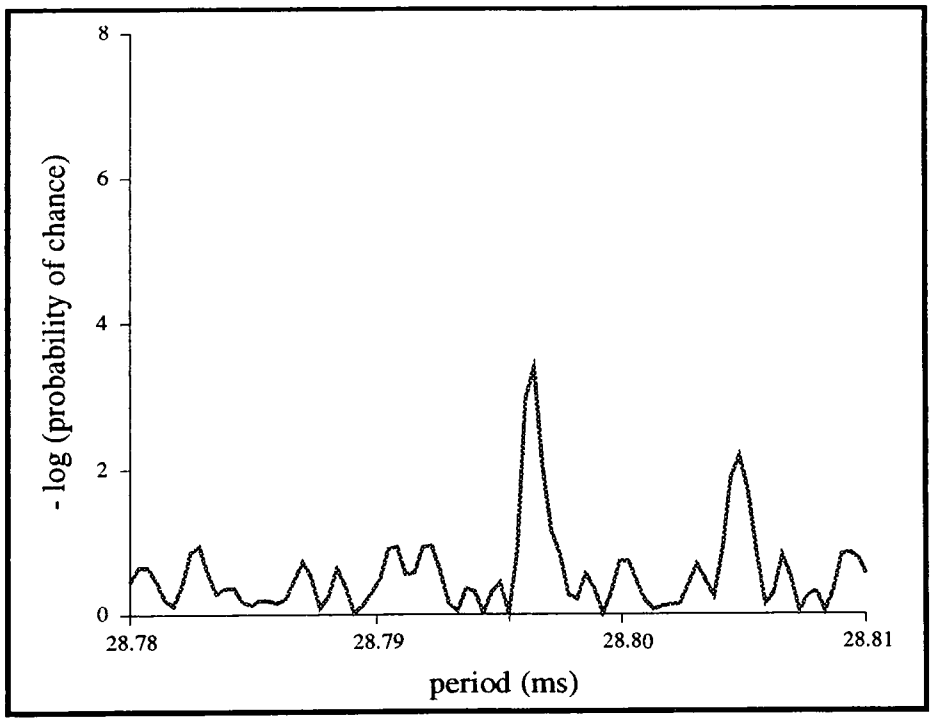

Fig. 7.3d(i) : probability of periodicity in the range 28.78 ms to 28.81 ms in the Mark III telescope dataset of 19/08/1987 (central channel only = 307 events).

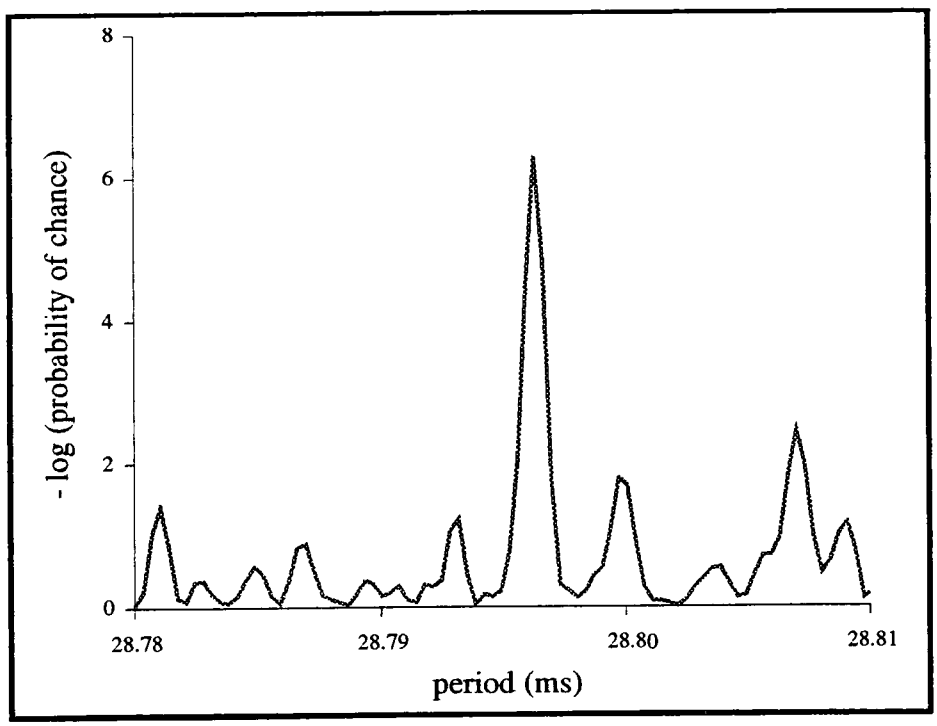

Fig. 7.3d(ii) : probability of periodicity in the range 28.78 ms to 28.81 ms in the Mark III telescope dataset of 15/08/1987 (central channel only = 537 events).

"raw" probabilities i.e. those obtained before the number of degrees of freedom, which are similar for both plots, are taken into account.

If the concurrence of these peak periodicities were merely coincidental, then the phase of the short period pulse would not be expected to be maintained from one observation to the next. The test for uniformity of phase was repeated on the two 800 s extract files, firstly combining them without the retention of relative phase information, as described in section 4.3.6(ii), and secondly by treating them as a single dataset of four days in duration, according to the method of section 4.3.6(i). The results of trials over the period range 28·795 to 28·797 ms were as follows:

	peak period (ms) ± 1 FI	raw prob. of chance	corrected prob. of chance
no relative phase info.	28·7962853 ± 0·0010	$3{\cdot}765 \times 10^{-9}$	$2{\cdot}137 \times 10^{-8}$
phase info. retained	28·7962916 ± 0·0000024	$6{\cdot}914 \times 10^{-13}$	$1{\cdot}909 \times 10^{-9}$

Clearly, if the number of trials have been correctly accounted for (3 per Fourier interval), then the results indicate that the retention of relative phase does not result in degradation of the periodic effect.

In order to establish whether or not this periodicity was restricted to the 800 s bins chosen on the basis of a slight excess count rate or the occurrence of φ_b, the test for uniformity of phase was applied to the entire 1987 dataset. Since no precise knowledge of the orbital elements of Sgr X-7 was available, no correction for the Doppler shift in pulse frequency due to orbital motion was attempted. However, an estimate of the possible magnitude of this effect was made. Given the reported orbital velocity of the primary of 70 km s^{-1} (Cowley, Crampton & Hutchings, 1982) and assuming an orbital inclination of 76°, equation 4.3f may be applied in order to determine the effect of Doppler shifting of the period of a steady

pulsator, assumed to be associated with the compact star. It was found that the pulse period observed at orbital phase 0·8 could translate to a maximum value at phase 0·75 of 28·797 ms and a minimum value at phase 0·25 of 28·784 ms. A search range of 28·78 to 28·80 ms was therefore chosen. The coherence times of a 28 ms signal at the ascending and descending nodes and at conjunction were estimated from equations 4.3g and 4.3f to be ~640 s and ~1400 s respectively. Events triggering the central channel only were selected and each data file was analysed in 800 s segments, each segment starting 200 s later than the one proceeding it. There was no evidence of periodicity on any nights other than those of the 15th and 19th of August. The periodicity which was observed during these two observations was restricted to an approximately 1200 s long section of each. When the same test was applied to data from the 15th and 19th of August containing only those events which triggered a single, off-source, guard-ring channel response, no pulsed signal was seen.

The test for uniformity of phase was re-applied to the two φ_b centred 800 s extract files of 15/08/1987 and 19/08/1987, in order to search for power in the second, third or fourth harmonics of the 28·796 ms period and at twice its value. None was found. For completeness, the data were folded at the period present in the earlier observation in order to produce a light curve for each 800 s segment. These are shown in figure 7.3e. As is consistent with the strong Rayleigh test result, both are sinusoidal rather than sharply peaked, and the maxima approximately coincide. Chadwick et al. (1985) noted that the Cyg X-3 VHE γ-ray pulse profile was broad, as were those of the x-ray binary bound pulsars in Her X-1 and 4U0115+63, as opposed to the short duty cycle of the isolated Crab pulsar. Thus, it is reasonable to suppose that were the Sgr X-7 system to support an accretion powered pulsar it would exhibit a smooth pulse profile.

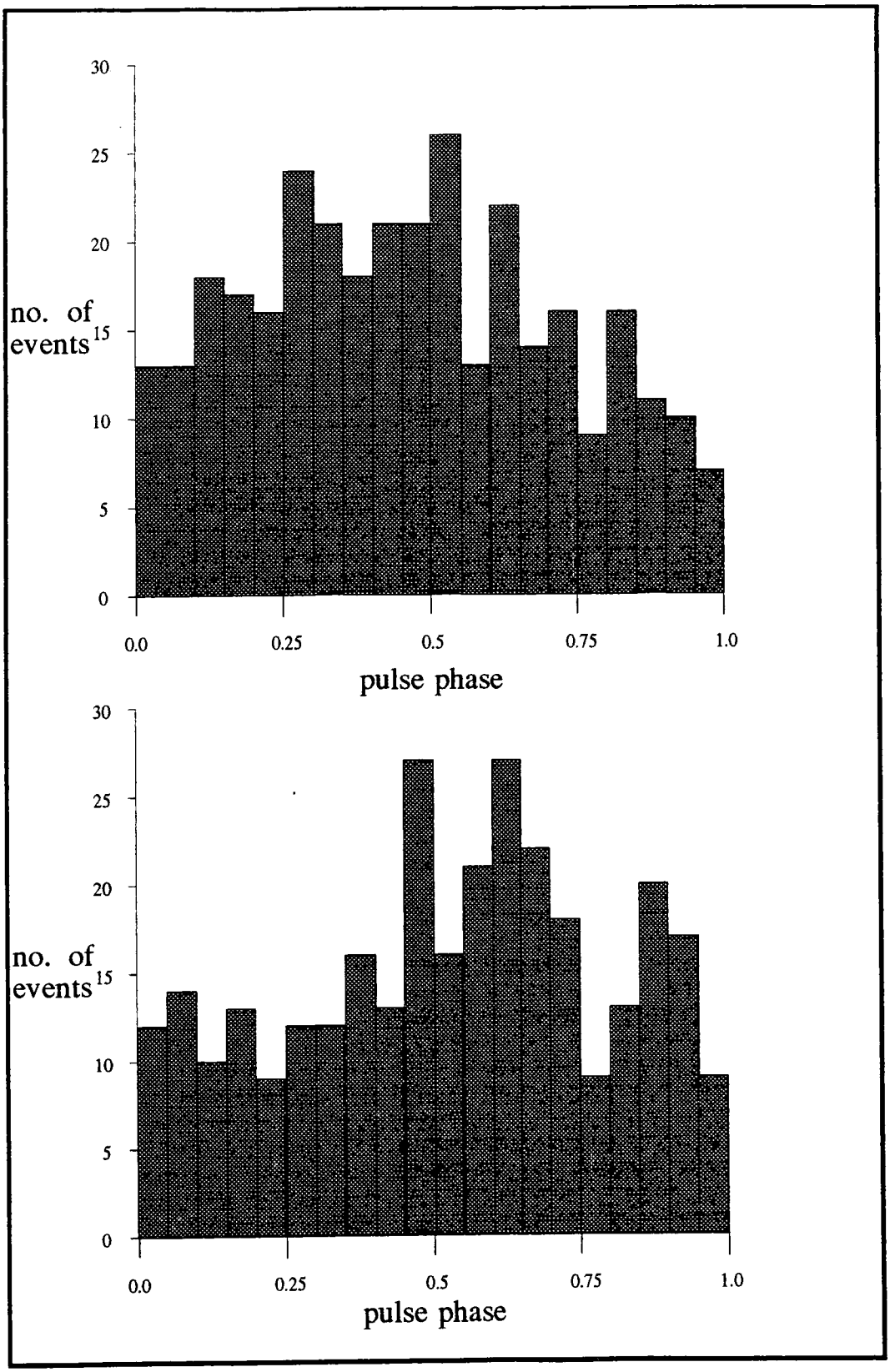

Fig. 7.3e : light curves for 800 s of data centred on orbital phase 0.8 (events triggering the central channel only) from observations made on the 15th (top) and 19th (bottom) of August 1987. The phase bin origin is arbitrary but common to both plots.

(ii) the June 1991 to September 1992 data

The real time count rate record of every observation was scanned for traces of an on-source event excess similar to that observed during the night of 15/08/1987. None was found.

The Mark V telescope data were considered unsuitable for periodic analysis as there was some doubt as to the stability of this instrument's internal clock.

For each occurrence of orbital phase 0·8 in the dataset, an 800 s long file was created, containing events which triggered the central channel only. This amounted to 27 files from the Mark III telescope and 26 from the Mark IV instrument, 19 of which were taken from simultaneous observations. The Rayleigh test for uniformity of phase was applied to each of these 800 s long data segments. From observations of Cyg X-3 spanning a period of $4^1/_2$ years, Chadwick et al. (1987) measured a "spin-down" period derivative for the 12·59 ms pulsar within this system of $2{\cdot}8 \times 10^{-14}$ s s^{-1}. If a period derivative of this order is assumed to apply to the 28 ms periodicity observed from Sgr X-7 on 15/08/1987, then by the end of the 1992 observing season this pulse period would be expected to have lengthened by ~4 μs. A trial period range from 28·78 to 28·81 ms was chosen in order to accommodate such a shift. Periodicity having a raw probability of chance occurrence of less than 0·001 was present on only two occasions, on the nights of 06/07/1991 and 19/08/1992 when only the Mark III telescope was in use (the extract files contained 321 and 226 events respectively). Neither fell at the exact pulse period observed in 1987. Once the number of trials performed was taken into account, these results were reduced to a probability of $9{\cdot}9 \times 10^{-3}$ of a 28·794 ms periodicity at φ_b on 06/07/1991 and a probability of $4{\cdot}7 \times 10^{-4}$ of pulsations at a 28·780 ms period at the same point in the orbit of Sgr X-7 on 19/08/1992.

The sliding bin technique was applied to test all available data for periodicity over the above range in 800 s sections stepped by 200 s. It was

confirmed by this method that the two peaks uncovered in extracts about orbital phase 0·8 were confined to within ~1000 s of this epoch. An interesting outcome of this analysis, though not of any statistical significance, was the appearance of a peak at the precise period observed on the night of 06/07/1991 in data taken on 15/07/1991. This pulse period was present in 800 s of data centred upon orbital phase 0·775, a time bin which just encompassed phase 0·8. It was a factor of 100 times less significant than the result of the same bin sliding test applied to the observation taken on 6/07/1991, and had not appeared in the extract file centred upon phase 0·8.

7.3.4 discussion

If the periodicity observed on the nights of 15/08/1987 and 19/08/1992 is considered to be a genuine pulsar signal, then it is consistent with a "spin up" at a rate of $1{\cdot}3 \times 10^{-13}$ s s^{-1}. It may be the case that in Cyg X-3 the pulsar spin-down trend is almost but not quite counterbalanced by spin-up during episodes of accretion, whereas in Sgr X-7 the latter effect is dominant. Accretion onto the surface of a neutron star may prove increasingly difficult as its spin quickens. It might be assumed that the luminosity of an accreting γ-ray pulsar would be enhanced during a period of mass accretion and thus it would be more frequently detected during the spin-up period, however, the central source might well be obscured by the extra "free" material in the system at this time so that selection effects were of the opposite sense.

The peak period observed in the 800s long extract from the Mark III telescope data of 15/08/1987 had an associated Rayleigh vector of magnitude 0·16, which (according to equation 4.4b) is equivalent to a flux of γ-rays above the telescope's threshold energy ~2×10^{-9} cm^{-2} s^{-1}. This corresponds to a source of luminosity $\geq 6 \times 10^{35}$ erg s^{-1} at 250 GeV and above at a distance of 2·5 kpc, which is not insupportable given the estimated

luminosity range of non-accreting pulsars of between 10^{32} and 10^{36} erg s^{-1}.

The candidate signal appears to be confined to a small region of the LMXB orbit near phase 0·8. This result is consistent with the model of the Sgr X-7 system put forward by White and Holt (1982) which includes a thickening of the accretion disc at this orbital phase (as viewed from Earth) near the region where the gas stream from the companion impinges upon it. It may be that the optical depth of the disc at this point is sufficient to support the creation of γ-rays via π^o production and decay (as described in section 6.3.3(i)) without extinction through re-absorption by e^+e^- pair production. It is to be expected that emission from a millisecond pulsar would be scattered and attenuated in the accretion disc corona at longer wavelengths - thus pulse coherence would be lost. Interestingly, it was at this orbital phase that Mason and Cordova (1982a) discovered a minimum in the UV light curve.

Brazier et al. (1990) reported that only two strong bursts of γ-rays were observed from the direction of Cyg X-3 during 350 hours of observation. The lack of burst activity from Sgr X-7 is therefore not unexpected. The significance of the apparent 28 ms pulsation is low and would not be worthy of comment were it not for the seeming orbital dependency of the emission. At least one further detection of a "burst" episode coincident with an increase in the fraction of pulsed events is required, before this object can be said with any certainty to contain a "γ-ray pulsar". Given the intermittent nature of γ-ray emission from many established sources, it would perhaps be better to devote observing time to objects having a well-charted pulse period at other energies. Hour long observations targeted on phase 0·8 of Sgr X-7's orbit might prove profitable.

7.4 PSR 1855+09, a binary radio pulsar

7.4.1 background information

PSR 1855+09 was first identified as a 5·4 ms pulsar in a binary orbit from the radio observations of Seglestein, Rawley, Stinebring, Fruchter & Taylor (1986). Six objects of this type which lie within the galactic disc have been well documented to date. From the spatial distribution of these and the sensitivity of sky surveys at radio wavelengths, Johnston and Bailes (1991) deduced an upper limit to the number of PSR 1855+09 type systems in the galaxy of 2500.

Segelstein, Rawley, Stinebring, Fruchter and Taylor found that the radio pulse profile of PSR 1855+09 was double peaked, and that the main pulse and the inter-pulse, separated by ~180°, shared a common polarisation mode indicative of emission from the vicinity of a single pole. Johnston and Bailes (1991) note that the presence of an inter-pulse implies a large beaming fraction and hence a high probability of detection. From radio timing measurements of the pulse period, P, and its first derivative, dP/dt, Rawley, Taylor and Davis (1988) estimated the surface magnetic field strength of the neutron star, B, from the relation $B \approx 3 \times 10^{19}\ P\ dP/dt$ (in cgs units) to be $3{\cdot}0 \times 10^{8}$ G. The companion star in this 12·3 day orbit has not yet been optically identified (Kulkarni, Djorgovski & Klemola, 1991). This suggests that it is of low luminosity and hence relatively old. The pulse timing measurements by Ryba and Taylor (1991) limit the companion's mass to approximately $0{\cdot}23 \pm 0{\cdot}02\ M_{sun}$, and are consistent with an orbital inclination, i, of ~90°. The distance to PSR 1855+09, d, has not yet been conclusively determined. The above authors were able to make radio measurements of sufficient precision to show the effects of the proper motion of PSR 1855+09 on pulse arrival times and determine an annual parallax for the system. This parallax measurement was consistent with a value of $d \geq 0{\cdot}6$ kpc at the 68 % confidence level. Hydrogen absorption

spectra had previously been used to confine this distance to $1{\cdot}6$ kpc $< d <$ $2{\cdot}0$ kpc on the basis of a galactic rotation model, whilst radio dispersion measurements gave $d < 1$ kpc. Ryba and Taylor (1991) chose a value of $d = 1{\cdot}1$ kpc, which was also assumed by Johnston and Bailes (1991), and is the value adopted here.

Using the comprehensive ephemeris produced by Ryba and Taylor (1991), which is given below, an estimate of the γ-ray luminosity of PSR 1855+09 may be made. According to the model of Usov (1983), charged particles accelerated in the region above the polar cap of a pulsar rotating at a period of a few milliseconds will emit curvature radiation, giving rise to a γ-ray flux which maximises in the 100 GeV region. By submitting the parameters of PSR 1855+09 given by Ryba and Taylor (1991) to the technique of Usov (1983), a flux at Earth of γ-rays having an energy $\geq$ 100 GeV of $\sim 1{\cdot}3 \times 10^{-10}$ cm^{-2} s^{-1} is predicted.

The PSR 1855+09 Ephemeris of Ryba & Taylor (1991)

Pulse Parameters

P (ms)	$5{\cdot}36210045404065(10)$
dP/dt (ss^{-1})	$1{\cdot}7835(3) \times 10^{-20}$
d^2P/dt^2 (s^{-1})	$-1{\cdot}0 \pm 1{\cdot}9 \times 10^{-31}$
ν (s^{-1})	$186{\cdot}494081670261(3)$
$d\nu/dt$ (s^{-2})	$-6{\cdot}2034(10) \times 10^{-16}$
$d^2\nu/dt^2$ (s^{-3})	$4 \pm 7 \times 10^{-27}$
t_o	JD $2447526{\cdot}0000566171(3)$

Orbital Parameters

asin(i) (lt s)	$9{\cdot}2307807 \pm 0{\cdot}0000003$
P_{orb} (s)	$1065067{\cdot}59082 \pm 0{\cdot}0012$
dP_{orb}/dt (ss^{-1})	$-5 \pm 8 \times 10^{-12}$
e	$2{\cdot}167 \pm 0{\cdot}004 \times 10^{-5}$
ω	$276{\cdot}299335 \pm 0{\cdot}003$ °
T_o	JD $2447530{\cdot}39335870 \pm 0{\cdot}003$

Position (J 2000)

Right Ascension	$18^h\ 57^m\ 36{\cdot}393521(10)^s$
Declination	09° 43' 17·3233(3)''

The figures in parentheses represent the uncertainties in the last digits quoted. Note that T_o is the time of periastron passage i.e. the point at

which the radial velocity of the radio source is a maximum. This point is offset from the ascending node by a fraction $\approx \omega/360^\circ$ of the orbit (ω is termed the "longitude of periastron").

7.4.2 previous analysis in Durham

The analysis of data recorded on this object by the University of Durham group up until summer 1991 has been documented in full by Brazier (1991). The results were presented by Bowden et al. (1991b).

A total of 56 Mark III telescope datafiles were searched for periodicity using the Rayleigh test for uniformity of phase described in section 4.3.3(i).

The event arrival times were reduced to the solar system barycentre (see section 4.1.2(ii)) using the co-ordinates of PSR 1855+09 given by Rawley, Taylor and Davis (1988). Brazier (1991) estimated that the errors in the Rawley, Taylor and Davis ephemeris were large enough to require relaxation of the orbital parameters when correcting the event times for the Doppler shift due to orbital motion in order to ensure the recovery of any periodicity, as described in section 4.3.5(ii). The Rayleigh test was applied to each individual file, at the exact pulse period given by the above authors and then at its second harmonic, whilst the data were focussed using a range of values of asin(i) and Φ. The number of degrees of freedom inherent in this "orbital sampling" was estimated from Monte Carlo simulations. No evidence of periodicity at the full period was found. At the second harmonic, one observation contained periodicity having a probability of occurrence by chance of $< 10^{-5}$. The periodic peak in this datafile (that recorded on 11/10/1988) was most significant when only those events were considered which triggered the central channel alone and which did not cause the charge registered by the surrounding guard ring channels to exceed 45% of the on-source value. This 45 % "soft cut" (described in chapter 5) was then applied to the dataset as a whole and the Rayleigh test

was repeated. 13 datafiles reduced in this manner were found to contain periodicity near the second harmonic of the pulse period having a probability of chance occurrence of $< 0{\cdot}1$, 7 more than would be expected from a selection of 56 files containing no real periodic signal. This was seen as some evidence of γ-ray emission from PSR 1855+09.

Since a single 3 hour observation would cover ~1 % of the 12 day long orbit, it was thought that, by plotting the Rayleigh power of the peak near the second harmonic of the pulse period versus the orbital phase of each observation, some evidence of a dependency of γ-ray signal strength upon the position of the neutron star might be obtained. By application of the Kolmogorov-Smirnov test for goodness of fit (Conover, 1980, 344) the probability that the apparent clustering of these data points about the descending node occurred purely by chance was found to be $0{\cdot}027 \pm 0{\cdot}004$.

7.4.3 the 1987 to 1992 dataset

A further 15 observations of PSR 1855+09 were made with the Mark III telescope during 1991 and 1992, bringing the total number of data files from this instrument (listed in figure 7.4a) to 71. PSR 1855+09 typically lay at a zenith angle of between 50° and 42°, the telescope was therefore operating at a threshold energy of ~450 GeV. All of these observations were taken in tracking mode apart from that made on 27/09/1989. This single chopped observation was treated as a gapped dataset.

Some data collected using the Mark IV telescope and the newly commissioned Mark V instrument also exists, but was regarded, as Mark IV telescope data obtained in 1990 previously had been, as suitable solely for use in the verification of any strong periodic signal see in contemporaneous Mark III telescope data.

date (UT)	duration (min.)	sky clarity	orbital phase*
29/05/1987	94	good	0.06
26/09/1989	107	good	0.06
09/09/1988	121	good	0.07
07/06/1989	223	poor	0.08
18/07/1987	256	good	0.09
18/09/1987	138	good	0.11
19/07/1987	138	v. poor	0.12
30/05/1987	176	good	0.13
27/09/1989	119	good	0.14
19/05/1990	99	excellent	0.14
10/09/1988	164	poor	0.15
28/05/1992	180	excellent	0.17
20/09/1990	106	good	0.18
19/09/1987	119	excellent	0.19
31/05/1987	87	good	0.21
28/09/1989	107	good	0.22
20/05/1990	147	good	0.22
21/07/1990	150	excellent	0.24
20/07/1987	304	good	0.25
29/05/1992	210	excellent	0.25
20/09/1987	139	excellent	0.27
25/04/1987	68	good	0.29
29/09/1989	94	good	0.30
12/09/1988	135	poor	0.32
07/10/1988	67	good	0.34
29/05/1989	129	v. poor	0.34
02/06/1987	156	good	0.37
30/09/1989	83	poor	0.38
28/06/1990	201	excellent	0.38
23/07/1990	135	poor	0.40
30/05/1989	152	v. poor	0.42
03/06/1987	205	v. good	0.45
01/10/1989	72	poor	0.46
10/06/1991	84	poor	0.48
23/07/1987	292	poor	0.49
09/10/1988	75	v. good	0.50

Figure 7.4a : the PSR 1855+09 dataset (Mark III telescope data from 1987 to 1992 inclusive).

* orbital phase with respect to perihelion at the mid-point of each observation, according to the ephemeris of Ryba and Taylor (1991).

date (UT)	duration (min.)	sky clarity	orbital phase*
31/05/1989	68	good	0.51
04/06/1987	223	v. good	0.54
23/05/1987	215	v. good	0.56
11/06/1991	158	good	0.56
21/09/1992	155	excellent	0.56
24/07/1987	285	good	0.58
10/10/1988	74	good	0.58
30/04/1990	108	excellent	0.61
28/08/1992	112	excellent	0.61
29/04/1987	60	v. good	0.62
22/07/1992	231	excellent	0.62
25/05/1990	242	poor	0.63
24/05/1987	224	excellent	0.64
12/06/1991	85	v. poor	0.64
19/06/1990	242	excellent	0.65
03/06/1992	276	poor	0.66
11/10/1988	70	good	0.67
29/09/1988	67	good	0.69
01/05/1990	164	excellent	0.69
23/07/1992	330	v. good	0.69
25/05/1987	195	excellent	0.72
13/06/1991	178	v. good	0.72
04/06/1992	207	v. good	0.74
12/10/1988	61	poor	0.75
02/05/1990	167	excellent	0.77
26/05/1987	219	good	0.81
14/06/1991	188	v. good	0.81
23/09/1989	97	good	0.82
03/05/1990	175	excellent	0.85
15/06/1991	196	poor	0.89
24/09/1989	120	good	0.89
07/09/1988	126	good	0.91
16/09/1987	117	good	0.95
16/06/1991	239	good	0.97
08/09/1988	147	good	0.99

Figure 7.4a cont. : the PSR 1855+09 dataset (Mark III telescope data from 1987 to 1992 inclusive).

* orbital phase with respect to perihelion at the mid-point of each observation, according to the ephemeris of Ryba and Taylor (1991).

7.4.4 recent analysis and results

The initial aim of this analysis was to build upon the results which Brazier (1991) achieved by searching over a range of orbital parameters, using instead the exact ephemeris supplied by Ryba and Taylor (1991) and including data collected in 1991 and 1992.

(i) a test for periodicity at the second harmonic

The arrival times of the events contained in the 71 Mark III telescope datafiles were corrected to the solar system barycentre using the position of PSR 1855+09 given by Ryba and Taylor (1991). The data were filtered to produce reduced files containing only those events which triggered the central channel alone. A 45% soft-cut selection was also applied to all data except those recorded in 1992, during which period the charge digitizers were inoperative.

The Rayleigh test for uniformity of phase was applied to each datafile in a search for periodicity near the second harmonic of the radio pulse period (hereafter referred to as the "half period"), over the range 2·681045 to 2·681055 ms. For a datafile of three hours duration the Fourier Interval (F.I.) in period within this range is of the order of 1 ns. The results of these tests are tabulated in figure 7.4b. The Rayleigh probabilities of chance occurrence shown here have been corrected for the number of trials performed in the specified period range. In deference to the null results previously obtained, no test was performed for periodicity at the full radio pulse period.

The Rayleigh probabilities of chance occurrence of periodicity within ± 1 F.I. of the half period (P_R) were combined using equation 4.31. The resulting logarithmic sum, distributed as chi-square with 142 degrees of freedom, gave an overall probability of chance occurrence of periodicity throughout the dataset of 94 %.

date (UT)	peak period (ms)	peak prob.	best prob. at P +/- 1 F.I.
29/05/1987	2.6810450	0.81	1.0
26/09/1989	2.6810486	0.44	1.0
09/09/1988	2.6810501	0.36	0.21
07/06/1989	2.6810508	0.55	0.20
18/07/1987	2.6810509	0.92	0.78
18/09/1987	2.6810525	0.42	1.0
19/07/1987	2.6810525	0.70	0.62
30/05/1987	2.6810462	0.18	1.0
27/09/1989	2.6810469	0.53	1.0
19/05/1990	2.6810515	0.62	1.0
10/09/1988	2.6810474	0.26	0.18
28/05/1992	2.6810499	0.25	0.070
20/09/1990	2.6810534	0.66	0.60
19/09/1987	2.6810534	0.051	0.46
31/05/1987	2.6810537	0.012	0.73
28/09/1989	2.6810516	0.42	0.41
20/05/1990	2.6810528	0.57	0.98
21/07/1990	2.6810500	0.37	0.14
20/07/1987	2.6810512	0.32	1.0
29/05/1992	2.6810509	0.0036	0.0061
20/09/1987	2.6810497	0.26	0.11
25/04/1987	2.6810450	0.18	0.69
29/09/1989	2.6810545	0.16	1.0
12/09/1988	2.6810518	0.38	0.33
07/10/1988	2.6810518	0.18	0.15
29/05/1989	2.6810496	0.16	0.063
02/06/1987	2.6810545	0.045	1.0
30/09/1989	2.6810534	0.37	0.69
28/06/1990	2.6810514	0.78	1.0
23/07/1990	2.6810526	0.51	0.88
30/05/1989	2.6810493	0.50	0.40
03/06/1987	2.6810462	0.24	0.33
01/10/1989	2.6810555	0.24	1.0
10/06/1991	2.6810471	1.0	1.0
23/07/1987	2.6810534	0.49	1.0
09/10/1988	2.6810453	0.28	0.43

Figure 7.4b : minimum Rayleigh probabilities of chance occurrence of periodicity in the range 2.681045 ms to 2.681055 ms (3rd column) and within one Fourier Interval of 2.6810502 ms (4th column).

date (UT)	peak period (ms)	peak prob.	best prob. at P +/- 1 F.I.
31/05/1989	2.6810519	0.20	0.29
04/06/1987	2.6810496	0.14	0.33
23/05/1987	2.6810521	0.026	1.0
11/06/1991	2.6810453	0.55	1.0
21/09/1992	2.6810495	0.39	0.18
24/07/1987	2.6810532	0.64	1.0
10/10/1988	2.6810542	0.29	1.0
30/04/1990	2.6810453	0.35	0.13
28/08/1992	2.6810488	0.20	0.86
29/04/1987	2.6810450	0.93	1.0
22/07/1992	2.6810485	0.094	1.0
25/05/1990	2.6810519	0.75	1.0
24/05/1987	2.6810520	0.75	1.0
12/06/1991	2.6810551	0.56	0.80
19/06/1990	2.6810457	0.54	0.79
03/06/1992	2.6810468	0.036	1.0
11/10/1988	2.6810522	0.000038	0.000036
29/09/1988	2.6810450	0.28	1.0
01/05/1990	2.6810460	0.059	1.0
23/07/1992	2.6810488	0.096	1.0
25/05/1987	2.6810548	0.17	1.0
13/06/1991	2.6810455	0.63	0.77
04/06/1992	2.6810481	0.28	1.0
12/10/1988	2.6810483	0.22	0.22
02/05/1990	2.6810502	0.049	0.012
26/05/1987	2.6810454	0.12	0.91
14/06/1991	2.6810514	0.77	1.0
23/09/1989	2.6810504	0.67	0.61
03/05/1990	2.6810488	0.24	1.0
15/06/1991	2.6810552	0.93	1.0
24/09/1989	2.6810450	0.57	1.0
07/09/1988	2.6810534	0.55	0.82
16/09/1987	2.6810515	0.38	0.46
16/06/1991	2.6810489	0.60	1.0
08/09/1988	2.6810551	0.44	1.0

Figure 7.4b cont. : minimum Rayleigh probabilities of chance occurrence of periodicity in the range 2.681045 ms to 2.681055 ms (3rd column) and within one Fourier Interval of 2.6810502 ms (4th column).

The expected frequency of occurrence of periodicity at various levels of significance in a dataset made up of 71 samples is given in the following table for comparison with those observed:

probability level (P)	expected frequency of $P_R \leq P$	observed frequency of $P_R \leq P$
1·0	71	71
0·3	21	15
0·1	7·1	5
0·03	2·1	3
0·01	0·7	2
0·000036	0·0025	1

(ii) orbital phase dependency

The observed cumulative frequency distribution of P_R only exceeds expectation for $P < 0{\cdot}03$. If the data contain a signal from PSR 1855+09 then it is clearly sporadic. Since the pulsar rotation and its spin-down rate are very stable it is reasonable to assume that no significant accretion takes place within the binary. Regulation of the strength of any γ-ray flux received from this system must therefore be attributed to geometrical effects, which would tend to regulate its "observability" as a function of orbital phase.

In order to test for a dependency of signal strength upon orbital phase, the peak Rayleigh power within ± 1 F.I. of the half period ($-\ln(P_R)$) was plotted in figure 7.4c versus the orbital phase (with respect to superior conjunction) at the mid-point of the corresponding observation. Note that in this figure eight points having $P_R = 1$ have been overwritten by others. By inspection, the distribution does not differ greatly from that shown in figure 2 of Bowden et al. (1991b). The addition of 15 new data points and restriction of the search range to within one F.I. of the expected period has slightly enhanced the impression of bimodality noted by Brazier (1991). It is difficult to assess the

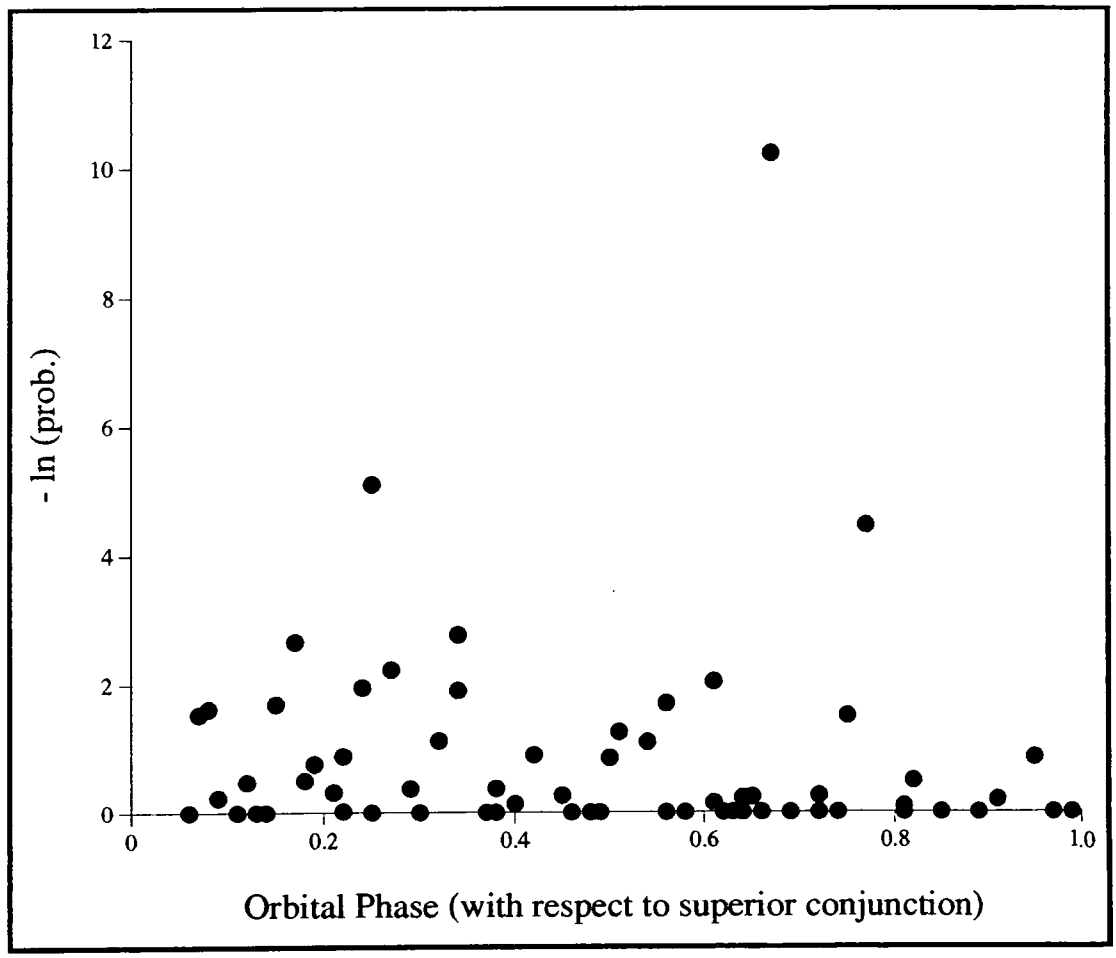

Fig. 7.4c : the Rayleigh probability of chance occurrence of periodicity within one Fourier Interval of 2.6810502 ms plotted (on a logarithmic scale) versus the orbital phase (with respect to superior conjunction) of PSR 1855+09 at the mid-point of each observation.

significance of the peaks apparent to the eye near the ascending and descending nodes, due to the restricted sample size and the uneven orbital sampling (the latter arose through the preferential observation of this system at or near those regions of the 12 day orbital cycle where activity had been tentatively identified from early analyses). For this reason, no attempt has been made here to search for a similar pattern in sub-sections of the 1987 to 1992 dataset.

If the observations produced equally weighted samples from a uniform distribution then the datafiles would exhibit similar Rayleigh powers at the trial period. Under the null hypothesis that the received power in the form of pulsed γ-rays is independent of orbital phase, the cumulative distribution of the Rayleigh power may be described by:

$$F(i) = \sigma(i) \left[\sum_{j=0}^{N} - \ln (P_R) \right]^{-1}$$

where

$$\sigma(i) = \sum_{j=0}^{i} - \ln (P_R)$$

and i is the ranking of an observation when all N observations are ordered according to their orbital phase measured from an arbitrary origin.

The observed cumulative distribution of Rayleigh powers as a fraction of their sum is shown in figure 7.4d. The deviation of this distribution from that expected under the aforementioned null hypothesis (displayed as a dashed line) was quantified using Watson's U_N^2 test for goodness of fit. The application of this test in the assessment of the significance of bimodality in a similar distribution has been described by Batschelet (1981, 79). The test statistic is:

$$U_N^2 = \Sigma v_i^2 - \Sigma (c_i v_i / N) + N [1/3 - (\bar{v} - 1/2)^2]$$

where $v_i = F(i)$, $\bar{v} = 1/N \Sigma v_i$ and $c_i = 2i - 1$.

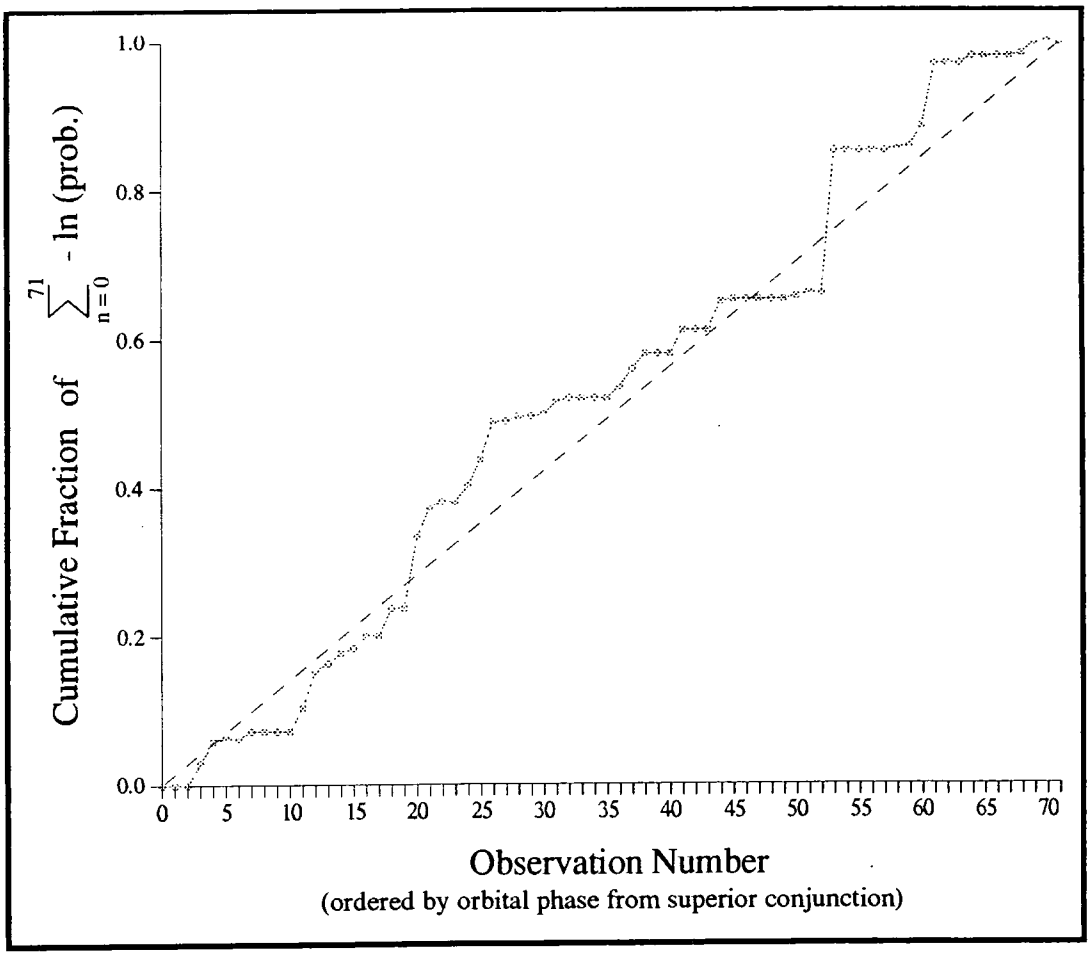

Figure 7.4d : accumulation of the Rayleigh power within one Fourier Interval of the second harmonic of the pulse period of PSR 1855+09 as the number of observations considered is increased. The dashed line represents the distribution expected if the pulsed signal strength (which may be zero) is not a function of orbital phase.

For the sample distribution illustrated in figure 7.4d, $U_N^2 = 0{\cdot}174$. Tabulated significance values for this statistic (Batschelet, 1981) show that the null hypothesis may be rejected at the 0·1 level but not at a significance of $\leq 0{\cdot}05$. There is therefore little evidence that the ability to detected pulsed γ-rays from PSR 1855+09 is dependent upon the position of the neutron star in its orbit at the time of observation. This result is dependent upon the assumption that the data points are equally weighted. This is not the case since the observations are of variable length and quality; however, as these factors are non-systematic, this approximation is perhaps a fair one.

(iii) a test for a narrow pulse profile

When Cerenkov event times are corrected for the effects of orbital motion using the radio ephemeris of Ryba and Taylor (1991), an implicit assumption is made that any γ-ray emission site within the PSR 1855+09 system is co-moving with that of the radio source. If this assumption is valid then the potential exists to produce light curves of the number of γ-ray like events observed versus the absolute *pulse* phase.

If the γ-ray flux from such an object is dominated by curvature radiation produced by charged particles spiralling along the magnetic field lines near the neutron star's polar caps, then the radio ephemeris must be applicable since the narrow radio beam is also assumed to be a product of particle acceleration in this confined region. If γ-rays arise primarily through particle acceleration in charge separated gaps in the pulsar's outer magnetosphere, then the maximum spatial separation of the γ-ray and radio production sites approximates to the radius of the neutron star's light cylinder given by $r = c/\Omega$. At the rotation rate of PSR 1855+09, $r \approx 250$ km, which is equivalent to a fraction of $\sim 1{\cdot}5 \times 10^{-5}$ of the pulsar's almost circular orbit. According to equation 4.3i, a change in orbital phase of this magnitude will never result in a shift in the

perceived pulse period in excess of 0·001 ns, so this effect, if present, will not be detectable in this experiment.

The accuracy with which events can be assigned an absolute pulse phase is therefore limited by the precision with which their arrival times at Earth are recorded. For example, where a 20 bin light curve is to be produced, by folding the event arrival times modulo a trial period p, from a dataset of duration t, a phase shift of one bin width or more between the beginning and end of the dataset would result from an error in the estimation of the clock slip rate of $\delta_{slip} \geq 0{\cdot}05\ p\ t^{-1}$. In the case of the PSR 1855+09 dataset, for which $t \approx 5$ years and $p \approx 5{\cdot}36$ ms, the current measured value of δ_{slip} is roughly equivalent to the limiting value in the above expression. Since the clock monitoring system has evolved since 1987, it is reasonable to assume that *absolute* pulse phase cannot be maintained throughout the dataset. The *relative* phase of pulse arrival times at the beginning and end of a 3 hour long observation is known to an accuracy of at least 1/2000 th of the width of a p/20 bin.

The χ^2 test for goodness of fit (described in section 4.3.4) was applied to the 71 light curves produced by folding the event arrival times in each observation at the full radio pulse period. The probability of chance occurrence of the deviation of each histogram from a flat light curve, P_x, was estimated from the corresponding value of χ^2_{19}. P_x was found to be less than 0·1 on only three occasions. It was felt that if the γ-ray light curve followed the pattern of the radio emission, having a pulse and an inter-pulse separated by 0·5 in phase, then folding the data at the half period might increase the chance of detection of a weak signal. Accordingly the above test was re-applied to light curves produced by folding the data at the half period, with the result that five histograms gave $P_x < 0{\cdot}1$, as shown in figure 7.4e.

According to Eadie et al. (1971), individual values of P_{xi} may be combined to form a test statistic, $\alpha = -2 \ln \Pi P_{xi}$, which is itself

date (UT)	no. of events*	prob. at P	prob. at P/2
29/05/1987	551	0.87	0.76
26/09/1989	2651	0.63	0.54
09/09/1988	1819	0.05	0.11
07/06/1989	6186	0.63	0.90
18/07/1987	2566	0.06	0.05
18/09/1987	2916	0.80	0.84
19/07/1987	757	0.68	0.18
30/05/1987	559	0.26	0.21
27/09/1989	3353	0.63	0.80
19/05/1990	615	0.17	0.30
10/09/1988	4873	0.12	0.16
28/05/1992	4974	0.46	0.27
20/09/1990	1232	0.92	0.59
19/09/1987	2374	0.14	0.45
31/05/1987	2522	0.46	0.67
28/09/1989	2120	0.18	0.08
20/05/1990	407	0.15	0.66
21/07/1990	4990	0.20	0.36
20/07/1987	3045	0.76	0.37
29/05/1992	3309	0.62	0.029
20/09/1987	2156	0.18	0.048
25/04/1987	323	0.30	0.49
29/09/1989	2266	0.28	0.62
12/09/1988	1241	0.73	0.27
07/10/1988	1405	0.19	0.20
29/05/1989	1920	0.60	0.76
02/06/1987	1679	0.84	0.19
30/09/1989	1470	0.69	0.63
28/06/1990	216	0.30	0.66
23/07/1990	1599	0.30	0.84
30/05/1989	2029	0.67	0.25
03/06/1987	1667	0.24	0.83
01/10/1989	1143	0.57	0.52
10/06/1991	170	0.91	0.49
23/07/1987	2760	0.41	0.54
09/10/1988	1841	0.69	0.90

Figure 7.4e : probabilities of chance occurrence of chi-square at the full pulse period and its second harmonic .

* events which triggered the central channel only (and which survived a 45 % soft cut selection, unless recorded in 1992 in which case no soft cut was applied).

date (UT)	no. of events*	prob. at P	prob. at P/2
31/05/1989	1481	0.13	0.48
04/06/1987	2140	0.14	0.70
23/05/1987	1425	0.69	0.76
11/06/1991	1417	0.55	0.35
21/09/1992	2197	0.68	0.32
24/07/1987	5909	0.37	0.38
10/10/1988	1359	0.31	0.67
30/04/1990	726	0.87	0.18
28/08/1992	2008	0.69	0.73
29/04/1987	1430	0.020	0.58
22/07/1992	4296	0.71	0.75
25/05/1990	655	0.44	0.44
24/05/1987	2199	0.21	0.93
12/06/1991	172	0.65	0.58
19/06/1990	5366	0.88	0.71
03/06/1992	6527	0.91	0.81
11/10/1988	1416	0.40	0.15
29/09/1988	1769	0.81	0.88
01/05/1990	2561	0.20	0.35
23/07/1992	4421	0.82	0.70
25/05/1987	2030	0.81	0.91
13/06/1991	1743	0.076	0.75
04/06/1992	5398	0.28	0.91
12/10/1988	874	0.16	0.56
02/05/1990	1148	0.024	0.16
26/05/1987	4776	0.62	0.72
14/06/1991	1460	0.90	0.93
23/09/1989	2567	0.62	0.91
03/05/1990	906	0.80	0.68
15/06/1991	1274	0.45	0.69
24/09/1989	2816	0.58	0.58
07/09/1988	2101	0.74	0.12
16/09/1987	1143	0.083	0.31
16/06/1991	1628	0.36	0.023
08/09/1988	2249	0.58	0.58

Figure 7.4e cont. : probabilities of chance occurrence of chi-square at the full pulse period and its second harmonic .

* events which triggered the central channel only (and which survived a 45 % soft cut selection, unless recorded in 1992 in which case no soft cut was applied).

distributed as χ^2 with 2 N degrees of freedom, from which to obtain P_x for the dataset as a whole. For application of the χ^2 statistic to be entirely valid it is required that, on average, the number of events in a single phase bin is in excess of five times the number of bins employed. Since the χ^2 test was chosen to complement the Rayleigh test, which is sensitive to broad features and may therefore cause a signal having a sharply peaked pulse profile to be overlooked, the number of bins in each light curve was not reduced in order that all files might meet this criterion. As a result, only those 34 datafiles containing more than 2000 events were included in the calculation of the overall values of P_x. Values of P_x = 72 % at the full pulse period, and P_x = 66 % at the half period were thus obtained.

7.4.5 discussion

There is no evidence to suggest that a γ-ray signal at the half period pervades the dataset. The strongest effect observed upon a single night was that of 11/10/1988 having a Rayleigh probability of occurrence by chance of $3{\cdot}6 \times 10^{-5}$. However, the data from this observation were included in the early tests which led to the decision to look for emission at the half period rather than at the full radio pulse period and from which the choice of a 45 % soft-cut was made. This probability should therefore be reduced by at least a factor of four, in which case the expected frequency of occurrence of a Rayleigh power of this strength in the dataset of 71 samples is 0·01. It is interesting to note that the Rayleigh probability of chance occurrence of periodicity during this observation obtained by Brazier (1991) after correction for the number of trials performed was $4{\cdot}7 \times 10^{-4}$. The use of an exact ephemeris rather than searching over a range of orbital parameters has improved upon this result only very slightly. The addition of data collected during 1991 and 1992 has served merely to reduce the significance of this single strong effect.

There is no statistically significant connection between the

results of the Rayleigh test and the orbital phase at the time of observation. This is hardly surprising given the absence of any orbital modulation of the closely studied radio flux from this object. A systematic variation in the γ-ray signal strength over the orbital cycle would necessarily be attributed to the presence of material along the line of sight to the pulsar. This intervening matter could absorb a steady γ-ray flux or act as a target for γ-ray production from a charged particle beam. There can, however, be few such targets in the PSR 1855+09 system as it does not appear to support accretion. The limb of the secondary is one potential site. However, since this is presumed to be a late-type, low mass star, alignment of the particle beam and its target as viewed from Earth would be short-lived. Brazier (1991) noted that the mass ratio of the two stars is too low to support the accumulation of matter at the Lagrangian points of the PSR 1855+09 system. She speculated that irradiation of the secondary could liberate sufficient material to form a curved wake behind it. Stenger (1984) calculated that the production of TeV γ-rays through the interaction of very high energy protons with hadronic material reached its maximum efficiency at a target column density of ≈ 50 g cm^{-2}. Ryba and Taylor (1991) placed an upper limit of 10^{-12} g cm^{-2} upon the column density of such ionised material within the PSR 1855+09 system, based upon the lack of attenuation of the pulsar's radio signal. The only evidence in support of a γ-ray flux modulated at the orbital period is that supplied by De Jager et al. (1990), who report that a signal pulsed at the half period was present in data collected on PSR 1855+09 using the atmospheric Cerenkov telescopes of the University of Potchefstroom. They noted that the effect was confined to the phase interval 0·92 to 0·02 with respect to superior conjunction. However, this phase region had received the greatest observational coverage (see also Brink et al., 1993).

7.5 PSR 1509-58, an isolated pulsar

7.5.1 background information

PSR 0531+21 and PSR 0833-45 were detected by both the COS-B and SAS-2 satellites (Hartman et al., 1979, Bennet et al., 1977) and were detected in subsequent observations at TeV energies (Rayner, 1989). Following the discovery of pulsed γ-ray emission from these isolated pulsars, which are embedded within the Crab and Vela X supernova remnants (SNRs) respectively, a search for x-ray pulsars was conducted using the Einstein Observatory, in the expectation of further fast pulsar - SNR associations. Amongst the SNRs targeted was MSH 15-52, which was found to contain PSR 1509-58, a source of 150 ms periodicity in the 0·2 to 4 keV range (Seward & Harnden, 1982).

The first radio observations of PSR 1509-58 revealed no shift in the pulse phase indicative of diurnal binary motion (Manchester, Tuohy & D'Amico, 1982). A year and a half had elapsed between the x-ray and radio measurements of the pulse period, yet they were in sufficiently close agreement to exclude any possibility of long term orbital motion. Thus, PSR 1509-58 is an isolated pulsar, and its emission is powered not by accretion from a companion but simply by rotational kinetic energy loss (Weisskopf et al., 1983).

Its discoverers estimated the surface magnetic field strength of PSR 1509-58 to be 15×10^{12} G, the second largest pulsar dipole field on record, and calculated its rate of kinetic energy loss to be in the region of 5×10^{37} erg s^{-1}. PSR 1509-58 is also remarkable in that its measured period derivative of $1{\cdot}5 \times 10^{-12}$ s s^{-1} is greater than that of any other isolated pulsar, being treble that of the Crab pulsar which previously held this distinction, which indicates that this object has existed in its current form for a mere one or two thousand years.

In spite of its youth, PSR 1509-58 is not prone to the glitch activity generally associated with pulsars having characteristic ages of less than

20,000 years (McKenna & Lyne, 1990). The stability of its rotation may indicate that the temperature of the recently formed neutron star is sufficiently high to allow the transfer of angular momentum from its core to its outer crust to remain relatively stress free. The regularity of this pulsar clock is such that the second derivative of its spin frequency may be measured, from which its braking index has been calculated and found to be less than that predicted. It has been suggested that this deficit may be due to the deformation of the neutron star's dipolar magnetic field by the outflowing energetic ions associated with a strong γ-ray source.

If the current rotational frequency of PSR 1509-58 is assumed to be considerably less than its original value, then, from equation 7.2a, the pulsar's characteristic age is found to be 1690 years (Manchester, Durdin & Newton, 1985). This estimate is consistent with the recent claim that SN 185, recorded by Chinese astronomers some 800 years before they witnessed the birth of the Crab pulsar, may have been the supernova explosion in which PSR 1509-58 was formed (Thorsett, 1992).

Doubt has been expressed in some quarters as to the validity of the association of PSR 1509-58 with the remnant MSH 15-52. The line of sight superposition of a pulsar upon a physically unrelated nebula is far from impossible, given the abundance of such remnants in the direction of the galactic plane. The nebula must be expanding into a region of the interstellar medium of particularly low density in order to have achieved its present extent during the lifetime of the pulsar. This scenario is consistent with the paradoxically high x-ray temperature and low surface brightness of the remnant. The x-ray spectral index of the pulsar and the optical extinction of the nebula give similar values for the neutral hydrogen column density (Seward, Harnden, Murdin & Clark, 1983). The 4·2 kpc distance to MSH 15-52 was established, from radio interferometric measurements of hydrogen line absorption, by Caswell, Murray, Roger, Cole and Cooke (1975).

7.5.2 previous VHE γ-ray observations

The University of Potchefstroom group surveyed a total of eighteen isolated radio pulsars using the atmospheric Cerenkov technique (Nel et al., 1992). Only PSR 1509-58 was seen to emit VHE γ-rays on a regular basis - during four out of ten dark moon periods between 1985 and 1988. This signal was absent from supplementary observations made over the following three years. The first observations made by this group consisted of 20·9 hours of tracked data collected over a period of 11 days in June 1985, at an estimated energy threshold of 2 TeV. When the on-source events were folded at the radio period of ~150 ms, a triple peaked light curve was produced (de Jager, Raubenheimer, North, Nel & van Urk, 1988). It was clear from the asymmetry of this light curve that this apparent ~50 ms variation was a harmonic of the γ-ray pulse period rather than the fundamental itself. It was found that the probability of chance occurrence of periodicity in the data, as calculated from the Rayleigh test for uniformity of phase, was minimised when the second harmonic of the radio period was considered in preference to the first or the fundamental. The above authors speculated that this triple peak phenomenon could be accommodated by the outer gap model of Cheng, Ho and Ruderman (1986) if one rather than two of the smaller gaps (labelled G' in figure 7.2) was quenched by emission from the others, or if γ-ray production in two outer gaps was supplemented by a flux of γ-rays from above one polar cap. This result is at variance with all other detections of VHE γ-rays from pulsars, which have always shown either singly or doubly peaked light curves.

The University of Potchefstroom group found evidence to suggest that the duty cycle of PSR 1509-58 consisted of continuous emission at the third harmonic of the radio period over about ten days, followed by an "off-state" of a similar duration (Nel, de Jager, Raubenheimer & North, 1989). From the observations taken in June 1985, the luminosity (above 2 TeV) of PSR 1509-58 was calculated to be $4{\cdot}7 \times 10^{34}$ erg s^{-1} (Nel, de Jager,

Raubenheimer, North & Brink, 1990). It should be noted that this result is based upon a Rayleigh test for emission at a period in the region of 50 ms, yet there is no indication that the number of degrees of freedom involved in the optimisation of the search range to include only the third harmonic of the radio period (based upon epoch folding of this very dataset) have been taken into account (Rayner, 1989).

PSR 1509-58 was observed by the Durham group in April 1987 (25 hours) and March 1989 (16 hours). The Rayleigh test was applied to search for periodicity in the range 150·4 to 150·5 ms, but none was found (Brazier et al., 1990). It was felt that relative phase could be said to be maintained between pulsed events over a month long observing session, but that the telescope timing was not sufficiently accurate to allow the production of a single light curve from data spanning two years. A twenty binned histogram of the number of events triggering the central channel alone versus the phase of the 150 ms pulse period corresponding to their arrival times, as calculated from the ephemeris of Manchester, Durdin and Newton (1985), was produced from each annual dataset. These light curves showed no structure. An upper limit to the flux, above 300 GeV, which if confined to a single bin would have produced a three standard deviation excess above expectation was estimated by the method described in section 4.4.1(iii) to be
$3{\cdot}4 \times 10^{-11}$ cm^{-2} s^{-1} from observations taken in 1987 and
$2{\cdot}2 \times 10^{-11}$ cm^{-2} s^{-1} from those made in 1989 (Rayner, 1989).

7.5.3 results from the Compton Gamma Ray Observatory

In January 1992, γ-rays in the energy range 20 keV to 2 MeV were reported to have been detected from PSR 1509-58 by the BATSE instrument aboard the Compton Gamma Ray Observatory (described in section 1.4.1(iii)). The energy spectrum observed was harder than that of the Crab pulsar seen by the same detector. The light curve signature consisted of a single peak which became narrower as the energy threshold was increased (Wilson et al.,

1992).

Analysis of data obtained in March 1992 using COMPTEL revealed a peak in the light curve around phase 0·47 in the 0·7 to 1 MeV band, but no pulse structure in the 1 to 30 MeV region (Carraminana, priv. comm.). When the data were subjected to a Z^2_3 test (described in section 4.3.3(ii)), which had been successfully applied in the detection of pulsed emission from the Crab pulsar, they were found not to conform to a flat light curve at the three standard deviation level (Bennet et al., 1993). The peak coincided with the pulse phase of the maximum in the 100 keV to 2 MeV energy range as determined from data recorded by OSSE (Hertz et al., 1993) and conformed to the 50 % duty cycle observed by BATSE.

PSR 1509-58 has not yet been detected by EGRET in the 20 MeV to 30 GeV region, although five other isolated pulsars have (Fichtel et al., 1992, Bennet et al., 1993).

7.5.4 the dataset

PSR 1509-58 was scheduled for observation by CGRO, as an OSSE secondary target over the period 19/3/1992 to 02/4/1992 and as the primary target from 15/10/1992 to 22/10/1992. It is visible from Bohena Settlement from March to June inclusive. It was observed on 08/3/1992 with the Mark III telescope, but no further time was allocated to data collection during this month as priority was given to the installation of the Mark V telescope. Three more observations were made in March 1993 (listed in figure 7.5a), during which the object reached culmination at 29°, corresponding to a threshold energy for the Mark III telescope of approximately 300 GeV. All of the observations of this object were made in tracking mode.

date (UT)	J.D. of observation	duration	sky clarity
08/03/92	2448690·083	255	good
19/03/93	2449066·112	176	excellent
23/03/93	2449070·116	100	good
28/03/93	2449075·137	170	poor

Figure 7.5a : the post 1989, Mark III telescope, PSR 1509-58 dataset (the Julian day number at the *beginning* of each observation is shown in the second column).

Information relating to PSR 1509-58 extracted from *The Princeton GRO/radio timing database*	
R.A. (2000)	15 h 13 m 55·6795 s
δ (2000)	-59° 8' 9·49"
T_o	JD 2448478·000000571
ν	6·6368504279262 s^{-1}
$d\nu/dt$	- 6·76745 x 10^{-11} s^{-2}
$d^2\nu/dt^2$	1·97 x 10^{-21} s^{-3}

Figure 7.5b : the PSR 1509-58 ephemeris of Johnston, Kaspi, Manchester, Lyne and D'Amico (1993).

7.5.5 recent analysis and results

The data were filtered in order to create files containing only those events which triggered the central channel alone. A parabolic fit was made to the count rate variation with zenith angle, in order to search for a brief excess which might be attributable to the activity of the target object rather than a thinning of any cloud cover. When a 300 s long bin was passed through each file in 60 s steps no such candidate "burst" was found.

A 20 bin light curve was produced for each file by folding the data modulo the pulse period (P) i.e. recorded event times were assigned an absolute phase (between 0 and 1) in accordance with the most recent ephemeris available in the Princeton GRO/radio timing database (presented in figure 7.5b) and placed in the corresponding phase bin of width 1/20, to produce a histogram of the number of on-source events versus pulse phase. The stated ephemeris is given as valid from JD 2447913 to JD 2449043; it is fair to assume that it may be extended to the epoch of the latest observations considered here given the absence of glitch behaviour from PSR 1509-58. The χ^2 test for goodness of fit described in section 4.3.4 was applied to each of these pulse phase histograms, in order assess the significance of any deviation of the number of events per bin from a uniform distribution.

Results from the CGRO showed that the light curve of PSR 1509-58 was single peaked in the 20 keV to 2 MeV region. Busetta et al. (1993) report evidence of a secular change in the shape of the light curve of the Vela pulsar at energies in the range 10 to 30 GeV, from the two narrow pulses observed during balloon experiments in 1981 to a broader feature showing "in-fill" between these pulses in recent COMPTEL observations. These authors also remark that emission between the two peaks in the light curve of the Crab pulsar is more intense in the spectral range covered by the EGRET instrument aboard the CGRO than at the lower energy region at which COMPTEL operates. It was felt that by re-binning the VHE γ-ray data at half

of the radio pulse period, some evidence of emission might be obtained by the combination of a weak signal separated by 180° in phase at the full pulse period. This was done and the χ^2 test was applied to the four 20 bin light curves obtained.

0·1 μs per day is an upper limit to the error in the measured value of the slip rate of the rubidium clock in use as a local time standard for the Bohena Settlement site (Rayner, priv. comm.). The relative arrival times of events in the 1992/1993 dataset may therefore be said to be known to an accuracy of 0·04 ms, or to $^1/_{100}$ th of the width of a single phase bin in the 20 bin light curves constructed by folding data at half of the radio pulse period of PSR 1509-58. This being the case, the data from all observations were combined to form the light curves, at the full 150 ms period and at its first harmonic, shown in figure 7.5c. The value of χ^2 and its associated probability are tabulated in figure 7.5d for light curves obtained from the individual observations and from the dataset as a whole, at both the full pulse period and its second harmonic.

The Rayleigh test was applied to each file in order to search for a signal at the third harmonic of the pulse period as reported by the University of Potchefstroom group (Nel, de Jager, Raubenheimer & North, 1989). These authors noted some slight variation in the peak to peak separation of the triple peaked light curves identified from three separate observations, hence the χ^2 test involving the retention of absolute phase information was deemed inappropriate to this investigation. For each observation, a range of trial periods was chosen to encompass five Fourier intervals (defined in section 4.3.2) to either side of the third harmonic of the radio period. The minimum Rayleigh probability of chance occurrence of periodicity in this range, corrected for the number of trials employed, is listed in figure 7.5d, together with the test period at which this "peak" appeared and the size of the Fourier interval.

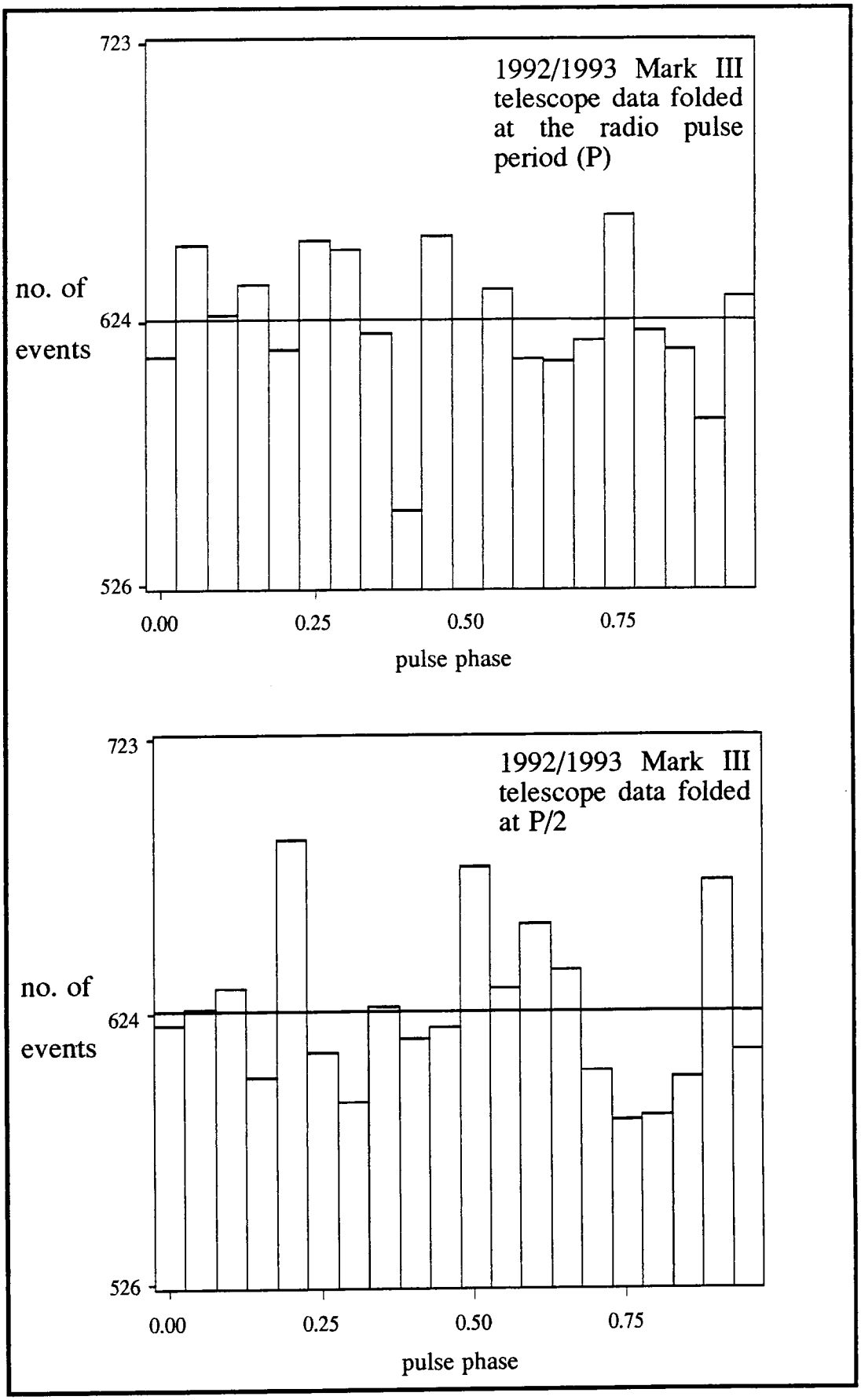

Figure 7.5c : light curves of PSR 1509-58 produced by binning events which triggered the central channel only according to the absolute phase of the radio pulse period, P, (above) and of P/2 (below) at the time of their arrival.

DATA \ TEST		the chi-square test for goodness of fit to a uniformly distributed light curve				Rayleigh test for phase uniformity within 5 F.I. of the third harmonic of the radio period	
		at the radio period, P		at P/2			
date (UT)	no. of events	chi-square	probability of chance	chi-square	probability of chance	peak period (ms)	probability of chance
08/03/1992	3667	17.00	0.55	19.89	0.38	50.23455 +/_ 0.00016	0.432
19/03/1993	4174	19.07	0.42	23.21	0.21	50.25129 +/_ 0.00024	0.053
23/03/1993	1757	15.01	0.68	19.22	0.41	50.25006 +/_ 0.00042	0.231
28/03/1993	2899	21.60	0.29	18.59	0.45	50.25121 +/_ 0.00025	0.194
total	12497	18.12	0.48	26.09	0.12		

Figure 7.5d : the results of tests for periodicity in the 1992/1993 PSR 1509-58 dataset.

7.5.6 conclusions

No evidence was found of pulsed emission from PSR 1509-58 in the 1992/1993 dataset. The light curve produced by folding all data at the pulse period did not exhibit the single maximum around phase 0·5 present in low energy γ-ray data from the CGRO. If a 5 % duty cycle is assumed, then a limit to the pulsed γ-ray flux from PSR 1509-58 at and above 250 GeV, may be calculated using equation 4.4d. A 3σ flux limit of $8{\cdot}9 \times 10^{-11}$ cm^{-2} s^{-1} is thus obtained (where a signal strength of 1% of the background flux is given by $\varphi_{1\%} \approx 6{\cdot}6 \times 10^{-11}$ cm^{-2} s^{-1}), which is slightly greater than those estimated from the 1987 and 1989 measurements because of the limited size of the new dataset.

The University of Potchefstroom group detected recurrent pulsed γ-ray emission from PSR 1509-58 at energies of approximately 2 TeV and above at a flux level of $3{\cdot}9 \pm 0{\cdot}9 \times 10^{-11}$ cm^{-2} s^{-1} during observations made between JD 2446227 and JD 2447382 (Nel, de Jager, Raubenheimer, North & Brink, 1990). When this object was targeted by the same group between JD 2447601 and JD 2448367 no further evidence of pulsed emission was found. An upper limit to the pulsed flux of $1{\cdot}2 \times 10^{-11}$ cm^{-2} s^{-1} was estimated from these data as a whole, although the energy threshold of the detector was increased from 2 TeV to 4 TeV during the course of these observations (Nel et al., 1992). These results were based upon the Rayleigh power present at the third harmonic of the radio pulse period. Since the Rayleigh probability of chance occurrence of periodicity at or near this ~50 ms period was never found to be less than 0·05 on a single night in the Durham 1992/1993 dataset, a null result was assumed and a flux limit was calculated for each observation, using equation 4.4c. These were then combined according to equation 4.4e to give an overall flux limit of $6{\cdot}4 \times 10^{-10}$ cm^{-2} s^{-1} at photon energies of ~250 GeV and above. If the index of the cosmic ray integral spectrum in the 5 TeV to 1 PeV region of -1·60 (Khrenov, 1993) is assumed to apply, such that the number of cosmic rays

detected is proportional to $E^{-1.6}$, then the above result at the Mark III telescope's 250 GeV threshold energy is equivalent to a flux limit at primary energies greater than 2 TeV of $2{\cdot}3 \times 10^{-11}$ cm^{-2} s^{-1}. This result is therefore consistent with the limit obtained from the University of Potchefstroom's most recent results and confirms that the γ-ray flux present in early observations made by this group is transient in nature.

The non-detection of PSR 1509-58 by EGRET does not bode well for its appearance at TeV energies. However, the discovery of high energy γ-rays from PSR 1055-52 by this instrument indicates that this isolated pulsar is a suitable alternative target.

7.6 47 Tucanae, a globular cluster

7.6.1 a foreword on globular clusters

Above and below the galactic disc, in which most star formation takes place at present, there lies a halo of more than one hundred spherical clusters of up to one million gravitationally bound stars. These "globular clusters" provide a large sample of stars in advanced evolutionary phases (Castellani, 1980).

Only about one ten thousandth of the mass of the galaxy is concentrated in globular clusters, yet they have been found to contain ten of the ~100 known x-ray binaries (Ray & Kluzniak, 1990). This suggests that the binary formation rate in these regions is enhanced by tidal capture of main sequence stars by neutron stars. Since the globular clusters consist of an old stellar population, it is reasonable to assume that any isolated pulsars formed in early supernova explosions will have spun-down and will no longer be powerful radio sources. Hence those millisecond pulsars observed must either have been "recycled" or must be the products of the later accretion induced collapse of white dwarfs, the lack of a companion star in some cases being attributed to its evaporation the pulsar wind of

the primary or to collisional disruption of the parent system.

Chen (1991) suggested that globular clusters might be strong γ-ray sources due to flux contributions from as many as one thousand millisecond pulsars per cluster. Only a few of these pulsars should be visible to radio astronomers due to the narrow beaming of emission at these wavelengths. Thus, an upper limit to the millisecond pulsar population might be better attained from observations at γ-ray energies. By assuming the period distribution of the twenty eight millisecond pulsars so far observed in globular clusters to be representative of all, the above author estimated the total pulsar "spin-down power" of a single globular cluster to be $\approx 10^{38}\ N_{500}$ erg s^{-1} where N_{500} is the number of millisecond pulsars present in units of 500. If an efficiency of γ-ray production via the outer magnetospheric gap mechanism similar to that of isolated pulsars is assumed, then the resulting γ-ray luminosity is given by:

$$L_{gamma} = 1{\cdot}5 \times 10^{36}\ N_{500}\ f \quad \text{erg s}^{-1} \qquad \text{eqn. 7.6}$$

where f is a beaming factor which approximates to unity.

In his paper entitled "Gamma Rays from Globular Clusters", Tavani (1993) states that according to the argument of Chen (above), in excess of 500 individual pulsed sources would be required to exist within a single globular cluster in order for it to be detected in the γ-ray region with the equipment currently available. This author estimates the sizes of the pulsar populations which could exist within a range of globular clusters by assuming that this is determined by the cluster mass, core star density and velocity dispersion. He finds that only one of the 48 clusters considered should have $N_{500} > 1$. However, he goes on to suggest that globular clusters may be strong γ-ray sources if they contain *interacting binary pulsars*, in the vicinity of which a strong unpulsed γ-ray flux is developed at a shock front where a pulsar wind encounters material evaporating from an irradiated companion star. This shock emission would be similar to that

observed from the supernova remnants surrounding young pulsars. The target material would absorb radio emission from the central "hidden pulsar" whilst remaining optically thin at x-ray energies and above. By inference from observations of the Crab nebula, Tavani (1993) estimated that at energies above 100 keV a flux of up to 10^{35} erg s^{-1} could be obtained from a hidden pulsar. As Spergel (1991) noted, the presence of a numerous pulsar population could account for the lack of free gas within globular clusters, since material released during stellar evolution could be carried out of the cluster by the relativistic particles and/or low frequency electro-magnetic radiation of pulsar winds.

7.6.2 background information on 47 Tucanae

Charles (1989) reviewed satellite x-ray surveys in search of sources which could be identified with globular clusters and found 21, of which the lone source associated with 47 Tucane (or NGC 104) was one of the nearest, having a x-ray luminosity of $10^{34.6}$ erg s^{-1}. Auriere, Koch-Miramond and Ortolari (1989) discovered a 120 s periodicity in the x-ray flux, suggestive of a cataclysmic variable or x-ray binary origin. De Jager et al. (1989) reported the detection of a γ-ray flux at energies above ~5 TeV pulsed at this 120 s period from the direction of 47 Tuc, having a peak luminosity of ~10^{36} erg s^{-1}. These authors stated that such a high γ-ray luminosity excludes the possibility that the source is a CV. A pulsed TeV γ-ray signal from 47 Tuc has yet to be confirmed by independent observers (see Mannings (1990) and Bowden (1993)). Paresce, De Marchi and Ferraro (1992) have since identified an optical counterpart to the periodic x-ray source (X0021.8-7221) from Hubble Space Telescope observations of the region. They report that the spectral characteristics of the object, a high x-ray to optical brightness ratio and an ultra violet excess typical of an accretion disc, are consistent with those of an intermediate polar CV.

In July 1991, Manchester et al. announced the discovery of ten

millisecond radio pulsars in 47 Tuc, bringing the total in this cluster to eleven and the overall globular cluster pulsar population count to approximately 30. None of these objects was detected in *every* observation, six exhibited binary orbital motion and one was consistently absent at the same orbital phase, suggestive of eclipse by an ablating companion. The Tavani (1993) estimate for the number of pulsars which may exist within 47 Tuc is 276. According to equation 7.6, these pulsars should support a γ-ray luminosity of 8×10^{35} erg s^{-1}. At a distance of 4·6 kpc (Webbink, 1985) the flux from 47 Tuc should, by this argument, be of the order of 3×10^{-10} erg cm^{-2} s^{-1}. By contrast, a single millisecond pulsar at this distance, assumed to exhibit the maximum spin-down power ($\sim 10^{36}$ erg s^{-1}) and efficiency of conversion of this power to γ-rays ($\sim 10^{-2}$) theoretically allowed, would give rise to a γ-ray flux at Earth of 4×10^{-12} erg cm^{-2} s^{-1}. If this flux were manifest entirely as 450 GeV γ-rays (i.e. at the threshold energy of the Durham Mark III telescope at a zenith angle of 45°) then the single pulsar would contribute 9×10^{-13} photons cm^{-2} s^{-1} to a total pulsed flux of $2{\cdot}5 \times 10^{-10}$ photons cm^{-2} s^{-1}. Since the sensitivity of the Mark III detector at this zenith angle is given by $\varphi_{1\%} \approx 8 \times 10^{-11}$ photons cm^{-2} s^{-1} (see section 4.4.2), it is clear that whilst the flux from the globular cluster pulsar population as a whole might appear as a 3 % signal in this instrument, individual millisecond pulse signatures are unlikely to be distinguished. If the hidden pulsar population hypothesis put forward by Tavani (1993) is correct, then the overall, effectively unpulsed, γ-ray flux from 47 Tuc may exceed that estimated above.

7.6.3 a search for unpulsed emission

(i) the dataset

47 Tuc was observed using the Mark III telescope in chopping mode on

seven occasions in August 1991. Of these datasets, the five listed in figure 7.6a were considered to be of sufficiently good quality, in terms of reported sky clarity and telescope response, to be subjected to a search for an unpulsed γ-ray signal. The object was viewed near its culmination, such that the target zenith angle was restricted to the range 42° to 46° throughout. The target direction was regularly alternated in order to obtain on-source and off-source data sets of equal duration, each made up of a series of two minute long exposures. This "chopping" mode of observation is described in detail in chapter three.

(ii) analysis and results

In order to confirm that the data were well-behaved, histograms were constructed of the on-source count rate, averaged over consecutive 240 s long bins, for each observation. At no point did the count rate differ by as much as three standard deviations from that expected (as determined from a parabolic fit to the count rate variation with zenith angle).

A simple summation of the number of events which triggered the central channel alone was performed, in order to determine whether the total count from the direction of 47 Tuc (n_{on}) exceeded that from a position offset from it by 2° in azimuth (n_{off}). These values are displayed for each observation and for the dataset as a whole in figure 7.6b. Also shown is the corresponding excess number of on-source counts, s, required, given n_{off}, in order for the null hypothesis (that no signal is present in the data sample) to be rejected at the 68 % confidence level (calculated according to the method described in section 4.3.1). Clearly, this value is attained in neither a single observation nor in the dataset as a whole. The null hypothesis cannot be rejected. According to equation 4.4a, the steady flux from 47 Tuc which would have resulted in its detection at the 3 σ level is $3{\cdot}1 \times 10^{-10}$ cm^{-2} s^{-1} at a zenith angle limited energy threshold of 450 GeV.

date (UT)	duration (min.)	sky clarity
07/08/1991	164	excellent
10/08/1991	167	excellent
11/08/1991	250	excellent
13/08/1991	152	excellent
14/08/1991	187	excellent

Fig. 7.6a : the selected 47 Tuc dataset.

date (UT)	n_{on}	n_{off}	$n_{on}-n_{off}$	s
07/08/1991	2090	2132	- 42	67
10/08/1991	2436	2481	- 45	72
11/08/1991	3137	3102	35	81
13/08/1991	2053	2003	50	65
14/08/1991	2300	2360	- 60	71
total	12016	12078	- 62	157

Fig. 7.6b : comparative totals of the number of events recorded from the source direction and from an off-source control region.

7.6.4 conclusions

An upper limit to the γ-ray flux from 47 Tuc above 0·1 GeV of 3×10^{-6} cm^{-2} s^{-1} was obtained using the COS-B satellite (Chen, 1991). If it is assumed that the detection of VHE γ-rays from this object would require a source spectrum harder than that of the cosmic ray background, then if the spectrum follows a power law of the form:

$$N_E = \text{a constant} \times \left[\varepsilon\right]^{-\alpha}$$

where N_E is the number of photons of energy ε, α must be < 1·6. Thus, at the Mark III telescope threshold energy of 450 GeV, from the above relation, a flux limit of:

$$N_{450} \geq 3 \times 10^{-6} \left[\frac{450}{0{\cdot}1}\right]^{-1{\cdot}6}$$

$$\geq 4 \times 10^{-12} \text{ cm}^{-2} \text{ s}^{-1}$$

is obtained, which is entirely compatible with the experimentally derived value of $N_{450} < 3{\cdot}1 \times 10^{-10}$ (which gives $\alpha \approx 1{\cdot}09$).

If a distance to 47 Tuc of 4·6 kpc is assumed, then a flux at Earth of $N_{450} \approx 3{\cdot}1 \times 10^{-10}$ cm^{-2} s^{-1} would be equivalent to a source luminosity at 450 GeV of $5{\cdot}6 \times 10^{35}$ erg s^{-1}. An upper limit to the flux from 47 Tuc obtained using EGRET (which operates in the 20 MeV to 30 GeV region) of the order of 5×10^{34} erg s^{-1} has recently been reported (Thompson, 1992), whilst the analysis of COMPTEL data on this object is underway.

From inspection of equation 4.4a and of the observed event count rate, it is clear that the reduction of the limiting value of N_{450} obtained by experiment to that estimated, from the COS-B result and the assumption of a simple power law source spectrum, would require of the order of 28 years worth of data of a similar quality. A concerted effort to increase the sensitivity of atmospheric Cerenkov telescopes is required.

CHAPTER EIGHT

Future Prospects for Atmospheric Cerenkov Astronomy

If the detection of VHE γ-rays is to become a powerful tool in the study of astronomical phenomena, the next generation of atmospheric Cerenkov telescopes must produce positive results which are "non-statistical". Target objects must be chosen with care, and an effort must be made to develop a truly efficient and reliable cosmic ray background rejection technique. As signal to noise ratios improve, so larger flux collecting areas may be introduced whilst maintaining a manageable volume of data. Thus the threshold energies of ground based detectors can be reduced in order to span the gap in the observable γ-ray spectrum between satellite experiments and the atmospheric Cerenkov technique.

8.1 signal enhancement

As pioneers of the Cerenkov light imaging technique, the Whipple collaboration have achieved the most statistically significant results to date (Fegan, 1992). A disadvantage of the imaging technique is that since reliance is placed upon one or two instruments of increasingly complex design, maintenance and development work substantially reduces the available observing time.

It is difficult to imagine how the mirror area of a single telescope could be increased far beyond current limits without encountering mechanical problems and prohibitive engineering costs. It has been suggested that solar collectors where many free standing mirror units focus light onto a single tower could have a role to play in atmospheric Cerenkov astronomy (Tumer, Kerrick, O'Neill, White & Zych, 1991). It would be interesting to compare the results from a large imaging telescope based upon a single dish with those obtained from a similar mirrored area

comprising an array of smaller instruments operating on the principle of guard ring rejection, and possibly incorporating inter-telescope timing information. Since many groups are financially constrained to choose between one approach and another, a true comparison of the relative worth of these techniques must await further source detections and a standardisation of the methodology and format of flux calculations. Indeed, Palfrey (1992) suggested that the time had come for the formation of an "international simulation working group", which would produce models of shower formation and Cerenkov emission against which the performance of the various techniques could be judged.

8.1.1 the Mark III/Mark V telescope upgrade

The Mark III and Mark V telescopes were refurbished in April 1993, in order to create a pair of simple imaging telescopes of identical performance (Bowden et al., 1993a).

An extra 2" PMT was added to the outer ring of tubes in the central detector package of the Mark V telescope to form a 31 pixel camera. Baffles were erected about each mirrored dish in order to reduce the amount of background light observed.

The central dish of the Mark III telescope made up of spherical mirror facets was replaced by a parabolic mirror, of reflective surface area 10 m^2, of the type used for the Mark V telescope. A 31 pixel camera identical to that of the Mark V instrument was installed in place of the central 7 PMT detector package of the Mark III telescope. The struts supporting this camera were extended so that a point source at infinity now produces an image of approximate diameter 2·5 cm at the PMTs' photocathodes, as is the case for the Mark V telescope.

The Mark III and Mark V telescopes, as they now stand, are shown in figure 8.1. During simultaneous viewing of the zenith, approximately 45% of all recorded Cerenkov flashes are registered by both instruments. The

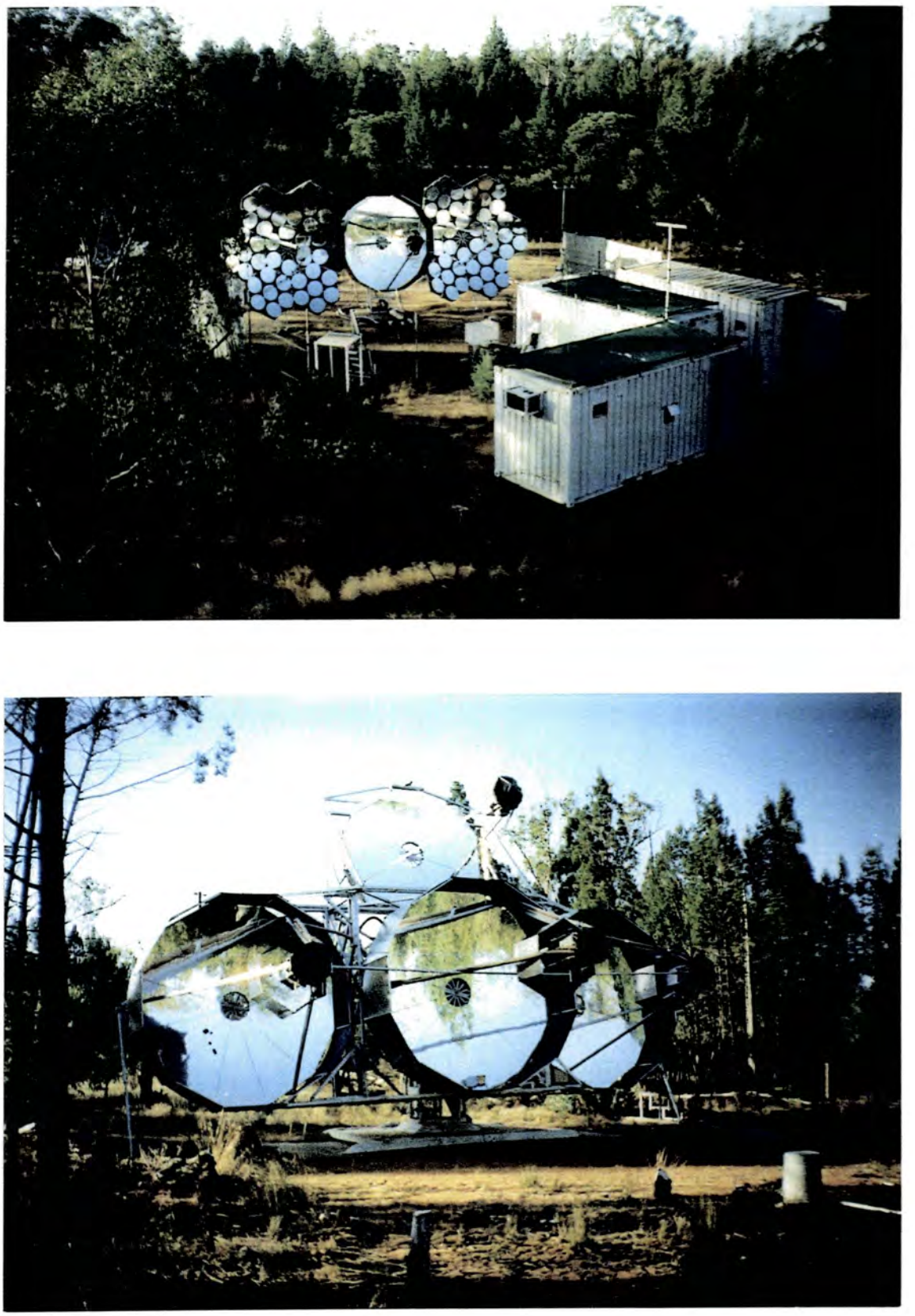

Figure 8.1 : the Mark III and Mark V telescopes (top and bottom frames respectively) after refurbishment in April 1993. Both telescopes are now equipped to record the image of each Cerenkov flash viewed by their central detector packages.

position of the centroid of a Cerenkov image in the field of view can be determined from a dual telescope response and used as a background event rejection criterion. It should be possible to apply this "stereo imaging" technique to intrinsically fainter flashes than the single telescope method which requires detailed information as to the angular extent and orientation of each image (see section 2.3.1(iii)). However, since only bright flashes tend to trigger more than one telescope, the threshold energy of the Mark III/Mark V stereo imaging pair will be similar to the ~450 GeV threshold energies of the two instruments when they are operated as independent imaging telescopes. One advantage of the stereo technique is that the normalisation of the PMT responses is less critical to the pinpointing of the centroid of a Cerenkov image than to the determination of a complete set of image parameters.

The Australian/Japanese CANGAROO project commenced stereo Cerenkov imaging in December 1992 (Edwards et al., 1993).

An obvious target for VHE γ-ray astronomers is the development of new ground-based instruments which will bridge the gap between the current energy threshold of atmospheric Cerenkov telescopes, of ~200 GeV, and the 30 GeV upper limit to photon detection by the EGRET instrument aboard the CGRO. Proponents of the imaging technique should beware, however, since the distinction between the well defined images of γ-ray initiated cascades and the irregular outline of hadronic showers may be blurred as the total amount of light required to trigger a response is reduced. The 10 GeV to 100 GeV energy range marks the maximum of the differential cosmic ray proton number spectrum, due partially to steering by interplanetary magnetic fields (Hillier, 1984). In this region, the particle flux density falls below that expected from the inverse power law relationship applicable to particle energies above 100 GeV. It is hoped that, as the pions produced by primary protons of increasingly lower energies will tend to decay to form muons rather than photonic pairs, γ-rays from celestial

objects will form a greater fraction of the cosmic ray flux detected by atmospheric Cerenkov telescopes having low energy thresholds (Orford, priv. comm.). However, there is some speculation to the effect that the flux of cosmic ray electrons, which does not decline until the energy per particle drops below ~10 GeV (Taira et al., 1993), may shroud any celestial γ-ray signal of energy < 100 GeV per photon, as electrons form secondary γ-rays at the top of the atmosphere.

8.1.2 the Mark VI telescope

The extraction of detailed information as to the shape and orientation of the image of a Cerenkov light pool requires a high photon density capable of triggering multiple PMTs. A large flux collecting area is therefore required. The 3-fold coincidence guard ring technique has been shown to be a successful method of cosmic ray background rejection (Brazier et al., 1989a), its greatest asset being its simplicity. It is intended that the University of Durham Mark VI telescope, which is currently under construction, will perform as an imaging telescope *and* require a three-fold coincidence from one central camera and detector packages facing two outer dishes. The Mark VI telescope is of a similar design to the Mark V, although an "upper" timing dish has been omitted from the new instrument and its linear dimensions are double those of the latter. Each of three parabolic mirrors constructed from 24 Mark V telescope type segments should bring light from a distant point source to an image of size ~0.25° FWHM. The detector packages will consist of a cluster of nineteen 2" photomultiplier tubes, each having a projected 0·5° aperture on the sky, in the focal plane of each outer dish and a 109 by ~0·25° pixel camera of 1" PMTs facing the central dish. A response from a single tube in each of the 19 PMT detectors together with any one of seven 1" tubes viewing the same area of sky will constitute an event. This telescope should have a threshold energy at the zenith, under a clear sky, of ~75 GeV. The central

detector package will also function as a Whipple type camera. The requirements of high resolution imaging are expected to raise the energy threshold for event acceptance to ~500 GeV. The Mark VI telescope is due to be commissioned at Bohena Settlement in June 1994.

8.2 VHE γ-ray source candidates

8.2.1 objects of promise in the Durham database

(i) accreting binary systems

Fresh evidence of pulsed VHE γ-ray emission from the x-ray binaries Vela X-1 and Cen X-3 has been found in data collected by the University of Durham group (Bowden et al., 1992b, Bowden et al., 1993b). These sources, and the XRBs Cyg X-3 and Her X-1 are seen to emit VHE γ-rays most often when the compact star is at or near the ascending node (Chadwick, McComb & Turver, 1992). This orbital phase dependency is attributed to the short-lived alignment of the particle accelerator and the target material within each system, and Earth. Whilst light at longer wavelengths may be scattered from its original path before leaving a matter rich system, those γ-rays which survive their passage through absorbing material generally retain their direction of emission. The orbital phase dependency of a VHE γ-ray flux may therefore provide otherwise unobtainable information as to the geometry of a binary system.

The Durham group detected a strong burst of activity from the Cataclysmic Variable AE Aquarii at phase 0.17 with respect to superior conjunction, and a second less significant burst episode at an orbital phase of 0·93 (Bowden et al., 1992). This could be interpreted as due to particles accelerated at the edge of an accretion disc which form γ-rays in the limb of the companion. An on-source count rate excess which may have been a sign of similar activity from another intermediate polar type CV,

H0253+193, unfortunately could not be assigned an orbital phase because no sufficiently accurate ephemeris was available. This class of object could provide an excellent test bed for the inference of system geometry from γ-ray observations, since their relative abundance has allowed optical astronomers to study them in greater detail than the more distant x-ray binaries.

It has been suggested that the success rate of VHE γ-ray astronomy, in terms of positive source detections, could be increased if objects were preferentially targeted for observation at a pre-selected phase of their orbits. This pre-supposes that source mechanisms are sufficiently well understood that γ-ray emission at other points in an orbit may be ruled out. It would be unfortunate if the drive to produce a large VHE γ-ray source catalogue were to overshadow the development of atmospheric Cerenkov astronomy as an investigative tool.

The continued growth in the size of flux collectors, and the refinement of background rejection techniques, should reduce the exposure time required for the detection of a signal of a certain strength. Coverage of the entire orbit of a given source should therefore become more attractive in the future, as only a few orbital cycles will need to be observed in order to obtain a significant result.

(ii) isolated pulsars

To date, six isolated pulsars have been detected by the CGRO (Fierro et al., 1993). Two of these, the Crab pulsar and Geminga unfortunately never rise to more than ~40° above the horizon at Bohena Settlement and therefore lie in the large zenith angle - high telescope threshold energy regime. The others, the Vela pulsar, PSR 1509-58, PSR 1706-44 and PSR 1055-52 which culminate at zenith angles of between 30° and 15° have been observed on several occasions during 1993. It is hoped that some positive results will be achieved as this database is extended during the

lifetime of the CGRO. The search for pulsations in VHE γ-ray data benefits greatly from the regularly updated pulsar ephemerides, which are provided by radio astronomers as support for the CGRO mission.

Pulsed VHE γ-rays detected from the Crab pulsar (Gibson et al., 1982, Tumer et al., 1985, Bhat et al., 1986) and from Geminga (Bowden et al., 1993, Vishwanath, Satyanarayana, Ramana-Murthy & Bhat, 1992) have firmly established isolated, strongly magnetised, rapidly rotating pulsars as targets for further atmospheric Cerenkov observations. A strong unpulsed flux of γ-rays of energy > 0·5 TeV has been observed from the direction of the Crab nebula by the Whipple collaboration, using the imaging technique at their Northern Hemisphere site (Vacanti et al., 1991). With the introduction of stereo imaging at Bohena Settlement, it will be interesting to see whether a significant unpulsed flux can be detected from the nebulae thought to be associated with the Vela pulsar, PSR 1509-58 and PSR 1706-44 (McAdam, Osborne & Parkinson, 1993).

8.2.2 collaborative projects

(i) active galactic nuclei

The EGRET instrument aboard the CGRO detected in excess of two dozen active galaxies during its first two years of operation.

A flux of relativistic particles may arise in the vicinity of an AGN through diffusive shock acceleration at the terminations of plasma jets (Quenby & Lieu, 1989) or, possibly, may result from the shock acceleration of protons undergoing spherical accretion onto a massive black hole at the galactic centre (Protheroe & Kazanas, 1983). Fast protons can interact with surrounding material to produce unstable neutral pions which decay to give a flux of γ-rays, which may then undergo inverse Compton scattering. The jet scenario has the advantage that the site of any γ-ray emission is somewhat removed from the dense core of the AGN where the likelihood of

photon absorption via pair production is greatest.

The EGRET γ-ray source catalogue does not include the active galaxy Centaurus A, although γ-rays from this object *were* detected by the OSSE and COMPTEL instruments which have lower energy thresholds than EGRET (Fichtel, 1992a). Centaurus A was the target of atmospheric Cerenkov observations by the University of Durham group in 1987 and 1988, during which no evidence of VHE γ-ray emission was found (Rayner, 1989).

In March 1992, the EGRET team reported the detection of γ-rays of energy > 1 MeV from three BL Lac type AGN, including one of the nearest, Markarian 421, which has a redshift, z, of 0·031 (Michelson et al., 1992). The Whipple group observed Mkn 421 using the atmospheric Cerenkov imaging technique and detected an unpulsed flux of γ-rays of energy > 0·5 TeV significant at the 6·3 standard deviation level (Punch et al., 1992). The same group found no evidence of VHE γ-ray emission from eight other AGN in the distance range given by $0{\cdot}055 \leq z \leq 2{\cdot}17$ (Fennell et al., 1992). One of these was 3C 279, an AGN which appeared to EGRET to be brighter than Mkn 421. The non-detection of 3C 279 may be due to the acknowledged time variability of its emission in the tens of GeV range, or it may be attributed to the fact that 3C 279 has a z of 0·54, at which distance the degradation of the γ-ray flux through pair production with the infrared background is thought to become significant (Kniffen et al., 1993).

The VHE γ-ray astronomy of AGN may be used to place an upper limit upon the intensity of the infrared background flux, direct measurements of which have been plagued by the heat radiated by dust within the solar system, and by the background noise associated with even the most efficiently cooled infrared detectors.

Stecker and De Jager (1993) derived an upper limit to the infrared background flux using the shape of the γ-ray spectrum of Mkn 421 as measured by the Whipple group and by EGRET. They assumed that the true source spectrum followed a simple power law over the 10^9 eV to 10^{12} eV

photon energy range. They then estimated the infrared flux density required in order to bring the VHE tail of the true spectrum down to the level observed, through the loss of extragalactic VHE photons to pair production. Their result falls between those obtained by direct measurement, and the values postulated from counts of the number of galaxies visible from Earth in the infrared and optical wavebands. It is consistent with an entirely "ordinary" origin of the infrared photons in the process of stellar evolution, implying that apocalyptic events need not be invoked. These authors predict that absorption of the γ-ray flux from VHE photon emitting AGN should become apparent at source distances given by $z \geq 0{\cdot}15$ to $0{\cdot}25$.

In order to deduce a rigorous upper limit to the infrared background flux from cosmic γ-ray energy spectra, a large sample of AGN is required. To avoid the introduction of a directional or instrumental bias, further observations of AGN should ideally be carried out by the entire community of atmospheric Cerenkov astronomers. In 1992 and 1993, the Durham group have begun to accumulate data on the AGN 3C 279, PKS 2135-147, PKS 2155-30 and PKS 0521-36, which have redshifts of approximately $0{\cdot}54$, $0{\cdot}2$, $0{\cdot}17$ and $0{\cdot}055$ respectively. Note that a z of $0{\cdot}5$ is equivalent to a distance of approximately 3000 Mpc.

VHE γ-ray groups should enlist the aid of other astronomers, in monitoring the instantaneous level of activity of AGN at different wavelengths. For instance, the Whipple group observed a threefold increase in the VHE γ-ray flux from Mkn 421. Variations of this magnitude were to be expected, since a fourfold increase in the intensity of the x-ray flux from this object (which lasted for three days and was classified as a short outburst) had previously been recorded by the Ariel V satellite (Marshall, Warwick & Pounds, 1981). Information as to whether an AGN was in a high or a low emission state at the time of atmospheric Cerenkov observations will be invaluable if far-reaching conclusions are to be made from a spectral survey.

(ii) γ-ray burst studies

Two decades after the discovery of γ-ray bursts, their origin remains a mystery. The point sources of this sporadic γ-ray emission, which lasts for a few seconds or a few tens of seconds, are seemingly isotropically distributed across the celestial sphere. Statistical tests performed on the measured brightness distribution have lead astronomers to the conclusion that the Gamma Ray Bursters (GRBs) must lie either within 1 kpc of Earth or beyond the local supercluster at ≥ 30 Mpc (Epstein & Hurley, 1988). The detection of periodicity on a timescale of a few seconds within a limited number of the outburst light curves is consistent with an origin in the vicinity of strongly magnetised neutron stars.

The Burst And Transient Source Experiment aboard the CGRO observed 400 cosmic γ-ray bursts during its first 20 months of operation. EGRET witnessed seven of these at energies of up to 0·2 GeV per photon. Schneid et al. (1992) reported that the burst witnessed by EGRET on 03/05/1991 was three orders of magnitude brighter above the 50 MeV level than the Vela pulsar had appeared to be to the same instrument (the Vela pulsar is the most intense, steady high energy source seen by EGRET). At the low energy end of the γ-ray spectrum, the distribution of the burst intensities recorded by the CGRO falls below that which would be expected from a spatially isotropic population of GRBs. According to Fichtel (1992a), this deviation may be due to the effects of redshifting over cosmological distances.

It has been suggested that GRBs lie in a halo about this galaxy, hence their isotropic appearance (Jennings, 1982). The Whipple group chose to test this model by observing M31, another spiral galaxy in the local group. Atmospheric Cerenkov data were scanned for potential burst episodes by using the imaging technique to select candidate γ-ray initiated events, then searching for a brief count rate excess over the background rate. The elliptical Cerenkov flash images selected in this manner were superimposed

upon a grid representing the telescope's focal plane, and the perpendicular distance, d, of the major axis of each from various points on the grid was calculated. A cluster of events having $d < 0{\cdot}08^{\circ}$ from a common point was to constitute a burst detection. No such burst was observed in the 11 hour long M31 dataset (Chantell et al., 1993). Since BATSE detects GRBs at a rate of approximately 1 per day, this result was hardly surprising.

Connaughton et al. (1993) endorse a wider application of the above atmospheric Cerenkov burst searching technique. They looked for an overlap between the areas of sky covered during the routine observation of various objects with the Whipple telescope, and the GRB sightings listed in the BATSE Burst Catalogue. Unfortunately, the narrow field of view and short duty cycle of atmospheric Cerenkov observations was such that no such overlap was found. However, these authors note that over the expected lifetime of BATSE (~8 years), a GRB must almost certainly fall within the field of view of at least one of the atmospheric Cerenkov telescopes in operation around the world. They themselves now intend to comb the entire 1988 - 1993 Whipple database for candidate GRBs. It is in this kind of search that the value of multiple telescope observations whether performed by a single group as at Bohena Settlement or through the collaboration of those operating observatories at similar longitudes becomes apparent; without independent confirmation of a burst episode, an instrumental or otherwise local origin cannot be ruled out.

8.3 peroration

It is clear that the rapid expansion of atmospheric Cerenkov facilities which is currently under way is fully justified. Early results have surpassed initial expectations by revealing a wide variety of VHE γ-ray source morphologies, from unipolar inductors to star - disc dynamos.

The discovery that x-ray binaries (e.g. Cygnus X-3) may support fast, VHE γ-ray emitting pulsars which are obscured from view at longer

wavelengths by a cocoon of accreting material, may shed some light upon the birth of millisecond pulsars in binary systems, a process which has long perplexed theoreticians.

Active Galactic Nuclei are an exciting new addition to the growing catalogue of VHE γ-ray sources. The development of this practical link between particle physics and cosmology will require the additional services of the Compton Gamma Ray Observatory. Long may the productive partnering of satellite experiments and atmospheric Cerenkov astronomy continue.

REFERENCES

Angel, J.R.P. (1978), *Ann. Rev. Astr. Ap.*, **16**, 487.

Antonov, R.A. et al. (1991), *Proc. 22nd Int. Cosmic Ray Conf.*, **2**, 664, Dublin.

Ascoli Balzanelli, A. & Ascoli, R. (1954), *Nuovo Cimento*, **11**, 562.

Auriere, M., Koch-Miramond, L. & Ortolani, S. (1989), *Astr. Ap.*, **214**, 113.

Bailey, J. (1981), *MNRAS*, **197**, 31.

Bailey, J., Hough, J.H., Gatley, I. & Axon, D.J. (1983), *Nature*, **301**, 223.

Balashov, V.V., Korotkikh, V.L. & Moskalenko, I.V. (1990), *Proc. 21st Int. Cosmic Ray Conf.* (Ed. Protheroe, R.J.), **4**, 416, Adelaide.

Basiuk, V. et al. (1989), *Proc. Int. Workshop on VHE Astronomy*, 41, Crimea.

Basiuk, V. et al. (1991), *Proc. Int. Conference on VHE Astronomy* (Ed. Matthews, J.), 65, Ann Arbor.

Bastian, T.S., Dulk, G.A. & Chanmugam, G. (1988), *Ap. J.*, **324**, 431.

Bath, G.T. (1976), *Structure & Evolution of Close Binary Systems* (Ed. Eggleton, P.P., Mitton, S. & Whelan, J.A.J.), Reidel Publishing, Dordrecht.

Bath, G.T., Pringle, J.E. & Whelan, J.A.J. (1980), *MNRAS*, **190**, 185.

Batschelet, E. (1981), *Circular Statistics in Biology*, Academic Press, London.

Bell, J.F., Bailes, M. & Bessell, M.S. (1993), *Nature*, **364**, 603.

Belvedere, G. (1989), *Accretion Disks and Magnetic Fields in Astrophysics* (Ed. Belvedere, G.), Kluwer Academic Publishers, Dordrecht.

Bennet, K. et al. (1977), *Astr. Ap.*, **61**, 279.

Bennet, K. et al. (1993), *Proc. 23rd Int. Cosmic Ray Conf.*, **1**, 172, Calgary.

Beuermann, K., Stella, L. & Patterson, J. (1987), *Ap. J.*, **316**, 360.

Bhat, P.N. et al. (1986), *Nature*, **319**, 127.

Blackett, P.M.S. (1948), Rep. Gassiot Comm. of the Royal Society on *Emission spectra of the night sky and aurora*, 34.

Boley, F.I. (1964), *Rev. Mod. Phys.*, **36**, 792.

Bowden, C.C.G. (1993) *Ph. D. Thesis, University of Durham.*

Bowden, C.C.G. et al. (1991), *Proc. 22nd Int. Cosmic Ray Conf.*, **1**, 429, Dublin.

Bowden, C.C.G. et al. (1991a), *Proc. 22nd Int. Cosmic Ray Conf.*, **1**, 356, Dublin.

Bowden, C.C.G. et al. (1991b), *Proc. 22nd Int. Cosmic Ray Conf.*, **1**, 396, Dublin.

Bowden, C.C.G. et al. (1992), *Astroparticle Phys.*, **1**, 47.

Bowden, C.C.G. et al. (1992a), *J. Phys. G*, **18**, 413.

Bowden, C.C.G. et al. (1992b), *J. Phys. G*, **18**, L127.

Bowden, C.C.G. et al. (1993), *J. Phys. G*, **19**, L29.

Bowden, C.C.G. et al. (1993a), paper presented at the Calgary workshop *Towards a Major Atmospheric Cerenkov Detector II*.

Bowden, C.C.G. et al. (1993b), *Proc. 23rd Int. Cosmic Ray Conf.*, **1**, 298, Calgary.

Brazier, K.T.S. (1991), *Ph. D. Thesis, University of Durham.*

Brazier, K.T.S. et al. (1989), *Experimental Astronomy*, **1**, 77.

Brazier, K.T.S. et al. (1989a), *Proc. 23rd ESLAB Symposium on Two Topics in X-Ray Astronomy* (Ed. Hunt, J. & Battrick, B.), ESA, Paris, **1**, 325.

Brazier, K.T.S. et al. (1990), *Proc. 21st Int. Cosmic Ray Conf.* (Ed. Protheroe, R.J.), **4**, 374, Adelaide.

Brink, C. et al. (1993), *Proc. 23rd Int. Cosmic Ray Conf.*, **1**, 334, Calgary.

Browning, R. & Turver, K.E. (1977), *Nuovo Cimento*, **38A**, 223.

Busetta, M. et al. (1993), *Isolated Pulsars*, (Ed. van Riper, K.A., Epstein, R. & Ho, C.), Cambridge University Press, Cambridge.

Carraminana, A. (1991), *Ph. D. Thesis, University of Durham.*

Cassiday, G.L. et al. (1989), *Phys. Rev. Lett.*, **62**, 383.

Castellani, V. (1980), *Globular Clusters*, (Ed. Hanes, D. & Madore, B.), Cambridge University Press, Cambridge.

Caswell, J.L., Murray, J.D., Roger, R.S., Cole, D.J. & Cooke, D.J. (1975), *Astr. Ap.*, **45**, 239.

Cawley, M.F. et al. (1990), *Experimental Astronomy*, **3**, 173.

Cerenkov, P.A. (1934), *Dokl. Akad. Nauk, SSSR*, **14**, 101.

Cerenkov, P.A. (1937), *Phys. Rev.*, **52**, 378.

Chadwick, P.M. (1987), *Ph. D. Thesis, University of Durham.*

Chadwick, P.M. et al. (1985), *Nature*, **318**, 642.

Chadwick, P.M. et al. (1987), *Very High Energy Gamma Ray Astronomy* (Ed. Turver, K.E.), Reidel Publishing, Dordrecht.

Chadwick, P.M., McComb, T.J.L. & Turver, K.E. (1992), *Towards a Major Atmospheric Cerenkov Detector* (Ed. Fleury, P. & Vacanti, G.), Editions Frontieres, Gif-sur-Yvette.

Chanmungam, G. & Brecher, K. (1985), *Nature*, **313**, 767.

Chantell, M. et al. (1993), *AIP Conference Proceedings* (Ed. Friedlander, M., Gehrels, N. & Macomb, D.J.), **280**, 833, St. Louis.

Charles, P.A. (1989), *Proc. of the 23rd ESLAB Symposium on two topics in X-ray Astronomy*, ESA SP-296, **1**, 129.

Chen, K. (1991), *Nature*, **352**, 695.

Cheng, K.S. & Ruderman, M. (1989), *Ap. J.*, **337**, L77.

Cheng, K.S. & Ruderman, M. (1991), *Ap. J.*, **373**, 187.

Cheng, K.S. et al. (1990), *Proc. 21st Int. Cosmic Ray Conf.* (Ed. Protheroe, R.J.), **4**, 374, Adelaide.

Cheng, K.S., Ho, C. & Ruderman, M.A. (1986), *Ap. J.*, **300**, 500.

Chiang, J. & Romani, R.W. (1992), *Ap. J.*, **400**, 629.

Connaughton, V. et al. (1993), *Proc. 23rd Int. Cosmic Ray Conf.*, 1, 112, Calgary.

Conover, W.J. (1980), *Practical Nonparametric Statistics*, J. Wiley & Sons, New York.

Cordes, J.M. & Helfand, D.J. (1980), *Ap. J.*, **239**, 640.

Cordova, F.A. & Mason, K.O. (1983), *Accretion-driven Stellar X-ray Sources* (Ed. Lewin, W.H.G. & van den Heuvel, E.P.J.), Cambridge University Press, Cambridge.

Cowley, A.P., Crampton, D. & Hutchings, J.B. (1982), *Ap. J.*, **255**, 596.

Curie, E. (1938), *Marie Curie*, William Heinemann, London.

de Jager, O.C. (1987), *Ph. D. Thesis, University of Potchefstroom.*

de Jager, O.C. & Meintjes, P.J. (1992), *Astr. Ap.*, **268**, 1.

de Jager, O.C. et al. (1989), *IAU Circular # 4858.*

de Jager, O.C. et al. (1990), *Nucl. Phys. B (Proc. Suppl.)* **14A**, 169, North-Holland Publishing, Amsterdam.

de Jager, O.C., Raubenheimer, B.C., North, A.R., Nel, H.I. & van Urk, G. (1988), *Ap. J.*, **329**, 831.

de Jager, O.C., Swanepoel, J.C.H. & Raubenheimer, B.C. (1989), *Astr. Ap.*, **221**, 180.

Dyakanov, M.N. et al. (1993), *Proc. 23rd Int. Cosmic Ray Conf.*, **4**, 303, Calgary.

Eadie, W.T. et al. (1971), *Statistical Methods in Experimental Physics*, North-Holland Publishing, Amsterdam.

Edwards, P.G. et al. (1993), *Proc. 23rd Int. Cosmic Ray Conf.*, **2**, 426, Calgary.

Edwards, P.J. (1990), *Ph. D. Thesis, University of Nottingham.*

Eggleton, P.P. (1976), *Structure & Evolution of Close Binary Systems* (Ed. Eggleton, P.P., Mitton, S. & Whelan, J.A.J.), Reidel Publishing, Dordrecht.

Epstein, R.I. & Hurley, K. (1988), *Astro. Lett. & Communications*, **27**, 229.

Erber, T. (1966), *Rev. Mod. Phys.*, **38**, 626.

Fegan, D.J. (1992), *Towards a Major Atmospheric Cerenkov Detector* (Ed. Fleury, P. & Vacanti, G.), Editions Frontieres, Gif-sur-Yvette.

Fennell, S. et al. (1992), *AIP Conf. Proc.*, **280**, 508.

Fermi, E. (1949), *Phys. Rev.*, **75**, 1169.

Fichtel, C.E. et al. (1992), preprint to appear in *Advances in Space Research*, Pergamon Press, New York.

Fichtel, C. E. (1992a), preprint to appear in *Proc. 16th Symposium on Relativistic Astrophysics*, Berkeley.

Fierro, J.M. et al. (1993), *Ap. J.*, **413**, L27.

Frank, I.M. & Tamm, Ig. (1937), *Dokl. Akad. Nauk, SSSR*, **14** (3), 109.

Gaisser, T.K. & Hillas, A. M. (1977), *Proc. 15th Int. Cosmic Ray Conf.*, **8**, 353, Plovdiv.

Gibson, A.I. et al. (1982), *Nature*, **296**, 833.

Gibson, A.I. et al. (1982a), *Proc. Int. Workshop on VHE Gamma Ray Astronomy.*, (Ed. Ramana-Murthy, P.V. & Weekes, T.C.), TIFR, Bombay.

Ginsburg, V.L. (1940), *Zh. fiz. SSSR*, **2**, 441.

Goeckel (1910), *Phys. Zeits.*, **11**, 280.

Griffiths, D. (1987), *Introduction to Elementary Particles*, J. Wiley & Sons, New York.

Griffiths, R.E. et al. (1978), *Nature*, **276**, 247.

Gunn, J.E. & Ostriker, J.P. (1969), *Nature*, **221**, 454.

Gursky, H. (1976), *Structure & Evolution of Close Binary Systems* (Ed. Eggleton, P.P., Mitton, S. & Whelan, J.A.J.), Reidel Publishing, Dordrecht.

Haefner, R., Schoembs, R. & Vogt, N. (1979), *Astr. Ap.*, **77**, 7.

Halpern, J.P. & Patterson, J. (1987), *Ap. J.*, **312**, L31.

Harding, A.K. (1990), *Nucl. Phys. B (Proc. Suppl.)* **14A**, 3, North-Holland Publishing, Amsterdam.

Harrison, T.E. (1990), *IAU Circular # 5114.*

Hartman, R.C. et al. (1979), *Ap. J.*, **230**, 597.

Heaviside, O. (1892), *Electrical Papers*, **2**, 494.

Hellier, C., Mason, K.O. & Rees Williams, O. (1992), *MNRAS*, **258**, 457.

Hellier, C., Mason, K.O., Smale, A.P. & Kilkenny, D. (1990), *MNRAS*, **224**, 39p.

Henrichs, H.F. (1983), *Accretion-driven Stellar X-ray Sources* (Ed. Lewin, W.H.G. & van den Heuvel, E.P.J.), Cambridge University Press, Cambridge.

Hertz, P. et al. (1993), *AIP Conf. Proc.*, **280**, 238.

Hess, V.F. (1911), *Phys. Zeits.*, **12**, 998.

Hillas, A.M. (1982), *J. Phys. G*, **8**, 1475.

Hillas, A.M. (1987), *Very High Energy Gamma Ray Astronomy* (Ed. Turver, K.E.), Reidel Publishing, Dordrecht.

Hillas, A.M. & Johnson, P.A. (1990), *Proc. 21st Int. Cosmic Ray Conf.* (Ed. Protheroe, R.J.), **4**, 19, Adelaide.

Hillas, A.M. & Patterson, J.R. (1987), *Very High Energy Gamma Ray Astronomy* (Ed. Turver, K.E.), Reidel Publishing, Dordrecht.

Hillier, R. (1984), *Gamma Ray Astronomy*, Clarendon Press, Oxford.

Jelley, J.V., (1958), *Cerenkov Radiation and its Applications*, Pergamon Press, London.

Jelley, J.V., (1987), *Very High Energy Gamma Ray Astronomy* (Ed. Turver, K.E.), Reidel Publishing, Dordrecht.

Jennings, M.C. (1982), *Ap. J.*, **258**, 110.

Johnston, S. & Bailes, M. (1991), *MNRAS*, **252**, 277.

Johnston, S., Kaspi, V.M., Manchester, R.N., Lyne, A.G. & D'Amico, N. (1993), *GRO/Radio Timing Data Base*, Princeton University.

Kamata, Y., Tawara, Y. & Koyama, K. (1991), *Ap. J.*, **379**, L65.

Katz, J.I. & Smith, I.A. (1988), *Ap. J.*, **326**, 733.

Kazanas, D. & Ellison, D.C. (1986), *Nature*, **319**, 380.

Kertzman, M.P. & Sembroski, G. (1991), *Proc. 22nd Int. Cosmic Ray Conf.*, **2**, 656, Dublin.

Khrenov, B.A. (1993), *Nuclear Physics B (Proc. Suppl.)*, **33A,B**, 18.

Kiraly, P. & Meszaros, P. (1988), *Ap. J.*, **333**, 719.

Kirk, J.G. & Trumper, J.E. (1983), *Accretion-driven Stellar X-ray Sources* (Ed. Lewin, W.H.G. & van den Heuvel, E.P.J.), Cambridge University Press, Cambridge.

Kirk, J.G. & Heavens, A.F. (1990), *Proc. 21st Int. Cosmic Ray Conf.* (Ed. Protheroe, R.J.), **4**, 93, Adelaide.

Kniffen, D.A. et al. (1993), *Ap. J.*, **411**, 133.

Koyama, K. et al. (1991), *Ap. J.*, **377**, 240.

Kraushaar, W.L. et al. (1972), *Ap. J.* **177**, 341.

Krys, A., Krys, E. & Wasilewski, A. (1991), *Proc. 22nd Int. Cosmic Ray Conf.*, **2**, 638, Dublin.

Kulkarni, S.R. & Thorsett, S.E. (1993), *Nature*, **364**, 579.

Kulkarni, S.R., Djorgovski, S. & Klemola, A.R. (1991), *Ap. J.*, **367**, 221.

Kurfess, J.D. et al. (1992), *Ap. J. Lett.*, **399**, 137.

Labay, J., Garcia, D., Canal, R. & Isern, J. (1989), *Proc. of the 23rd ESLAB Symposium on two topics in X-ray Astronomy*, ESA SP-296, **1**, 489.

Lang, K.R. (1986), *Astrophysical Formulae*, Springer-Verlag, New York.

Lasota, J.P., Hameury, J.M. & King, A.R. (1989), *Accretion Disks and Magnetic Fields in Astrophysics* (Ed. Belvedere, G.), Kluwer Academic Publishers, Dordrecht.

Liebert, J. (1980), *Ann. Rev. Astron. Astrophys.*, **18**, 363.

Link, B., Epstein, R.I. & Van Riper, K.A. (1992), *Nature*, **359**, 616.

Longair, M.S. (1981), *High Energy Astrophysics*, Cambridge University Press, Cambridge.

Lang, K.R. (1986), *Astrophysical Formulae*, Springer-Verlag, New York.

Lorrain, P. & Corson, D.R. (1970), *Electromagnetic Fields and Waves*, W.H. Freeman and Co., New York.

Lyne, A.G. & Graham-Smith, F. (1990), *Pulsar Astronomy*, Cambridge University Press, Cambridge.

Macrae, J.H.K. (1985), *Ph. D. Thesis, University of Durham.*

Mallet, L. (1926) *C.R. Acad. Sci. (Paris)*, **183**, 274.

Manchester, R.N. & Taylor, J.H. (1977), *Pulsars*, Freeman, San Francisco.

Manchester, R.N., Durdin, J.M. & Newton, L.M. (1985), *Nature*, **313**, 374.

Manchester, R.N. et al. (1991), *Nature*, **352**, 219.

Manchester, R.N., Tuohy, I.R. & D'Amico, N. (1982), *Ap. J.*, **262**, L31.

Mannings, V.G. (1990), *Ph. D. Thesis, University of Durham.*

Mannings, V.G. (1992), *Astr. Ap.*, **258**, 335.

Mardia, K.V. (1972), *Statistics of Directional Data*, Academic Press, London.

Marshall, N., Warwick, R.S. & Pounds, K.A. (1981), *MNRAS*, **194**, 987.

Mason, K.O. & Cordova, F.A. (1982), *Ap. J.*, **255**, 603.

Mason, K.O. & Cordova, F.A. (1982a), *Ap. J.*, **262**, 253.

Mason, K.O. et al. (1980), *Ap. J.*, **242**, L109.

McAdam, W.B., Osborne, J.L. & Parkinson, M.L. (1993), *Nature*, **361**, 516.

McKenna, J. & Lyne, A.G. (1990), *Nature*, **343**, 349.

Meintjes, P.J. et al. (1992), *Ap. J.*, **401**, 325.

Meyhandan, R. et al. (1991), *Proc. 22nd Int. Cosmic Ray Conf.*, **1**, 384, Dublin.

Michelson, P.F. et al. (1992), *IAU Circular # 5470.*

Naylor, T. & Podsiadlowski, Ph. (1993), *MNRAS*, **262**, 929.

Nel, H.I., de Jager, O.C., Raubenheimer, B.C. & North, A.R. (1989), *Timing Neutron Stars* (Ed. Ogelman, H. & van den Heuvel, E.P.J.), Kluwer Academic Publishers, Dordrecht.

Nel, H.I., de Jager, O.C., Raubenheimer, B.C., North, A.R. & Brink, C. (1990), *Ap. J.*, **361**, 181.

Nel, H.I. et al. (1992), *Ap. J.*, **398**, 602.

Orford, K.J.O. (1991), *Experimental Astronomy*, **1**, 305.

Palfrey, T.R. (1992), *Towards a Major Atmospheric Cerenkov Detector* (Ed. Fleury, P. & Vacanti, G.), Editions Frontieres, Gif-sur-Yvette.

Paresce, F., De Marchi, G. & Ferraro, F.R. (1992), *Nature*, **360**, 46.

Patterson, J. (1981), *Ap. J. Suppl. Ser.*, **45**, 517.

Patterson, J. & Halpern, J.P. (1990), *Ap. J.*, **361**, 173.

Patterson, J.R. & Hillas, A.M. (1983), *J. Phys. G*, **9**, 1433.

Patterson, J., Williams, G. & Hiltner, W.A. (1981), *Ap. J.*, **245**, 618.

Payne-Gaposchkin, C.H. (1977), *Astron. J.*, **82**, 665.

Petterson, J.A. (1983), *Accretion-driven Stellar X-ray Sources* (Ed. Lewin, W.H.G. & van den Heuvel, E.P.J.), Cambridge University Press, Cambridge.

Podsiadlowski, Ph. (1991), *Nature*, **350**, 136.

Pringle, J.E. et al. (1987), *MNRAS*, **255**, 73.

Protheroe, R.J. (1977), *Ph. D. Thesis, University of Durham.*

Protheroe, R.J. (1982), *J. Phys. G*, **8**, L165.

Protheroe, R.J. & Kazanas, D. (1983), *Ap. J.*, **265**, 620.

Protheroe, R.J. & Patterson, J.R. (1984), *J. Phys. G*, **10**, 841.

Protheroe, R.J. & Stanev, T. (1992), *Towards a Major Atmospheric Cerenkov Detector* (Ed. Fleury, P. & Vacanti, G.), Editions Frontieres, Gif-sur-Yvette.

Punch, M. et al. (1992), *Nature*, **358**, 477.

Quenby, J.J. & Lieu, R. (1989), *Nature*, **342**, 654.

Ramana-Murthy, P.V. & Wolfendale, A.W. (1986), *Gamma Ray Astronomy*, Cambridge University Press, Cambridge.

Rao, M.V.S. & Sinha, S. (1988), *J. Phys. G*, **14**, 811.

Rappaport, S.A. & Joss, P.C. (1983), *Accretion-driven Stellar X-ray Sources* (Ed. Lewin, W.H.G. & van den Heuvel, E.P.J.), Cambridge University Press, Cambridge.

Rawley, L.A., Taylor, J.H. & Davis, M.M. (1988), **326**, 947.

Ray, A. & Kluzniak, W. (1990), *Nature*, **344**, 415.

Rayner, S.M. (1989), *Ph. D. Thesis, University of Durham.*

Rees, M. (1989), *Accretion Disks and Magnetic Fields in Astrophysics* (Ed. Belvedere, G.), Kluwer Academic Publishers, Dordrecht.

Rice, S.O. (1944), *Bell System Technical Journal*, **23**, 282.

Ritter, H. (1990), *Astr. Ap. Suppl. Ser.*, **85**, 1179.

Robinson, E.L. (1976), *Ann.Rev. Astron. Ap.*, **14**, 119.

Robinson, E.L., Shafter, A.W. & Balachandran, S. (1991) *Ap. J.*, **374**, 298.

Robinson, E.L. & Warner, B. (1984), *Ap. J.*, **277**, 250.

Ruderman, M.A. & Sutherland, P.G. (1975), *Ap. J.*, **196**, 51.

Rutherford & Cooke (1903), *Phys. Rev.*, **16**, 183.

Rybicki, G.B. & Lightman, A.P. (1979), *Radiative Processes in Astrophysics*, J. Wiley & Sons, New York.

Ryba M.F. & Taylor, J.H. (1991), *Ap. J.*, **371**, 739.

Schneid, E.J. et al. (1992), *Astr. Ap.*. **255**, L13.

Schoembs, R. & Vogt, N. (1980), *Astr. Ap.*, **88**, 66.

Schoembs, R. & Vogt, N. (1981), *Astr. Ap.*, **97**, 185.

Schönfelder, V. (1989), *Cosmic Gamma Rays, Neutrinos and Related Astrophysics* (Ed. Shapiro, M.M. & Wefel, J.P.), Kluwer Academic Publishers, Dordrecht.

Segelstein, D.J., Rawley, L.A., Stinebring, D.R., Fruchter, A.S. & Taylor, J.H. (1986), *Nature*, **322**, 714.

Seifert, W., Ostreicher, R., Wunner, G. & Ruder, H. (1987), *Astr. Ap.*, **183**, L1.

Seward, F.D. & Harnden, F.R. (1982), *Ap. J.*, **256**, L45.

Seward, F.D., Harnden, F.R., Murdin, P. & Clark, D.H. (1983), *Ap. J.*, **267**, 698.

Shapiro, S.L. & Teukolsky, S.A. (1983), *Black Holes, White Dwarfs & Neutron Stars*, J.Wiley & Sons, New York.

Silberberg, R., Tsao, C.H. & Letaw, J.R. (1993), *Particle Astrophysics & Cosmology* (Ed. Shapiro, M.M., Silberberg, R. & Wefel, J.P.), Kluwer Academic Publishers, Dordrecht.

Slane, P. & Fry, W.F. (1989), *Ap. J.*, **342**, 1129.

Spergel, D.N. (1991), *Nature*, **352**, 221.

Standish, E.M. (1982), *Astr. Ap.*, **114**, 297.

Stecker, F.W. & De Jager, O.C. (1993), *Ap. J.*, **415**, 71.

Stenger, V.J. (1983), *Hawaii DUMAND Center Report HDC-5-83*, University of Hawaii.

Stenger, V.J. (1984), *Ap. J.*, **284**, 810.

Taira, T. et al. (1993), *Proc. 23rd Int. Cosmic Ray Conf.*, **2**, 128, Calgary.

Tajima, T. & Gilden, D. (1987), *Ap.J.*, **320**, 741.

Takano, S. et al. (1989), *IAU Circular # 4745.*

Tavani, M. (1993), *Ap. J.*, **407**, 135.

Thompson, D.J. et al. (1992), *Nature*, **359**, 615.

Thorsett, S.E. (1992), *Nature*, **356**, 690.

Tumer, O.T. et al. (1985), *Proc. 19th Int. Cosmic Ray Conf.*, **1**, 139, La Jolla.

Tumer, O.T., Hammond, J.S., Zych, A.D. & MacCallum, C. (1990), *Nucl. Phys. B (Proc. Suppl.)*, **14A**, 176, North-Holland Publishing, Amsterdam.

Tumer, O.T., Hammond, J.S., White, R.S. & Zych, A.D. (1990), *Proc. 21st Int. Cosmic Ray Conf.* (Ed. Protheroe, R.J.), **2**, 155, Adelaide.

Tumer, O.T., Kerrick, A.D., O'Neill, T.J., White, R.S. & Zych, A.D. (1991), *Proc. 22nd Int. Cosmic Ray Conf.*, **2**, 634, Dublin.

Tuohy, I.R., Mason, K.O., Garmire, G.P. & Lamb, F.K. (1981), *Ap. J.*, **245**, 183.

Usov, V.V. (1983), *Nature*, **305**, 409.

Usov, V.V. (1988), *Pis'ma Astron. Zh.*, **14**, 606.

Vacanti, G. et al. (1991), *Ap.J.*, **377**, 467.

van den Heuvel, E.P.J. (1976), *Structure & Evolution of Close Binary Systems* (Ed. Eggleton, P.P., Mitton, S. & Whelan, J.A.J.), Reidel Publishing, Dordrecht.

van den Heuvel, E.P.J. (1987), *High Energy Phenomena Around Collapsed Stars* (Ed. Pacini, F.), Reidel Publishing, Dordrecht.

van der Klis, M. (1989), *Ann. Rev. Astron. Ap.*, **27**, 517.

van der Woerd & Heise, J. (1987), *MNRAS*, **225**, 141.

van der Woerd, H. et al. (1987), *Astr. Ap.*, **182**, 219.

Vishwanath, P.R., Satyanarayana, G.P., Ramana-Murthy, P.V. & Bhat, P.N. (1992), *IAU Circular # 5612.*

Walpole, R.E. (1982), *Introduction to Statistics*, Macmillan Publishing, New York.

Wang, Y.M. (1986), *Astrophysics & Space Science*, **121**, 193.

Warner, B. (1976), *Structure & Evolution of Close Binary Systems* (Ed. Eggleton, P.P., Mitton, S. & Whelan, J.A.J.), Reidel Publishing, Dordrecht.

Warner, B. & Brickhill, A.J. (1978), *MNRAS*, **182**, 777.

Webbink, R.F. (1985), *Dynamics of Star Clusters* (Ed. Goodman, J. & Hut, P.), Cambridge University Press, Cambridge.

Weekes, T.C. & Turver, K.E. (1977), *Proc. of the 12th ESLAB Symp.*, E.S.R.O., Frascati.

Weisskopf, M.C. et al. (1983), *Ap. J.*, **267**, 711.

White, N.E. (1989), *Astr. Ap. Rev.*, **1**, 85.

White, N.E. & Holt, S.S. (1982), *Ap. J.*, **257**, 318.

Williams, G. et al. (1979), *Nature*, **281**, 48.

Wilson, J.G. & Wouthuysen, S.A. (1967), *Progress in Elementary Particle and Cosmic Ray Physics*, **9**, North-Holland Publishing, Amsterdam.

Wilson, R.B. et al. (1992), *IAU Circular # 5429.*

Zukerman, B., Becklin, E.E., McLean, I.S. & Patterson, J. (1992), *Ap. J.*, **400**, 665.